MEDICAL UNIVERSITY OF VIENNA

Identifying Novel Degraders and Resistance Mechanisms in Targeted Protein Degradation

Doctoral Thesis at the Medical University of Vienna

for obtaining the academic degree

Doctor of Philosophy

Submitted by

Alexander Hanzl, MSc

Supervisor:

Georg E Winter, PhD

CeMM Research Center for Molecular Medicine

Lazarettgasse 14, AKH BT 25.3, 1090 Vienna, Austria

Vienna, September 2022

Table of Contents

Declaration

This doctoral thesis is presented in a cumulative format and contains two research manuscripts as well as a review article. Alexander Hanzl is the sole author of this theses with input from his supervisor Georg Winter and is the first author on all included articles. Most of the herein described experiments and analysis were performed in the laboratory of Georg Winter at the Research Center for Molecular Medicine of the Austrian Academy of Sciences (CeMM) in Vienna, Austria. The presented work was aided by other members of the Winter laboratory, as well as collaborators in the laboratories of Alessio Ciulli at the University of Dundee and Eric Fischer at the Dana Farber Cancer Institute. Detailed author contributions are highlighted in the prologue section to each original research article as well as in the author contribution statements therein.

Chapter 1.4.4 was published in **Current Opinion in Chemical Biology** and has been reprinted with permission from the publisher Elsevier Inc.

Targeted protein degradation: current and future challenges.

Alexander Hanzl, Georg E. Winter (2020), Curr Opin Chem Biol *56*, 35-41.

The manuscript in Chapter 2.1 is accepted at **Nature Chemical Biology** and is reprinted with permission by the publisher Springer Nature Ltd.

Functional E3 ligase hotspots and resistance mechanisms to small-molecule degraders.

Alexander Hanzl, Ryan Casement*, Hana Imrichova*, Scott J. Hughes, Eleonora Barone, Andrea Testa, Sophie Bauer, Jane Wright, Matthias Brand, Alessio Ciulli and Georg E. Winter (2022); Nat Chem Biol, accepted manuscript. * These authors contributed equally

The manuscript in Chapter 2.2 is currently submitted at **Cell Chemical Biology** and under consideration.

Tracing E3 Ligase Abundance Empowers Degrader Discovery at Scale.

Alexander Hanzl, Eleonora Barone, Sophie Bauer, Hong Yue, Radosław P. Nowak, Elisa Hahn, Eugenia V. Pankevich, Christoph Bock, Eric S. Fischer, Georg E. Winter (2022).Cell Chem Biol, submitted manuscript

Abstract

Targeted protein degradation (TPD) presents a novel pharmacologic paradigm, where a protein of interest (POI) is intentionally depleted by hijacking cellular protein turnover systems. Small molecule ‘degraders’ have been identified to recruit target proteins to E3 ligases, thereby directing ubiquitination onto these neosubstrates. As a result, the POI is earmarked for proteasomal degradation, and its potentially disease-promoting functions are impeded. This strategy is advantageous due to its catalytic turnover at low drug concentrations compared to conventional inhibition and further opens new avenues to target proteins previously thought ‘undruggable’.

With increasing clinical investigations of degrader molecules, we anticipated emergence of therapy resistance which might differ from described resistance mechanisms to inhibitors. We set out by performing targeted sequencing of near-haploid cells that acquired spontaneous resistance to small-molecule degraders. Resistance mutations emerged preferentially on the E3 ligase within the drug-induced ternary complex interface with the POI. We next evaluated the impact of all possible mutations in that interface via deep mutational scanning. This captured E3 ligase hotspots presenting neosubstrate- and chemotype specificity, deepening our insights into the structural determinants of drug induced ternary complexes. We further identified and functionally annotated mutations that were described in degrader treated refractory multiple myeloma patients. By comparing spontaneous resistance emergence between two commonly adopted E3s in TPD, we also characterized key determinants of these ligases to increase success for future therapy development.

Aiming to exploit this knowledge in the second part of this thesis, we set out to design an E3 ligase selective approach for degrader discovery. Building on previous characterization of cullin RING E3 ligase (CRL) regulatory circuits and their modulation, we develop a scalable assay reporting on drug induced changes to the interactome of a CRL. We benchmark this method with both heterobifunctional PROtein Targeting Chimeras (PROTACs) and small monovalent molecular glue degraders. In a proof-of-concept high-throughput screen, we identify chemically distinct molecular glue degraders functionally mimicking previously identified compounds. Finally, we chart the large space of over 250 E3 ligases amendable to this approach to mark the possibilities for scalable identification of degraders specific to a ligase of interest. Overall, this work highlights important factors for TPD resistance and presents the first scalable approach to E3 ligase selective degrader discovery.

Zusammenfassung

Der gezielte Abbau von Proteinen (Targeted Protein Degradation) stellt eine neue pharmakologische Strategie dar, bei der Zielproteine mittels Moleküle an E3-Ligasen binden und so ubiquitiniert werden. Infolgedessen werden diese Proteine für den proteasomalen Abbau vorgemerkt und ihre potenziell krankheitsfördernden Funktionen verhindert. Diese Strategie ist aufgrund ihrer katalytischen Wirkweise im Vergleich zur konventionellen Inhibition vorteilhaft. Sie eröffnet darüber hinaus neue Wege Proteine, die bisher außerhalb des Wirkungsbereichs der Pharmakologie lagen, zu erreichen.

Mit zunehmenden klinischen Studien von diesen neuen gezielten Abbaumolekülen antizipieren wir das Auftreten von Therapieresistenzen, die sich von bisher beschriebenen Resistenzmechanismen gegen Inhibitoren unterscheiden werden. Daher sequenzierten wir zunächst Zellen, die spontan Resistenz gegen gezielte Abbaumoleküle entwickelten und fanden Mutationen bevorzugt innerhalb der E3-Ligase an der Schnittstelle des induzierten ternären Komplexes mit dem Zielprotein. Im nächsten Schritt bewerteten wir die Auswirkungen aller möglichen Mutationen an dieser Schnittstelle durch gezielte Mutagenisierung. Auf diese Weise wurden E3-Ligase-Aminosäuren mit Neosubstrat- und Abbaumolekül-Spezifität erfasst, was tiefe Einblicke in die strukturellen Notwendigkeiten dieser ternären Komplexe aufzeigte. Darüber hinaus konnten wir Mutationen beschreiben, die in Patienten auftreten nach einer Diagnose mit wiederkehrendem Multiplem Myelom und nach Behandlung mit solchen Abbaumolekülen. Durch den Vergleich des spontanen Aufkommens von Resistenzen zwischen zwei häufig eingesetzten E3 Ligasen zum gezielten Abbau von Proteinen, charakterisieren wir zusätzlich Eigenschaften dieser Ligasen, um den Erfolg zukünftiger Therapieentwicklungen zu steigern.

Um dieses Wissen zu verwerten, entwickelten wir im zweiten Teil dieser Arbeit einen E3-Ligasen-selektiven Ansatz für die Identifizierung neuer gezielter Abbaumoleküle. Aufbauend auf einer früheren Charakterisierung der cullin-RING-E3-Ligase (CRL) Regulierung und ihrer Modulation beschreiben wir eine skalierbare Analyse, die über molekülinduzierte Veränderungen der Interaktionen einer Ligase berichtet. Wir validieren diese Methode sowohl mit bifunktionalen als auch mit kleinen monovalenten gerzielten Abbaumolekülen. In einer Machbarkeitsstudie identifizieren wir neue molekulare Abbaumoleküle, mit ähnlicher Wirkweise zu bereits bekannten. Insgesamt hebt diese Arbeit wichtige Faktoren für die TPD-Resistenz hervor und stellt den ersten skalierbaren Ansatz für die Suche nach E3-Ligase selektiven Abbaumolekülen dar.

Acknowledgements

This thesis marks the culmination of a long road for me, which I perceive to not have walked alone but with the continuing support and encouragement of many people in my life. Without the assistance and backup from each one of you, I would surely not be where I am today.

First and foremost, I want to thank my PhD mentor Georg for a sheer million reasons that I could not have hoped for a better teacher, role model and supervisor. I feel eternally grateful for endless project discussions, encouragements and endorsements which were the main drivers for my scientific development. I do not take such a mentorship for granted and hope that the future will still provide many opportunities for keeping close contact.

I also want to highlight the contribution of every person (past and present) at CeMM to the excellent scientific but also familiar environment which hugely impacted my traineeship. In no other place so far have I experienced a similar solidarity and team spirit which emerges from the commitment of every individual starting at admin and facility support and reaching to faculty. Thank you!

I want to thank the many people that have contributed directly to projects I have been lucky enough to work on. That includes Matthias, who layed the scientific base for one of the projects and entrusted it to me. Hana and Ryan, who continuously put efforts into publishing this work. Sophie, Ele and Elisa for their assistance and giving me the chance to work together with them.

All of the current and previous Winter lab members have generated an environment that allowed me to grow tremendously both professionally and personally and I hope that I could also contribute to similar success stories for some of you.

I am grateful to my close friends Berni, Zezi and Max for pushing me outside my scientific and work-related bubble and giving me additional perspectives as well as always offering emotional relief. I want to thank my more organized half, Anna, for all the childish moments, her continuous support and understanding for long workdays and my science delusions.

Last but not least, I want to thank my family for always giving me the security of a safe haven which I luckily have not had to make use of too many times yet. My sisters for providing refreshingly diverging points of view on life and my parents for their permanent effort to support all of us, in every possible way. Without all of you this would not have been possible for me!

List of abbreviations

AA	amino acid
ADCC	Antibody-Dependent Cell-mediated Cytotoxicity
ADME	Absorption, Distribution, Metabolism, Excretion
ALL	Acute Lymphocytic Leukemia
APC	Anaphase-Promoting Complex
BET	Bromodomain Extra-Terminal protein
BTB	Broad complex, Tramtrack, Bric-a-brac
CAND1	Cullin-Associated, NEDD8-Dissociated protein 1
CAR	Chimeric Antigen Receptor
Cas9	CRISPR-associated protein 9
CDK4	Cyclin-Dependent Kinase 4
CDK6	Cyclin-Dependent Kinase 6
CLL	Chronic Lymphocytic Leukemia
CML	Chronic Myeloid Leukemia
COP9	Constitutive Photomorphogenesis 9
CRBN	Cereblon
CRISPR	Clustered Regularly Interspaced Short Palindromic Repeats
CRL	Cullin-RING ligase
CSN	COP9 Signalosome
DCAF	DDB1- and CUL4 associated factor
DDB1	DNA-Damage Binding protein 1
DNMT	De Novo MethylTransferase
DUB	Deubiquitinase
E1	Ubiquitin-activating enzyme
E2	Ubiquitin-conjugating enzyme
E3	Ubiquitin ligase
EMT	Epithelial-To-Mesenchymal transition
FDA	Food and Drug Administration
GIST	GastroIntestinal Stromal Tumor
GO	Gene Ontology
HDAC	Histone Deacetylase
HECT	Homologous to E6AP C-Terminus
HER	Human Epidermal growth factor Receptor
IAA	Indole Acetic Acid
IAP	Inhibitor of Apoptosis Protein
IBR	In-Between-RING
IMiD	ImmunoModulatory Drug
MG	Molecular Glue
NAE	NEDD8-Activating Enzyme
NEDD8	Neural precursor cell Expressed, Developmentally Downregulated 8
PROTAC	PROteolysis TArgeting Chimera
RBR	RING-between-RING
RING	Really Interesting New Gene
SCF	SKP, Cullin, F-box containing complex
SERD	Selective Estrogen Receptor Degrader
SERM	Selective Estrogen Receptor Modulator
sgRNA	single guide RNA
SMI	Small Molecule Inhibitor
SOCS/BC	Suppressor Of Cytokine Signaling/ elongin-BC
SR	Substrate Receptor
STK	Serine/Threonine Kinase
TPD	Targeted rotein degradation
UPS	Ubiquitin-Proteasome System
VHL	Von Hippel-Lindau

List of Figures

1. Introduction

1.1 Characterization and Underpinnings of Cancer

Cancer is an overarching term for a collection of pathophysiological diseases that can affect and originate from every tissue of the human body. Global statistical analysis has shown that in 2020 alone an estimated 20 million new cases of cancer and 10 million cancer related deaths were recorded (Ferlay et al., 2021). This apparent clinical need has historically led to classify the great diversity of cancer maladies by site and tissue of origin. The vast heterogeneity of these malignancies among individual patients and even tumors is however unified by a necessity to adhere to a set of biological traits. These underpinning principals are thought to ensure onset and progression of aberrant tumor growth and are commonly known as the “hallmarks of cancer” (Hanahan and Weinberg, 2000; Hanahan and Weinberg, 2011). The core set of ten hallmark capabilities includes: Evading growth suppression, cellular death and immune destruction while enabling proliferative signaling, replicative immortality, vascularization, metastasis, and deregulation of cellular metabolism, which is supported by genomic instability and tumor-promoting inflammation. Recently four additional emerging hallmarks and enabling characteristics have been proposed including non-mutational epigenetic reprogramming (Hanahan, 2022)(Figure 1). Accumulated in a highly variable fashion for each individual tumor these unifying principals emerge at all stages of disease development and in many cases represent targets of therapeutic intervention.

The diverse classification of cancers is further elevated by the inherent genetic heterogeneity. The genomic revolution and subsequent large scale tumor sequencing efforts have yielded an additional layer of characterization by common genomic alterations. These efforts spurred the hunt for molecular underpinnings of oncogenesis and thereby high-profile therapeutic targets (Futreal et al., 2004). It is generally believed that mutations in a small number of genes important for cancer growth (oncogenes) or growth inhibition (tumor suppressors) can drive single cells to develop malignant growth.

Given the aforementioned hallmark of genomic instability most cancers develop an increased genomic mutational burden. This results in driver mutations that are essential for disease progression and so-called passenger or by-stander mutations. Typically, driver mutations are highly prevalent throughout the heterogenetic tumor as they are selected for in an evolving cancer tissue (Pon and Marra, 2015; Stratton et al., 2009). Passenger mutations

can remain functionally inconsequential but also over time adopt a tumor progressing role based on the environmental conditions (Roche-Lestienne et al., 2002). Some of these cases will be discussed in further detail in the cancer resistance chapter (1.3) of this work.

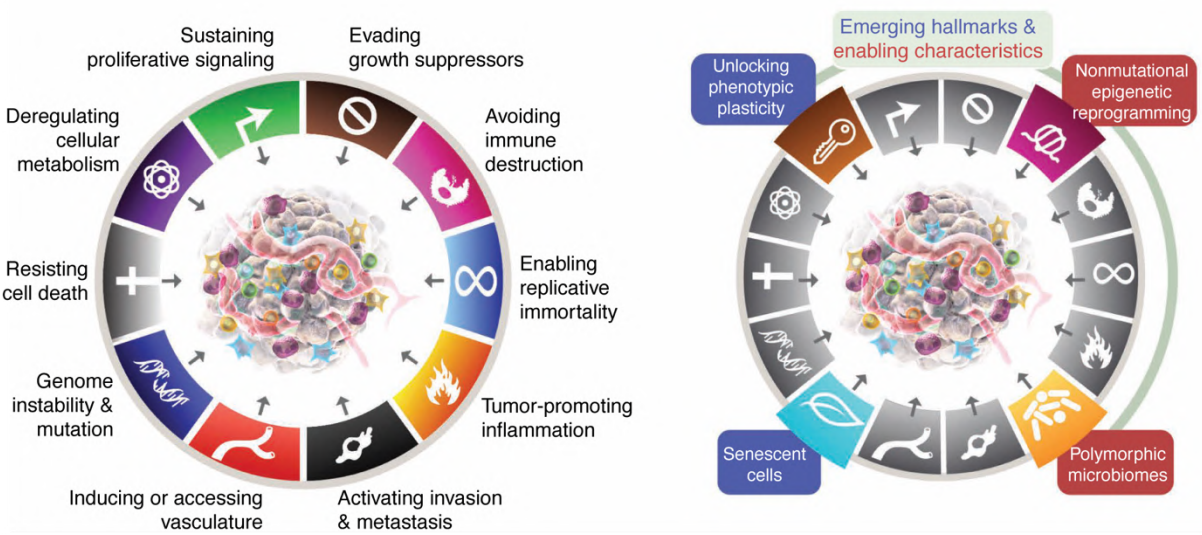

Figure 1. The hallmarks of cancer in 2022.

Reprinted from Cancer Discov 12, 31-46., Hanahan, D., Hallmarks of Cancer: New Dimensions, 2022, with permission from AACR

1.1.1 Multiple Myeloma

Most cancers depend on driver mutations which converge on regulation of cell proliferation and genomic integrity (Martincorena et al., 2017). Being no exception to this rule, multiple myeloma has a recurrent role throughout this thesis and therefore serves here as an example to introduce some of these genes. As a type of blood cancer originating in plasma cells of the bone marrow, the malignant mature B-lymphoid cells display large patient and tumor heterogeneity (Bolli et al., 2014; Lohr et al., 2014). Clonal aberrant plasma cell expansion during disease progression ultimately competes for the bone marrow niche leading to malfunctioning hematopoiesis and suppression of the immune system. Disease onset is in most cases marked by large chromosomal alterations or hyperdiploidy. In about 40 per cent of cases chromosome translocations lead to juxtaposition of cell cycle and signaling genes (f.e. *CCND1*, *CCND3* and *FGFR3*) to the highly expressed immunoglobulin heavy chain (*IgH*) locus (Chapman et al., 2011a). This is in most cases however not sufficient to drive malignant progression which often coincides with activation or somatic mutation of common oncogenic drivers such as *MYC*, *KRAS*, *TP53* and *BRAF* (Walker et al., 2018). In the case of multiple myeloma, drug repurposing efforts have uncovered thalidomide and analogous immunomodulatory imid drugs (IMiDs) as potential therapies. These have since been adopted to clinical standard of care, greatly improving patient outcomes (Raza et al., 2017). One of the

molecular modes of action of IMiDs later identified, proved instrumental to the establishment of targeted protein degradation (TPD) as a viable pharmacological concept.

1.2 Current State of Cancer Treatment

In the beginning of the 20th century treatment of cancer was mainly performed by surgical removal of solid tumors. The school of thought was to remove extensive parts of healthy tissue via radical surgery. At the same time discovery of X-ray mediated antineoplastic activity marked the beginnings of radiotherapy. Both of these treatment methods have been extensively improved and, in most cases, still represent at least a part of therapeutic cancer intervention today (Schirrmacher, 2019).

The third pillar, chemotherapy, was first introduced in the 1940s and has since consistently increased in importance for patient care. Successful treatment of cancers with chemical or biological agents is often achieved by targeting the hallmarks discussed earlier. In many cases these therapeutics focus on vulnerabilities of cancer cells due to their aberrant growth and dependency thereon. As cancers present in highly diverse varieties so do their therapeutic counterparts. In the following some of the most commonly used treatment agents are discussed in more detail.

1.2.1 Conventional Chemotherapy

The rise of chemotherapy in the mid of the 20th century led to identification of several therapeutic modalities with general antiproliferative (cytotoxic) effect. These agents intervene in cellular processes important for rapidly dividing cells and therefor affect preferentially malignant cells. However rapidly regenerating healthy cells (f.e. in gastrointestinal or oral cavity tissue) are similarly affected thereby limiting the therapeutic dose window these drugs can be used in. Furthermore, the divergent markup of tumors leads to malignant cells with varied cell growth characteristics and thereby diverse susceptibility to each chemotherapeutic agent respectively (Rahbari et al., 2016; Russo et al., 2016). To address this heterogeneity, combination treatments targeting different aspects of cellular growth have been introduced and shown tremendous success.

Antimetabolites:

Antifolates have been first reported in 1948 with the discovery of antineoplastic effects of aminopterin, which started the field of antimetabolite chemotherapeutics (Farber and Diamond, 1948). Successor molecules such as methotrexate (MTX) were identified as dihydrofolate reductase (DHFR) inhibitors and are still used to day in high dose treatment regimens (Pui et al., 2009). These drugs affect intracellular folate homeostasis and thereby

the synthesis of DNA building block precursors. Newer versions of this modality such as pemetrexmed and pralatrexate incorporate a second mode of action as prodrugs. Upon conversion to polyglutamates these drugs also inhibit thymidylate synthase (TS) and thereby purine synthesis potentially contributing to their therapeutic activity (Allegra et al., 1987).

5-fluoropyrimidines (5-FU) have been designed based on the observation that radiolabeled uracil is preferentially incorporated in rat liver cancers (Heidelberger et al., 1957). They incorporate at least two modes of action, first via inhibition of TS and thereby dTTP precursor deprivation and second via their direct incorporation into nucleic acid strands (Santi et al., 1974).

Nucleoside analogues constitute the third class of antimetabolite drugs. Arabinose nucleosides were originally identified and isolated from natural sources and inhibit DNA polymerase α. They are incorporated into DNA and terminate chain elongation ultimately leading to apoptosis (Kufe et al., 1984; Townsend and Cheng, 1987). Purine analogues such as 6-mercaptopurine (6-MP) exert their antineoplastic activity by DNA incorporation leading to coding errors in replication. They also incorporate in RNA and inhibit *de novo* purine synthesis, but these effects are thought to be less contributing (Sahasranaman et al., 2008).

Antimitotic Drugs

Drugs targeting mitosis have been mostly identified from anti-cancer activities in natural compound screening efforts (Wani and Horwitz, 2014). Agents such as vinca alkaloids (f.e. vinblastine), taxanes (f.e. paclitaxel) and eribulin have been found to target microtubule dynamics at low drug dose while inhibiting their polymerization at higher doses. These effects converge on aberrant mitotic spindle assembly and mitotic blockade. Furthermore, new antitubulin drugs with different modes of tumor delivery such as nanoparticle packaging or as antibody drug conjugates have recently been approved for leukemia and lymphomas (Bighin et al., 2013; Douer, 2016). Interestingly, targeting mitotic kinases and other factors important for mitosis have not yet come to fruition.

Alkylating and Methylating Agents

Historically, alkylating drugs were the first nonhormonal chemical compounds showing antineoplastic activity. Based on the discovery that nitrogen mustards depleted leukocytes, the first chemotherapeutics were used to treat lymphomas (Goodman and Wintrobe, 1946; Jacobson et al., 1946). Alkylating agents such as cyclophosphamide act on guanin bases of DNA leading to reactive intermediates which attack nucleophilic sites. This leads to DNA cross-linking and other forms of DNA damage which stall DNA replication if not repaired. Next to utilization in many different cancers there has also been renewed interest in these agents,

as they lead to altered gene expression and thereby neo-antigen presentation for immunotherapy, a topic discussed in the targeted therapy chapter of this thesis.

Platinum Analogues

Cisplatin and subsequent analogues with reduced off targets such as carboplatin and oxaliplatin exert their cytotoxicity via covalent binding to purine DNA bases. This leads to local denaturing which must be repaired by nucleotide excision repair (NER) and double strand break (DSB) repair. Ultimately, cells are arrested at the G2M phase of the cell cycle and undergo cell death (Amable et al., 2019). Platinum drugs have synergistic activities with a wide range of other anticancer agents due their activity throughout the cell cycle. Considering the tumor heterogeneity discussed at the beginning of this chapter, this poses a significant advantage. Additionally, platinum agents sensitize tumor cells to radiation, as DNA-Pt adducts interfere with DSB repair (Boeckman et al., 2005).

Bacterial Derived Topoisomerase Inhibitors

Anthracycline chemotherapeutics such as doxorubicin are antibiotics that act on topoisomerases (TOP), which cleave DNA to locally reduce stress from supercoiling or intwining. Particularly, during DNA replication topoisomerases activity is essential for replication fork stability (Delgado et al., 2018). The mode of action of doxorubicin includes stabilization of the TOP2 complex in a covalently DNA bound state at DSB sites, inhibition of the catalytic activity of TOP2, increasing reactive oxygen species and stimulating apoptosis. More narrow TOP targeting agents include the TOP1 inhibitor topotecan and etoposide. Systemic toxicities and adverse effects have also led to development of tumor specific delivery of TOP inhibitors (Ogitani et al., 2016).

Other Therapeutic Agents

Bleomycin is another bacterial derived DNA damaging drug that induces single- and double-strand breaks via an iron mediated oxidative cleavage of the deoxyribose backbone of DNA (Chabner).

1.2.2 Targeted Chemotherapy

All the above-mentioned therapeutic approaches target cellular processes and inflict damage also in healthy not just malignant cells. This limits the therapeutic window to where next to tumor killing properties, adverse effects are still manageable. While drug combinations and optimized treatment schedules can broaden this window of opportunity, the genomic revolution in life sciences has shed light on a novel set of drug targets which is expanding rapidly. Careful scientific pursuit of the molecular underpinnings of different cancers aided by large scale gene mapping efforts such as the human genome project has revealed concepts

of oncogenic addiction (Weinstein, 2002). Cancers in their neoplastic behavior can become dependent on the malfunction of a set of gene(s). Targeted treatment of these factors entails the promise of specific cytotoxicity to cancer cells while leaving healthy tissue unharmed and thereby allowing a greater therapeutic window. Targeting of these neoplastic factors via chemical or biological agents has repeatedly been successful by improving patient care and progression free survival (PFS). However targeted therapies elicit a very specific selective pressure on a rapidly evolving system and therefore have seen an inevitable rise of cancer resistance. Clinically, patients often experience a spectacular response at the onset of treatment and thereby a benefit of disease management, which is however paired with only minor improvements in long-term overall survival. Mechanisms of acquired therapy resistance are typically however not limited to any specific drug and therefore often also translate to classical anti-proliferative chemotherapy.

Biological drugs

Monoclonal Antibodies

The first monoclonal antibody treatment in cancer was approved in 1998 and targeted the B-cell marker CD20 (Coiffier et al., 1998). The impressive initial results led to more than 40 different antibody-based treatments in current clinical use. These in general aim to target important functional hallmarks such as angiogenesis, proliferation, and evasion from the immune system. Mechanisms to achieve responses are almost as varied as their cellular targets and include: (i) fixation of complement factors, (ii) direct target inhibition by binding transmembrane proteins and locking their function or (iii) signaling immune effector cells (natural killer (NK) and T cells) in a process called antibody dependent cell mediated cytotoxicity (Singh et al., 2018). Furthermore, antibody drug conjugates can facilitate local specificity of delivered inhibitory or cytotoxic compounds (iv). Finally, antibodies can be directed at extracellular soluble factors such as cytokines and hormones to elicit their therapeutic effect (v).

Targets include the human epidermal growth factor receptor family (HER2) in metastatic breast cancer by blocking its intracellular signalling (Harbeck et al., 2013). EGFR also presents a high profile target in colorectal cancer bound by cetuximab (Fornasier et al., 2018). To target the local angiogenic effect of vascular endothelial growth factor (VEGF), antibodies have been developed to bind the secreted ligand and block its receptor interaction (Ferrara et al., 2004).

Focus on the immune evasion of tumors so called checkpoint inhibitors have recently gained a lot of interest and shown exceptional results in clinics (Hodi et al., 2010). These monoclonal antibodies target surface antigens on tumor cells which allow their evasion of T

cell mediated killing. Specifically Cytotoxic T-lymphocyte-Associated Protein 4 (CTLA-4) and programmed death ligand 1 (PD-L1) are often overexpressed in cancer cells and upon binding with their counterpart receptors on T-cells activate signaling cascades which in turn inhibit T cell activation. In normal conditions this system is fine tuned to maintain immune tolerance to self-antigens, which the tumor hijacks for its immune evasion. Successful approvals for antibodies (ipilimumab, nivolumab and others) against both these tumor antigens have revolutionized the field of cancer immunotherapy. Especially cancers with high mutational burden and thereby higher likelihood of generating neo-antigens have evolved to utilize these immune evading pathways and respond exceptionally well to these treatments.

Adoptive Cellular Therapy

The concept of immune cell transfer to cancer patients with the goal of therapeutic benefits has gained a lot of interest with recent clinical results. The admission of anti-CD19 chimeric antigen receptor (CAR) T cell therapy in B-Cell leukemias and lymphomas in 2017 constituted another clinical milestone in cancer therapy. Several different immune cells have been adopted in clinical trial settings including NK lymphocytes, cytokine-induced killer T cells and tumor-infiltrating lymphocytes (Rosenberg and Restifo, 2015). In general these modalities aim to isolate and expand immune cells of the patient and engineer them to obtain activity against a tumor specific antigen. In the case of the aforementioned CAR-T cells this is accomplished by expression of an artificial T cell receptor against the mature B cell surface marker CD19. Upon reintroduction to the patient these CAR-T cells don't target healthy B cell precursors, allowing for reconstitution of a normal B cell compartment (Lulla et al., 2018). Clinical limitations of these therapies lie in their high cost of manufacturing as they are individually produced per patient and toxicities based on excessive immune responses such as graft vs. host disease (GVHD).

Small Molecule Inhibitors

Macromolecular targeted therapies as the above discussed biological agents have seen increasing importance in clinics. At the same time, advancements in drug discovery and disease understanding have similarly expanded the second field of targeted therapies characterized by protein inhibition via small molecules (Figure 2). Small molecule inhibitors (SMIs) in most cases target disease relevant enzymes at the active site in a substrate competitive manner. Alternative modes of action include allosteric binding (outside the enzymatic pocket) leading to steric protein structure changes, and induction or disruption of protein-protein interactions (PPIs). Binding to the site of interest is typically achieved by compound – protein surface complementation facilitated by electrostatic interactions or hydrophobicity. Furthermore, SMIs can act in a reversible or irreversible fashion via covalently

attaching to the protein of interest (POI) (Roskoski, 2016). Main advantages of SMIs over biological agents lie in their pharmacokinetics (drug delivery and bioavailability) and their inherently more scalable manufacturing and storage. To date the US Food and Drug Administration (FDA) has approved over 90 small molecule drugs for use in cancer therapy. In the latter, many of the currently clinically used SMIs will be discussed according to their target spectrum.

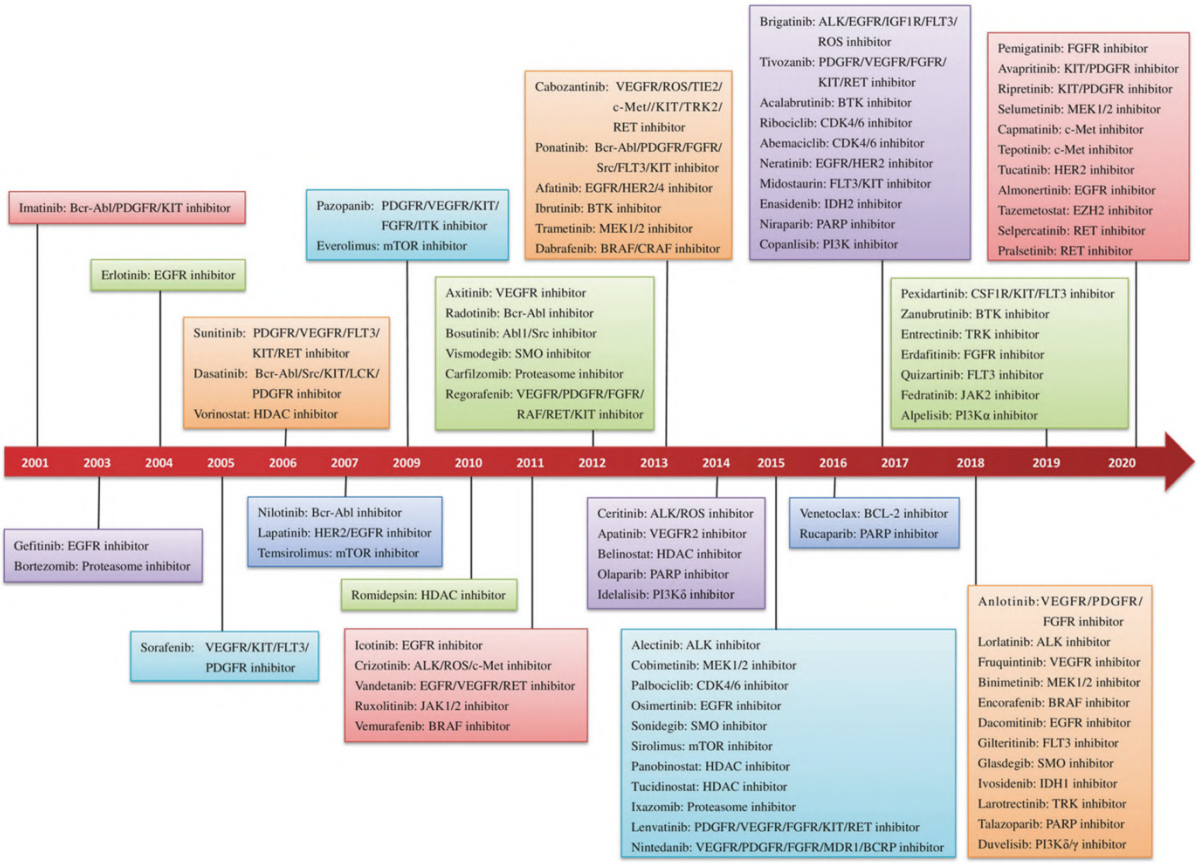

Figure 2. A timeline of approvals of small molecule inhibitors for anti-cancer therapy

Reprinted from Signal Transduction and Targeted Therapy 6, 201., Zhong, L., Li, Y., Xiong, L., Wang, W., Wu, M., Yuan, T., Yang, W., Tian, C., Miao, Z., Wang, T., and Yang, S. (2021). Small molecules in targeted cancer therapy: advances, challenges, and future perspectives., under the Creative Commons CC BY license.

Kinase Inhibitors

Kinases are enzymes catalyzing the transfer of terminal phosphate groups from ATP to hydroxyl moieties on their substrate. They comprise a protein family of 535 members collectively called the human kinome (Wilson et al., 2018). Kinases often preform the initial activation event for signaling cascades controlling a plethora of cellular processes such as proliferation, differentiation of migration. Given their central role in these basic prerequisites of cellular survival and identity, they are often found dysregulated in human cancers. As such Kinases represent the best studied family of oncogenic target genes with around 38 clinically

approved inhibitors to date (Ferguson and Gray, 2018). Kinases can be generally classified by their substrate residues into two groups: tyrosine kinases (TKs) and serine/threonine kinases (STKs).

In the group of tyrosine kinases, the BCR-ABL fusion represents one of the historically most important targets. It is the first target to which a SMI was approved in an oncology setting (Druker et al., 1996). The oncogenic fusion gene between the TK ABL1 and the breakpoint cluster region (BCR) on chromosome 22 produces a 210 kDa oncoprotein in nearly all cases of chronic myeloid leukemia (CML) and 20 % of acute lymphoblastic leukemia (ALL). The protein fusion allows autophosphorylation and drives cellular proliferation. Due to its high prevalence it was originally proposed as a biomarker for patient stratification and BCR-ABL inhibition produced spectacular clinical results spurring the field of targeted therapy (Deininger et al., 2005). Subsequent identification of resistance mutations led to development of second and third generation inhibitors, which are also under evaluation for solid tumors (Rossari et al., 2018). Another TK of considerable interest is the HER family kinase receptor EGFR specifically in non-small cell lung cancer (NSCLC). In this case abnormal activation of the kinase function often is driven by mutation, spurring the successful drug discovery efforts to generate mutant specific inhibitors (Lynch et al., 2004). Other high profile tyrosine kinase targets include: ALK, c-MET, FLT3 and angiogenesis targeting though VEGF inhibition (Zhong et al., 2021).

The second group are serine/threonine kinases, which include several factors active in the RAS-RAF-MAPK-ERK pathway. This signaling cascade important for proliferation is therapeutically exploited on several levels. Firstly, via the oncogene BRAF which is often dysregulated through a V600E mutation, to which ATP competitive inhibitors such as vemurafenib have been developed (Chapman et al., 2011b). Secondly, MEK1 inhibitors have also been employed in combination with BRAF inhibitors (Flaherty et al., 2012). Lastly, RAS mutants which until recently have been considered “undruggable” due to their lack of an enzymatic pocket (and thereby not belonging to kinases), have also been successfully exploited (Ostrem et al., 2013). STKs also include cyclin dependent kinases (CDKs) instrumental for efficient cell cycle progression whose disruption has shown promise in breast cancer (Spring et al., 2020). Finally, the PI3K-AKT-mTOR pathway controlling apoptosis and cellular growth presents another therapeutic intervention point, as it is often found activated via mutations or amplification (Fruman et al., 2017).

Epigenetic Inhibitors

Epigenetics describes the study of influences on gene expression mediated via higher level modifications than by alteration of the genetic sequence. These modifications typically are

deposited by so called ‘writer’ proteins on DNA or the chromatin fiber affecting the transcription machinery’s access. These epigenetic marks include chemical modifications such as acetylation, methylation and many others which can be specifically bound by ‘reader’ and ‘eraser’ proteins through functional domains (f.e. bromodomains). These epigenetic effectors can lead to recruitment of co-factors to deposit or remove additional marks or facilitate chromatin remodeling (Tarakhovsky, 2010). As functionally this higher-level regulation affects gene expression many cancers have developed a dependency on epigenetic modifications. This is further emphasized by its recent promotion to a hallmark status (Hanahan, 2022). While numerous inhibitors to epigenetic regulatory proteins have been developed only a few have found clinical success.

Methylation marks can be found both on DNA and histone proteins, which facilitate the ordered arrangement of the DNA strands. In both cases these marks in a broad sense lead to silencing of the specific genomic region, although selective histone tail methylation can also have other functional consequences. DNA methyltransferases (DNMTs) have been shown to repress tumor suppressor transcription in cancers and have been successfully targeted by the nucleoside analogues azacitidine and decitabine (Kantarjian et al., 2006). A histone methyl transferase (HMT) function is carried out by the polycomb repressor complex 2 (PRC2) whose central component EZH2 deposits epigenetic modifications involved in proliferation, adhesion and DNA damage (Duan et al., 2020). Dysfunctional EZH2 is often linked to oncogenesis and disease progression and hence efforts have been driven to obtain approval for inhibitors targeting its active site (Bhat et al., 2021; Gounder et al., 2020).

The second major epigenetic modification is acetylation of histone tails which is commonly found to be an activating signal for the specific locus. This mark is deposited by histone acetyl transferases (KMTs) and removed by histone deacetylases (HDACs). Specifically for HDACs several pan- as well as selective inhibitors have been approved for clinical use in cancers (Falkenberg and Johnstone, 2014). Readers of histone acetylation comprise other promising targets for therapeutic intervention. Most notably upon which are the bromodomain extra-terminal (BET) protein family. Among these proteins BRD4 is known to facilitate upregulation of oncogenes such as MYC and BCL2 (Cochran et al., 2019). JQ1, a BET inhibitor recurrent throughout this thesis, competitively inhibits the acetyl-lysine active site of bromodomains (Delmore et al., 2011). While clinical development of JQ1 has been discontinued, other BET inhibitors are still explored in a wide variety of different cancers (Cochran et al., 2019).

Proteostasis Targeting Drugs

Protein turnover and homeostasis (‘proteostasis’) plays a central role in fundamental cellular processes including cell growth and proliferation as well as stress response to DNA

damage and unfolded proteins (UPR) (Reed, 2006). The ubiquitin proteasome system as its central player is responsible for approx. 80 % of protein degradation activity (Collins and Goldberg, 2017). As malignant cells depend on rapid proliferation, they also necessitate efficient protein turnover to remove misfolded or mutated proteins (Adams, 2004). The 26S proteasome is a 2.5 mDa complex and facilitates the proteolytic cleavage of substrates earmarked by ubiquitin chains into short peptides. The specific cascade of ubiquitin transfer and subsequent degradation will be discussed in the chapters. Proteasome inhibitors in general aim to target the catalytic subunits involved in the final proteolytic step, blocking general substrate engagement. In the early 2000s the FDA approved the proteasome inhibitor bortezomib with its chymotrypsin inhibition activity on the 26S proteasome and anti-neoplastic effects in hematological malignancies (Richardson et al., 2003). Especially the treatment success in multiple myeloma (MM) prompted efforts to improve selectivity in following versions such as carfilzomib (Kuhn et al., 2007). Overall survival benefits led to proteasome inhibitors as the first line treatment in MM cases often in combination with immunomodulatory and other drugs.

Immunomodulatory Drugs

Immunomodulatory drugs (IMiDs) such as thalidomide were rediscovered for cancer treatment after causing potentially the most tragic case of adverse effects in pharmacology history. In the early 1950s, thalidomide was initially developed and marketed for morning sickness during pregnancy. Its widespread use led to tragic cases of teratogenicity and subsequent market withdrawal (Speirs, 1962). Due to its later identified immune-modulatory effects it was subsequently evaluated in several inflammatory conditions and eventually approved for erythema nodosum leprosum (ENL) (Hales, 1999). This approval allowed off-label use in other diseases under guidelines to prevent pregnancy exposure and ultimately facilitated its discovery as an anticancer therapeutic (Singhal et al., 1999). The mechanism of action of thalidomide and its IMiD analogues lenalidomide and pomalidomide is multimodal. At least four modes of action have been described: (i) indirect effects via induction of cytokine secretion of bone marrow stromal cells in the tumorigenic niche (Chauhan et al., 1996); (ii) antiangiogenic effects via tumor necrosis factor α (TNF-α) inhibition (Moreira et al., 1993); (iii) increasing the antitumor immune response via NK cell mediated cytotoxicity (Davies et al., 2001); (iv) direct antitumor effects in multiple myeloma cells due to targeted degradation of essential factors. The discovery of this final mechanism of action took nearly 60 years but has since revolutionized efforts in drug discovery. While the molecular details of this mode of action will be discussed in a later chapter, it is principled around recruitment of zinc-finger domain containing proteins to a ubiquitinating E3 ligase complex which ultimately leads to its

proteasomal degradation (Ito et al., 2010). Many of these targets are transcription factors (TFs) vitally important for correct embryonic development explaining the teratogenic effects of these drugs (Gandhi et al., 2014; Krönke et al., 2014; Lu et al., 2014). Soon after thalidomide's approval in multiple myeloma, the second generation IMiD lenalidomide with increased efficacy entered the market. It has since topped the charts of small molecule drug sales for several years, highlighting its tremendous use as a first line treatment in combination with proteasome inhibitors and the anti-inflammatory drug dexamethasone. Given this success, drug discovery efforts poured into designing yet more potent IMiDs such as pomalidomide (Richardson et al., 2019), but also into expanding its pharmacologic notion to other targets.

Other Inhibitors

The space of cancer therapeutics is vast and very competitive. While the above examples span across a large spectrum of the most widely used agents, several small molecule inhibitors not fitting any of the mentioned categories, have not been discussed yet. To generate a more complete overview, details to BCL-2, hedgehog and PARP inhibitors will be given.

B-cell lymphoma (BCL) 2 proteins comprise several factors entailing pro- and anti-apoptotic mediating functions. Protein-protein interactions within this family regulate the apoptotic state of the cell. The BCL-2 gene itself codes for one of the anti-apoptotic proteins and is often found dysregulated especially in hematological cancers (Ashkenazi et al., 2017). Efforts to target the PPI interface of BCL-2 resulted in the approval of venetoclax in chronic lymphoid leukemia (CLL) cases (Ashkenazi et al., 2017).

The hedgehog (HH) pathway is an essential conserved signaling cascade for embryonic development. With several feedback mechanisms and ligand mediated events, a part of this pathway centers on activation of the transmembrane protein Smoothened (SMO). Active SMO promotes expression via the glioma associated oncogenic TFs GLI1, GLI2 and GLI3 and can be miss regulated by abnormal ligand levels or mutations (Pak and Segal, 2016). Several inhibitors of the HH pathway have been approved for their anticancer activity in basal cell carcinoma and AML via targeting SMO (Basset-Séguin et al., 2017; Cortes et al., 2020; Migden et al., 2015).

One of the previously discussed hallmarks of cancer is genomic instability giving rise to mutational burden which helps adaptation in a quickly evolving system. A fine balance for genomic integrity in cancer cells is ensured by dysregulation of the several orthogonal DNA repair mechanisms. This intricate equilibrium exposes several points of potential therapeutic intervention. Breast cancer is often coinciding with mutations in the tumor suppressors *BRCA1*

and *BRCA2* which have central roles in DSB repair, rendering some of the repair pathways dysfunctional (King et al., 2003). As DNA repair is still vitally important for these cancer cells, they depend on other repair factors, which upon deletion have a “synthetic lethal” effect (O'Neil et al., 2017). One of these proteins is Poly ADP-ribose polymerase 1 (PARP1), which facilitates recruitment of repair factors to single strand breaks (SSBs). Upon its catalytic inhibition SSBs often turn into DSBs during replication, which in turn can only be repaired in an error-prone fashion when *BRCA* genes are deleted. Cumulatively, this shifts the balance to inexorable genomic instability leading to anti-neoplastic effects (Vyas and Chang, 2014). Several PARP inhibitors have been approved also possessing additional benefits such as PARP trapping most notably olaparib (Lord and Ashworth, 2017). Many of these inhibitors also have synergistic activity with other DNA damaging agents previously discussed (such as platinum based agents or taxanes).

1.3 Cancer Resistance Mechanisms

The advances in treatment of cancer outlined above have led to a steady improvement for patients. Overall survival (OS) across different malignancies at one, five and ten years after diagnosis has risen by more than 50 per cent in 40 years (Quaresma et al., 2015). However, in only a short list of maladies treatment is curative. Resistance to treatment regimen has become a challenge of highest importance and is similarly shared between classical chemotherapeutic approaches and targeted therapies. Within targeted therapies immunotherapies have resulted in distinct treatment responses. While only subsets of patients react to such therapies, they tend to have a more lasting effect with increased long term overall survival. For most other targeted therapies clinicians report an overwhelming initial response lasting in tremendous increases in short term progression free survival (PFS) which unfortunately do not translate into increased overall survival >10 years after diagnosis (Ledford, 2016). It is thus critically important for the scientific community to understand the possibilities for acquired cancer resistance adaptations to benefit patients via stratification and efficient treatment monitoring.

Considerable research effort has let to classification of resistance mechanisms into intrinsic and extrinsic events. Intrinsic resistance can be seen as pre-existing to the tumor before treatment onset. Extrinsic events are acquired as a result of the treatment. Recently, the clinical relevance of such an isolated consideration of cancer resistance is being challenged however (Vasan et al., 2019). A more integrated approach is emerging, where inherent properties of cancers (such as heterogeneity, aberrant growth, etc.) are the biological cause of resistance leading to a specific molecular response. A molecular understanding over these

biological underpinnings at the level of the whole organism is subject to current research and will be out of the scope of this thesis. However, a close dissection of the molecular explanation for the resistance can yield a foundation for the mechanistic explorations in the results part of this work. All of the following examples however have to be seen in the wider context of tumor heterogeneity with ever evolving diverse subpopulations in constant exchange with the tumor microenvironment (TME).

One central mechanism for resistance is the control of intracellular drug concentrations. This is generally regulated by transporter proteins mediating uptake and efflux of metabolites, signaling factors and drugs. The ABC transporter family comprises 48 members many of which have been implicated in resistance to classical chemotherapeutics such as etoposide, taxanes and doxorubicin (Wu et al., 2014). In general, upregulation of certain transporters can lead to multi drug resistance via the ATP dependent efflux of therapeutic agents.

Especially targeted therapies are highly vulnerable to modification of their target proteins. Many tyrosine kinase inhibitors fall into this fallacy, where a secondary mutation leaves the target unaffected by the drug. For example, inhibition of EGFR leads in almost half of the patients to develop the “gatekeeper” mutation T790M, which allows enhanced ATP binding and thereby activity while blocking the drug engagement (Yu et al., 2014). Subsequent inhibitor adaptations led to a back and forth between drug discovery efforts and tumor evolution in response. Other cellular mechanisms such as epigenetic alterations or non-coding RNAs can also lead to target dysregulation and subsequent resistance (Ohata et al., 2017).

Some classical chemotherapeutic agents such as doxorubicin and cisplatin base their therapeutic window on the malignant growth and proliferation of cancer cells. Their anticancer activity is dependent on the fast cycling of cells. At the same time these drugs, as a secondary consequence, lead to an arrest of proliferation (senescence), for example via activation of the tumor suppressor p53. This therapy induced senescence can increase the stemness properties and subsequent escape from the senescent state leading to resistant subpopulations (Milanovic et al., 2018).

DNA damaging as well as DNA repair targeted therapeutics mediate their anti-neoplastic effect via the activity of DNA repair processes. With a variety of orthogonal repair mechanisms, upregulation of essential factors can mitigate some of the drug effects and lead to resistance emergence (Ceppi et al., 2006; Gerson, 2004).

Conceptually, cancer therapeutics ideally elicit their response in the malignant cell while keeping health cells unharmed. By transitioning their cell state they can therefore evade their dependency on the targeted pathways and generate resistant subpopulations. One of such

mechanisms is the epithelial-to-mesenchymal transition of cancer cells mediated through signaling cascades and epigenetic changes (Fischer et al., 2015). In many cases the relevant factors overlap with stemness processes highlighting a link to so called cancer stem cells (Oshimori et al., 2015; Shibue and Weinberg, 2017).

Taken together many of the above outlined mechanisms co-exist in a given tumor state and potentially arise only at certain times or through selection via a specific treatment. Approaches to clinically tackle cancer resistance include an early detection of the primary disease, treatments to increase the tumor response, therapeutic monitoring and consequent adaptive therapeutic intervention (Vasan et al., 2019).

1.4 Targeted Protein Degradation (TPD)

Cancer drug discovery faces several difficult challenges. Many of the problems that come with biological agents have been discussed in the introduction of inhibitor centric targeted therapies. Fighting malignancies with small molecule protein inhibitors is however itself subject to conceptual limitations.

First, inhibitors aim to block an enzymatic function of the POI. In most cases this is achieved by limiting accessibility of a (co)-substrate to the active site. Given that only a small subset of proteins present relevant in a disease setting, this notion limits the available ligand space for drug discovery immensely (Martincorena et al., 2017). On top of this many of the high-profile targets don't entail an enzymatic function and therefore drop out of the conventional ligandable protein space (Behan et al., 2019). This view is centered around the fact that successfully targeted binding pockets on proteins tend to be evolutionarily and functionally conserved and are therefore few across the proteome (Hopkins and Groom, 2002). Recent whole proteome ligandability studies are challenging this view but have yet to translate into clinical success (Wang et al., 2019). Approaches such as these allow for the unlocking of many high-profile targets such as scaffolding proteins and transcription factors (for instance MYC, RAS-proteins, etc.) (Behan et al., 2019). Furthermore, the nature of conserved binding pockets throughout protein families, typically leads to undesired off-target inhibition of a particular chemical probe. A classic example of this issue are kinase inhibitors, which rarely show confined selectivity among this protein family (Ferguson and Gray, 2018).

Targeted protein degradation (TPD) has recently seen a meteoric rise in interest as it promises solutions to several of the aforementioned challenges. At its core TPD aims to deplete a POI from the cell via a degradation pathway. Several conceptual approaches have been realized to achieve this including lysosome and autophagy targeting chemical and

biological agents (Zhao et al., 2022). From a patient centric drug discovery view the method of small molecule directed target ubiquitination and degradation has shown the most promise (Dale et al., 2021). Many of the advantages of this approach over protein inhibition are discussed in detail in the review in chapter 1.4.4. In the preceding text an introduction of the underlying biological systems that allow such a mechanism of action is given.

1.4.1 The Ubiquitin Proteasome

In a steady-state system protein half-lives vary greatly from time scales in minutes to days. Especially regulatory proteins mediating cellular adaptations have high turnover rates allowing fast responses to stimuli (Savitski et al., 2018; Zecha et al., 2018). Cells have evolved several pathways for selective and bulk removal of proteins and even whole compartments (Ciechanover, 2005). Autophagy describes the process of material encapsulation in membrane bordered autophagosomes which fuse with lysosomes containing proteases and hydrolytic enzymes. This leads to the endosomal digestion of protein aggregates and organelles. The second major pathway for protein disposal is centered around the 26S ubiquitin proteasome already briefly introduced in chapter 1.2.2.

The 26S proteasome serves as the final catalytic degrading entity for ~ 80 per cent of the human proteome (Collins and Goldberg, 2017). It is a 2.5 mDa complex comprised of a 20S core cylinder capped by two 19S enzymatic caps which help in the recruiting and modification of proteins for subsequent degradation (Baumeister et al., 1998). The catalytic protease activity is centered within the inner cavity of this complex ensuring the spatial confinement and selective targeting of proteolysis (Bedford et al., 2010). The N-terminal threonine protease activity leads to substrate cleavage resulting in up to 24 aa polypeptides which can be subsequently transported to the ribosome for repurposing. Substrate recognition is mediated via ubiquitin chain modifications with the help of receptors such as Rpn10 and Rpn13 (Lu et al., 2015).

1.4.2 Post Translational Ubiquitin Modification

Ubiquitin (Ub) is the central signaling protein modification deposited typically on lysine residues of substrate proteins to elicit subsequent degradation, translocation or activity modulation. It is a 76 aa – 8.5 kDa small globular protein conserved among eukaryotes and expressed from precursor genes or as monomeric 3- or 9-part repeats (*UBB* and *UBC*). Preferentially deposited on lysine residues, it itself carries several lysines for ubiquitin chain modification. The ubiquitination of substrates is performed through a cascade of sequential enzymatic steps. This is initiated by the ATP dependent thiol-esterification between the C-terminal end of ubiquitin and a cysteine residue on one of two human E1 ubiquitin-activating

enzymes (Figure 3). The second step is the transfer of ubiquitin to one of ~40 E2 ubiquitin-conjugating enzymes in a transesterification. Finally, most of the around 600 human E3 ubiquitin ligases recruit a protein of interest and a loaded E2 and facilitate a ligation between the C-terminal G76 of ubiquitin and the amino group of a lysine on the POI.

Protein ubiquitination does not represent a one-way street to degradation. With a variety of different post-translational modification options ubiquitin is one of the functionally most diverse protein mark. In its simplest form as mono-ubiquitination, it is implicated in cellular processes ranging from chromatin regulation and DDR to endocytosis (Hicke, 2001). Furthermore, its tendency to generate self-linked chains via its seven different lysine residues potentiates the complexity of PTMs collectively referred to as 'ubiquitin code' (Komander and Rape, 2012; Yau et al., 2017). The most abundant chain linkage happens via lysine K48 and is also the signal to proteasomal degradation. For this, at least 4 consecutive monomers must be deposited to sterically allow the funneling into the 26S proteasome (Thrower et al., 2000). Local ubiquitin density is another contributing factor for recruitment of proteasome receptors Rpn10/13 and efficient degradation (Lu et al., 2015).

With so many different functions for this PTM, cells have also evolved enzymes to remove and modify ubiquitination (Komander et al., 2009). This activity is held among deubiquitinases (DUBs) and facilitates for instance the recycling of ubiquitin by the 19S caps of the proteasome.

The wide variety of E3 ligases allows for the necessary substrate specificity of ubiquitination reactions. E3 ligases have evolved to contain different hared protein domains and associated complexes by which they are classified today. The three major classes include the RING-between-RING (RBR) ligases, the large HECT ligases and the really interesting new gene (RING) E3 ligases. The latter comprise the largest complexity with ~579 members, half of which are typically found in multi-component modular complexes centered around 7 different cullin backbone scaffolding proteins.

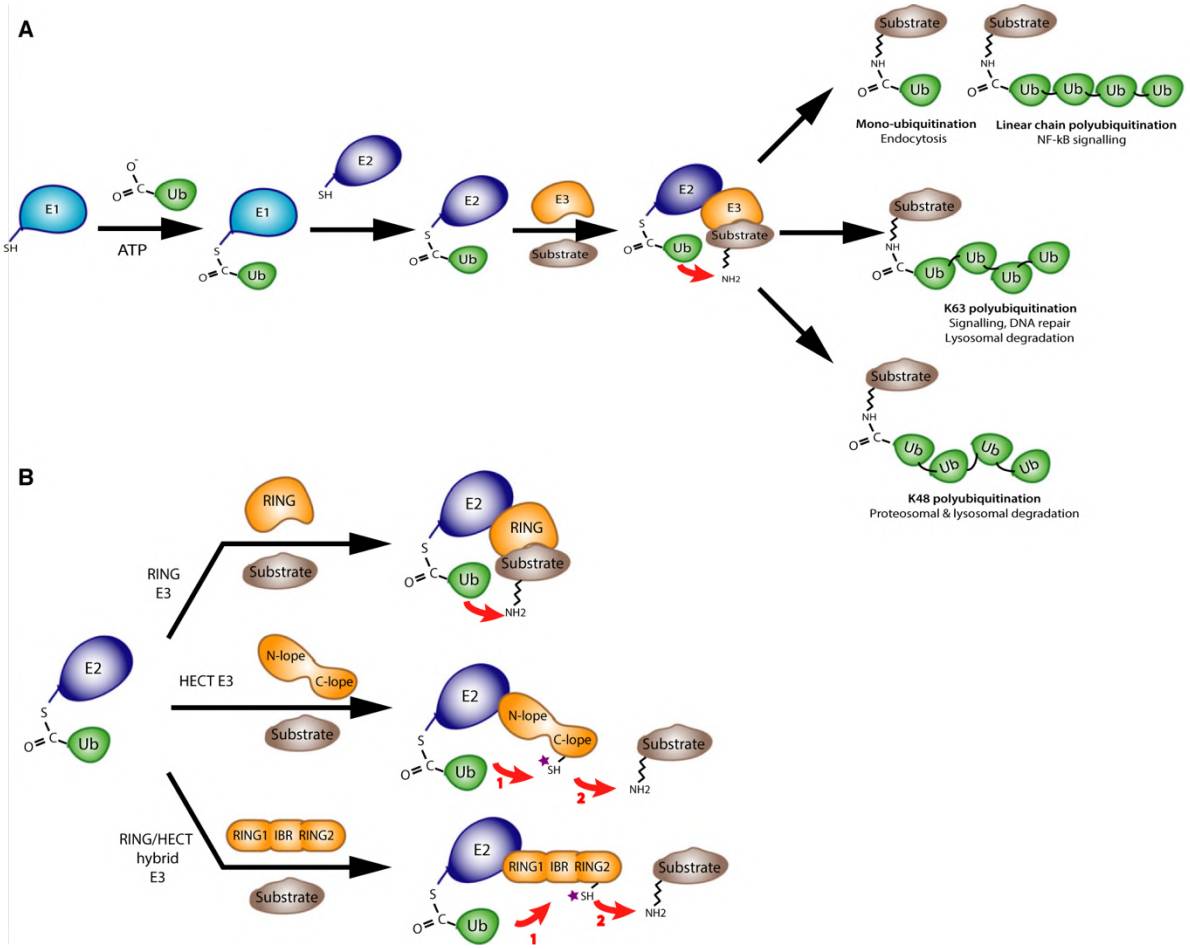

Figure 3. The cellular ubiquitination pathway (A) and different classes of E3 ligases (B)

Reprinted from FEBS J 282, 2076-2088., Seirafi, M., Kozlov, G., and Gehring, K. (2015). Parkin structure and function., under the Creative Commons CC BY NC ND license with permission from John Wiley and Sons.

1.4.3 Cullin-RING ligases (CRLs)

An estimated 20 % of the human proteome is under proteostatic control of cullin RING ligases (Soucy et al., 2009). Due to their modular complex assembly, they are regulating a vast variety of cellular processes and functions, many of which are likely not yet identified due to the inherent difficulties of pinpointing E3 ligase-substrate relationships (Emanuele et al., 2011). CRLs share structural consensus features which dictate their regulation and dynamics. The central structural entity is always one of the scaffolding cullin backbones: CUL1, CUL2, CUL3, CUL4A, CUL4B, CUL5 and CUL7. The C-terminal part of this scaffold binds RBX1 (RBX2 in the case of CUL2) which in turn recruits the ubiquitin loaded E2 (Kamura et al., 1999). The N-terminal end on the other hand binds adapter proteins which serve as a recruitment site for substrate specifying factors called substrate receptors (SR).

Every CUL scaffold enables a specific set of adaptor-SR combinations to recruit their substrates and facilitate their ubiquitination through induced proximity to a loaded E2 enzyme.

CUL1 binds the SKP1 adapter and F-box motive SRs hence them generally being referred to as SCF ligases. CUL7 similarly interacts with SKP1 but has so far only been shown to serve as a scaffold for the FBX29 SR. For CUL2 and CUL5 an adapter pair has evolved (Elongin B and Elongin C, ELOB/C) which is interacting with the SOCS family substrate receptors. CUL4A and CUL4B share the same adaptor protein in DDB1 and its substrate receptors (DCAFs) have been shown to interact with both scaffolds, though usually a preference is observed. Finally for CUL3 scaffolds, the adapter protein and SR evolved to a single entity in the form of BTB domain containing proteins.

This divers and complex modular system necessitates control mechanisms to flexibly adapt its target ubiquitination spectrum to the cellular needs. At the level of substrate binding, in many cases PTMs regulate the ubiquitination as in the case of the hypoxia inducible factor 1 α (HIF1A). Under normal physiological conditions HIF1A is hydroxylated on a proline residue and degraded via the $CUL2^{VHL}$ E3 ligase. Upon hypoxic exposure this substrate loses its hydroxylation and stabilizes within minutes highlighting the immediate response possible through this system (Ivan et al., 2001; Jaakkola et al., 2001). Another layer of regulation is mediated through a conserved lysine residue on the CUL backbones near the RBX1 binding site. This Lys represents the attachment site of a small ubiquitin like modifier called NEDD8 which activates the CRL E3 ligase by stabilization of RBX1 bound to a loaded E2 (Baek et al., 2020; Kawakami et al., 2001).

Centered around the attachment and removal of this NEDD8 mark a small set of factors regulate the activity of all CRLs (Figure 4). CUL scaffolds are neddylated via a ubiquitin like cascade initiated by the E1 NEDD8 activating enzyme (NAE1) and one of two E2s (UBE2F or UBE2M) followed by ligation via an E3 ligase. In its neddylated state the CRL is stabilized as a complex and primed for ubiquitination of recruited substrates. The ubiquitination activity however often exceeds substrate availability and is therefore also targeted towards the substrate receptor itself in a process termed ‘autodegradation’ (Wolf et al., 2003). This mechanism is also supported by the fact that E3 ligase SRs are among proteins with the shortest half-lives (Li et al., 2021; Savitski et al., 2018). Autodegradation has also been shown to be preventable by increased substrate availability via biochemical dissection (Li et al., 2004).

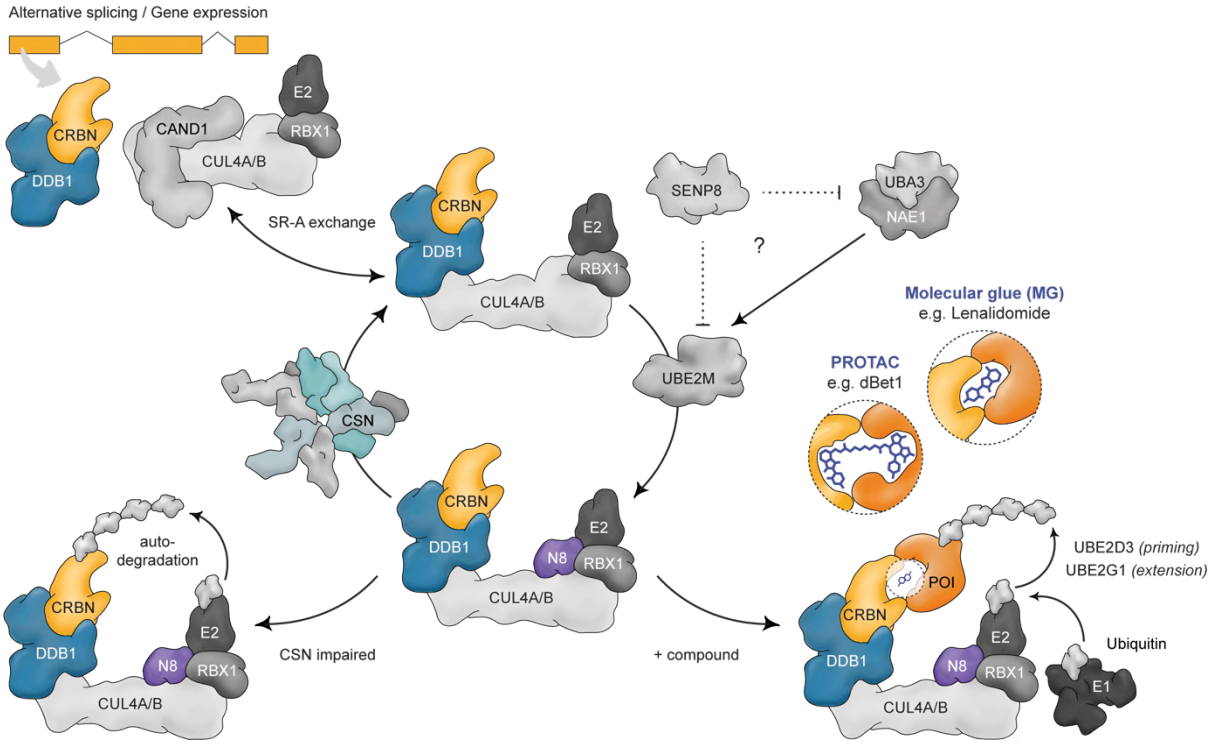

Figure 4. The regulatory cycle of Cullin RING ligases exemplified by CRL4.

Reprinted from Cell Chem Biol 28, 1048-1060., Scholes, N. S., Mayor-Ruiz, C., and Winter, G. E. (2021). Identification and selectivity profiling of small-molecule degraders via multi-omics approaches., with permission from Elsevier.

The priming NEDD8 mark on CUL scaffolds is again removed by the catalytic subunit CSN5 of the ~350 kDa COP9 signalosome complex (Cavadini et al., 2016; Lingaraju et al., 2014). In its deneddylated state CUL backbones are subject to competing binding from adapter-SR pairs and cullin-associated NEDD8-dissociated proteins 1 and 2 (CAND1 and its paralog CAND2). CAND1 wraps around the CUL scaffold and dissociates the binding of adapter-SR pairs highlighting its importance for SR exchange mechanisms. Tripartite SR-CUL-CAND1 complexes present an unstable intermediate conformation between stable CUL-CAND1 binding and stable neddylated SR-CUL-RBX1 E3 ligases (Pierce et al., 2013). In an attempt to target vulnerabilities of this fine balance in CRL regulation, several chemical probes have been designed and later extensively used to unravel biological details of these complex mechanisms. These include an inhibitor of NAE1 blocking the neddylation of all CUL scaffolds and conversely an inhibitor of CSN5 blocking NEDD8 removal (Schlierf et al., 2016; Soucy et al., 2009).

The extent of the plasticity of the cullin-RING ligase system has recently been showcased by several reports making use of these chemical probes and global interaction proteomics. Approximately half of the CUL scaffolds are bound and inactivated by CAND1, ready for incorporation of adaptor-SRs, which are almost exclusively found in paired complexes

(Reichermeier et al., 2020; Reitsma et al., 2017). These adapter-SR pairs occur in excess to their CUL scaffolds leaving most of them in an unbound state. This highlights the poised steady-state of the CRL ubiquitin system and its ability to quickly respond to cellular changes. Another layer of evidence for cell-state specific CRL modulation is that the CUL bound fraction for each SR can vary up to 200-fold, even though overall abundances for SRs only differ by 4-fold (Reichermeier et al., 2020).

The determinants of the CUL bound adapter-SR pool have also been slowly unraveled. Previously substrate availability has been implicated in affecting SR autodegradation and abundance (Li et al., 2004). Drug induced degradation has shed light on how substrate availability is a main driver of CRL remodeling (Reitsma et al., 2017). Upon small-molecule mediated neo-substrate recruitment of RBM39 to the $CUL4^{DCAF15}$ E3 ligase, the fraction of DCAF15 bound to CUL4 increases by ~2-fold. On the other hand, for the CRBN SR already a high fraction is found interacting with the CUL4 scaffold at a steady-state and neo-substrate recruitment had only marginal effects on this fraction (Reichermeier et al., 2020). Co-treatment with the NAE1 inhibitor MLN4924 blocked the CUL scaffold remodeling and thereby neo-substrate degradation (Reichermeier et al., 2020). Similarly, CSN5 inhibition by CSN5i-3 is preventing the dynamic SR exchange, but it also locks the bound adapter-SR pairs in active CRLs and thereby leads to induced autodegradation (Mayor-Ruiz et al., 2019). Given cell line differences in this autodegradation potential, this together paints a picture of a cell state specific cullin RING ligase repertoire, which is efficiently modulated to stimuli through changes in substrate availability.

1.4.4 A Review of Current and Future Challenges in TPD

In the following, a detailed review of targeted protein degradation, its recent advances and future directions is given. The author of this thesis conceived and wrote this review together with his supervisor. As an author of this review, rights are retained to include a full reprint of the article in this thesis. Other rights remain with the publisher Elsevier Inc. and the journal Current Opinion in Chemical Biology.

Available online at www.sciencedirect.com

ScienceDirect

Current Opinion in Chemical Biology

Targeted protein degradation: current and future challenges

Alexander Hanzl and Georg E. Winter

Abstract

Traditional approaches in the development of small-molecule drugs typically aim to inhibit the biochemical activity of functional protein domains. In contrast, targeted protein degradation aims to reduce overall levels of disease-relevant proteins. Mechanistically, this can be achieved via chemical ligands that induce molecular proximity between an E3 ubiquitin ligase and a protein of interest, leading to ubiquitination and degradation of the protein of interest. This paradigm-shifting pharmacology promises to address several limitations inherent to conventional inhibitor design. Most notably, targeted protein degradation has the potential not only to expand the druggable proteome beyond the reach of traditional competitive inhibitors but also to develop therapeutic strategies of unmatched selectivity. This review briefly summarizes key challenges that remain to be addressed to deliver on these promises and to realize the full therapeutic potential of pharmacologic modulation of protein degradation pathways.

Addresses

CeMM Research Center for Molecular Medicine of the Austrian Academy of Sciences, 1090 Vienna, Austria

Corresponding author: Winter, Georg E (GWinter@cemm.oeaw.ac.at)

Current Opinion in Chemical Biology 2020, **56**:35–41

This review comes from a themed issue on **Next Generation Therapeutics**

Edited by **Gonçalo Bernardes** and **Raphaël Rodriguez**

For a complete overview see the Issue and the Editorial

Available online 2 January 2020

https://doi.org/10.1016/j.cbpa.2019.11.012

Keywords

Targeted protein degradation, PROTACs, Molecular glues, Chemical biology, E3 ligase.

The framework of chemically induced protein dimerization

Proximity and interactions between proteins underpin most cellular processes. This leaves their dynamic modulation as an important goal in chemical biology and ligand discovery. Several strategies to induce protein–protein interactions (PPIs) have been innovated and are summarized in an excellent recent review [1]. Historically, the concept of inducing novel PPIs through small molecules goes back to immunosuppressive natural products, such as rapamycin and FK506. Mechanistically, both bind the protein FKBP12, thus inducing novel interactions with the mechanistic target of rapamycin kinase (mTOR) and the phosphatase calcineurin, respectively. As a consequence of this drug-induced neoassociation, several activities of mTOR and calcineurin are modulated [2–4]. Thus, both small molecules act as 'chemical neomorphs' that achieve their cellular effect by inducing PPIs that otherwise do not occur in nature. Another example of such a chemical neomorph is the plant hormone indole-3-acetic acid (IAA, auxin). Auxin induces molecular proximity between the ubiquitin ligase substrate receptor TIR1 and a family of transcriptional regulators called Aux/IAAs [5,6]. As a consequence, IAAs get ubiquitinated and degraded by the proteasome. Thus, auxin modulates the function of the SCF^{TIR1} ligase, enabling molecular recognition and degradation of a protein it would not recognize in its absence. The notion that small molecules can artificially change the target spectrum of cellular effectors of the ubiquitin–proteasome system, in particular of E3 ubiquitin ligases, represents the core concept of targeted protein degradation (TPD) [7].

Monovalent molecular glues and heterobifunctional degraders

Conceptually, there are two chemical strategies to alter the substrate spectrum of an E3 ubiquitin ligase (Figure 1). First, E3 ligases can be reprogrammed by monovalent small molecules, often referred to as 'molecular glues' (MGs). Auxin is a prime example of how a MG connects an E3 ligase (SCF^{TIR1}) and the target protein. Ligand binding to the E3 ligase alters protein interface properties, leading to dimerization with a neosubstrate. Similarly, the clinically approved drug thalidomide and its analogs, collectively called 'immunomodulatory drugs' or IMiDs, were found to act via a MG-type mechanism, namely, by reprogramming the target spectrum of the E3 ligase $CRL4^{CRBN}$. After the initial identification of the substrate receptor Cereblon (CRBN) as the cellular target of thalidomide, seminal studies uncovered that IMiD binding to CRBN leads to recruitment and proteasomal degradation of zinc finger (ZF) proteins IZKF1 and IKZF3 [8–10]. In general, MGs such as IMiDs orchestrate molecular recognition

Figure 1

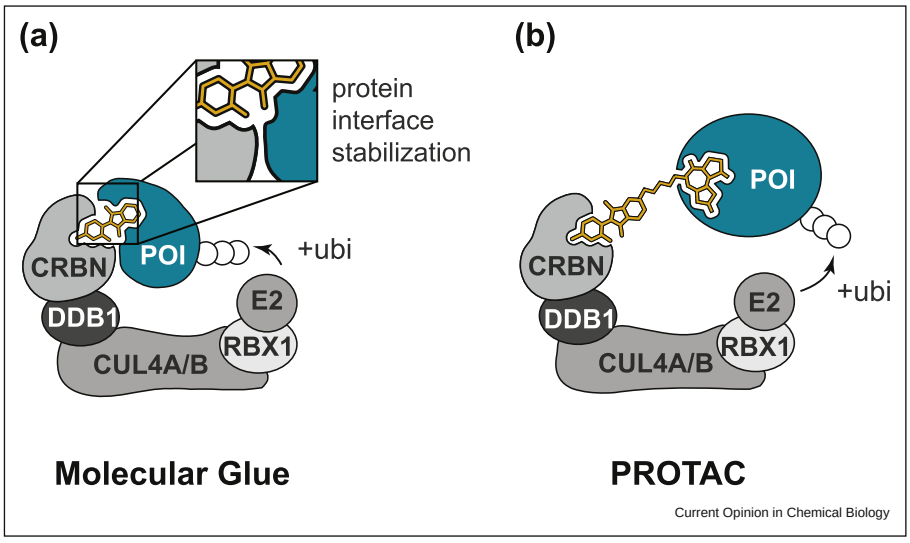

Schematic comparison of molecular glues and PROTACs. **(a)** Molecular glues are monovalent compounds that induce the dimerization of two proteins (here: an E3 ligase substrate receptor and a neosubstrate). Compound-induced proximity is often characterized by multiple interactions between the two proteins, resulting in high binding cooperativity. **(b)** PROTACs are heterobifunctional degraders that can individually bind to the E3 ligase and the protein of interest. Simultaneous binding induces molecular proximity and ensuing ubiquitination and degradation of the POI. In contrast to MGs, PROTAC-mediated dimerization is less dependent on compatible protein surfaces and associated binding cooperativity. PROTAC, proteolysis targeting chimeras; MG, molecular glue; POI, protein of interest.

between the E3 ligase and the neosubstrate in a highly cooperative manner (Figure 1A). This means that the MG typically induces novel PPIs between the E3 ligase and the target protein which contribute to the formation of a trimeric E3:MG:target protein complex. Notably, IMiDs *per se* have no measurable binding affinity to their degraded targets but hijack an entire surface patch on CRBN to induce productive dimerization [11]. While this outlines the exciting possibility of degrading unliganddable proteins, the discovery of E3 modulating MGs has so far mostly been serendipitous and cannot be easily generalized for other targets and target classes.

The major alternative to MGs is heterobifunctional degraders, which consist of one ligand binding to a ubiquitin ligase and a second ligand designed to engage a protein of interest (POI). Both ligands are connected by a flexible linker of suitable length to allow simultaneous binding to the E3 and the POI, leading to molecular proximity (Figure 1B). Productive ternary complex formation ultimately leads to ubiquitination and degradation of the POI. Such heterobifunctional degraders are often referred to as proteolysis targeting chimeras (PROTACs) [12]. First PROTAC concepts relied on peptidic agents with limited cellular efficacy. However, over the past couple of years, significant progress has been made with nonpeptidic heterobifunctional molecules [13–15]. These efforts enabled the targeted degradation of a range of proteins with well-defined ligand binding sites, such as bromodomain proteins and kinases [16,17]. Among a small group of E3 ligases that can be harnessed for PROTAC development, CRBN and the von Hippel-Lindau tumor suppressor (VHL) stand out in terms of their versatility and *in vivo* compatibility [13,18,19]. Other accessible E3 ligases include MDM2 and cIAP1 [20,21]. The modular nature of PROTACs comes with tangible upsides but also considerable challenges. First, it allows a rational and straightforward design simply by exchanging the target-binding warhead. On the other hand, their molecular weight (typically above 800 Da) poses a challenge for pharmacokinetic optimization [22]. Furthermore, as PROTACs are required to individually bind both the target protein and the E3 ligase, the associated degradable space is limited to proteins that can efficiently be liganded with small molecules. In the following, we want to highlight some of the recent discoveries and trends in the field of PROTACs and MGs and put emphasis on some of the remaining key challenges.

Exploiting selectivity of TPD

Conventional pharmacologic inhibition of a protein typically depends on ligand binding at a functional site, which often is conserved throughout enzyme families. This poses a challenge for selective inhibitor design, as showcased, for instance, by the field of kinase inhibitors [23]. In contrast, TPD requires not only compound binding but also positioning of the E3 and the POI in a configuration conducive to ternary complex formation.

Finally, tripartite binding must occur in a manner that ensures accessibility of lysine residues within the ubiquitination zone of the ligase. Notably, recent studies have uncovered that these requirements can provide an avenue toward the design of highly selective degraders starting from more promiscuous targeting ligands. First observations of target discrimination through TPD where made with MZ1, a PROTAC that prompted preferential BRD4 degradation even though using a pan-bromodomain and extraterminal (BET) protein binding targeting ligand [14,24]. Moreover, when the multikinase inhibitor SNS-032 was conjugated to thalidomide to create a putative multikinase degrader, the resulting compound selectively degraded CDK9, despite retaining a multikinase binding spectrum [25]. Further studies have systematically addressed this phenomenon by generating CRBN- or VHL-based degraders based on additional multikinase inhibitor warheads [16,17]. Although the degraders would still bind to hundreds of kinases, degradation was achieved for only 10–20% of the targets across different cellular backgrounds. In addition, it was shown that the degradable target spectrum was dependent on the hijacked E3 ligase. Subtle changes in linker configuration were sufficient to generate isoform-specific degraders of the p38 mitogen-activated protein kinase (MAPK) family [26]. Together, these studies also highlighted that binding affinity to the POI was not correlated to its degradability. Further supporting the notion that degraders can elicit unprecedented selectivity, structural dissection of BET PROTACs led to the first rational development of a BRD4-selective degrader. Mechanistically, selectivity was dictated by protein–protein interface determinants outside of the ligand binding pocket on the POI [27,28]. Furthermore, subtle modification of the E3 ligase binder allows controlling for residual inhibitory consequences of the PROTAC [29].

Collectively, these studies have shown how selectivity of otherwise promiscuous scaffolds can be achieved through TPD and lead to highly specific degraders. This was ultimately exploited in a disease-relevant context by generating PROTACs capable of selectively degrading CDK6 over CDK4 [29,30]. Selective CDK6 degraders could emerge as valuable therapeutic options in hematologic malignancies and will enable addressing kinase-independent scaffolding functions [31,32].

Expanding the scope of E3 ligases via covalent ligands

Rational identification of novel E3 ligands is a challenging task and most discoveries so far have happened serendipitously. The covalently acting natural product nimbolide is an example of such a finding. To elucidate the mechanism of action of nimbolide, activity-based proteomic profiling was applied, leading to the identification of the E3 ligase RNF114 as the primary target [33]. Other studies have explored the rational identification of covalent interactors of the E3 ligases. Gel-based activity-based proteomic profiling was used to screen for covalent binders of RNF4, identifying several probes with varying specificity for RNF4 over other proteins [34]. In another approach, broad cysteine-reactive probes were conjugated to an FKBP12 ligand and tested for their ability to degrade FKBP12 [35]. This led to the identification of a covalent ligand of the CRL4 substrate receptor DCAF16.

An important question was if the different covalent E3 binders could further be developed as E3 recruitment elements in a heterobifunctional degrader design. All of these studies assayed degradability of BET proteins by synthesizing PROTACs that connect the novel covalent E3 ligands to the known BET bromodomain antagonist JQ1 [24]. RNF114- and DCAF16-based degraders were selective for BRD4. The RNF4-based PROTAC however caused destabilization of a broader range of proteins including BRD4. Although effects of covalent binding of a POI through PROTACs have been studied previously, potential advantages and disadvantages of degraders that covalently engage the E3 ligase still remain to be experimentally validated [36]. Conceptually, these could include the reduction of the requirement for a ternary binding event to a binary interaction. Further ligand optimization will be required to develop second-generation, *in vivo* compatible degraders.

Exploring the limits of CRBN modulation with MGs

Although first PROTAC molecules recently entered clinical investigations, MG degraders, such as the aforementioned IMiDs, are already routine treatment options for different B-cell neoplasms. Generalizing and rationalizing the discovery of novel MGs thus marks a key future challenge. This could be achieved by further exploring the limits of the 'degradable space' in reach of the $CRL4^{CRBN}$ ligase complex or by chemically unlocking novel ligases. The first evidence that the $CRL4^{CRBN}$ ligase complex can be hijacked for the degradation of proteins other than the initially identified IKZF1/3 surfaced when CK1α was identified as an additional target of lenalidomide [37]. Soon, several additional IMiD targets such as GSPT1, ZFP91, and SALL4 were described [38–41]. This growing list motivated the first comprehensive assessment of the spectrum of neosubstrates that can be degraded by reprogramming $CRL4^{CRBN}$ with IMiD-like MGs [42]. Since the Cys_2-His_2 (C2H2)ZF domains of known substrates were sufficient for drug-induced recruitment, it was reasoned that IMiDs may degrade other proteins containing this feature. Indeed, four novel neosubstrates were identified using a scalable protein stability reporter assay. Structural and sequence homology

analysis revealed that the overall ZF fold, rather than a particular linear amino acid sequence, is required for IMiD-based recruitment to the $CRL4^{CRBN}$ interface. This enabled a computational prediction of neosubstrates via a holistic docking approach, leading to the identification of several additional proteins that can biochemically be recruited to CRBN after IMiD treatment. Further chemistry efforts will be required to develop chemical matter that can expand on these efforts. Forthcoming studies will likely take advantage of these modern-day docking strategies to predict 'glueable' interfaces between POIs and E3s, which might enable the prioritization of novel MG scaffolds.

MG approaches to other ubiquitin ligases

Recent research revealed that the molecular mechanism of IMiDs might not be a unique phenomenon. The arylsulfonamide indisulam and structurally related analogs were shown to induce the degradation of the splicing factor RBM39 by chemically reprogramming the substrate receptor DCAF15 [43,44]. Three recent independent studies have provided the structural and biochemical workup that unequivocally confirmed that indisulam and related aryl sulfonamides indeed function via a MG mechanism analogous to the IMiD pharmacology [45–47]. All three studies characterized a complex of DCAF15:DDB1:DDA1 together with an aryl sulfonamide recruiting RBM39. Of note, these compounds bind to DCAF15 with a significantly lower affinity than IMiDs bind to CRBN. Consistent with a model of high cooperativity, RBM39 binding greatly improves complex stability. In unbiased proteomics experiments, RBM23 is the only other destabilized protein after indisulam treatment [45]. Mechanistically, this is explained by high sequence conservation between their RRM domains involved in indisulam-induced molecular recognition. This remarkable selectivity likely stems from the buried surface area

Figure 2

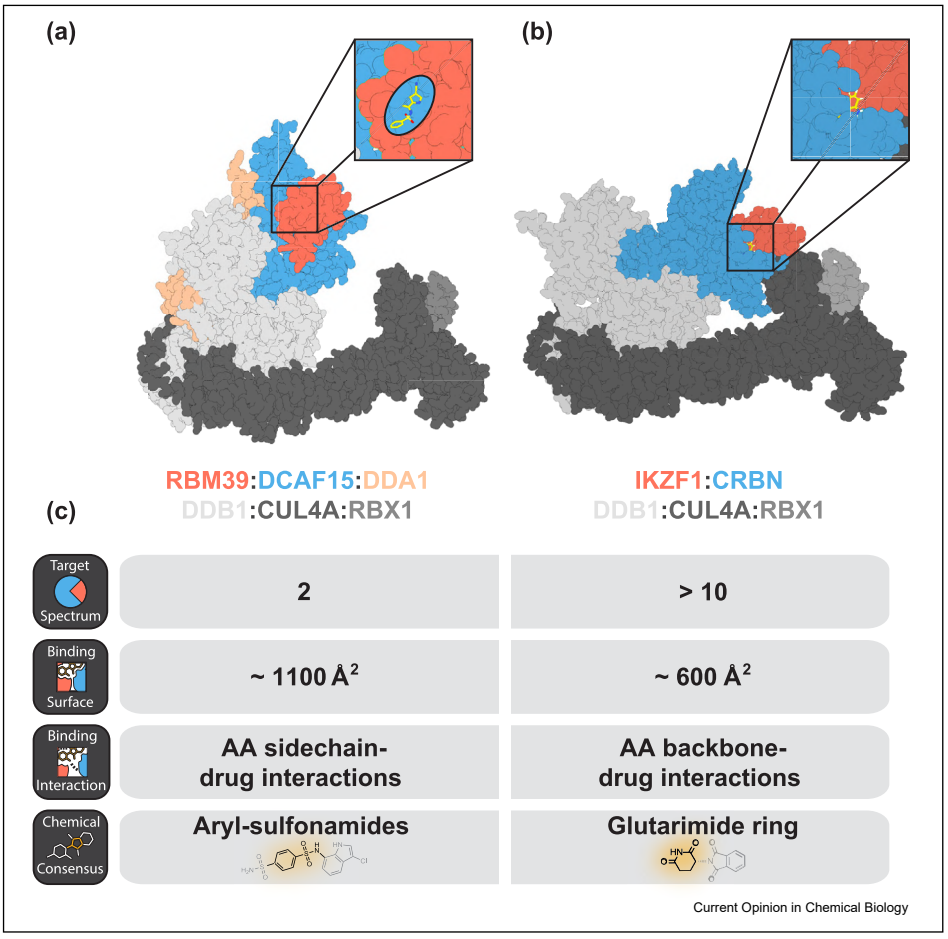

Comparision of DCAF15- and CRBN-based molecular glue degraders. **(a)** A structure of DCAF15 (PDB: 6PAI) bound to indisulam, the RRM2 domain of RBM39 and DDB1 aligned with a structure of DDB1:CUL4A:RBX1 (PDB 6PAI). **(b)** A structure of CRBN (PDB: 6H0F) in complex with pomalidomide, the ZF2 domain of IKZF1 and DDB1 aligned with a structure of DDB1:CUL4A:RBX1 (PDB 6PAI). **(c)** Comparision of general properties of DCAF15- and CRBN-based molecular glues.

between DCAF15 and RBM39, which is approximately twice as large as that of CRBN and its neosubstrates (Figure 2). Furthermore, indisulam binding involves significant side chain interactions in the ternary complex resulting in increased specificity. This leads all three studies to the conclusion that the DCAF15:indisulam surface will likely not allow the same promiscuous target spectrum as the CRBN:IMiD interface. However, new chemical matter could potentially adopt some of the RBM39:DCAF15 interactions and thereby allow other targets to be degraded.

In addition to developing MGs that recruit true neosubstrates, another promising approach is to chemically reinforce known substrate—E3 interactions that are altered in the disease. One such example is β-catenin, a Wnt signaling effector protein. β-Catenin is often mutated at Ser33 and Ser37 [48]. This disrupts a phosphodegron recognized by the $SCF^{\beta-TrCP}$ cullin-RING ligase, leading to stabilization of β-catenin and associated oncogenic consequences [49]. A recent study developed several biochemical screens coupled to structure-informed lead optimization to identify a compound that can re-enhance binding and ubiquitination of mutant β-catenin [50]. This marks the first successful study with the rationale of finding MGs for a specific ligase:substrate pair and provides a blueprint for similar future endeavors.

Collectively, the field of TPD has matured to a level where its generalizable nature is widely accepted. We will increasingly learn how to leverage some of the challenges that are associated with degrader design to our advantage to develop small molecules with unprecedented selectivity and potency. We believe that key challenges in the field will be to chemically unlock a larger number of ligases and to further rationalize the development of monovalent MGs. In addition, with the first heterobifunctional degraders in clinical trials, initial promising results on safety and druglikeness will have to be solidified (NCT03888612 and NCT04072952). This also leads to important considerations on anticipating, detecting, and circumventing associated resistance mechanisms. Along these lines, recent studies have shown that mutations in E3 ligase complexes or regulators thereof can lead to resistance to different types of degraders [51—53]. Similarly, CRBN mutations/loss of functions have been linked to the clinical mechanism of IMiD resistance, but their relevance have not fully been resolved [54,55]. Importantly, IMiDs are known to also act via a multiple indirect mechanisms, including T-cell and NK-cell modulation [56,57]. It thus remains to be seen how tumors will cope with the selective pressure of TPD therapies that function primarily via cell-autonomous mechanisms.

Conflict of interest statement

Nothing declared.

Acknowledgements

The Center for Molecular Medicine (CeMM) and the Winter Laboratory are supported by the Austrian Academy of Sciences. This work was further supported by a FWF (Fonds zur Foerderung der Wissenschaftlichen Forschung) grant to Georg Winter (project number P30271). We thank Matthias Brand for assistance with figure design. We want to apologize to colleagues whose work could not be included and highlighted in this review because of space limitations.

References

Papers of particular interest, published within the period of review, have been highlighted as:

* of special interest
** of outstanding interest

1. Stanton BZ, Chory EJ, Crabtree GR: **Chemically induced proximity in biology and medicine**. *Science* 2018, **359**. eaao5902–11.

2. Liu J, Farmer JD, Lane WS, Friedman J, Weissman I, Schreiber SL: **Calcineurin is a common target of cyclophilin-cyclosporin A and FKBP-FK506 complexes**. *Cell* 1991, **66**: 807–815.

3. Griffith JP, Kim JL, Kim EE, Sintchak MD, Thomson JA, Fitzgibbon MJ, Fleming MA, Caron PR, Hsiao K, Navia MA: **X-ray structure of calcineurin inhibited by the immunophilin-immunosuppressant FKBP12-FK506 complex**. *Cell* 1995, **82**: 507–522.

4. Stan R, McLaughlin MM, Cafferkey R, Johnson RK, Rosenberg M, Livi GP: **Interaction between FKBP12-rapamycin and TOR involves a conserved serine residue**. *J Biol Chem* 1994, **269**:32027–32030.

5. Tan X, Calderon-Villalobos LIA, Sharon M, Zheng C, Robinson CV, Estelle M, Zheng N: **Mechanism of auxin perception by the TIR1 ubiquitin ligase**. *Nature* 2007, **446**: 640–645.

6. Kepinski S, Leyser O: **Auxin-induced SCFTIR1-Aux/IAA interaction involves stable modification of the SCFTIR1 complex**. *Proc Natl Acad Sci* 2004, **101**:12381–12386.

7. Lai AC, Crews CM: **Induced protein degradation: an emerging drug discovery paradigm**. *Nat Rev Drug Discov* 2017, **16**: 101–114.

8. * Ito T, Ando H, Suzuki T, Ogura T, Hotta K, Imamura Y, Yamaguchi Y, Handa H: **Identification of a primary target of thalidomide teratogenicity**. *Science* 2010, **327**:1345–1350.
This study shows uncovered CRBN as the cellular target of thalidomide.

9. * Lu G, Middleton RE, Sun H, Naniong M, Ott CJ, Mitsiades CS, Wong KK, Bradner JE, Kaelin WG: **The myeloma drug lenalidomide promotes the cereblon-dependent destruction of ikaros proteins**. *Science* 2014, **343**:305–309.
Together with Krönke et al., this study highlights that lenalidomide modulates, rather than inhibits the function of the CRBN E3 ligase complex, leading to degradation of the neo-substrates IKZF1 and IKZF3.

10. * Kronke J, Udeshi ND, Narla A, Grauman P, Hurst SN, McConkey M, Svinkina T, Heckl D, Comer E, Li X, *et al.*: **Lenalidomide causes selective degradation of IKZF1 and IKZF3 in multiple myeloma cells**. *Science* 2014, **343**:301–305.
Together with Lu et al., this study highlights that lenalidomide modulates, rather than inhibits the function of the CRBN E3 ligase complex, leading to degradation of the neo-substrates IKZF1 and IKZF3

11. Chamberlain PP, Hamann LG: **Development of targeted protein degradation therapeutics**. *Nat Chem Biol* 2019, **86**:129.

12. Sakamoto KM, Kim KB, Kumagai A, Mercurio F, Crews CM, Deshaies RJ: **Protacs: chimeric molecules that target proteins to the Skp1-Cullin-F box complex for ubiquitination and degradation**. *Proc Natl Acad Sci* 2001, **98**:8554–8559.

13. ** Winter GE, Buckley DL, Paulk J, Roberts JM, Souza A, Dhe-Paganon S, Bradner JE: **Phthalimide conjugation as a strategy for in vivo target protein degradation**. *Science* 2015, **348**: 1376–1381.

This study outlined the first all-chemical and *in vivo* compatible strategy for rational degrader design via CRBN reprogramming

14. Zengerle M, Chan K-H, Ciulli A: **Selective small molecule induced degradation of the BET bromodomain protein BRD4**. *ACS Chem Biol* 2015, **10**:1770–1777.

15. Lu J, Qian Y, Altieri M, Dong H, Wang J, Raina K, Hines J, Winkler JD, Crew AP, Coleman K, *et al.*: **Hijacking the E3 ubiquitin ligase cereblon to efficiently target BRD4**. *Chem Biol* 2015, **22**:755–763.

16. * Huang H-T, Dobrovolsky D, Paulk J, Yang G, Weisberg EL, Doctor ZM, Buckley DL, Cho J-H, Ko E, Jang J, *et al.*: **A chemoproteomic approach to query the degradable kinome using a multi-kinase degrader**. *Cell Chem Biol* 2018, **25**:88–99. e6.

Two comprehensive investigations of degrome of multi-kinase binding PROTACs including an assessment of how different ligases affect the spectrum of degradable targets

17. * Bondeson DP, Smith BE, Burslem GM, Buhimschi AD, Hines J, Jaime-Figueroa S, Wang J, Hamman BD, Ishchenko A, Crews CM: **Lessons in PROTAC design from selective degradation with a promiscuous warhead**. *Cell Chem Biol* 2018, **25**:78–87. e5.

Two comprehensive investigations of degrome of multi-kinase binding PROTACs including an assessment of how different ligases affect the spectrum of degradable targets

18. Pettersson M, Crews CM: **PROteolysis TArgeting Chimeras (PROTACs) - past, present and future**. *Drug Discov Today Technol* 2019, **31**:15–27.

19. Bondeson DP, Mares A, Smith IED, Ko E, Campos S, Miah AH, Mulholland KE, Routly N, Buckley DL, Gustafson JL, *et al.*: **Catalytic in vivo protein knockdown by small-molecule PROTACs**. *Nat Chem Biol* 2015, **11**:611–617.

20. Schneekloth AR, Pucheault M, Tae HS, Crews CM: **Targeted intracellular protein degradation induced by a small molecule: en route to chemical proteomics**. *Bioorg Med Chem Lett* 2008, **18**:5904–5908.

21. Itoh Y, Ishikawa M, Naito M, Hashimoto Y: **Protein knockdown using methyl bestatin-ligand hybrid molecules: design and synthesis of inducers of ubiquitination-mediated degradation of cellular retinoic acid-binding proteins**. *J Am Chem Soc* 2010, **132**:5820–5826.

22. Edmondson SD, Yang B, Fallan C: **Proteolysis targeting chimeras (PROTACs) in "beyond rule-of-five" chemical space: recent progress and future challenges**. *Bioorg Med Chem Lett* 2019, **29**:1555–1564.

23. Müller S, Chaikuad A, Gray NS, Knapp S: **The ins and outs of selective kinase inhibitor development**. *Nat Chem Biol* 2015, **11**:818–821.

24. Filippakopoulos P, Qi J, Picaud S, Shen Y, Smith WB, Fedorov O, Morse EM, Keates T, Hickman TT, Felletar I, *et al.*: **Selective inhibition of BET bromodomains**. *Nature* 2010, **468**:1067–1073.

25. Olson CM, Jiang B, Erb MA, Liang Y, Doctor ZM, Zhang Z, Zhang T, Kwiatkowski N, Boukhali M, Green JL, *et al.*: **Pharmacological perturbation of CDK9 using selective CDK9 inhibition or degradation**. *Nat Chem Biol* 2017, **14**:1–14.

26. * Smith BE, Wang SL, Jaime-Figueroa S, Harbin A, Wang J, Hamman BD, Crews CM: **Differential PROTAC substrate specificity dictated by orientation of recruited E3 ligase**. *Nat Commun* 2019, **10**:1–13.

A structural and biochemical survey of PROTAC mediated target selectivity across isoforms of kinase family.

27. Gadd MS, Testa A, Lucas X, Chan K-H, Chen W, Lamont DJ, Zengerle M, Ciulli A: **Structural basis of PROTAC cooperative recognition for selective protein degradation**. *Nat Chem Biol* 2017, **13**:514–521.

28. Nowak RP, DeAngelo SL, Buckley D, He Z, Donovan KA, An J, Safaee N, Jedrychowski MP, Ponthier CM, Ishoey M, *et al.*: **Plasticity in binding confers selectivity in ligand-induced protein degradation**. *Nat Chem Biol* 2018, **14**:706–714.

29. Brand M, Jiang B, Bauer S, Donovan KA, Liang Y, Wang ES, Nowak RP, Yuan JC, Zhang T, Kwiatkowski N, *et al.*: **Homolog-selective degradation as a strategy to probe the function of CDK6 in AML**. *Cell Chem Biol* 2019, **26**:300–306. e9.

30. Jiang B, Wang ES, Donovan KA, Liang Y, Fischer ES, Zhang T, Gray NS: **Development of dual and selective degraders of cyclin-dependent kinases 4 and 6**. *Angew Chem Int Ed* 2019, **58**:6321–6326.

31. Kollmann K, Heller G, Schneckenleithner C, Warsch W, Scheicher R, Ott RG, Schäfer M, Fajmann S, Schlederer M, Schiefer A-I, *et al.*: **A kinase-independent function of CDK6 links the cell cycle to tumor angiogenesis**. *Cancer Cell* 2013, **24**:167–181.

32. Tigan A-S, Bellutti F, Kollmann K, Tebb G, Sexl V: **CDK6-a review of the past and a glimpse into the future: from cell-cycle control to transcriptional regulation**. *Oncogene* 2016, **35**:3083–3091.

33. Spradlin JN, Hu X, Ward CC, Brittain SM, Jones MD, Ou L, To M, Proudfoot A, Ornelas E, Woldegiorgis M, *et al.*: **Harnessing the anti-cancer natural product nimbolide for targeted protein degradation**. *Nat Chem Biol* 2019, **15**:747–755.

34. Ward CC, Kleinman JI, Brittain SM, Lee PS, Chung CYS, Kim K, Petri Y, Thomas JR, Tallarico JA, McKenna JM, *et al.*: **Covalent ligand screening uncovers a RNF4 E3 ligase recruiter for targeted protein degradation applications**. *ACS Chem Biol* 2019, https://doi.org/10.1021/acschembio.8b01083.

35. ** Zhang X, Crowley VM, Wucherpfennig TG, Dix MM, Cravatt BF: **Electrophilic PROTACs that degrade nuclear proteins by engaging DCAF16**. *Nat Chem Biol* 2019, **15**:737–746.

This study outlines a rational approach towards the identification of novel covalent E3 ligands that are suited as recruitment elements for heterobifunctional degraders

36. Tinworth CP, Lithgow H, Dittus L, Bassi ZI, Hughes SE, Muelbaier M, Dai H, Smith IED, Kerr WJ, Burley GA, *et al.*: **PROTAC-mediated degradation of Bruton's tyrosine kinase is inhibited by covalent binding**. *ACS Chem Biol* 2019, **14**:342–347.

37. Krönke J, Fink EC, Hollenbach PW, MacBeth KJ, Hurst SN, Udeshi ND, Chamberlain PP, Mani DR, Man HW, Gandhi AK, *et al.*: **Lenalidomide induces ubiquitination and degradation of CK1α in del(5q) MDS**. *Nature* 2015, **523**:183–188.

38. Matyskiela ME, Lu G, Ito T, Pagarigan B, Lu C-C, Miller K, Fang W, Wang N-Y, Nguyen D, Houston J, *et al.*: **A novel cereblon modulator recruits GSPT1 to the CRL4(CRBN) ubiquitin ligase**. *Nature* 2016, **535**:252–257.

39. An J, Ponthier CM, Sack R, Seebacher J, Stadler MB, Donovan KA, Fischer ES: **pSILAC mass spectrometry reveals ZFP91 as IMiD-dependent substrate of the CRL4CRBN ubiquitin ligase**. *Nat Commun* 2017, **8**:15398.

40. Matyskiela ME, Couto S, Zheng X, Lu G, Hui J, Stamp K, Drew C, Ren Y, Wang M, Carpenter A, *et al.*: **SALL4 mediates teratogenicity as a thalidomide-dependent cereblon substrate**. *Nat Chem Biol* 2018, **14**:981–987.

41. Donovan KA, An J, Nowak RP, Yuan JC, Fink EC, Berry BC, Ebert BL, Fischer ES: **Thalidomide promotes degradation of SALL4, a transcription factor implicated in Duane Radial Ray syndrome**. *eLife* 2018, **7**:154.

42. ** Sievers QL, Petzold G, Bunker RD, Renneville A, Słabicki M, Liddicoat BJ, Abdulrahman W, Mikkelsen T, Ebert BL, Thomä NH: **Defining the human C2H2 zinc finger degrome targeted by thalidomide analogs through CRBN**. *Science* 2018, **362**, eaat0572.

A comprehensive study investigating the the structural relationship between degradable zinc finger proteins and the IMiD:CRBN complex that also innovated computational methods to predict targets within the reach of IMiD-based CRBN reprogramming.

43. ** Han T, Goralski M, Gaskill N, Capota E, Kim J, Ting TC, Xie Y, Williams NS, Nijhawan D: **Anticancer sulfonamides target splicing by inducing RBM39 degradation via recruitment to DCAF15**. *Science* 2017, **356**, eaal3755.

This study describes the serendipitous finding that the anti-cancer activity of selected aryl sulfonamides is due to redirecting the activity of the E3 ligase DCAF15 to degrade the splicing factor RBM39

44. Uehara T, Minoshima Y, Sagane K, Sugi NH, Mitsuhashi KO, Yamamoto N, Kamiyama H, Takahashi K, Kotake Y, Uesugi M, *et al.*: **Selective degradation of splicing factor CAPERα by anticancer sulfonamides**. *Nat Chem Biol* 2017, **13**:675–680. - PubMed - NCBI.

45. Bussiere DE, Xie L, Srinivas H, Shu W, Burke A, Be C, Zhao J, Godbole A, King D, Karki RG, *et al.*: **The structural basis of Indisulam-mediated recruitment of RBM39 to the DCAF15-DDB1-DDA1 E3 ligase complex**. *bioRxiv* 2019, **44**:737510.

46. Faust TB, Yoon H, Nowak RP, Donovan KA, Li Z, Cai Q, Eleuteri NA, Zhang T, Gray NS, Fischer ES: **Structural complementarity facilitates E7820-mediated degradation of RBM39 by DCAF15**. *Nat Chem Biol* 2019, **355**:1–8.

47. Du X, Volkov OA, Czerwinski RM, Tan H, Huerta C, Morton ER, Rizzi JP, Wehn PM, Xu R, Nijhawan D, *et al.*: **Structural basis and kinetic pathway of RBM39 recruitment to DCAF15 by a sulfonamide molecular glue E7820**. *Structure* 2019, **27**: 1625–1633.e3.

48. Nusse R, Clevers H: **Wnt/β-Catenin signaling, disease, and emerging therapeutic modalities**. *Cell* 2017, **169**:985–999.

49. Rubinfeld B, Robbins P, El-Gamil M, Albert I, Porfiri E, Polakis P: **Stabilization of beta-catenin by genetic defects in melanoma cell lines**. *Science* 1997, **275**:1790–1792.

50. Simonetta KR, Taygerly J, Boyle K, Basham SE, Padovani C, Lou Y, Cummins TJ, Yung SL, Soly von SK, Kayser F, *et al.*: **Prospective discovery of small molecule enhancers of an E3 ligase-substrate interaction**. *Nat Commun* 2019, **10**:1–12.

51. Mayor-Ruiz C, Winter GE: **Identification and characterization of cancer vulnerabilities via targeted protein degradation**. *Drug Discov Today Technol* 2019, **31**:81–90.

52. Zhang L, Riley-Gillis B, Vijay P, Shen Y: **Acquired resistance to BET-PROTACs (Proteolysis-Targeting chimeras) caused by genomic alterations in core components of E3 ligase complexes**. *Mol Cancer Ther* 2019, **18**:1302–1311.

53. Ottis P, Palladino C, Thienger P, Britschgi A, Heichinger C, Berrera M, Julien-Laferriere A, Roudnicky F, Kam-Thong T, Bischoff JR, *et al.*: **Cellular resistance mechanisms to targeted protein degradation converge toward impairment of the engaged ubiquitin transfer pathway**. *ACS Chem Biol* 2019, https://doi.org/10.1021/acschembio.9b00525.

54. Kortüm KM, Mai EK, Hanafiah NH, Shi C-X, Zhu Y-X, Bruins L, Barrio S, Jedlowski P, Merz M, Xu J, *et al.*: **Targeted sequencing of refractory myeloma reveals a high incidence of mutations in CRBN and Ras pathway genes**. *Blood* 2016, **128**:1226–1233.

55. Thakurta A, Gandhi AK, Waldman MF, Bjorklund C, Ning Y, Mendy D, Schafer P, Lopez-Girona A, Lentzsch S, Schey SA, *et al.*: **Absence of mutations in cereblon (CRBN) and DNA damage-binding protein 1 (DDB1) genes and significance for IMiD therapy**. *Leukemia* 2014, **28**:1129–1131.

56. Gandhi AK, Kang J, Havens CG, Conklin T, Ning Y, Wu L, Ito T, Ando H, Waldman MF, Thakurta A, *et al.*: **Immunomodulatory agents lenalidomide and pomalidomide co-stimulate T cells by inducing degradation of T cell repressors Ikaros and Aiolos via modulation of the E3 ubiquitin ligase complex CRL4(CRBN.)**. *Br J Haematol* 2014, **164**:811–821.

57. Hagner PR, Chiu H, Ortiz M, Apollonio B, Wang M, Couto S, Waldman MF, Flynt E, Ramsay AG, Trotter M, *et al.*: **Activity of lenalidomide in mantle cell lymphoma can be explained by NK cell-mediated cytotoxicity**. *Br J Haematol* 2017, **179**: 399–409.

1.4.5 Approaches to Identify Small-Molecule Protein Degraders

The previous sections have outlined the history and current state of the targeted protein degradation field. The vast clinical application potential highlighted a need to rapidly identify additional E3 ligase interacting molecules. This would expand the diversity for PROTAC development, as well as empower novel molecular glue degrader discovery. However especially the latter category of degraders remained elusive and most examples to date have been identified by chance during mode-of-action analysis of cellular cytotoxic molecules. Strategies that allow the intentional discovery of direct E3 ligase modulating molecules have turned into a holy grail in the field of TPD and can be roughly categorized (see Figure 5) by their design: target- and E3-ligase driven or agnostic (Domostegui et al., 2022). In the following, these strategies will be briefly introduced to lay a foundational context for the second part of the results section of this thesis.

Methods for unbiased degrader identification in a target and E3 ligase independent fashion, have so far exclusively been employed to discover cyclin K degraders (Mayor-Ruiz et al., 2020; Słabicki et al., 2020). Correlating E3 ligase expression and drug sensitivity across a large collection of cancer cell lines, could bioinformatically pair previously known MG degraders such as indisulam to their targeted substrate receptor DCAF15. Similarly, CRL adapter protein DDB1 expression could be linked with toxicity of the pan-cyclin dependent kinase (CDK) inhibitor (*R*)-CR8 indicating an E3 ligase dependent MOA (Słabicki et al., 2020). Careful chemical genetic and structural elucidation unveiled a molecular glue type interaction between DDB1, CR8 and CDK12 (or its paralog CDK13). This in turn, recruits the common CDK12 interaction partner cyclin K for subsequent ubiquitination and degradation.

Given the dynamic regulation of CRLs in cells mediated by a select set of central factors discussed in chapter 1.4.3, conceptually a loss-of-function of such a factor could have detrimental effects on degrader efficacy. This notion has been developed and made use of in a parallel study to the above mentioned via an unbiased phenotypic screening approach with engineered cell lines (Mayor-Ruiz et al., 2020). The generation of cancer cell lines deficient for CRL neddylation by mutation of the NEDD8 depositing enzyme UBE2M allowed comparative cytotoxic chemical screening. A difference in drug efficacy between $UBE2M^{WT}$ and $UBE2M^{MUT}$ cells was observed for several tested molecules, among which were previously discussed aryl sulfonamide MG degraders. Surprisingly, a chemically distinct set of molecules emerged as cyclin K degraders (as discussed above) form a plethora of orthogonal chemical genetic characterization. Together these two accounts present approaches to discover cytotoxic degrader compounds in a target and E3 ligase independent manner.

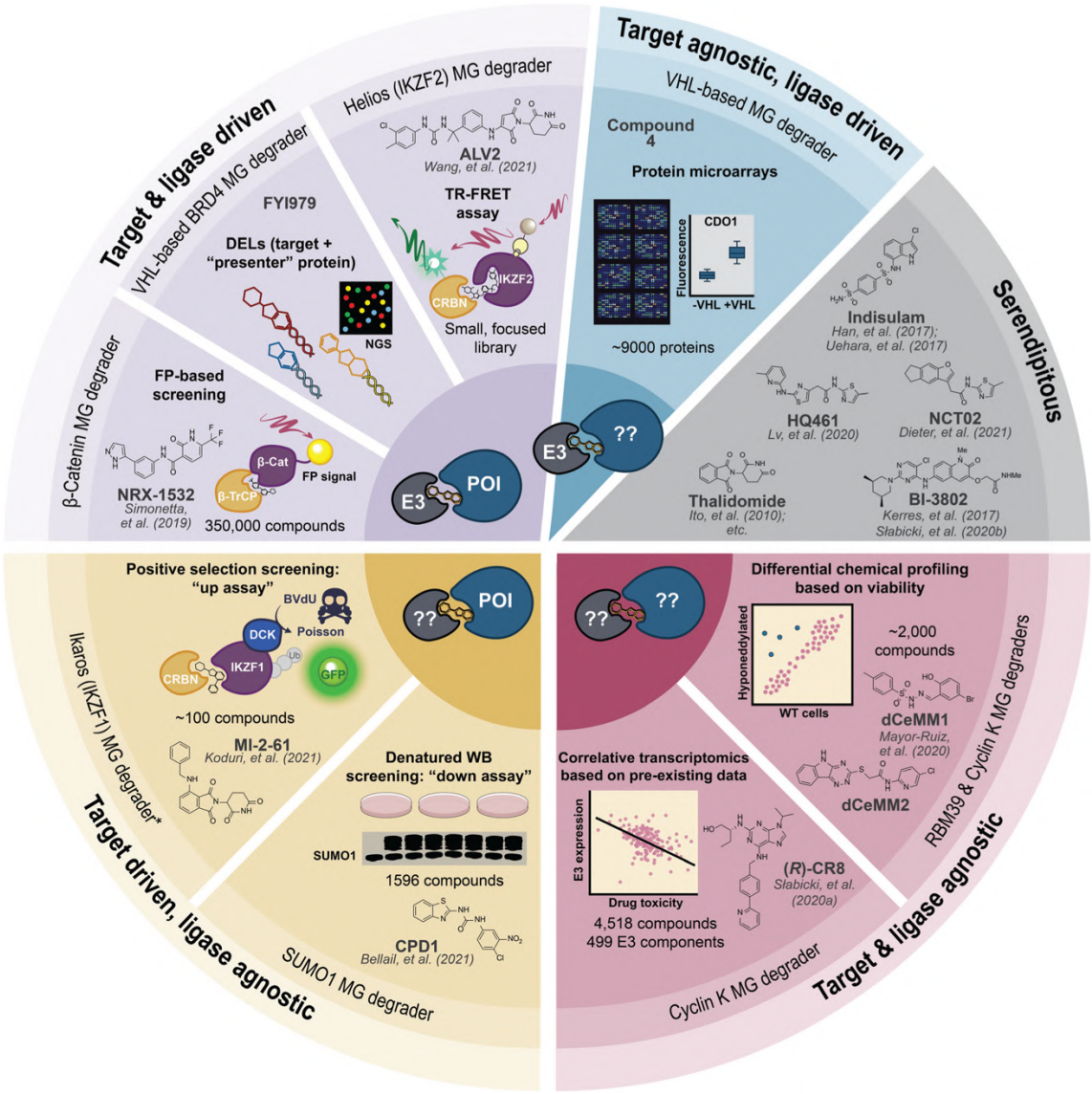

Figure 5. Approaches to rational molecular glue degrader identification.

Reprinted from Chem Soc Rev 51, 5498-5517., Domostegui, A., Nieto-Barrado, L., Perez-Lopez, C., and Mayor-Ruiz, C. (2022). Chasing molecular glue degraders: screening approaches., with permission from the Royal Society of Chemistry.

Following the success of chemically diversifying IMiDs to expand the degradable zinc-finger target space (discussed in chapter 1.4.4.) (Sievers et al., 2018b), similar ambitions were aimed towards targeting VHL. Original VHL binding molecules were however designed in peptide mimicry to disrupt the interaction of VHL and its endogenous substrate HIF1α (Galdeano et al., 2014). Hence, the recently communicated recruitment of CDO1 (involved in cysteine metabolism) to VHL via small molecules strikes even more surprisingly (Domostegui et al., 2022). In this case, recombinant protein microarrays were used, and it presents the only E3 ligase targeted approach to degrader discovery with the exception of the results highlighted in the second part of this thesis.

A few iterations of targeted approaches identifying POI specific degraders have recently emerged. Given the nature of TPD, in most cases these measure the levels of the POI in a scalable manner. An elegant twist to this notion was introduced by fusing deoxycytidine kinase (DCK) to the target protein (in this case IKZF1). DCK converts the exogenously supplemented non-natural nucleoside BVdU to a toxic product and thereby allows for positive selection screening for the degraded target (Koduri et al., 2021). Other approaches for target selective degrader screening have made use of biochemical assays such as fluorescence polarization. Reconstituting natural substrate recognition between oncogenic mutant β-catenin and the CUL1 SR β-TrCP elicits antineoplastic effects by disrupting downstream transcriptional programs (Simonetta et al., 2019).

Taken together, the rational discovery of E3 ligase modulators has been at the center of attention for targeted protein degradation. Nonetheless, to date only few records have emerged from this race, especially when screening in a target independent manner. Most assays by design report exclusively on cytotoxic molecules, thereby limiting the potential target space significantly. While computational modeling promises to reduce the experimental screening space through compound preselection, it has so far been limited to ternary complex optimization for PROTAC design (Weng et al., 2021; Zaidman et al., 2020). Prospective virtual screening, while attaining increasing interest in the field of TPD, has yet to deliver on these promises (Domostegui et al., 2022).

1.5 Aims of this Thesis

Small molecule-mediated targeted protein degradation presents a novel pharmacologic approach to patient therapy. Following the great excitement from biotech and pharma industry, several iterations of this paradigm are currently under clinical investigation and being employed for patient therapy. This thesis aimed to chart key requirements for TPD by investigating cellular resistances that emerge spontaneously and after deliberate mutation of key factors involved. We discovered that acquired resistance mutations to TPD point towards the importance of the E3 ligase substrate receptor for efficient ligand induced degradation. Given this, we set out to map functional E3 ligase hotspots via deep mutational scanning of the ternary complex interface. Linking our profiling to patient tumor sequencing data allowed us to delineate functional consequences of clinically emerging resistance mutations. Given this experience with TPD resistance we next set out to design and validate a phenotypic scalable screening assay that allows identification of small-molecule E3 ligase modulators. We extensively benchmark this approach and identify chemically distinct molecular glue degraders of RBM39 and RBM23.

Overall, we aimed to address the following points:

(i) Are inherent characteristics of E3 ligases such as essentiality affecting the emergence of resistance?

(ii) How is mutation of the protein surface topology affecting ligand-induced ternary complex formation and neo-substrate degradation?

(iii) What is the involvement of functional E3 ligase residues in patient derived resistances to TPD?

(iv) Can we devise methods to scaleably screen for modulators of E3 ligase substrate engagement?

2. Results

2.1 Functional E3 Ligase Hotspots and Resistance Mechanisms to Small-Molecule Degraders

2.1.1 Prologue

Compared to protein inhibitors, where resistances converge on the immediate drug target or its signaling network, degraders depend on cellular cascades to elicit their therapeutic response. Several studies have previously set out to identify genetic dependencies for targeted protein degradation.(Shirasaki et al., 2021; Mayor-Ruiz et al., 2019; Liu et al., 2019) These have highlighted common factors whose loss-of-function affects efficacy of one or several different small-molecule degraders. However, as these results were obtained in engineered LOF settings, they do not recapitulate an accurate picture of therapy resistance.

In the following work we set out to chart the genetic consequences of spontaneous resistance to TPD. We make use of the two most commonly adopted CRL E3 ligase substrate receptors CRBN and VHL to delineate effects of SR inherent characteristics on resistance emergence. We find that essentiality of the SR correlates with frequency and type of resistance mutations. Furthermore, genetic alterations following long-term degrader treatment were enriched in the ternary complex interface initiated between the E3 ligase and the neo-substrate. To further deepen our understanding of this ternary complex topology, we queried all SR residues in the vicinity of the degrader binding site via a deep mutational scanning approach. By comparing different degrader molecules, we identified functional E3 ligase hotspots that mediate neo-substrate specific and even degrader specific resistance. Furthermore, these SR positions overlap with treatment refractory patient tumor mutations allowing us to functionally annotate clinical resistance mechanisms.

The author of this thesis conceptualized this work together with Matthias Brand and the supervisor Georg Winter and performed hybrid capture and mutational scanning assays with the assistance of co-authors. Validation experiments were conducted together with members of the Winter Lab and biochemical characterization was contributed by collaborators. The specific author contributions can further be taken from the respective section in the publication.

2.1.2 Results

Results section 2.1.2 contains a full reprint of the manuscript ‘Functional E3 Ligase Hotspots and Resistance Mechanisms to Small-Molecule Degraders’ by Alexander Hanzl et al. currently accepted at Nature Chemical Biology. The author of this thesis is an author of the article and thus retains the right to include a reprint in full in this thesis. Other rights remain with the publisher Springer Nature Limited and the journal Nature Chemical Biology.

Functional E3 ligase hotspots and resistance mechanisms to small-molecule degraders

Alexander Hanzl[1], Ryan Casement[2*], Hana Imrichova[1*], Scott J. Hughes[2,3], Eleonora Barone[1], Andrea Testa[2,3], Sophie Bauer[1,4], Jane Wright[2], Matthias Brand[1,4], Alessio Ciulli[2,#] and Georg E. Winter[1,#]

Affiliations

[1] CeMM Research Center for Molecular Medicine of the Austrian Academy of Sciences, 1090 Vienna, Austria

[2] Division of Biological Chemistry and Drug Discovery, School of Life Sciences, University of Dundee, James Black Centre, Dundee, UK

[3] present address: Amphista Therapeutics Ltd., Newhouse, UK

[4] present address: Proxygen GmbH, 1030 Vienna, Austria

[*]these authors contributed equally

[#]correspondence to a.ciulli@dundee.ac.uk and gwinter@cemm.oeaw.ac.at

Abstract

Targeted protein degradation is a novel pharmacology established by drugs that recruit target proteins to E3 ubiquitin ligases. Based on the structure of the degrader and the target, different E3 interfaces are critically involved, thus forming defined “functional hotspots”. Understanding disruptive mutations in functional hotspots informs on the architecture of the assembly, and highlights residues susceptible to acquire resistance phenotypes. Here, we employ haploid genetics to show that hotspot mutations cluster in substrate receptors of hijacked ligases, where mutation type and frequency correlate with gene essentiality. Intersection with deep mutational scanning revealed hotspots that are conserved or specific for chemically distinct degraders and targets. Biophysical and structural validation suggests that hotspot mutations frequently converge on altered ternary complex assembly. Moreover, we validated hotspots mutated in patients that relapse from degrader treatment. In sum, we present a fast and widely accessible methodology to characterize small-molecule degraders and associated resistance mechanisms.

Introduction

Proximity-inducing pharmacology is a therapeutic paradigm of current great interest in academia and industry[1]. It is based on small molecules that co-opt the function of one protein by inducing a naturally non-occurring or non-consequential interaction with another protein[2]. One of the most powerful embodiments of proximity-inducing pharmacology is the concept of targeted protein degradation (TPD). In TPD, small-molecule "degraders" induce the molecular proximity between an E3 ubiquitin ligase and a protein of interest (POI), leading to the poly-ubiquitination and proteasomal degradation of the POI[3]. Degraders are typically categorized either as heterobifunctional PROTACs, or as monovalent molecular glues. Many of the E3 ligases that are currently amenable to TPD are members of the large family of cullin RING E3 ubiquitin ligases (CRL)[4–6]. CRLs are modular protein assemblies that are organized around a central cullin backbone. This also includes the two ligases most commonly hijacked by degraders that have reached clinical evaluation or approval, namely $CRL2^{VHL}$ and $CRL4^{CRBN}$ [7]. The specificity of substrate recognition among CRLs is conveyed by more than 250 different substrate receptors (SR), such as the aforementioned cereblon (CRBN) and von Hippel-Lindau disease tumor suppressor (VHL). In physiological settings, SRs recognize substrates for instance based on posttranslational modifications. The underpinning molecular recognition is hence based on complementary and co-evolved protein surfaces. Based on the natural, highly diversified function of SRs, they are ideal entry points for small-molecule modulation.

While naturally occurring substrate recognition is evolutionary optimized, small-molecule degraders often induce the formation of *de novo* protein-protein interactions[2,8,9]. As a result, degraders rely on an optimal exploitation of the structural plasticity of both involved protein surfaces and leveraging PPI energetics from the induced proximity. Successfully designed degraders induce a tripartite binding between SR, degrader, and POI, which is correctly positioned and sufficiently stable to ensure effective poly-ubiquitination and degradation of the POI. While cooperativity of the ternary complex formation is not required, it is often positively correlated with degrader potency[10–12]. Hence, variations in the geometry and PPIs of the states reflecting the drug-induced ternary complex ensemble may give rise to different "functional hotspots" in the hijacked ligase. We define functional hotspots as the repertoire of amino acid residues that affect drug potency upon substitution. Identification of such hotspots would allow prediction of putative mechanisms of degrader resistance. This could consequently further advance our understanding of cellular determinants of degrader efficacy[13–16]. Inspired by advances in the field of overcoming kinase inhibitor resistance[17], we anticipate that a detailed map of functional SR hotspots could inform on strategies to optimize degrader design to overcome or even prevent resistance acquisition.

Currently, identification of functional hotspots is predominantly driven by structural biology. Structural elucidation has been instrumental in shaping our understanding of TPD, and also empowers predictive computational models of ternary complex assembly[18–21]. However, it also faces some crucial limitations. Among others, structures (i) present a static snapshot of an otherwise dynamic system, (ii) might lack resolution especially at dynamic interfaces, (iii) don't consider stoichiometry found in a cellular environment and (iv) often depend on truncated protein constituents lacking posttranslational modifications. Complementary in solution technologies, such as Hydrogen Deuterium Exchange Mass

Spectrometry (HDX-MS) and small-angle X-ray scattering, can provide a more dynamic perspective, even though many of the aforementioned aspects and limitations similarly apply[22,23].

Here we set out to bridge this gap by integrating genomics approaches that enable an *in cellulo*, functional readout to identify E3 ligase hotspots that dictate degrader efficacy. We leverage human haploid genetics to describe how the resistance frequency and mutation types are different for PROTACs hijacking the non-essential SR CRBN and the essential SR VHL. Further focusing on the two SRs, we show that cellular reconstitution of loss of function clones with deep mutational scanning (DMS) libraries enables the scalable identification of functional hotspots. Variant enrichment under degrader selection revealed neo-substrate and ternary-complex specific, as well as chemotype selective functional hotspots for CRBN and VHL. Mechanistically, specific hotspots often converge on defects in ternary complex assemblies, as shown by biophysical assays using fully recombinant proteins. Integrating the resulting functional landscapes with crystallographic structural data shows that some of the validated hotspots can be rationalized based on the observed ternary complex structure, implying high complementarity of both approaches. In other cases, existing structures fail to resolve the often profound, functional differences. This indicates that DMS provides a resolution that is partially outside the reach of structural characterization. Finally, integration of DMS data with available clinical data suggests that functional CRBN hotspots are mutated in multiple myeloma patients relapsing from treatment with lenalidomide and pomalidomide, two CRBN-based molecular glue degraders.

In sum, we present a fast, scalable, and experimentally widely accessible methodology that supports the dissection of functional determinants of drug-induced neo-substrate recognition and degradation. This empowers the characterization and optimization of small-molecule degraders and informs on resistance mechanism of putative clinical relevance.

Results

Resistance Mechanisms differ between CRBN- and VHL PROTACs

Conceptually, complete loss-of-function of an essential gene poses a disadvantageous mechanism to evade selective pressure elicited by a drug. Here, we focused our efforts on the two most-commonly adopted SRs CRBN and VHL, both of which are hijacked by degraders in clinical use or entering clinical trials[7]. Mining publicly available data from the DepMap Consortium, *CRBN* presents as a non-essential gene across 1070 cell lines that were profiled via genome-scale CRISPR/Cas9 knockout screens (**Fig. 1A**)[24]. Despite its well-established role as a tumor suppressor in renal carcinoma[25], *VHL* proved essential in 935 of the profiled cell lines. To determine if this difference in essentiality is reflected in differential resistance acquisition, we focused on two BET Bromodomain targeting PROTACs: dBET6 (*CRBN*-based) and ARV-771 (*VHL*-based) that have matched cellular potency, including in the near-haploid human leukemia cell line KBM7 (**Extended Data Fig. 1A**)[26,27]. First, we validated the essentiality of *VHL* in KBM7 cells by CRISPR/Cas9-mediated disruption of *VHL* in competitive growth assays (**Extended Data Fig. 1B**). Previous studies have shown that *CRBN* loss is inconsequential for KBM7 proliferation[15]. KBM7 cells, which are a frequently used tool to study mechanisms of drug resistance are thus a valid model to capture the overall essentiality profile of both ligases.[28–30]. We next

determined the resistance frequency in KBM7 cells via outgrowth experiments after single dose treatments with either dBET6 or ARV-771. Despite their matched cellular efficacy, occurrence of resistant clones was ten-fold increased after exposure to dBET6 compared to ARV-771 (**Fig. 1B**). To identify mutations underpinning these quantitative differences, we isolated pools of drug-resistant clones and subjected them to a hybrid capture based targeted sequencing approach (**Extended Data Fig. 1C**). This strategy covers all members of the respective CRL ligase complexes, CRL regulatory proteins as well as the recruited POIs (**Supplementary Table 1**). In dBET6 resistant cells, we identified the majority of disruptive alterations directly in *CRBN*, while other members of the $CRL4^{CRBN}$ ligase complex were not affected (**Fig. 1C, Supplementary Table 2**). In contrast, cells resistant to ARV-771 featured a lower proportion of genetic defects directly in *VHL* and an equal number of alterations in various other components of the $CRL2^{VHL}$ complex, such as *CUL2* and *ELOB*. We found a higher fraction (55 %) of frameshifts and gained stop-codons in *CRBN*. In contrast, the majority (60%) of alterations in *VHL* were missense point mutations (**Fig. 1D** and **E, Supplementary Table 2**). Together, these data implicate the SR as the most frequently mutated CRL component in degrader-resistant clones. However, both the frequency and the type of alterations appear to be influenced by the essentiality of the co-opted SR. In case of hijacking VHL, the fitness costs associated with directly mutating the essential SR favors mutations acquired in other complex members, such as *CUL2*. Supporting these results, loss of *CUL2* has previously been reported as an acquired resistance mechanism to VHL-based PROTACs in OVCAR8 cells[16].

Figure 1

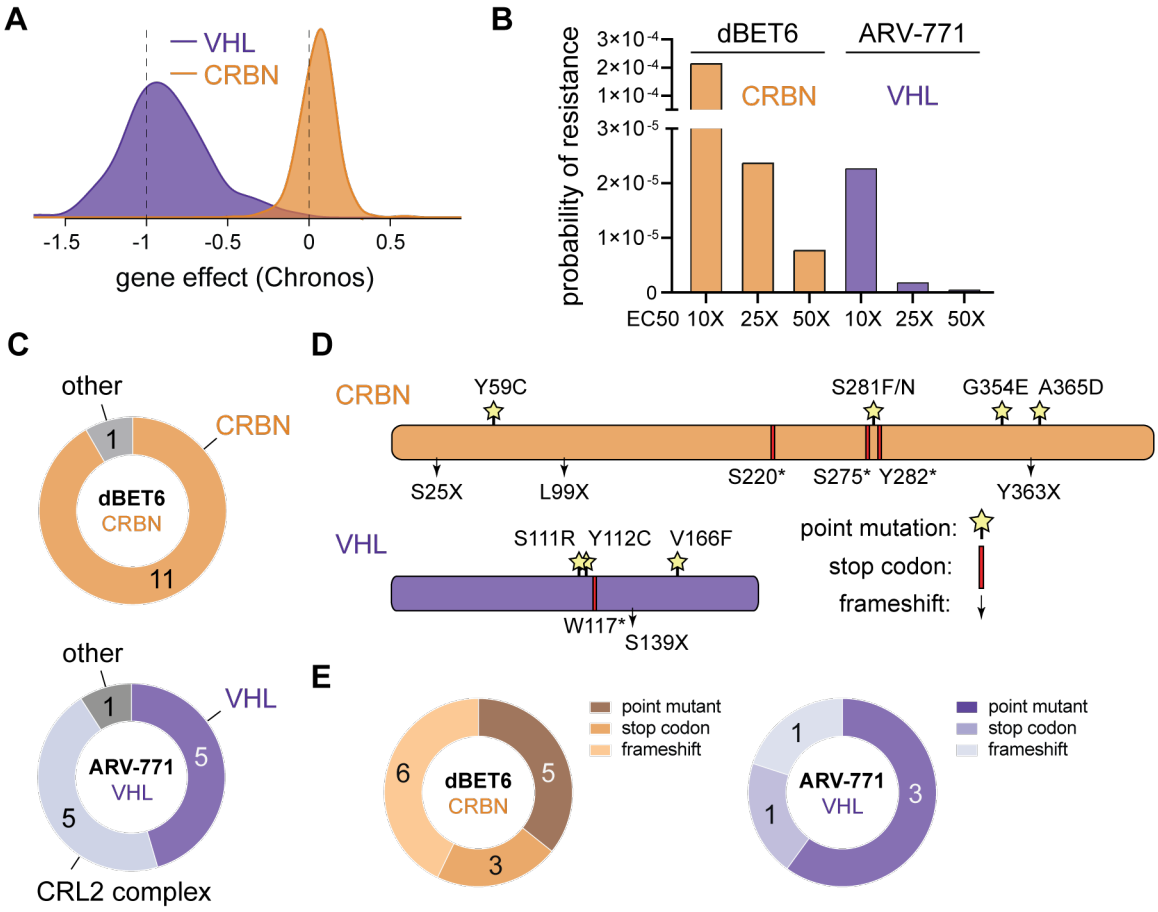

Figure 1. Quantitative and Qualitative Differences in Degrader Resistance
(A) Distribution of CRBN and VHL deletion effect (Chronos) across 1070 cancer cell lines. Data taken from Broad Institute DepMap Consortium (22Q1, public).
(B) Probability of resistance in KBM7 cells treated at 10, 25 and 50 times EC_{50} with CRBN (dBET6) and VHL (ARV-771) based BET-bromodomain targeting PROTACs.
(C) Number of spontaneous degrader resistance mutations in the substrate receptor (CRBN, VHL), the corresponding Cullin-RING-Ligase (CRL) complex and other degradation associated genes identified in KBM7 cells treated with dBET6 and ARV-771 (10, 25 and 50 times EC_{50}) for 8 to 14 days via targeted hybrid-capture and next-generation sequencing (see also **Extended Data Fig. 1**).
(D) Depiction of CRBN and VHL mutations identified by hybrid-capture sequencing in drug-resistant cell pools. Stars indicate point mutations. Red bars indicate premature stop codons. Arrows indicate frameshift mutations.
(E) Number of spontaneous degrader resistance alterations in the substrate receptor (CRBN, VHL) binned according to mutation type (point mutations, gained stop codons, frameshifts).
See also **Extended Data Fig. 1** and **Supplementary Tables 1** and **2**.

DMS Identifies Functional Hotspots of General Relevance

Many point mutations were identified proximal to the degrader binding pocket and the predicted neo-substrate interface, highlighting the importance of the SR in orchestrating ternary complex formation (**Extended Data Fig. 1D** and **E**). To systematically investigate the surface topology of both SRs at an amino acid resolution, we designed DMS libraries for all VHL and CRBN positions in proximity of the degrader binding site (< 10 Å, **Fig. 2A**) covering 1442 and 1738 different variants, respectively. Noteworthy, DMS strategies have previously been successfully employed to investigate functional relationships between small molecules and target proteins[31,32]. Here, we surmised that when coupled with a selectable readout, variant libraries could inform on functional hotspots in the respective SR. Considering the specific molecular architecture of the drug-induced ternary complex, such hotspots could either be conserved over different degraders, or specific for a particular compound.

To initially ensure quality control, we sequenced the prepared libraries and mostly identified expected missense variants (**Extended Data Fig. 2A).** Furthermore, an even distribution of possible substitutions was present for almost all residues (**Extended Data Fig. 2B**, see also Methods section). Next, to establish proof of concept, we reconstituted *VHL*-deficient RKO colon carcinoma cells ($VHL^{-/-}$), with the corresponding variant library. Selective pressure was applied through treatment with five different VHL-based PROTACs for seven days. The assayed PROTACs either target BRD4 and related BET bromodomain family proteins (MZ1[33], ARV-771[26] and macroPROTAC-1[34]), or the BAF complex subunits SMARCA2/4 for degradation (ACBI1[35]). To sample greater diversity of PROTAC exit vectors and linkers, we additionally designed AT7 (**1**) as an analogue of the previously disclosed AT1[10]. While AT7, similar to AT1, branches out of the VHL ligand *tert*-butyl group via a thioether linker, it bears a fluoro-cyclopropyl capping group instead of the methyl group of AT1 (**Extended Data Fig. 2C**). This capping group is known to enhance the binding affinity to VHL as well as aid new PPIs within PROTAC ternary complexes[35,36]. In cellular assays, AT7 exhibited potent cytotoxicity and BRD4 degradation (**Extended Data Fig. 2D** to **G**). All degraders blocked the proliferation of RKO cells in a *VHL* dependent manner, enabling sufficient selective pressure (**Extended Data Fig. 2E** and **H**). After the selection, VHL variants that conferred a proliferative advantage were identified via next generation sequencing by their enrichment over an unselected (vehicle-treated) population. We initially validated the robustness of this experimental setup between biological replicates (R = 0.92, **Extended Data Fig. 3A**). Averaging $\log_2$

fold-enrichment for each mutation across all 5 degraders generated a map of consensus VHL hotspots (**Fig. 2B**). As expected, residues of shared relevance primarily localized to the binding pocket of the closely related VHL ligands of the various assayed PROTACs (**Fig. 2C**). Hotspots were highly robust and conserved over a wide concentration range (**Extended Data Fig. 3B**).

We next aimed to expand our analyses to CRBN, assaying two BET PROTACs (dBET6, dBET57), and two molecular glue degraders (CC-885, CC-90009) degrading GSPT1 (**Fig. 2D** and **Extended Data Fig. 3C**)[37,38]. As observed for VHL, functional CRBN hotspots that were enriched across all tested degraders localized to the glutarimide (ligand-) binding pocket. (**Extended Data Fig. 3D**). In sum, the presented deep mutational scanning approach empowered the robust and reproducible identification of functional hotspots of general relevance over different degrader modalities, ligases and neo-substrates.

Figure 2

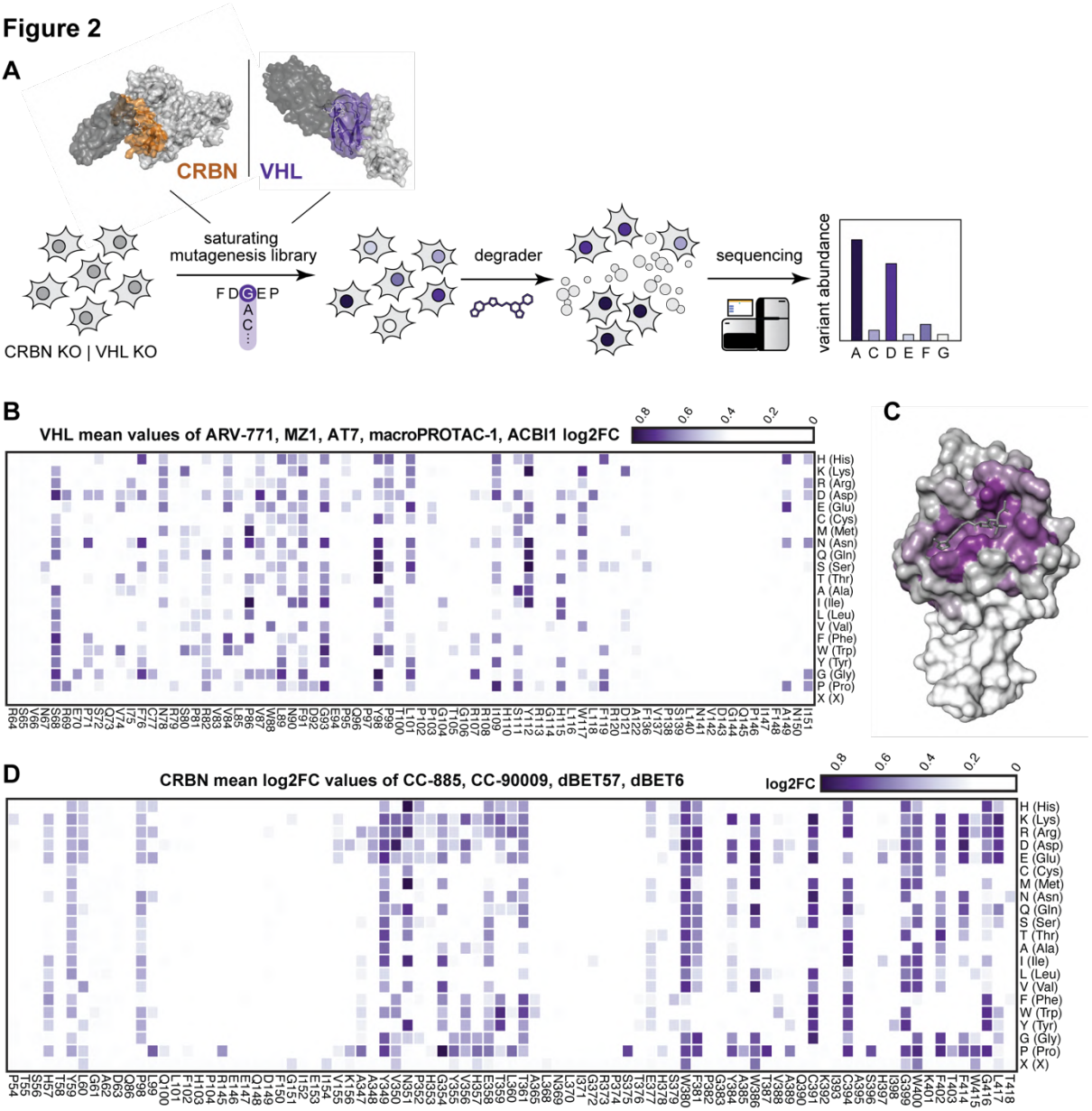

Figure 2. Deep Mutational Scanning Locates Functional Hotspots of General Relevance in the Degrader Binding Pocket
(A) Deep-mutational-scanning approach to identify resistance conferring CRBN and VHL mutants in 10 Å proximity (colored ochre and purple) of the ligand binding site via next-generation sequencing.
(B) Heatmap depicting mean log2 fold-enrichment of VHL mutations normalized to maximum log2 fold-changes vs. DMSO across 5 degraders (500 nM ARV-771, 500 nM MZ1, 500 nM AT7, 2 μM macroPROTAC-1, 2 μM ACBI1) treated for 7 days. n = 2 independent measurements.
(C) Surface structure of VHL bound by VHL Ligand VH032, PDB 4W9H[50]. Median log2 fold-enrichment of all VHL mutations over DMSO across 5 degrader treatments (see **Fig. 2B**) is mapped in purple to dark grey onto positions mutated in the library.
(D) Heatmap depicting mean log2 fold-enrichment of CRBN mutations normalized to maximum log2 fold-changes vs. DMSO across 4 degraders (500 nM dBET6, 500 nM dBET57, 500 nM CC-90009, 500 nM CC-885) treated for 7 days. n = 3 independent measurements.
See also **Extended Data Fig. 2** and **3**.

Characterizing Neo-Substrate Specific Functional VHL Hotspots

To focus the resolution towards unique, potentially substrate-specific, hotspots, we compared enrichments for the SMARCA2/4 PROTAC ACBI1[35] to the average enrichment of all assayed BET degraders (**Fig. 3A**). This allowed identification of the functional hotspots VHL^{N67}, VHL^{R69} and VHL^{H110}, which appear to be specifically required to sustain the activity of ACBI1, while they seem inconsequential for the tested BET PROTACs. In support of this, published co-crystal structures and TR-FRET data previously validated the importance of VHL^{R69} in $SMARCA2^{BD}$ recognition within the ternary complex[35]. To further confirm the specificity of these hotspots, we generated single point mutant reconstitutions in $VHL^{-/-}$ RKOs and assessed cellular fitness following drug treatments (**Fig. 3B** and **Extended Data Fig. 4A** to **D**). Indeed, mutating VHL^{N67} rescued the efficacy of ACBI1 without modulating the efficacy of BET PROTACs. These differences functionally converge on an altered neo-substrate degradation. In cells expressing a VHL^{N67} mutant, ACBI1 failed to induce SMARCA2/4 degradation at conditions where profound degradation is observed in isogenic VHL^{WT} cells. In contrast, BRD3/4 destabilization by the assayed BET degraders was unaffected by VHL^{N67} mutation (**Fig. 3C** and **Extended Data Fig. 4E**). Given the positioning of VHL^{N67} at the VHL:SMARCA2/4 binding interface yet not in direct contact with the PROTAC itself (**Fig. 3E**), we surmised that the lack of SMARCA2/4 degradation with the VHL^{N67} mutant might mechanistically be caused by defects in integrity and stability of the ternary complex. To address this, we established fluorescence polarization experiments assessing the extent to which ternary complex formation and cooperativity of the induced tripartite binding is affected by the VHL mutation. Specifically, PROTAC binding to purified *wildtype*, or mutated VHL-ElonginC-ElonginB (VCB) was measured in absence and presence of recombinant $SMARCA4^{BD}$ or $BRD4^{BD2}$. This led us to identify that mutations in VHL^{N67} (here VHL^{N67Q}) decrease the ternary complex affinity and cooperativity of ACBI1 binding to $SMARCA4^{BD}$ by ~7-fold (**Fig. 3D**). In contrast, the affinity and cooperativity of the VHL:MZ1 binary complex to $BRD4^{BD2}$ was largely unaffected by mutations in VHL^{N67} (within 2-fold those of wild-type, **Fig. 3D**). In the ternary crystal structure of a close ACBI1 analogue in complex with VCB and $SMARCA4^{BD}$ (PDB: 6HR2), the side chain of VHL^{N67} sits against the protein-protein interface sandwiched between VHL^{R69} and VHL^{F91} (**Fig. 3E**). While the asparagine side chain does not interact directly with SMARCA4, neighboring residues contribute PPIs. Therefore, any unfavorable VHL^{N67} changes can negatively impact ternary complex formation. In

contrast, in the ternary crystal structures of BET degraders such as MZ1[10] (PDB: 5T35), VHL^{N67} is distal from the induced PPI and does not impact ternary complex formation, explaining why VHL^{N67} was not a hotspot for the assayed BET degraders (**Extended Data Fig. 4F**).

Of note, the dose range and experimental setup of our DMS strategy was geared to reveal resistance-causing mutations. Accordingly, DMS also identified VHL^{H110L} as a mutation that causes resistance to ACBI1, which we could validate via single point mutant reconstitutions (**Fig. 3A** and **B**). Intriguingly, this mutation simultaneously sensitized cells to treatment with certain BET PROTACs, such as MZ1 (5-fold) or ARV-771 (6-fold, **Fig. 3B** and **Extended Data Fig. 4G** and **H**). This highlights VHL^{H110L} as potentially "versatile" in nature, meaning that its effect can be either sensitizing, neutral or resistance-causing, based on the assayed drug. Intriguingly, this sensitization effect was not uniform for all tested BET PROTACs. ARV-771, MZ1 and the macrocyclic BET degrader macroPROTAC-1[34] showed higher levels of augmentation, while sensitization for AT7 appeared attenuated (**Extended Data Fig. 4H**). This was further supported by BRD4 degradation upon PROTAC treatment in VHL^{H110L} expressing cells (**Fig. 3F** and **Extended Data Fig. 4I**). In an effort to understand these nuanced functional effects, we solved the cocrystal structure of the ternary complex between $BRD4^{BD2}$: AT7:VCB to a resolution of 3.0 Å (**Fig. 3G**). Remarkably, despite the unique linker geometry and increased lipophilicity, the ternary structure of AT7 proved largely conserved in relation to the cocrystal ternary structures of both MZ1[10] and macroPROTAC-1[34]. While there are no discernable changes in key PPIs, the entire bromodomain shifts laterally (r.m.s.d. of 2.1 Å) to accommodate the new PROTAC molecular architecture (**Extended Data Fig. 4J**). As in the structure of MZ1 and macroPROTAC-1, VHL^{H110} sits underneath the bromodomain in a hydrophobic patch formed by $BRD4^{W374}$, $BRD4^{L385}$ and the di-methyl thiophene of the JQ1 warhead (**Extended Data Fig. 4F** and **K**). It is therefore structurally plausible that a mutation of VHL^{H110} to a hydrophobic residue such as leucine at this position could have a beneficial impact on ternary binding affinity by enhancing favorable hydrophobic interactions. In contrast to the role VHL^{H110} plays in the BET ternary structures, the SMARCA4 ternary structure reveals an alternative side-chain conformation. Here VHL^{H110} points back towards the VHL ligand and forms a bridging hydrogen bond to a highly coordinated water trapped at the core of the ternary structure (**Fig. 3E**). Mutation of this histidine to a lipophilic residue, such as leucine, would drastically change this water environment. Additionally, the substitution of the planar side chain of histidine for the bulky branched side chain in leucine is likely to cause a steric clash at closely located PPIs.

Finally, our DMS analysis highlighted the functional hotspot VHL^{Y112}, which was also found mutated in our assessment of spontaneous resistance mechanisms (**Fig. 1D** and **3A**). Intriguingly, the mutant VHL^{Y112C} elicited selective resistance to BET degraders while having nearly no effect on ACBI1 potency (**Extended Data Fig. 4L**). Together, this showcases how our comparative analysis of systematic amino acid mutation can elucidate functional hotspots that modulate drug-induced degradation in a neo-substrate selective manner. Many of the functional consequences of individual mutations can be rationalized from a structural perspective. However, as exemplified via VHL^{H110L}, DMS data can provide a layer of functional resolution that is not immediately obvious from structure-centric approaches.

Figure 3

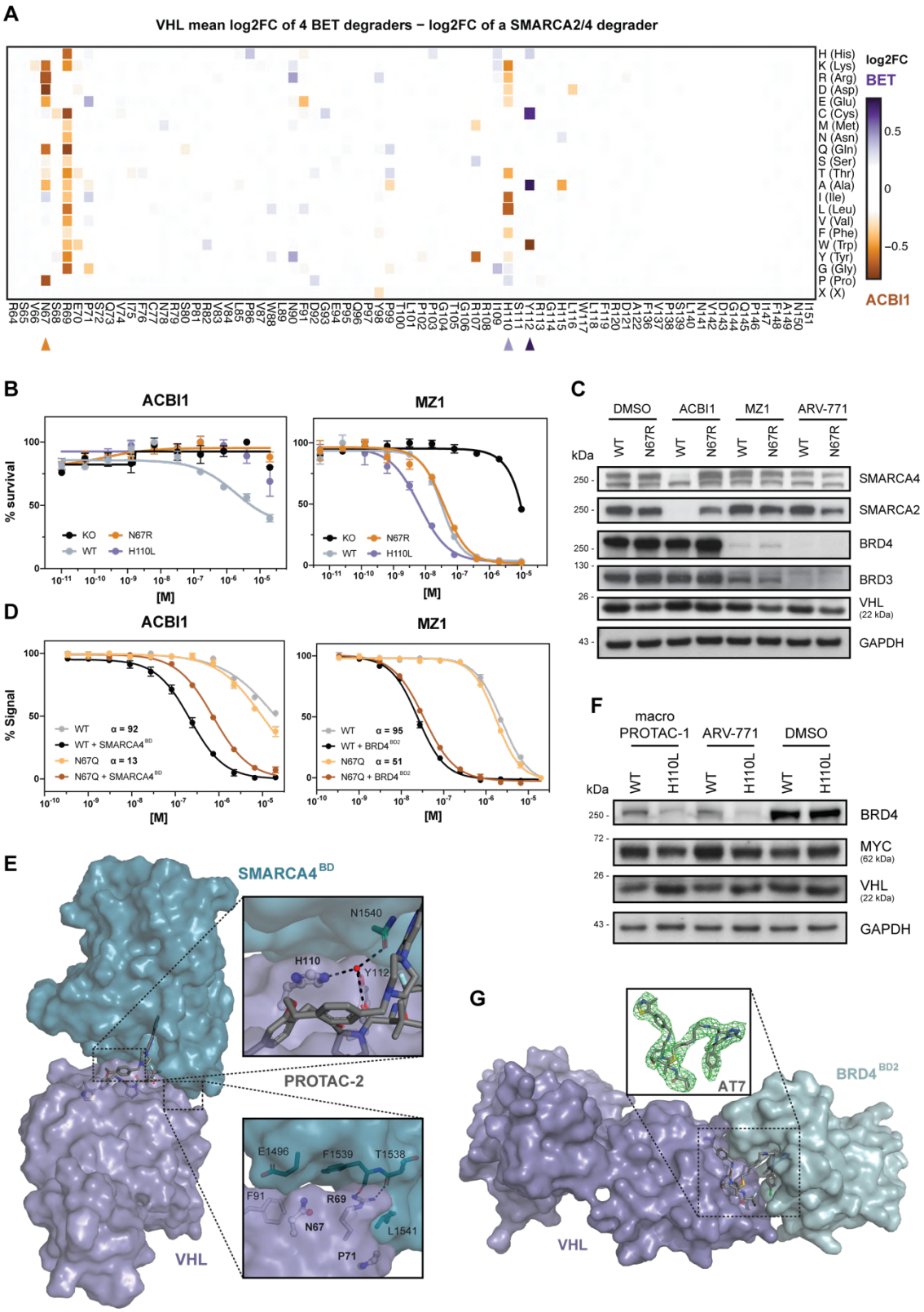
A
VHL mean log2FC of 4 BET degraders − log2FC of a SMARCA2/4 degrader
log2FC
BET
ACBI1
B
ACBI1
MZ1
% survival
KO
WT
N67R
H110L
[M]
C
DMSO
ACBI1
MZ1
ARV-771
WT
N67R
kDa
SMARCA4
SMARCA2
BRD4
BRD3
VHL
(22 kDa)
GAPDH
D
% Signal
WT α = 92
WT + SMARCA4 BD
N67Q α = 13
N67Q + SMARCA4 BD
WT α = 95
WT + BRD4 BD2
N67Q α = 51
N67Q + BRD4 BD2
E
SMARCA4 BD
N1540
H110
Y112
PROTAC-2
E1496
F1539
T1538
F91
R69
N67
L1541
P71
VHL
F
macro
PROTAC-1
ARV-771
DMSO
H110L
BRD4
MYC
(62 kDa)
VHL
(22 kDa)
GAPDH
G
AT7
BRD4 BD2
VHL

Figure 3. Functional VHL Hotspots Identified by DMS Show Neo-Substrate Dependent Resistance and Sensitivity to PROTAC Treatment

(A) Heatmap depicting differential log2 fold-enrichment of VHL mutations normalized to maximum log2 fold-changes vs. DMSO between the mean of 4 BET PROTACs (500 nM ARV-771, 500 nM MZ1, 500 nM AT7, 2 μM macroPROTAC-1) and the SMARCA2/4 PROTAC ACBI1 (2 μM). Treated for 7 days; n = 2 independent measurements.

(B) Dose-resolved, normalized viability after 4 d treatment (ACBI1, left) and 3 d treatment (MZ1, right) in RKO $VHL^{-/-}$ cells with over-expression of VHL^{WT}, VHL^{N67R} or VHL^{H110L}. Mean ± s.e.m.; n = 3 independent treatments.

(C) Protein levels in RKO $VHL^{-/-}$ cells with over-expression of VHL^{WT} or VHL^{N67R} treated with DMSO, ACBI1 (2.5 μM, 4h), MZ1 (75 nM, 2h) and ARV-771 (50 nM, 2h). Representative images of n = 2 independent measurements.

(D) Fitted curves from fluorescence polarization competition assays measuring displacement of a VHL peptide from either WT or mutant VCB protein by ACBI1 (left) or MZ1 (right) in the presence or absence of saturating concentrations of $SMARCA4^{BD}$ or $BRD4^{BD2}$ protein. Mean ± s.d.; n = 3 technical replicates.

(E) Cocrystal structure of PROTAC-2 (close analogue to ACBI1) in a ternary complex with VHL-ElonginC-ElonginB and $SMARCA4^{BD}$ (PDB 6HAX).

(F) Protein levels in RKO $VHL^{-/-}$ cells with over-expression of VHL^{WT} or VHL^{H110L} treated with DMSO, macroPROTAC-1 (250 nM, 2h), ARV-771 (12.5 nM, 90 min). Representative images of n = 2 independent measurements.

(G) Cocrystal structure of AT7 in a ternary complex with VHL-ElonginC-ElonginB and $BRD4^{BD2}$ solved to a resolution of 3.0 Å. The omit difference electron density map (Fo−Fc) is shown in green in the inset panel, superimposed around AT7 and contoured at 3σ.

See also **Extended Data Fig. 4**.

VHL Resistance Hotspots Are Specific to Distinct Degraders

We next set out to identify differential hotspots among degraders with an overlapping neo-substrate spectrum, as exemplified by the tested BET PROTACs. Comparative analysis of DMS enrichments revealed that VHL^{P71} is selectively critical for the efficacy of MZ1 and macroPROTAC-1(**Fig. 4A** and **Extended Data Fig. 5A**). These findings were subsequently validated in individual reconstitution experiments (**Fig. 4B, C** and **Extended Data Fig. 5B**). Previous structural elucidation of the MZ1-induced ternary complex has revealed a role of VHL^{P71} by extending the $BRD4^{WPF}$ shelf through additional CH-pi interactions with $BRD4^{W374}$ (**Fig. 4D**)[10]. This interfacial positioning of P71 prompted us to again investigate whether the underlying molecular mechanism is connected to altered assembly affinity of the ternary complex. Fluorescence polarization assays indicated that the binding cooperativity between MZ1, $BRD4^{BD2}$ and VCB is significantly (6-7 fold) affected upon introducing the VHL^{P71I} mutation (**Fig. 4E**). A similar effect was also observed for macroPROTAC-1. In contrast, the cooperativity of ARV-771-induced ternary complex formation is not affected (**Fig. 4E**), suggesting that the ARV-771-induced ternary complex features a unique architecture that is likely distinct from the architecture observed for MZ1.

In sum, we show that DMS empowers a functional segregation of different drug-induced, ternary complexes that involve identical neo-substrates. This is best exemplified by complexes induced by the BET protein degrader ARV-771, which has, intriguingly, at least in our hands so far proven intractable to structural exploration via crystallography.

Figure 4

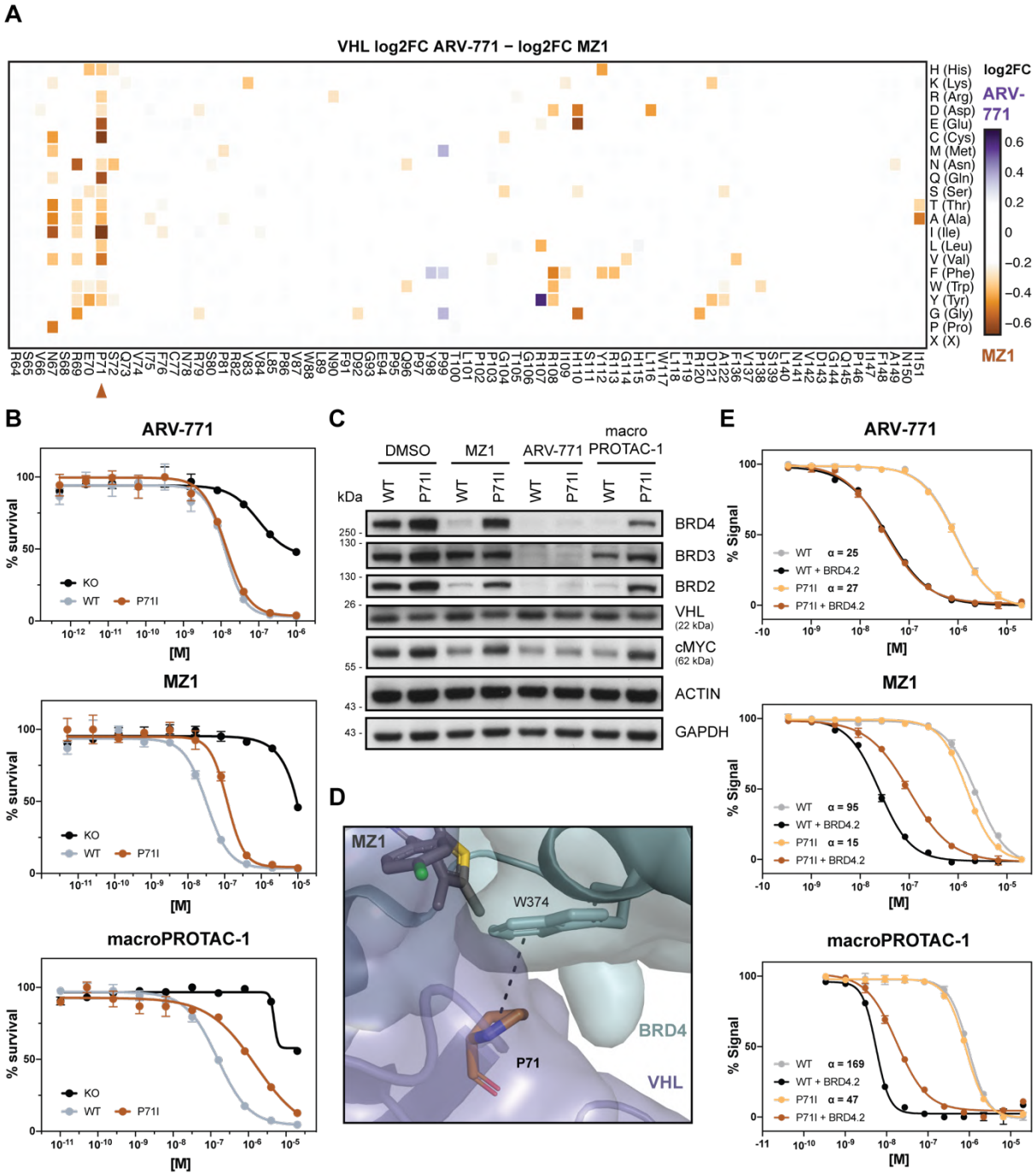

Figure 4. VHL^{P71} is a Functional Hotspot for Degrader Specific Resistance

(A) Heatmap depicting differential log2 fold-enrichment of VHL mutations normalized to maximum log2 fold-changes vs. DMSO between BET bromodomain targeting PROTACs ARV-771 (500 nM, 7d) and MZ1 (500 nM, 7d). n = 2 independent measurements.

(B) Dose-resolved, normalized viability after 3d treatment with ARV-771 (top), MZ1 (center) and macroPROTAC-1 (bottom) in RKO VHL$^{-/-}$ cells with over-expression of VHL^{WT} or VHL^{P71I}. Mean ± s.e.m.; n = 3 independent treatments.

(C) Protein levels in RKO VHL$^{-/-}$ cells with over-expression of VHL^{WT} or VHL^{P71I} treated with DMSO, MZ1 (37.5 nM, 90 min), ARV-771 (25 nM, 90 min) or macroPROTAC-1 (480 nM, 90 min). Representative images of n = 2 independent measurements.

(D) Cocrystal structure of MZ1 in a ternary complex with VHL-ElonginC-ElonginB and BRD4^{BD2} (PDB 5T35) depicting an interaction between VHL^{P71} and the BRD4^{WPF} shelf.

(E) Fitted curves from fluorescence polarization competition assays measuring displacement of a VHL peptide from either WT or mutant VCB protein by PROTACs in the presence or absence of saturating concentrations of partner protein. Mean ± s.d.; n = 3 technical replicates

Functional CRBN Hotspots Are Mutated in Relapsing Patients

Next, we turned our focus to CRBN, the only E3 ligase that to date is clinically validated via the FDA-approved molecular glue degrader lenalidomide and related analogs (collectively often referred to as immunomodulatory drugs, IMiDs). This gives us the chance to identify functional hotspots that differentiate between the two paradigmatic small-molecule degrader modalities: heterobifunctional PROTACs and monovalent molecular glues. Moreover, we hypothesized that DMS might elucidate functional hotspots involved in resistance mechanisms that are of clinical relevance.

First, we aimed to identify functional CRBN hotspots that show selectivity for molecular glue degraders or PROTACs. We utilized our DMS approach to systematically elucidate functional consequences of CRBN mutations on the efficacy of CC-90009, a clinical-stage molecular glue degrader targeting GSPT1[38]. Comparing CRBN variant enrichment after selection with CC-90009 or the BET PROTAC dBET6[27] yielded functional CRBN hotspots relevant to either of both classes of degrader modality (**Fig. 5A**). Among the enriched, glue-selective hotspots, we identified V388 as a key determinant of cellular efficacy of CC-90009. Intriguingly, this site corresponds to position 391 in mouse *Crbn*, which features the critical isoleucine variant that is responsible for the lack of IMiD activity in mouse cells, hence masking the teratogenicity of thalidomide[39]. Of note, DMS analysis resolves the importance of isoleucine, but also indicates that most other substitutions at this position are disruptive. Next, we aimed to expand our survey of functional CRBN hotspots, validating two CC-90009 selective mutants ($CRBN^{E377K}$ and $CRBN^{N351D}$, **Fig. 5B** and **Extended Data Fig. 6A**). Interestingly, mutations in $CRBN^{N351}$ showed a highly specific, versatile behavior for different degraders. While cellular expression of $CRBN^{N351D}$ prompted resistance to CC-90009, it was inconsequential for dBET6 (**Fig. 5A** and **B**). Simultaneously, it led to a marked sensitization (15-fold shift in EC_{50}) to the CDK9-targeting PROTAC THAL-SNS-032[40] (**Extended Data Fig. 6B** and **C**). This differential potency correlated with target degradation levels, highlighting the intricate functional differences that can be uncovered by our DMS analysis (**Fig. 5C Extended Data Fig. 6D** for $CRBN^{E377K}$). Upon inspection of the ternary structure of CC-90009 (PDB: 6XK9), $CRBN^{N351}$ is found proximal to the protein-protein interface and is in a position to directly interact with the backbone carbonyls of GSPT1 (**Fig. 5D**). In contrast the structure of dBET6 (PDB:6BOY) reveals that $CRBN^{351}$ is far from the PPI and is thus unlikely to have an effect on ternary complex formation.

We next focused on the $CRBN^{H397}$ position. Interestingly, our DMS data suggested that mutation to only the negatively charged amino acids aspartate or glutamate abrogated the cellular and degradation efficacy of the BET PROTAC dBET57 (**Extended Data Fig. 6E**). We validated that this mutational effect is not observed for the closely related dBET6 (**Fig. 5B, E** and **F** and **Extended Data Fig. 6F**). Intriguingly, mutations in this position also prompted resistance to molecular glue degraders (**Fig. 5A** and **B** and **Extended Data Fig. 6G**). Furthermore, a mutation in $CRBN^{H397}$ was also identified in a multiple myeloma (MM) patient who presented refractory to IMiD treatment [41]. Upon closer inspection, several mutations in relapsed patients, such as $CRBN^{P352S}$, $CRBN^{F381S}$ and $CRBN^{H57D}$ overlapped with CRBN hotspots identified by DMS (**Fig. 2D, 5G** and **H** and **Extended Data Fig. 6G** and **H**)[42].

Taken together, we report CRBN hotspots that modulate degrader efficacy selectively as well as universally, and which, upon mutation, can either cause resistance or sensitization. Some but not all of these effects could be rationalized via structural investigation. Importantly, DMS also highlighted functional hotspots that are disrupted by mutations in patients relapsing from IMiD treatment.

Figure 5

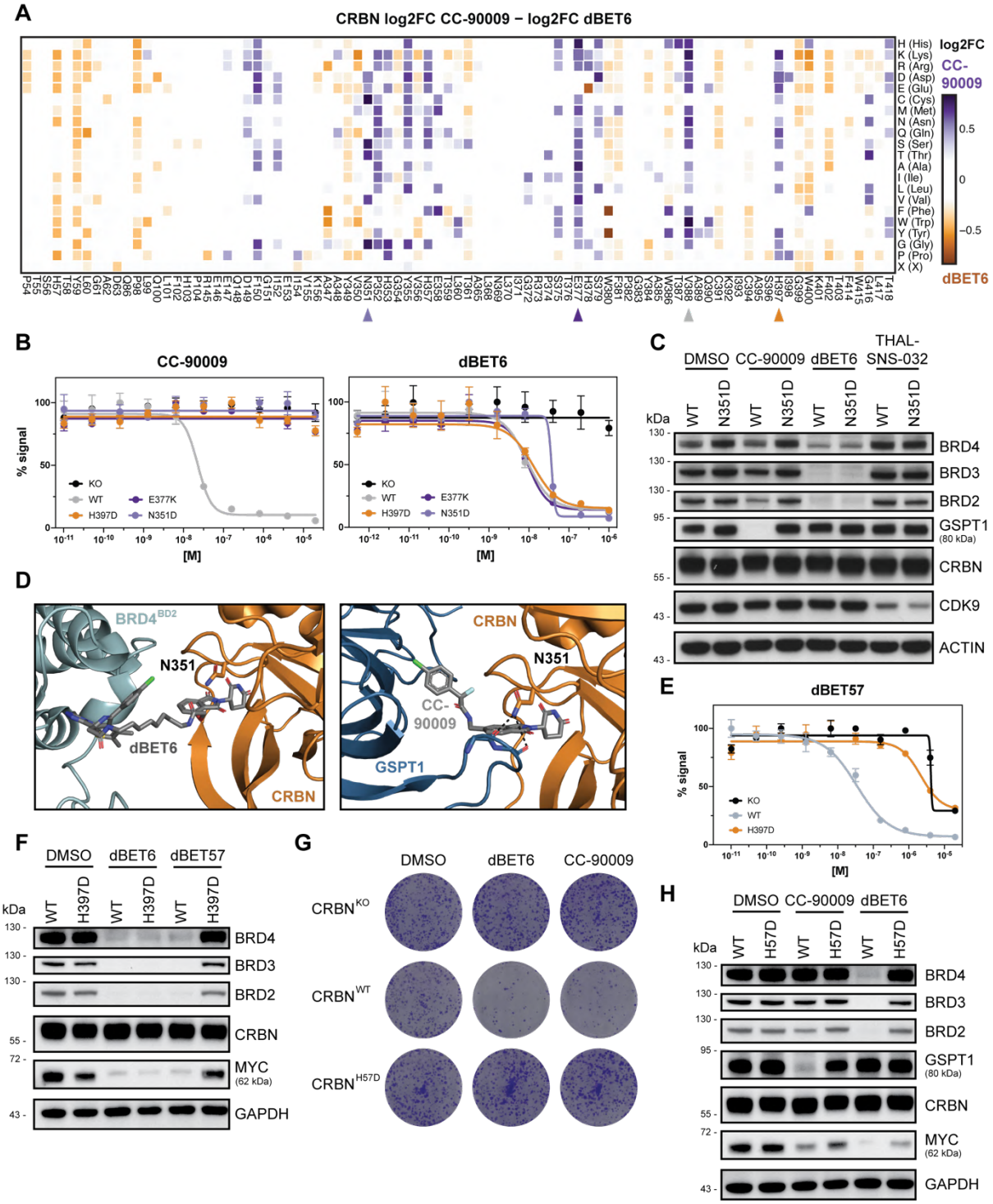

Figure 5. Functional CRBN Hotspots Show Degrader Selectivity and are Mutated in Refractory Multiple Myeloma Patients

(A) Heatmap depicting differential log2 fold-enrichment of CRBN mutations normalized to maximum log2 fold-changes vs. DMSO between BET bromodomain targeting PROTAC dBET6 (500 nM, 7 d treatment) and the GSPT1 targeting molecular glue CC-90009 (500 nM, 7 d treatment). n = 3 independent measurements.

(B) Dose-resolved, normalized viability after 3 d treatment with CC-90009 and dBET6 in RKO $CRBN^{-/-}$ cells with over-expression of $CRBN^{WT}$, $CRBN^{E377K}$, $CRBN^{N351D}$ and $CRBN^{H397D}$. Mean ± s.e.m.; n = 3 independent treatments.

(C, F and H) Protein levels in RKO $CRBN^{-/-}$ cells with over-expression of $CRBN^{WT}$, $CRBN^{N351D}$, $CRBN^{H397D}$ or $CRBN^{H57D}$ treated with DMSO, CC-90009 (50 nM, 6 h), dBET6 (15 nM, 2 h), dBET57 (240 nM, 2 h) or THAL-SNS-032 (200 nM, 2 h). Representative images of n = 2 independent measurements.

(D) Cocrystal structure of dBET6 (left) and CC-90009 (right) in a ternary complex with CRBN and $BRD4^{BD2}$ (PDB 6BOY) or GSPT1 (PDB 6XK9) depicting PPIs of $CRBN^{N351}$ and the GSPT1.

(E) Dose-resolved, normalized viability after 3 d treatment with dBET57 in RKO $CRBN^{-/-}$ cells with over-expression of $CRBN^{WT}$ and $CRBN^{H397D}$. Mean ± s.e.m.; n = 3 independent treatments.

(G) Depiction of clonogenic assays via crystal violet staining. Cells were treated for 10 days at EC90 of the degrader (30 nM dBET6, 60 nM CC-90009). Representative of n = 2 independent measurements.

See also **Extended Data Fig. 6**.

Discussion

An essential step in targeted protein degradation is the drug-induced formation of a ternary complex[10,43]. Enabled by the plasticity of a given protein-protein interface, structurally diverse degraders can prompt ternary assemblies of different architectures[2,9]. We hypothesize that, based on the specific geometry of a given assembly, mutations altering the surface topologies of the involved proteins can disrupt the drug-induced molecular proximity, preventing target degradation and ultimately leading to drug resistance. Here, we focus our efforts on CRBN and VHL. In the presented examples, we leverage cytotoxic effects of drugs resulting from degradation of widely essential proteins. Hence, variant selection was based on an altered cellular fitness as a downstream readout for drug-induced target degradation. Noteworthy, the presented DMS approach could also be combined with FACS-based readouts, thus expanding its reach also to non-essential targets or pathways. Based on the resistance-causing mutations we initially identified via targeted re-sequencing in near-haploid human cells, we have focused the mutational scanning on residues that are proximal to the degrader binding site. This focus was chosen to obtain a relatively manageable library size of around 1500 variants each, yet prevented the identification of hotspots outside the dimerization interface.

In general terms, we anticipate that multi-layered maps of functional E3 hotspots can advance our understanding of determinants of drug-induced substrate recognition by E3 ligases. We perceive this approach to be highly complementary and synergistic with efforts in structural biology of degrader ternary complexes. It provides scalable and functional information in the context of a cellular environment involving native protein components. For TPD-compatible E3 ligases lacking structural data, design of variant libraries and mechanistic interpretations will arguably be more challenging [6]. However, protein structure prediction and ternary complex modeling could offer insights, particularly in cases where the degrader binding site on the E3 could be mapped[44,45]. Additionally, or in absence of interpretable predictions, one could initially scan the entire gene CRISPR-tiling to then dissected functionally relevant interfaces in-depth via DMS.

Intriguingly, some of the identified and validated functional hotspots could not sufficiently be rationalized based on existing structural models. Among others, this is exemplified by functional hotspots that involve the BET PROTAC ARV-771. Based on the presented DMS data, for instance exemplified by VHL^{P71I} and VHL^{H110L}, it is conceivable that ARV-771 induces a ternary complex of a different geometry than the ones previously resolved for MZ1[10] or macroPROTAC-1[34]. In support of these predictions are the observations that (i) ARV-771-induced ternary complex assemblies have thus far proven to be unsuccessful to crystallization efforts; (ii) ARV-771 and MZ1 displayed distinct intra-BET bromodomain cooperativity profiles in FP ternary complex assays[46]. Hence, this and related observations emerging from this study underscore that nuanced, differentiated mutational profiles and sensitivities can arise even with degraders which share otherwise highly similar chemical structures, mechanisms, and cellular activities.

Finally, we hope that our multi-layered maps of functional hotspots in CRBN and VHL will also inform potential resistance mechanisms, as well as ways to overcome them by altered degrader design. In line with previous studies that employed CRISPR/Cas9 screens[13–15], we show that most emerging mutations occur directly in the SR of the involved E3 ligase. Of note, our sequencing strategy is limited in detecting copy number loss or splicing defects, and hence doesn't cover the full spectrum of possible causative mutations. Intriguingly, our data highlight that the essentiality of the co-opted SR appears to correlate with the frequency, type and topology of the identified alterations, even though we can't exclude the contribution of additional factors. While it appears reasonable to conclude that resistance-causing mutations will be enriched in the ligase, mutations can also arise on the neo-substrate, as for instance reported for CDK12-targeting PROTACs[47]. Moreover, an elegant recent study described a complementary approach, which is based on a CRISPR-suppressor scanning strategy, to identify resistance-causing mutations that are localized in neo-substrates of known molecular glue degraders[48].

Which mutations will turn out to be clinically relevant will only be revealed when additional degraders will be clinically evaluated. As of now, evidence from clinical practice is only available for CRBN-based IMiDs, such as lenalidomide and pomalidomide. Accumulating data has shown that up to one-third of patients refractory to pomalidomide treatment present with various types of CRBN alterations[41,42,49]. In support of a potential clinical relevance of our DMS approach, we found that a number of the identified hotspots are disrupted in patients relapsing from IMiD treatment. Some of the identified hotspots appeared to be specific for molecular glues, such as $CRBN^{P352}$, while others were similarly required for PROTAC potency, for example $CRBN^{F381}$. Of note, our DMS reconstitution mimics the scenario of homozygous mutations, while mutations in patients might also be heterozygous. Future data on clinical trials of CRBN-based glue degraders, such as CC-90009, and CRBN-based PROTACs, such as ARV-471 (targeting the estrogen receptor) and ARV-110 (targeting the androgen receptor) or VHL-based PROTACs, such as DT-2216 (targeting Bcl-xL) will likely shed light on additionally clinically relevant functional hotspots[7].

Acknowledgements:

We thank the Biomedical Sequencing Facility at CeMM for assistance with next-generation sequencing, Charlotte Crowe (Ciulli Lab) for the gift of purified BET bromodomain protein, the Diamond Light Source

for beamtime (BAG proposal MX14980-13) and Johannes Bigenzahn (Superti-Furga Lab) for the gift of plasmids. CeMM and the Winter laboratory are supported by the Austrian Academy of Sciences. The Winter lab is further supported by funding from the European Research Council (ERC) under the European Union's Horizon 2020 research and innovation program (grant agreement 851478), as well as by funding from the Austrian Science Fund (FWF, projects P32125, P31690 and P7909). The Ciulli laboratory's work on PROTACs has received funding from the European Research Council (ERC) under the European Union's Seventh Framework Programme (FP7/2007-2013) as a Starting Grant to A.C. (grant agreement No. ERC-2012-StG-311460 DrugE3CRLs). R.C. is funded by a PhD studentship from the UK Biotechnology and Biological Sciences Research Council (BBSRC) under the EastBio doctoral training programme (BB/M010996/1). Biophysics and drug-discovery activities at Dundee were supported by Wellcome Trust strategic awards 100476/Z/12/Z and 094090/Z/10/Z, respectively. For the purpose of open access, the authors have applied a Creative Commons Attribution (CC BY) licence to any Author Accepted Manuscript version arising.

Author contributions statement:

A.H., M.B. and G.E.W. conceptualized this study. A.H. and M.B. designed and conducted hybrid capture assays. A.H., S.B. and M.B. designed and conducted deep mutational scanning assays. A.H., S.B. and E.B. generated cell lines and conducted cellular mutant validation including immunoblotting and drug sensitivity assays. M.B. and H.I. analyzed and visualized hybrid capture and deep mutational scanning data. A.C. and A.T. designed AT7 compound and A.T. synthesized the compound. R.C. expressed and purified recombinant proteins, performed fluorescence polarization measurements and compound synthesis. S.J.H. solved cocrystal structure. J.W. performed degradation and cell viability assays for AT7. A.C. and G.E.W. supervised the work. H.I., A.H. and R.C. generated figures with input from all authors. A.H., R.C., A.C. and G.E.W. wrote the manuscript with input from all authors.

Competing interest statement

S.B. is an employee at Proxygen, a company that is developing molecular glue degraders. M.B. is scientific founder, shareholder, and employee at Proxygen. G.E.W. is scientific founder and shareholder at Proxygen and Solgate and the Winter lab receives research funding from Pfizer. A.C. is a scientific founder, shareholder, and advisor of Amphista Therapeutics, a company that is developing targeted protein degradation therapeutic platforms. S.J.H. and A.T. are currently employees of Amphista Therapeutics. The Ciulli laboratory receives or has received sponsored research support from Almirall, Amgen, Amphista Therapeutics, Boehringer Ingelheim, Eisai, Merck KaaG, Nurix Therapeutics, Ono Pharmaceutical and Tocris-Biotechne. The other authors are not aware of any affiliations, memberships, funding, or financial holdings that might be perceived as affecting the objectivity of this work.

References

1. Deshaies, R. J. Multispecific drugs herald a new era of biopharmaceutical innovation. *Nature* **580**, 329–338 (2020).
2. Gerry, C. J. & Schreiber, S. L. Unifying principles of bifunctional, proximity-inducing small molecules. *Nat Chem Biol* **16**, 369–378 (2020).
3. Hanzl, A. & Winter, G. E. Targeted protein degradation: current and future challenges. *Curr Opin Chem Biol* **56**, 35–41 (2020).
4. Petroski, M. D. & Deshaies, R. J. Function and regulation of cullin-RING ubiquitin ligases. *Nat Rev Mol Cell Biol* **6**, 9–20 (2005).
5. Harper, J. W. & Schulman, B. A. Cullin-RING Ubiquitin Ligase Regulatory Circuits: A Quarter Century Beyond the F-Box Hypothesis. *Annu Rev Biochem* **90**, 403–429 (2021).
6. Kramer, L. T. & Zhang, X. Expanding the landscape of E3 ligases for targeted protein degradation. *Current Research in Chemical Biology* **2**, 100020 (2022).
7. Békés, M., Langley, D. R. & Crews, C. M. PROTAC targeted protein degraders: the past is prologue. *Nat Rev Drug Discov* (2022) doi:10.1038/S41573-021-00371-6.
8. Kozicka, Z. & Thomä, N. H. Haven't got a glue: Protein surface variation for the design of molecular glue degraders. *Cell Chem Biol* **28**, 1032–1047 (2021).
9. Maniaci, C. & Ciulli, A. Bifunctional chemical probes inducing protein-protein interactions. *Curr Opin Chem Biol* **52**, 145–156 (2019).
10. Gadd, M. S. *et al.* Structural basis of PROTAC cooperative recognition for selective protein degradation. *Nat Chem Biol* **13**, 514–521 (2017).
11. Nowak, R. P. *et al.* Plasticity in binding confers selectivity in ligand-induced protein degradation. *Nat Chem Biol* (2018) doi:10.1038/s41589-018-0055-y.
12. Zorba, A. *et al.* Delineating the role of cooperativity in the design of potent PROTACs for BTK. *Proc Natl Acad Sci U S A* **115**, E7285-e7292 (2018).
13. Shirasaki, R. *et al.* Functional Genomics Identify Distinct and Overlapping Genes Mediating Resistance to Different Classes of Heterobifunctional Degraders of Oncoproteins. *Cell Rep* **34**, (2021).
14. Sievers, Q. L., Gasser, J. A., Cowley, G. S., Fischer, E. S. & Ebert, B. L. Genome-wide screen identifies cullin-RING ligase machinery required for lenalidomide-dependent CRL4(CRBN) activity. *Blood* **132**, 1293–1303 (2018).
15. Mayor-Ruiz, C. *et al.* Plasticity of the Cullin-RING Ligase Repertoire Shapes Sensitivity to Ligand-Induced Protein Degradation. *Mol Cell* **75**, 849-858.e8 (2019).
16. Zhang, L., Riley-Gillis, B., Vijay, P. & Shen, Y. Acquired Resistance to BET-PROTACs (Proteolysis-Targeting Chimeras) Caused by Genomic Alterations in Core Components of E3 Ligase Complexes. *Mol Cancer Ther* **18**, 1302–1311 (2019).
17. Ferguson, F. M. & Gray, N. S. Kinase inhibitors: the road ahead. *Nat Rev Drug Discov* **17**, 353–377 (2018).
18. Zaidman, D., Prilusky, J. & London, N. ProsetTac: Rosetta based modeling of PROTAC mediated ternary complexes. *J Chem Inf Model* **60**, 4894–4903 (2020).
19. Bai, N. *et al.* Rationalizing PROTAC-Mediated Ternary Complex Formation Using Rosetta. *J Chem Inf Model* **61**, 1368–1382 (2021).
20. Drummond, M. L. & Williams, C. I. In Silico Modeling of PROTAC-Mediated Ternary Complexes: Validation and Application. *J Chem Inf Model* **59**, 1634–1644 (2019).
21. Sievers, Q. L. *et al.* Defining the human C2H2 zinc finger degrome targeted by thalidomide analogs through CRBN. *Science (1979)* **362**, (2018).
22. Eron, S. J. *et al.* Structural Characterization of Degrader-Induced Ternary Complexes Using Hydrogen-Deuterium Exchange Mass Spectrometry and Computational Modeling: Implications for Structure-Based Design. *ACS Chem Biol* **16**, 2228–2243 (2021).
23. Dixon, T. *et al.* Atomic-Resolution Prediction of Degrader-mediated Ternary Complex Structures by Combining Molecular Simulations with Hydrogen Deuterium Exchange. *bioRxiv* 2021.09.26.461830 (2021) doi:10.1101/2021.09.26.461830.
24. Meyers, R. M. *et al.* Computational correction of copy number effect improves specificity of CRISPR-Cas9 essentiality screens in cancer cells. *Nat Genet* **49**, 1779–1784 (2017).
25. Latif, F. *et al.* Identification of the von Hippel-Lindau disease tumor suppressor gene. *Science* **260**, 1317–1320 (1993).
26. Raina, K. *et al.* PROTAC-induced BET protein degradation as a therapy for castration-resistant prostate cancer. *Proc Natl Acad Sci U S A* **113**, 7124–7129 (2016).

27. Winter, G. E. *et al.* BET Bromodomain Proteins Function as Master Transcription Elongation Factors Independent of CDK9 Recruitment. *Mol Cell* **67**, 5-18.e19 (2017).
28. Forment, J. v. *et al.* Genome-wide genetic screening with chemically mutagenized haploid embryonic stem cells. *Nat Chem Biol* **13**, 12–14 (2017).
29. Volz, J. C., Schuller, N. & Elling, U. Using Functional Genetics in Haploid Cells for Drug Target Identification. *Methods Mol Biol* **1953**, 3–21 (2019).
30. Winter, G. E. *et al.* The solute carrier SLC35F2 enables YM155-mediated DNA damage toxicity. *Nat Chem Biol* **10**, 768–773 (2014).
31. Suiter, C. C. *et al.* Massively parallel variant characterization identifies NUDT15 alleles associated with thiopurine toxicity. *Proc Natl Acad Sci U S A* **117**, 5394–5401 (2020).
32. Awad, M. M. *et al.* Acquired Resistance to KRAS G12C Inhibition in Cancer. *N Engl J Med* **384**, 2382–2393 (2021).
33. Zengerle, M., Chan, K. H. & Ciulli, A. Selective Small Molecule Induced Degradation of the BET Bromodomain Protein BRD4. *ACS Chem Biol* **10**, 1770–1777 (2015).
34. Testa, A., Hughes, S. J., Lucas, X., Wright, J. E. & Ciulli, A. Structure-Based Design of a Macrocyclic PROTAC. *Angew Chem Int Ed Engl* **59**, 1727–1734 (2020).
35. Farnaby, W. *et al.* BAF complex vulnerabilities in cancer demonstrated via structure-based PROTAC design. *Nat Chem Biol* **15**, 672–680 (2019).
36. Soares, P. *et al.* Group-Based Optimization of Potent and Cell-Active Inhibitors of the von Hippel-Lindau (VHL) E3 Ubiquitin Ligase: Structure-Activity Relationships Leading to the Chemical Probe (2S,4R)-1-((S)-2-(1-Cyanocyclopropanecarboxamido)-3,3-dimethylbutanoyl)-4-hydroxy-N-(4-(4-methylthiazol-5-yl)benzyl)pyrrolidine-2-carboxamide (VH298). *J Med Chem* **61**, 599–618 (2018).
37. Matyskiela, M. E. *et al.* A novel cereblon modulator recruits GSPT1 to the CRL4(CRBN) ubiquitin ligase. *Nature* **535**, 252–257 (2016).
38. Surka, C. *et al.* CC-90009, a novel cereblon E3 ligase modulator, targets acute myeloid leukemia blasts and leukemia stem cells. *Blood* **137**, 661–677 (2021).
39. Fink, E. C. *et al.* Crbn I391V is sufficient to confer in vivo sensitivity to thalidomide and its derivatives in mice. *Blood* **132**, 1535–1544 (2018).
40. Olson, C. M. *et al.* Pharmacological perturbation of CDK9 using selective CDK9 inhibition or degradation. *Nat Chem Biol* (2017) doi:10.1038/nchembio.2538.
41. Barrio, S. *et al.* IKZF1/3 and CRL4 CRBN E3 ubiquitin ligase mutations and resistance to immunomodulatory drugs in multiple myeloma. *Haematologica* **105**, E237–E241 (2020).
42. Gooding, S. *et al.* Multiple cereblon genetic changes are associated with acquired resistance to lenalidomide or pomalidomide in multiple myeloma. *Blood* **137**, 232–237 (2021).
43. Roy, M. J. *et al.* SPR-Measured Dissociation Kinetics of PROTAC Ternary Complexes Influence Target Degradation Rate. *ACS Chem Biol* **14**, 361–368 (2019).
44. Jumper, J. *et al.* Highly accurate protein structure prediction with AlphaFold. *Nature 2021 596:7873* **596**, 583–589 (2021).
45. Scholes, N. S., Mayor-Ruiz, C. & Winter, G. E. Identification and selectivity profiling of small-molecule degraders via multi-omics approaches. *Cell Chem Biol* **28**, 1048–1060 (2021).
46. Klein, V. G., Bond, A. G., Craigon, C., Lokey, R. S. & Ciulli, A. Amide-to-Ester Substitution as a Strategy for Optimizing PROTAC Permeability and Cellular Activity. *J Med Chem* **64**, 18082–18101 (2021).
47. Jiang, B. *et al.* Discovery and resistance mechanism of a selective CDK12 degrader. *Nat Chem Biol* **17**, 675–683 (2021).
48. Gosavi, P. M. *et al.* Profiling the Landscape of Drug Resistance Mutations in Neosubstrates to Molecular Glue Degraders. *ACS Cent Sci* acscentsci.1c01603 (2022) doi:10.1021/ACSCENTSCI.1C01603.
49. Kortum, K. M. *et al.* Targeted sequencing of refractory myeloma reveals a high incidence of mutations in CRBN and Ras pathway genes. *Blood* **128**, 1226–1233 (2016).
50. Galdeano, C. *et al.* Structure-guided design and optimization of small molecules targeting the protein-protein interaction between the von Hippel-Lindau (VHL) E3 ubiquitin ligase and the hypoxia inducible factor (HIF) alpha subunit with in vitro nanomolar affinities. *J Med Chem* **57**, 8657–8663 (2014).
51. Joung, J. *et al.* Genome-scale CRISPR-Cas9 knockout and transcriptional activation screening. *Nat Protoc* **12**, 828–863 (2017).
52. Guzmán, C., Bagga, M., Kaur, A., Westermarck, J. & Abankwa, D. ColonyArea: an ImageJ plugin to automatically quantify colony formation in clonogenic assays. *PLoS One* **9**, (2014).

53. Barnett, D. W., Garrison, E. K., Quinlan, A. R., Strömberg, M. P. & Marth, G. T. BamTools: a C++ API and toolkit for analyzing and managing BAM files. *Bioinformatics* **27**, 1691–1692 (2011).
54. Bolger, A. M., Lohse, M. & Usadel, B. Trimmomatic: a flexible trimmer for Illumina sequence data. *Bioinformatics* **30**, 2114–2120 (2014).
55. Li, H. & Durbin, R. Fast and accurate short read alignment with Burrows-Wheeler transform. *Bioinformatics* **25**, 1754–1760 (2009).
56. McLaren, W. *et al.* The Ensembl Variant Effect Predictor. *Genome Biol* **17**, (2016).
57. McKenna, A. *et al.* The Genome Analysis Toolkit: a MapReduce framework for analyzing next-generation DNA sequencing data. *Genome Res* **20**, 1297–1303 (2010).
58. van Molle, I. *et al.* Dissecting Fragment-Based Lead Discovery at the von Hippel-Lindau Protein:Hypoxia Inducible Factor 1α Protein-Protein Interface. *Chem Biol* **19**, 1300–1312 (2012).
59. Potterton, E., Briggs, P., Turkenburg, M. & Dodson, E. A graphical user interface to the CCP4 program suite. *Acta Crystallogr D Biol Crystallogr* **59**, 1131–1137 (2003).
60. Chen, V. B. *et al.* MolProbity: all-atom structure validation for macromolecular crystallography. *Acta Crystallogr D Biol Crystallogr* **66**, 12–21 (2010).

Materials and Methods

Cell lines, tissue culture and lentiviral transduction

KBM7 cells were obtained from T. Brummelkamp and grown in IMDM supplemented with 10% FBS and 1% penicillin/streptomycin (pen/strep). All other cells were obtained from ATCC or DSMZ. RKO, 293T and HeLa cells were cultured in DMEM supplemented with 10% FBS and 1% pen/strep. MOLM-13 and MV4;11 were grown in RPMI, 10% FBS and 1% pen/strep. pSpCas9(BB)-2A-GFP (PX458) was obtained through Addgene (48138) and used to transiently express sgRNA against CRBN and VHL in RKO cells (see Supplementary Table 5). Clones were single cell seeded and checked for CRBN/VHL deletion via PCR on gDNA or Western blotting. pENTR221_CRBN_WT (a gift from J. Bradner) and pDONR223_VHL_WT (Addgene 81874) were used to generate single CRBN and VHL variants via Q5 site-directed mutagenesis (New England Biolabs, E0554S) and subsequently cloned via Gibson Assembly in the pRRL-EF1a-XhoI-IRES-BlastR plasmid (gift from J. Bigenzahn and G. Superti-Furga) using the NEBuilder HiFi DNA Assembly Mix (New England Biolabs, E2621L). The CRBN/VHL WT and point mutant plasmids were used for lentivirus production and subsequent transduction in RKO CRBN$^{-/-}$ and VHL$^{-/-}$ clones, respectively.

For lentiviral production, 293T cells were seeded in 10 cm dishes and transfected at approx. 80 % confluency with 4 µg target vector, 2 µg pMD2.G (Addgene 12259) and 1 µg psPAX2 (Addgene 12260) using PEI (PolyScience, 24765-100) and following standard protocol. [51] Viral supernatant was harvested after 60 h, filtrated and stored in aliquots at -80 °C for transduction.

Colony formation assays

Cells were seeded in 6 well plates at a cell density of 1’000 cells/well and treated with DMSO or the indicated drug. After 10 days, cell colonies were stained with Crystal Violet (Cristal Violet 0.05% w/v, Formaldehyde 1%, 1x PBS, Methanol 1%) for 20 min, washed with water and dried. Colony number and density were quantified with ImageJ (US National Institutes of Health, ColonyArea plugin)[52].

Cell viability assays

Cells were seeded in 96- well plates at a cell density of 5000 cells per well and treated for 3 or 4 days with DMSO or drug at ten different 1:5 serial diluted concentrations. Starting concentrations of the drugs: ACBI1 20 μM (Boehringer Ingelheim, opnme), ARV-771 1 μM (MedChem Express, HY-100972), MZ1 10 μM, AT7 10 μM, macroPROTAC-1 20 μM, CC-90009 20 μM (MedChem Express, HY-130800), dBET6 1 μM (MedChem Express, HY-112588), dBET57 20 μM (MedChem Express, HY-123844). Each treatment was performed in biological triplicates. Cell viability was assessed via the CellTiter Glo assay according to manufacturer instructions (CellTiter-Glo Luminescent Cell Viability Assay, Promega G7573). Luminescence signal was measured on a Multilabel Plate Reader Platform Victor X3 model 2030 (Perkin Elmer). Survival curves and half-maximum effective concentrations (EC50) were determined in GraphPad Prism version 8.4.2 by fitting a nonlinear regression to the log10 transformed drug concentration and the relative viability after normalization of each data point to the mean luminescence of the lowest drug concentration.

Western blot analysis

PBS-washed cell pellets were lysed in RIPA Buffer (50 mM Tris-HCl pH 8.0, 150 mM NaCl, 1% Triton X-100, 0.5% sodium deoxycholate, 0.1% SDS, 1× Halt protease inhibitor cocktail, 25 U ml^{-1} Benzonase). Lysates were cleared by centrifugation for 15 min at 4 °C and 20,000*g*. Protein concentration was measured by BCA according to the manufacturer's protocol (Fisher Scientific Pierce BCA Protein Assay Kit, 23225) and 4X LDS sample buffer was added. Proteins (20 μg) were separated on 4-12% SDS-PAGE gels and transferred to nitrocellulose membranes. Membranes were blocked with 5% milk in TBST for 30 min at RT. Primary antibodies were incubated in milk or TBST alone for 1 h at RT or 4°C overnight. Secondary antibodies were incubated for 1 h at RT. Blots were developed with chemiluminescence films. Primary antibodies used: BRD4 (1:1000, Abcam, ab128874), BRD3 (1:1000, Bethyl Laboratories, A302-368A), BRD2 (1:1000, Bethyl Laboratories, A302-582A), SMARCA4 (1:1000, Bethyl Laboratories, A300-813A), SMARCA2 (1:1000, Cell Signaling Technology, #6889), cMYC (1:1000, Santa Cruz Biotechnology, sc-764), GSPT1 (1:1000, Abcam, ab49878), CDK9 (1:1000, Cell Signaling Technology, 2316S), CRBN (1:2000, kind gift of R. Eichner and F. Bassermann), VHL (1:1000, Cell Signaling Technology, 2738), ACTIN (1:5000, Sigma-Aldrich, A5441-.2ML), GAPDH (1:1000, Santa Cruz Biotechnology, sc-365062). Secondary antibodies used: Peroxidase-conjugated AffiniPure Goat Anti-Rabbit IgG (1:10000, Jackson ImmunoResearch, 111-035-003) and Peroxidase-conjugated AffiniPure Goat Anti-Mouse IgG (1:10000, Jackson ImmunoResearch, 115-035-003).

Resistance rate determination

KBM7 cells (4 x 10^6) were treated at a single dose relative to the degraders EC_{50} values in 3-day dose response assays (see also **Extended Data Fig. 1A**) in 20 ml of media. Cells were then seeded into 384-well plates at 50 μl per well and after 21 days, wells with proliferating cells were counted for each treatment. To correct for wells containing more than one resistant cell, the probability *p* of obtaining resistant cells was calculated via a binomial distribution using the count of wells lacking resistant cells

according to the following formula, where n is 10000 (cells per well) and P(x = 0) is the fraction of non-outgrowing wells on the plate.

$$P(x = 0) = \binom{n}{x}(1-p)^n$$

Acquired resistance mutation identification by hybrid capture

Generation of acquired drug resistant cells and hybrid-capture library preparation for next-generation sequencing

One hundred million KBM7 cells were treated with DMSO or 10X (100 nM), 25X (250 nM), 50X (500 nM) EC_{50} of dBET6 or ARV in 50 ml medium. After 25 d, Ficoll-gradient centrifugation with Lymphocyte Separation Media (Corning, COR25-072-CV) was performed according to manufacturer's protocols. Cells were recovered for one day, counted and PBS washed pellets were stored at -80 °C for subsequent gDNA extraction (QIAamp DNA Mini, QIAGEN 51304). DNA content was determined with Qubit dsDNA HS Kit (Thermo Fisher, Q32854) and 500 ng of the gDNA was subjected to DNA library preparation using the NEBNext Ultra II FS DNA Library Prep kit for Illumina (New England Biolabs, E7805S) following manufacturer's instructions (protocol for inputs >100 ng). Fragments were size-selected using AMPure XP beads (Beckman Coulter, 10136224) for fragments of 150-350 bp. Adaptor-ligated DNA was amplified in five cycles by PCR using NEBnext Multiplex Oligos for Illumina (Set1 E7335 and Set2 E75000). For hybrid capture, xGen Gene Capture Pools for the 29 genes of interest were purchased from IDT (see **Supplementary Table 1**) and 500 ng of DNA was used as input. Hybridization was performed for 16h following the supplier's protocols, including the xGen Universal Blocker-TS Mix (IDT, 1075475) blocking oligos. Post-capture PCR was performed with the NEBNext High-Fidelity 2X PCR Master Mix (NEB, M0541S) for 14-20 cycles. Sequencing libraries were quantified using the Qubit dsDNA HS Kit (Thermo Fisher Q32854) and analyzed on an Agilent 2100 Bioanalyzer before sequencing on a HiSeq 4000 lane (50 bp single-end).

NGS data analysis

Raw sequencing reads were converted to fastq files using the bamtools convert (v2.5.1)[53]. Sequencing adapters and low-quality reads were trimmed using the Trimmomatic tool (v0.39) in SE mode with standard settings[54]. Reads were aligned to the hg38/GRCh38 assembly of the human reference genome using aln and samse algorithms from the bwa package (v0.7.17)[55]. Unmapped reads were removed using the CleanSam function from the Picard toolkit (v2.25.1, Broad Institute GitHub Repository). Reads were sorted and duplicate reads filtered using the SortSam and MarkDuplicates Picard tools. Read groups were added by the Picard AddOrReplaceReadGroups tool.

The Mutect2 function from the GATK (v4.1.8.1) was used to call variants. The variants were annotated using the Ensembl Variant Effect Predictor tool (v103.1)[56]. Coding variants with greater than 2-fold enrichment in allele frequency (as determined by Mutect2) upon drug treatment compared to the wild-type population were considered hits (see also **Supplementary Table 2**).

Deep mutational scanning screens

Design, cloning and lentiviral production of the DMS library.

Amino acid residues within 10 Å of the VHL-ligand 1 and thalidomide binding pockets on VHL and CRBN respectively were determined via PyMol (v2.3.5) and selected for site saturation library design by TWIST Biosciences. Pooled libraries of mutant VHL (1442 variants) and CRBN (1738 variants) were introduced into the XhoI digested backbone pRRL-EF1a-XhoI-IRES-BlastR with NEBuilder 2x HiFi assembly (New England Biolabs). The assembly mix was purified via isopropanol precipitation and electroporated into Stbl4 bacteria (Thermo Fisher, 11635018) at 1.2 kV, 25 µF and 200 Ω. After recovery, the bacterial suspension was plated on LB Agar plates containing Ampicillin for selection. Dilutions of the bacterial suspension were plated and counted to determine a library coverage of 135x and 54x for VHL and CRBN libraries respectively. Quality control of the library distribution was performed via next-generation sequencing of the plasmid preparation as outlined for the screens below, except that the mentioned PCR was performed for 5 cycles. 1442 of 1500 possible VHL variants and 1738 of 1740 CRBN substitutions were recovered in the libraries. The VHL library included an abundant mutant (F119I) caused by library synthesis, which had no functional inconsequence. Lentiviral supernatant was produced as mentioned earlier and concentrated using Lenti-X concentrator (Takara, 631232) followed by storage at -80°C in aliquots.

Deep mutational scanning library screens

Eight million RKO CRBN$^{-/-}$ or VHL$^{-/-}$ were transduced at a MOI of 0.3 yielding a calculated library representation of 1664 and 1380 cells per variant for VHL and CRBN respectively. For each transduction one million cells were seeded in a 12-well plate with 8 µgml^{-1} polybrene (SantaCruz, SC-134220), the titrated amount of lentivirus filled to 1 ml with culture media. The plate was centrifuged at 765 x g for 1 h at 37°C and cells were detached after 6 h of incubation at 37°C, pooled and expanded. 48 hrs after transduction, pools were selected by adding 20 µgml^{-1} blasticidine for 7 days. Independent mutational scanning resistance screens were performed in replicates by treating 2.5 million cells, splitting and retreating after 4 days and harvesting 2.5 million cell pellets after a total of 7 day treatment with the indicated drug and dose.

Library preparation for next-generation sequencing

Genomic DNA (gDNA) was extracted from frozen cell pellets following the QIAamp DNA Mini Kit (Qiagen, 51304). VHL and CRBN variant cDNAs were amplified via PCR from gDNA with primers CRBN_GA_fwd & rev and VHL_GA_fwd & rev respectively. Primer sequences are available in **Supplementary Table 5**. The total isolated gDNA was processed in batches of 5 µg per PCR reaction with Q5 polymerase (NEB, M0491L). One PCR reaction contained 10 µl 5x reaction buffer, 10 µl 5x GC enhancer, 2.5 µl primer mix containing 10 µM forward and reverse primer each, 1 µl dNTP mix (10 µM each), 1 µl Q5 polymerase and nuclease-free water to bring the reaction volume to 50 µl. Target amplification was achieved by performing: 30 s initial denaturation at 95°C; next for 20 to 28 cycles: 15 s at 95°C, 30 s at 57°C and 2 min at 72°C; followed by a final extension for 5 min at 72°C. The cycle number for specific amplification of the 700 base-pair (VHL) and 1.4 kilo-base-pair (CRBN) targets was confirmed by agarose gel electrophoresis. PCR reactions for each treatment were pooled and purified using AMPure XP beads (Beckman Coulter, 10136224) according to standard protocol for double-sided clean up in a 0.3:1 and 1:1 ratio. The purity and integrity of the PCR products were analysed on an Agilent 2100 Bioanalyzer following manufacturer recommendations for high sensitivity DNA chips

(Agilent, 5067-4626). Sequencing libraries were prepared using Nextera DNA Library Prep Kit (Illumina, FC-131-1024) following standard manufacturer instructions for amplicon libraries. This cuts the PCR products and tags resulting pieces with adapter sequences for the following sequencing. After purification of the fragmented and PCR amplified DNA libraries, quality control was performed by analysis on an Agilent 2100 Bioanalyzer following manufacturer recommendations for high sensitivity DNA chips (Agilent, 5067-4626). Final sequencing libraries were pooled in equimolar amounts and sequenced running 50-bp single-end reads on a HiSeq4000.

NGS data analysis

Raw sequencing reads were converted to fastq format using samtools (v1.10). Sequencing adapters were removed, and low-quality reads were filtered using the Trimmomatic tool (v0.39) in SE mode with standard settings[54]. Short reads were aligned to the expression cassette using aln algorithm from the bwa software package (v0.7.17) with the -n 5 parameter allowing for 5 mismatches, followed by bwa samse command to generate SAM files[55]. Alignment files were sorted using SortSam function from the Picard toolkit (v2.25.1, Broad Institute GitHub Repository). Mutation calling was performed using the AnalyzeSaturationMutagenesis tool from GATK (v4.1.8.1)[57]. Given our sequencing strategy, 98.89 % of reads constituted wild type sequences and were therefore filtered out during this step. Next, relative frequencies of variants were calculated for each interrogated position and variants that were covered by less than 1 in 10,000 reads in the DMSO sample were excluded from further quantitative analysis. Read counts for each variant were then normalized to total read count of each sample and log2FCs of treatment over DMSO were calculated. To correct for differential drug potency, we next normalized each variant to the maximum log2 fold-change over DMSO. For drug comparisons, log2 fold-changes over DMSO were subtracted. Given the sequencing of 50-bp reads, cDNAs harbouring two mutations (from synthesis errors) in greater distance will not be detected as multiple mutations with this strategy and hence present as 2 separate variants. Heatmaps were generated using pheatmap (v1.0.12) package in R (v4.1.2). Mapping of median resistance scores per residue on protein structures was performed using the PyMOL software (v2.5.2, Schrödinger LLC) using publicly available protein structures of CRBN (PDB: 6BOY) and VHL (PDB: 4W9H).

Competition growth experiments

KBM7 cells constitutively expressing Cas9_Blast (Addgene #52962) were transduced with lentivirus expressing sgRNAs against *VHL, GAPDH, RPL5* or in the gene desert of *MYC* in the GFP vector LRG (Lenti_sgRNA_EFS_GFP) (Addgene #65656, see **Supplementary Table 5**). GFP-expressing cells were mixed with GFP-negative cells at a 1:1 ratio. The mixed populations were grown for 21 days, and monitored by flow cytometry in 7-day intervals. Data was analyzed with FlowJo (gating strategy see **Supplementary Figure 3**) and percentages of the respective GFP populations were normalized to day 0.

Recombinant protein generation

Protein production for SMARCA4, BRD4.2 and the WT VCB complex was carried out as previously described[10,35]. The VCB mutants, in which R67 and P71I of VHL (54-213) were mutated to glutamine

and isoleucine respectively, were generated using a Q5 site directed mutagenesis kit (NEB, E0554S) according to the manufacturer's instructions and expressed and purified as for VCB. Mass spectrometry analysis and agarose gel electrophoresis was carried out to ensure purity of the recombinant proteins (see **Supplementary Figure 3**).

Fluorescence polarization

FP competitive binding assays were performed as described previously[58], with all measurements taken using a PHERAstar FS (BMG LABTECH) with fluorescence excitation and emission wavelengths (λ) of 485 and 520 nm, respectively. Assays were run in triplicate using 384-well plates (Corning, 3544), with each well solution containing 15 nM VCB protein, 10 nM 5,6-carboxyfluorescein (FAM)-labeled HIF-1α peptide (FAM-DEALAHypYIPMDDDFQLRSF, "JC9"), and decreasing concentrations of PROTACs (11-point, 3-fold serial dilution starting from 40 μM) or PROTACs:bromodomain (11-point, 3-fold serial dilution starting from 40 μM PROTAC: 80 μM bromodomain into buffer containing 40 μM of bromodomain). All components were dissolved from stock solutions using 100 mM Bis–Tris propane, 100 mM NaCl, 1 mM DTT, pH 7.0, to yield a final assay volume of 15 μL. DMSO was added as appropriate to ensure a final concentration of 2% v/v. Control wells containing VCB and JC9 with no compound or JC9 in the absence of protein were also included to allow for normalization. IC_{50} values were determined for each titration using nonlinear regression analysis with Prism (GraphPad). Cooperativity values (α) for each PROTAC were calculated using the ratio: $\alpha = IC_{50}$ (− bromodomain)/ IC_{50} (+ bromodomain).

Crystallography

The ternary complex VCB: AT7:Brd4^{BD2} was prepared by combining VCB, Brd4^{BD2}, and AT7 in a 1:1:1 molar ratio and incubating for 15 min at RT. Crystals were grown at 20 °C using the hanging drop diffusion method by mixing equal volumes of ternary complex solution and a crystallization solution containing 10% (w/v) PEG 8000, 0.1 M Tris-HCl (pH 7.5) and 0.1 M $MgCl_2$. Crystals were ready for harvest within 24 h and were flash-frozen in liquid nitrogen using 20% (v/v) ethylene glycol in liquor solution as a cryoprotectant. Diffraction data were collected at Diamond Light Source beamline I24 using a Pilatus 6M-F detector at a wavelength of 0.9750 Å. Reflections were indexed and integrated using XDS, and scaling and merging were performed with AIMLESS in CCP4i (v7.1.018)[59]. The crystals belonged to space group P_{32}, with two copies of the ternary complex in the asymmetric unit. The structure was solved by molecular replacement using MOLREP and search models derived from the coordinates for the VCB:MZ1:Brd4^{BD2} ternary complex (PDB entry 5T35). The initial model underwent iterative rounds of model building and refinement with COOT and REFMAC5, respectively. All riding hydrogens were excluded from the output coordinate files but included for refinement. Compound geometry restraints for refinement were prepared with the PRODRG server. Model geometry and steric clashes were validated using the MOLPROBITY server.[60] The structure has been deposited in the protein data bank (PDB: 7ZNT); data collection and refinement statistics are presented in **Supplementary Table 4.** Interfaces observed in the crystal structure were calculated using PISA, and all figures were generated using PyMOL.

Data availability

Raw and analysed mutational scanning and hybrid capture datasets (Figures 1 to 5, S1 and S3 to 5) are available in the Gene Expression Omnibus database under accession code GSE198280. For their analysis the human reference genome (hg38/GRCh38 assembly, GenBank ID 883148) was used. Atomic coordinates and structure factors for the new protein structure VCB:AT7:Brd4^{BD2} is available at the protein data bank (PDB: 7ZNT). All data generated and analysed in this study are included in this published article, its Supplementary Information, the mentioned databases or are available from the corresponding authors upon request.

Code availability

All code used for analysis of the experimental data is available at https://github.com/GWinterLab/TPDR.

Extended Data Figure 1

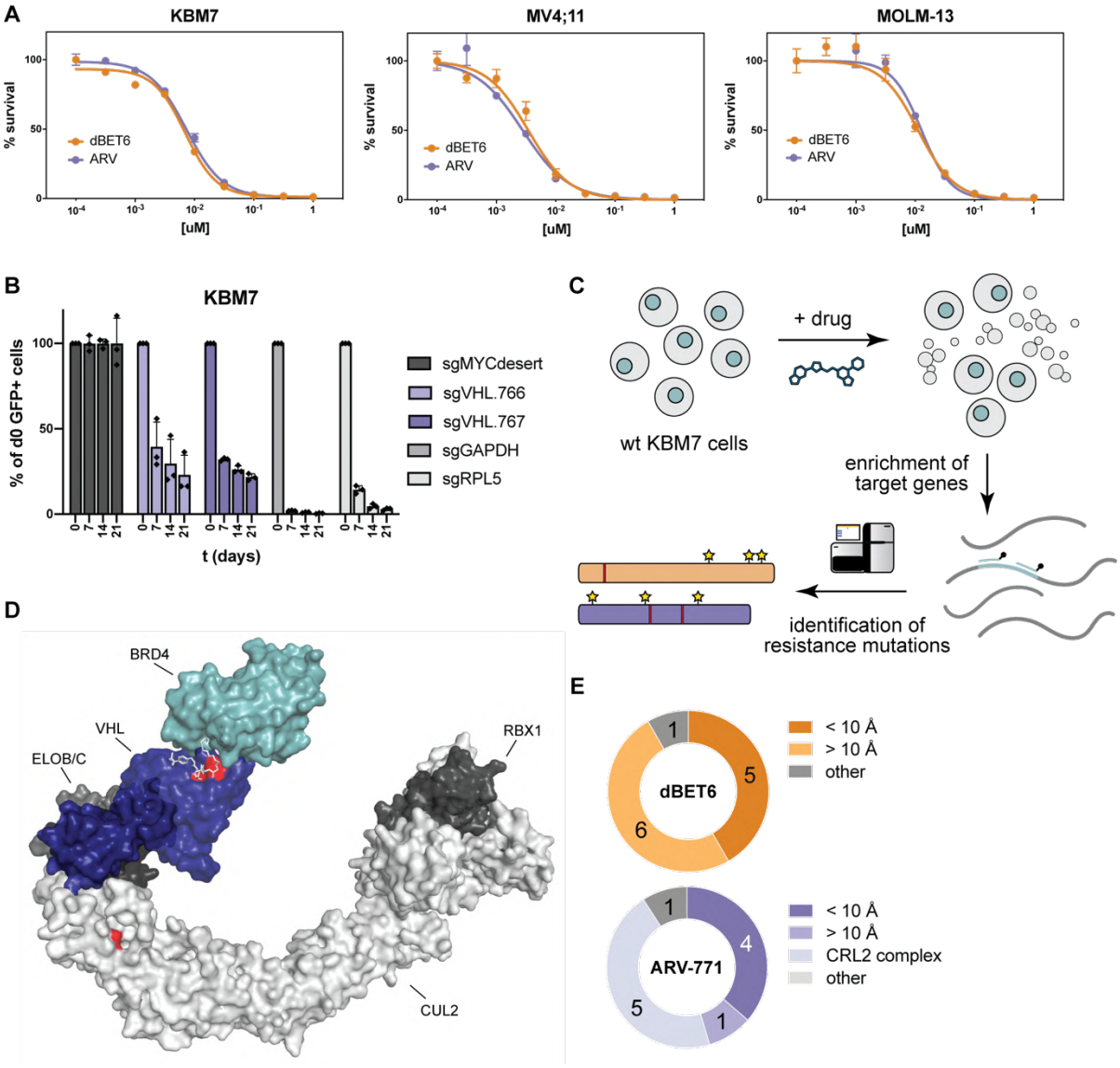

Extended Data Figure 1.

(A) Dose-resolved, normalized viability after 3 d treatment (dBET6 or ARV-771) in KBM7, MV4;11 and MOLM-13 cells. Mean ± s.e.m.; n = 3 independent treatments.

(B) Histogram depicting growth competition experiments. WT control KBM7 cells were mixed with mCherry and Cas9 expressing KBM7 cells harboring sgRNAs against the indicated genes. Pools were flow cytometry quantified at days 0, 7, 14 and 21 and mCherry percentages were normalized to day 0 percentage and to a non-targeting control sgRNA (sgMYCdesert). Data points are mean of 3 biological replicates.

(C) Scheme of targeted hybrid-capture approach coupled to next-generation sequencing to identify mutations in spontaneously resistant cells.

(D) Structure depiction of the CUL2-VBC-MZ1-BRD4 complex (PDBs: 5N4W, 5T35). Residues marked in red were identified in hybrid capture analysis. See also **Figure 1** and **Supplementary Table 2**.

(E) Number of spontaneous degrader resistance alterations in the substrate receptor (CRBN, VHL, colored) binned by their distance to the degrader binding site. See also **Figure 1D** and **Supplementary Table 2**.

Extended Data Figure 2

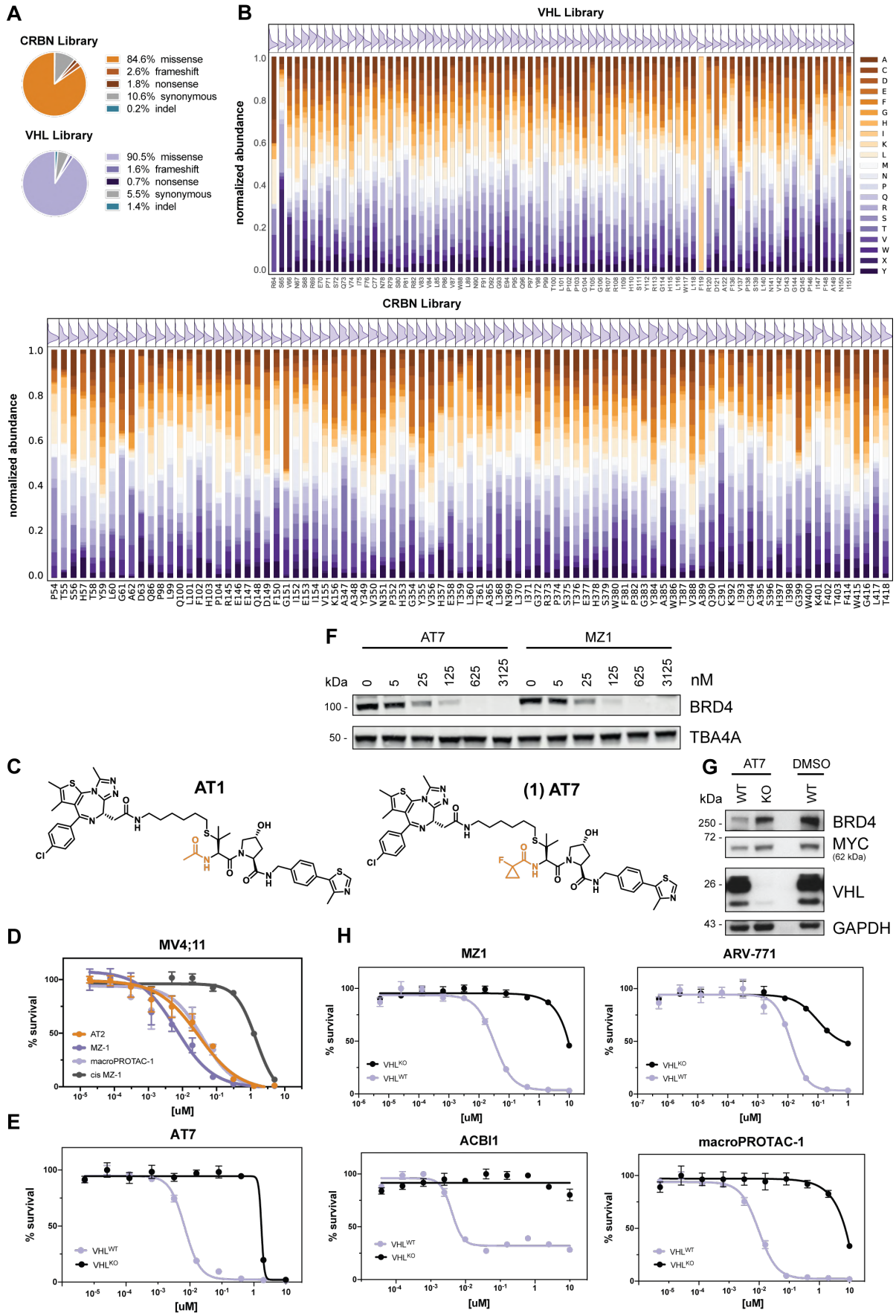

Extended Data Figure 2.

(A) Pie charts depicting the distribution of different alterations identified by sequencing the mutational scanning libraries for CRBN (top) and VHL (bottom).

(B) Stacked bar graphs and density distributions of residue wise normalized abundance of mutants identified in the DMS libraries for VHL (top) and CRBN (bottom).

(C) Chemical structure comparison of the degraders AT1 and AT2.

(D) Dose-resolved, normalized viability after 3 d treatment with MZ-1, macroPROTAC-1, cis MZ-1 (a non VHL binding control of MZ-1 or AT2 in MV4;11 cells. Mean ± s.e.m.; n = 3 independent treatments.

(E) Dose-resolved, normalized viability after 3 d treatment (AT2) in RKO VHL$^{-/-}$ cells with over-expression of VHL^{WT}. Mean ± s.e.m.; n = 3 independent treatments.

(F) Protein levels in HeLa cells treated with MZ-1 or AT2 (18h, indicated concentration).

(G) Protein levels in RKO VHL$^{-/-}$ cells with over-expression of VHL^{WT} treated with DMSO or AT2 (60 nM, 2 h).

(H) Dose-resolved, normalized viability after 4 d treatment (ACBI1) and 3 d treatment (ARV-771, MZ-1, macroPROTAC-1) in RKO VHL$^{-/-}$ cells with over-expression of VHL^{WT}. Mean ± s.e.m.; n = 3 independent treatments.

Extended Data Figure 3

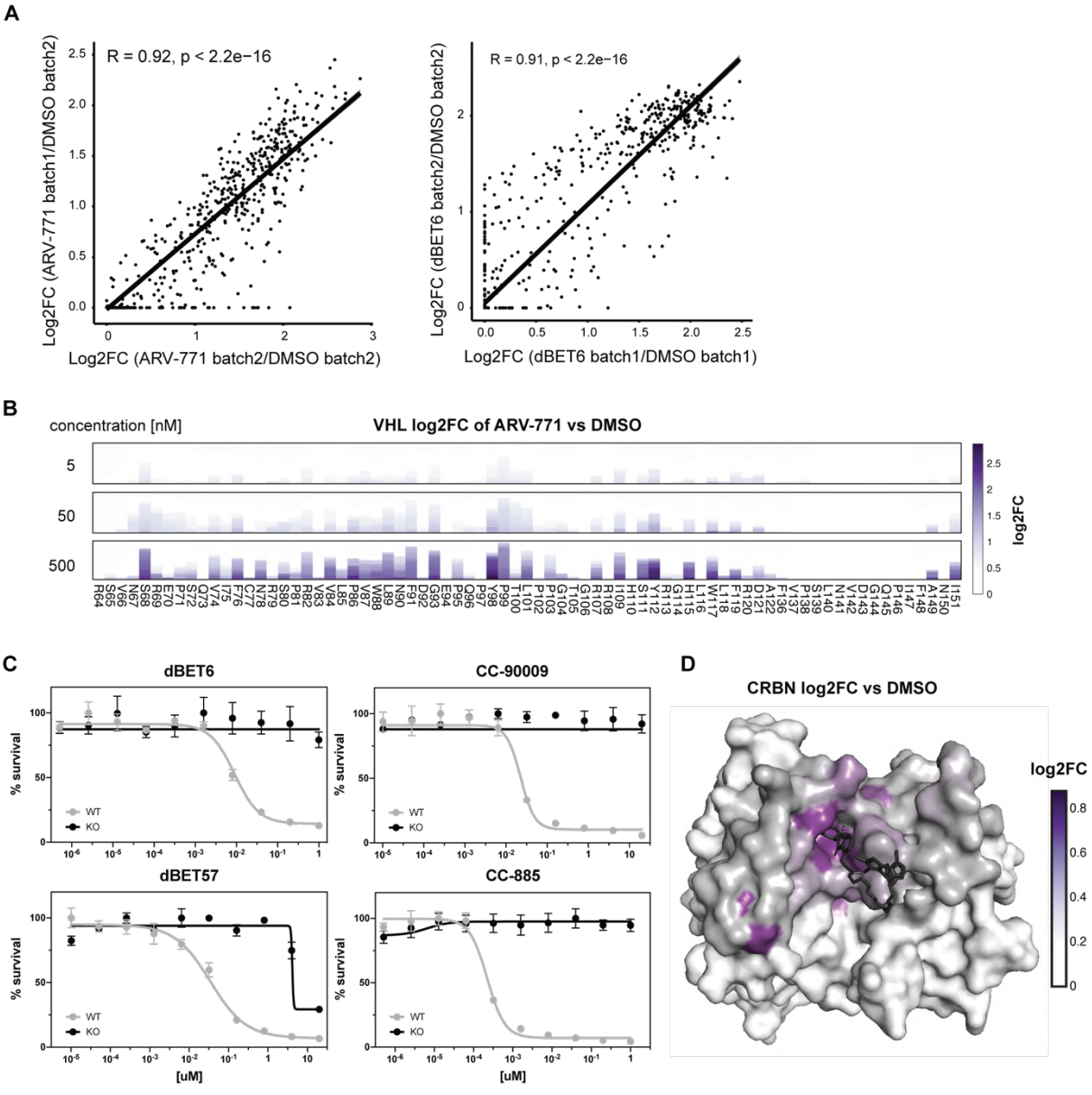

Extended Data Figure 3.

(A) Scatter plot depicting log2 fold-enrichment between different batch mutational scanning resistance measurements of VHL (500 nM ARV-771) or CRBN mutations (500 nM dBET6) normalized to DMSO after 7-day treatment. The rank-based measure of association was estimated via Spearman's rho statistic and reported P-values were calculated via asymptotic two-sided *t* approximation without adjustments for multiple comparisons.

(B) Stacked bar graphs of log2 fold-enrichment of VHL mutants normalized to DMSO treated with the indicated concentrations of ARV-771 for 7 days. n = 2 independent measurements.

(C) Dose-resolved, normalized viability after 3 d treatment with dBET6, CC-90009, dBET57 or CC-885 in RKO $CRBN^{-/-}$ cells with over-expression of $CRBN^{WT}$. Mean ± s.e.m.; n = 3 independent treatments.

(D) Surface structure of CRBN bound by dBET6 (PDB 6BOY). Median log2 fold-enrichment of all CRBN mutations over DMSO across 4 degrader treatments (see **Figure 2D**) is mapped in purple to dark grey onto positions mutated in the CRBN library.

Extended Data Figure 4.

(A and B) Dose-resolved, normalized viability after 4 d treatment (ACBI1) and 3 d treatment (MZ-1) in RKO $VHL^{-/-}$ cells with over-expression of VHL^{WT}, VHL^{R69G} or VHL^{N67Q}. Mean ± s.e.m.; n = 3 independent treatments.

(C and D) Depiction of clonogenic assays via crystal violet staining. RKO $VHL^{-/-}$ cells with over-expression of VHL^{WT}, VHL^{R69G}, VHL^{N67R} or VHL^{N67Q} were treated for 10 days at EC90 of the degrader (2.5 uM ACBI1, 50 nM ARV-771, 75 nM MZ-1).

(E) Protein levels in RKO $VHL^{-/-}$ cells with over-expression of VHL^{WT} or VHL^{N67Q} treated with DMSO, MZ-1 (75 nM, 2 h), ARV-771 (50 nM, 2 h) or ACBI1 (2.5 uM, 4 h).

(F) Cocrystal structure of MZ-1 in a ternary complex with VHL-ElonginC-ElonginB and $BRD4^{BD2}$ (PDB: 5T35).

(G) Heatmap depicting differential log2 fold-enrichment of the VHL^{H110} mutations normalized to DMSO after treatment with ARV-771 (500 nM, 7d). n = 2 independent measurements.

(H) Dose-resolved, normalized viability after 3d treatment AT2 (top), macroPROTAC-1 (bottom, left) or ARV-771 (bottom, right) in RKO $VHL^{-/-}$ cells with over-expression of VHL^{WT} or VHL^{H110L}. Mean ± s.e.m.; n = 3 independent treatments.

(I) Protein levels in RKO $VHL^{-/-}$ cells with over-expression of VHL^{WT} or VHL^{H110L} treated with DMSO or AT2 (60 nM, 2 h). Representative images of n = 2 independent measurements.

(J) Overlay of Cocrystal structures of AT2 (grey, purple, blue) and MZ1 (black, PDB:5T35) in a ternary complex with VHL-ElonginC-ElonginB and $BRD4^{BD2}$ showing a lateral shift of $BRD4^{BD2}$.

(K) Cocrystal structure of AT2 in a ternary complex with VHL-ElonginC-ElonginB and $BRD4^{BD2}$. See also Figure 3.

(L) Dose-resolved, normalized viability after 4 d treatment (ACBI1) and 3 d treatment (MZ-1, ARV-771) in RKO $VHL^{-/-}$ cells with over-expression of VHL^{WT} or VHL^{Y112C}. Mean ± s.e.m.; n = 3 independent treatments.

Extended Data Figure 4

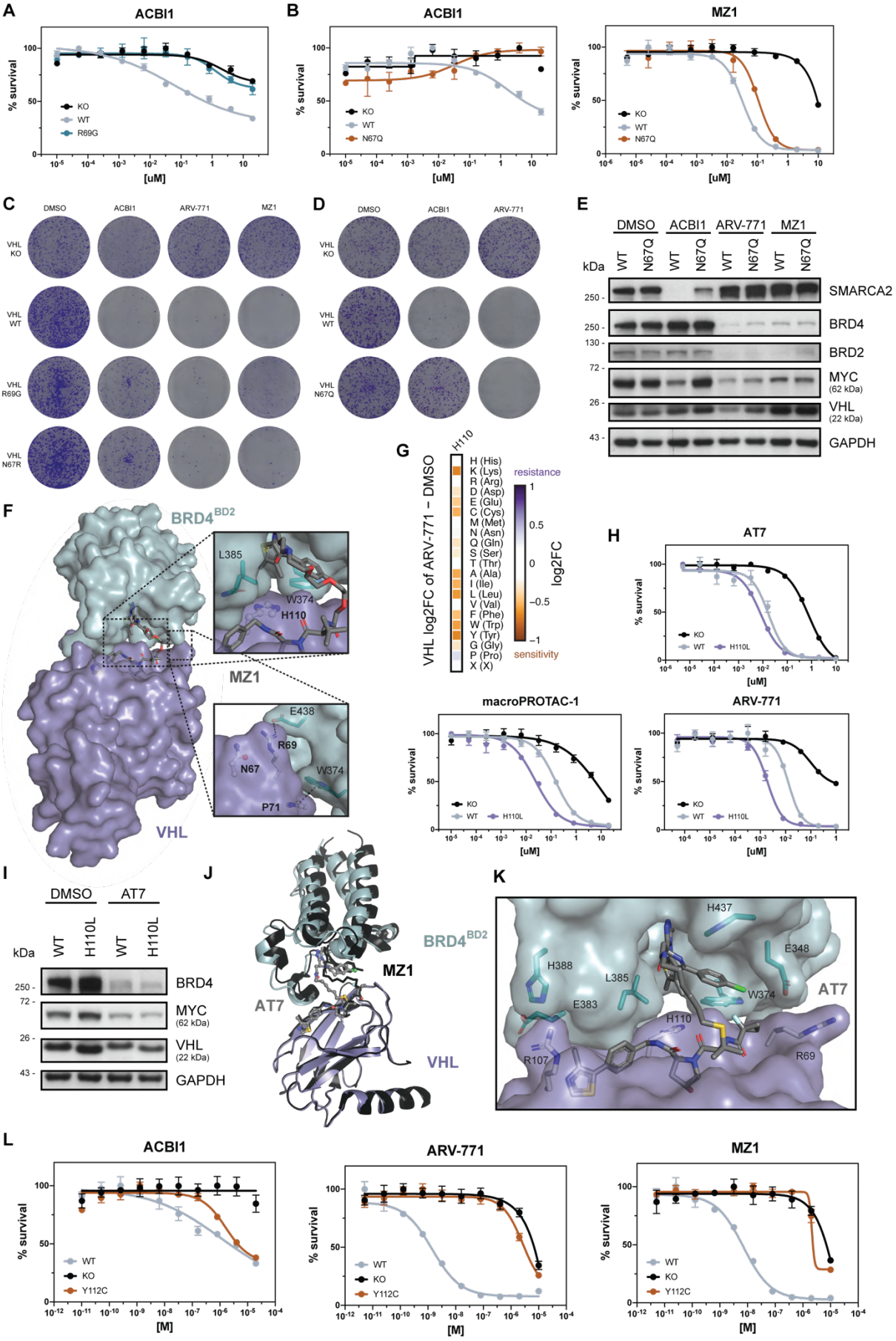

Extended Data Figure 5

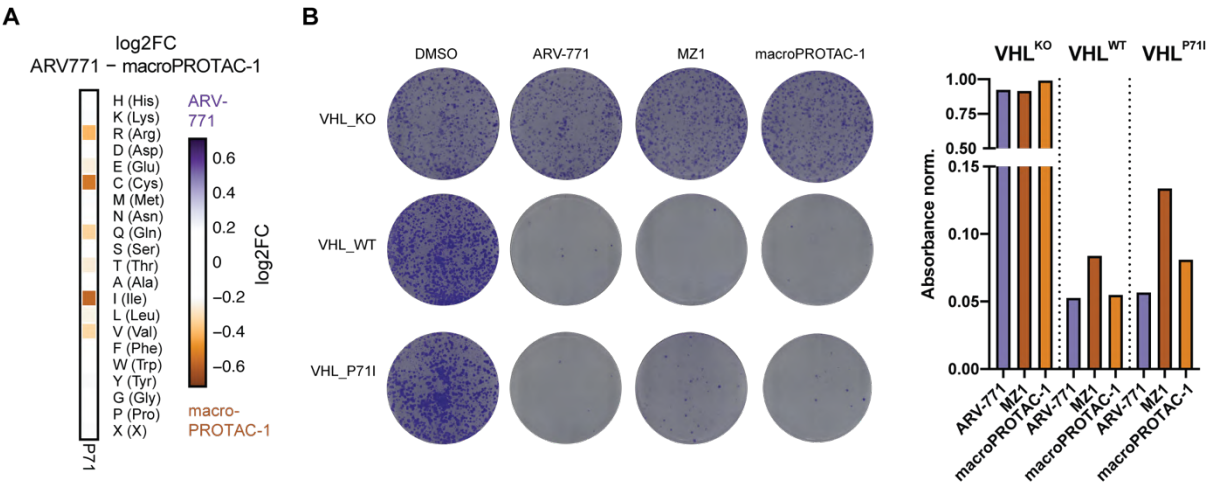

Extended Data Figure 5.
(A) Heatmap depicting differential log2 fold-enrichment of the VHL^{P71} mutations normalized to DMSO between treatment with ARV-771 (500 nM, 7d) and macroPROTAC-1 (2 uM, 7d). n = 2 independent measurements.
(B) Depiction (left) and quantification (right) of clonogenic assays via crystal violet staining. RKO $VHL^{-/-}$ cells with over-expression of VHL^{WT} or VHL^{P71I} were treated for 10 days at EC90 of the degrader (50 nM ARV-771, 75 nM MZ-1, 1 uM macroPROTAC-1).

Extended Data Figure 6.
(A, C and F) Depiction of clonogenic assays via crystal violet staining. RKO $CRBN^{-/-}$ cells with over-expression of $CRBN^{WT}$, $CRBN^{E377K}$, $CRBN^{N351D}$ or $CRBN^{H397D}$ were treated for 10 days with DMSO, 30 nM dBET6, 60 nM CC-90009, 480 nM dBET57 or the indicated concentration of THAL-SNS-032.
(B and G) Dose-resolved, normalized viability after 3 d treatment with THAL-SNS-032, dBET6 or CC-90009 in RKO $CRBN^{-/-}$ cells with over-expression of $CRBN^{WT}$, $CRBN^{N351D}$, $CRBN^{H397Y}$ or $CRBN^{H57D}$. Mean ± s.e.m.; n = 3 independent treatments.
(D) Protein levels in RKO $CRBN^{-/-}$ cells with over-expression of $CRBN^{WT}$ or $CRBN^{E377K}$ treated with DMSO, CC-90009 (50 nM, 6 h) or dBET6 (15 nM, 2 h). Representative images of n = 2 independent measurements.
(E) Heatmap depicting differential log2 fold-enrichment of $CRBN^{H397}$ mutations normalized to DMSO with dBET57 treatment (500 nM, 7d). n = 3 independent measurements.
(H) Quantification of clonogenic assays via crystal violet extraction and measurement of absorption at 590 nM. RKO $CRBN^{-/-}$ cells with over-expression of $CRBN^{WT}$ or $CRBN^{H57D}$ were treated for 10 days with DMSO, 30 nM dBET6, 60 nM CC-90009, 480 nM dBET57 or 0.6 nM CC-885. See also Figure 5.
nts are mean of 3 biological replicates.
(C) Scheme of targeted hybrid-capture approach coupled to next-generation sequencing to identify mutations in spontaneously resistant cells.
(D) Structure depiction of the CUL2-VBC-MZ1-BRD4 complex (PDBs: 5N4W, 5T35). Residues marked in red were identified in hybrid capture analysis. See also Figure 1 and Supplementary Table 2
(E) Number of spontaneous degrader resistance alterations in the substrate receptor (CRBN, VHL, colored) binned by their distance to the degrader binding site. See also **Figure 1D** and **Supplementary Table 2**.

Extended Data Figure 6

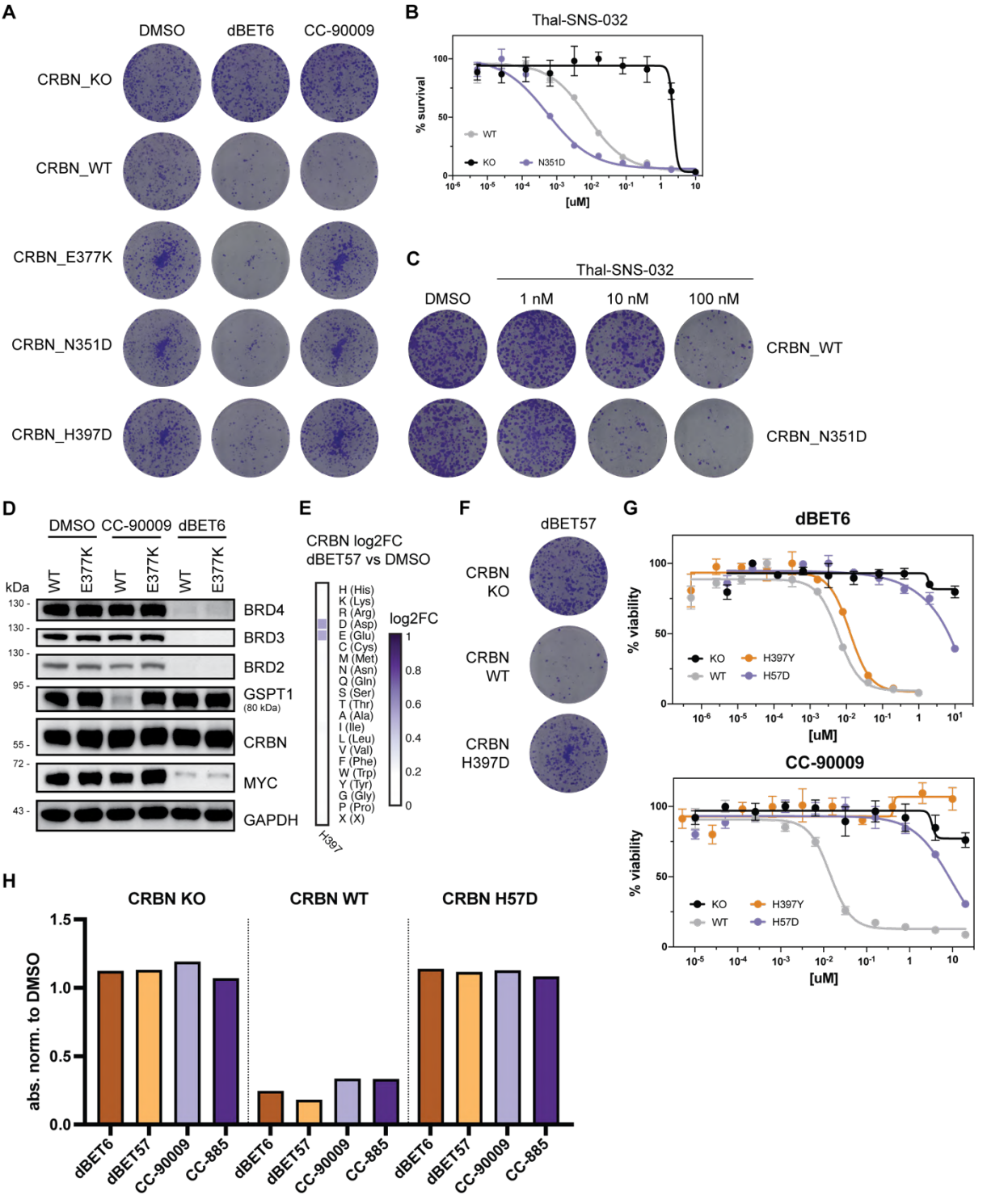

Supplementary Note

Table of Contents:

Supplementary Table 1:

List of genes included in xGen Gene Capture Pool

Gene	Function	Median DepMap CRONOS score
BRD2	target	-0.34
BRD3	target	0.11
BRD4	target	-1.05
CAND1	SR exchange	-0.32
CAND2	SR exchange	0.03
COPS2	de-neddylation	-1.15
COPS3	de-neddylation	-0.88
COPS4	de-neddylation	-0.98
COPS5	de-neddylation	-1.61
COPS6	de-neddylation	-1.50
COPS7A	de-neddylation	-0.03
COPS7B	de-neddylation	0.05
COPS8	de-neddylation	-1.11
COPS8	de-neddylation	-1.11
COPS9	de-neddylation	-0.14
CRBN	CRL4 subunit	0.00
CUL2	CRL2	-0.51
CUL4A	CRL4	-0.03
CUL4B	CRL4	-0.01
DDB1	CRL4 subunit	-1.95
ELOB	CRL2 subunit	-1.46
ELOC	CRL2 subunit	-1.17
GPS	de-neddylation	-0.69
NAE1	neddylation	-1.31
RBX1	CRL subunit	-1.34
UBA3	neddylation	-0.93
UBE2F	neddylation	-0.01
UBE2G1	E2 enzyme	-0.03
UBE2M	neddylation	-1.21
UBE2R2	E2 enzyme	-0.04
VHL	CRL2 subunit	-0.96

Supplementary Table 3: Degraders applied in this study

Degrader	Structure	Targets	ref.
ARV-771	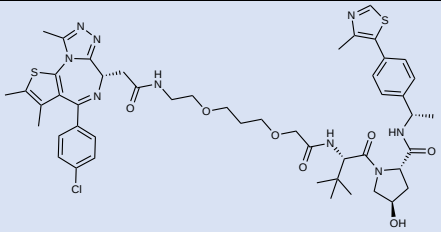	BRD4, BRD3, BRD2	ref. 26
MZ-1	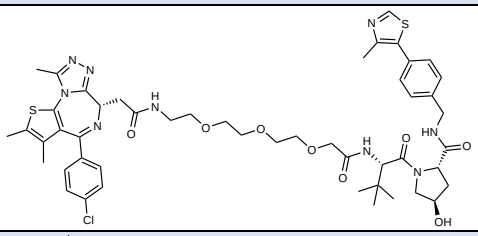	BRD4, BRD3, BRD2	ref. 33
cis-MZ-1	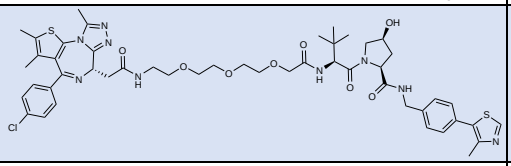	non VHL interacting inhibiting BRD4, BRD3, BRD2	ref. 33
macroPROTAC-1	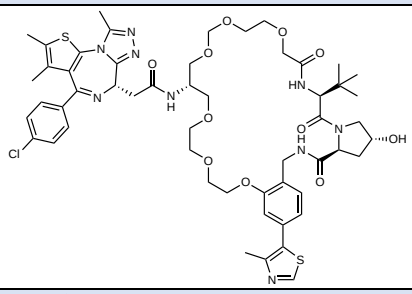	BRD4, BRD3, BRD2	ref. 34
AT7	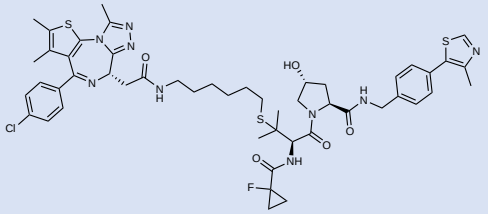	BRD4, BRD3, BRD2	this publication
ACBI-1	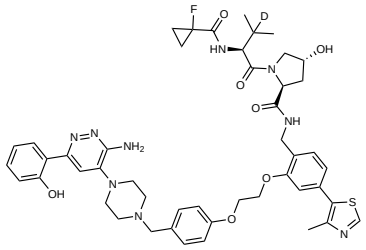	SMARCA2, SMARCA4, PBRM1	ref. 35
dBET6	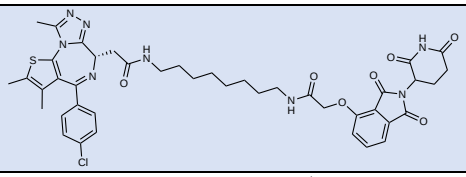	BRD4, BRD3, BRD2	ref. 27
dBET57	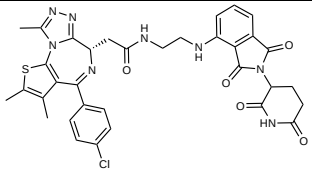	BRD4, BRD3, BRD2	ref. 11
CC-885	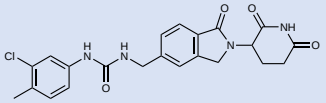	GSPT1	ref. 37
CC-90009 (Eragidomide)	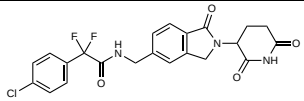	GSPT1	ref. 38

Supplementary Table 4: Crystallographic data collection and refinement statistics.

Data Collection	
Space Group	$P3_2$
Cell Dimensions	
a, b, c (Å)	82.6, 82.6, 169.6
α, β, γ, (°)	90.0, 90.0, 120.0
Resolution (Å)	65.9 – 3.0 (3.2 – 3.0)*
No. unique reflections	25970 (4234)
R_{merge} (%)	23.1 (96.6)
I/σ (I)	9.4 (5.3)
$CC_{1/2}$	99.2 (71.3)
Completeness (%)	100.0 (100.0)
Redundancy	9.9 (10.2)
Refinement	
R_{work}/R_{free} (%)	21.3/25.1
R.m.s. deviations	
Bond lengths (Å)	0.007
Bond angles (°)	1.363

* Values in parentheses are for highest-resolution shell.

Supplementary table 5. Oligo sequences

sgRNAs cloned into the plasmid pSpCas9(BB)-2A-GFP Addgene (48138)	
Gene Name	**Sequence**
CRBN	TGTATGTGATGTCGGCAGAC
VHL	GCGATTGCAGAAGATGACCT

sgRNAs cloned into the plasmid Lenti_sgRNA_EFS_GFP (Addgene #65656)	
Gene Name	**Sequence**
VHL (766)	CGCCGCATCCACAGCTACCG
VHL (767)	AGAGATGCAGGGACACACGA
GAPDH	GATCCCTCCAAAATCAAGTG
RPL5	GATCTATGAAGGCCAAGTGG

Oligos for amplification of CRBN and VHL for DMS	
Primer Name	**Sequence**
CRBN_GA fwd	aggtgtcgtgacgtacgggatcccaggaccATGGCCGGCGAAGGAG
CRBN_GA rev	gggggggggcggaattaattcctactacTTACAAGCAAAGTATTACTTTGTCTGGAC
VHL_GA fwd	aggtgtcgtgacgtacgggatcccaggaccatgccccggagggcggag
VHL_GA rev	gggggggggcggaattaattcctactactcaatctcccatccgttgatgtgcaatgcg

Supplementary Figure 1: VHL deep mutational scanning results

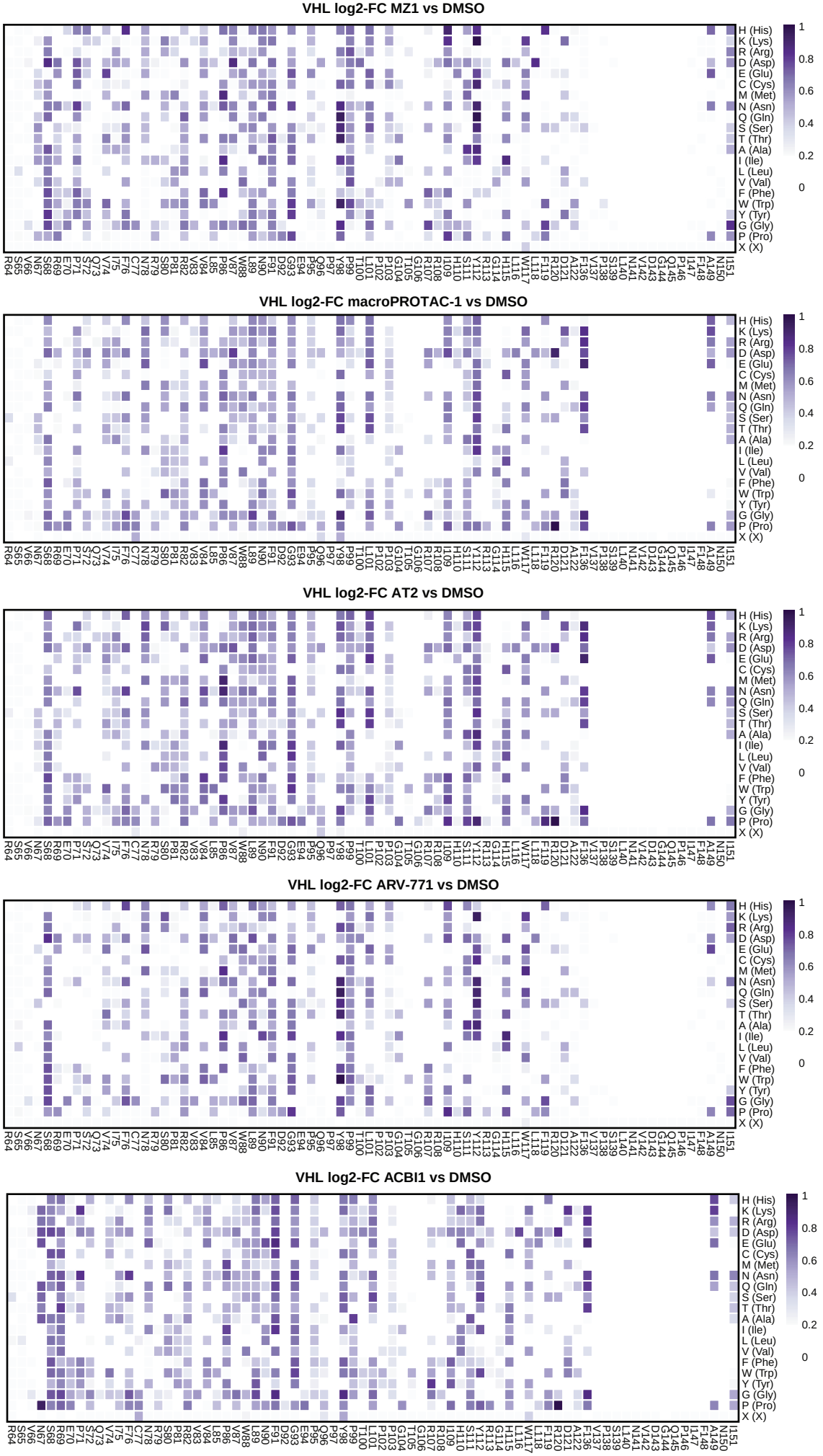

Supplementary Figure 2: CRBN deep mutational scanning results

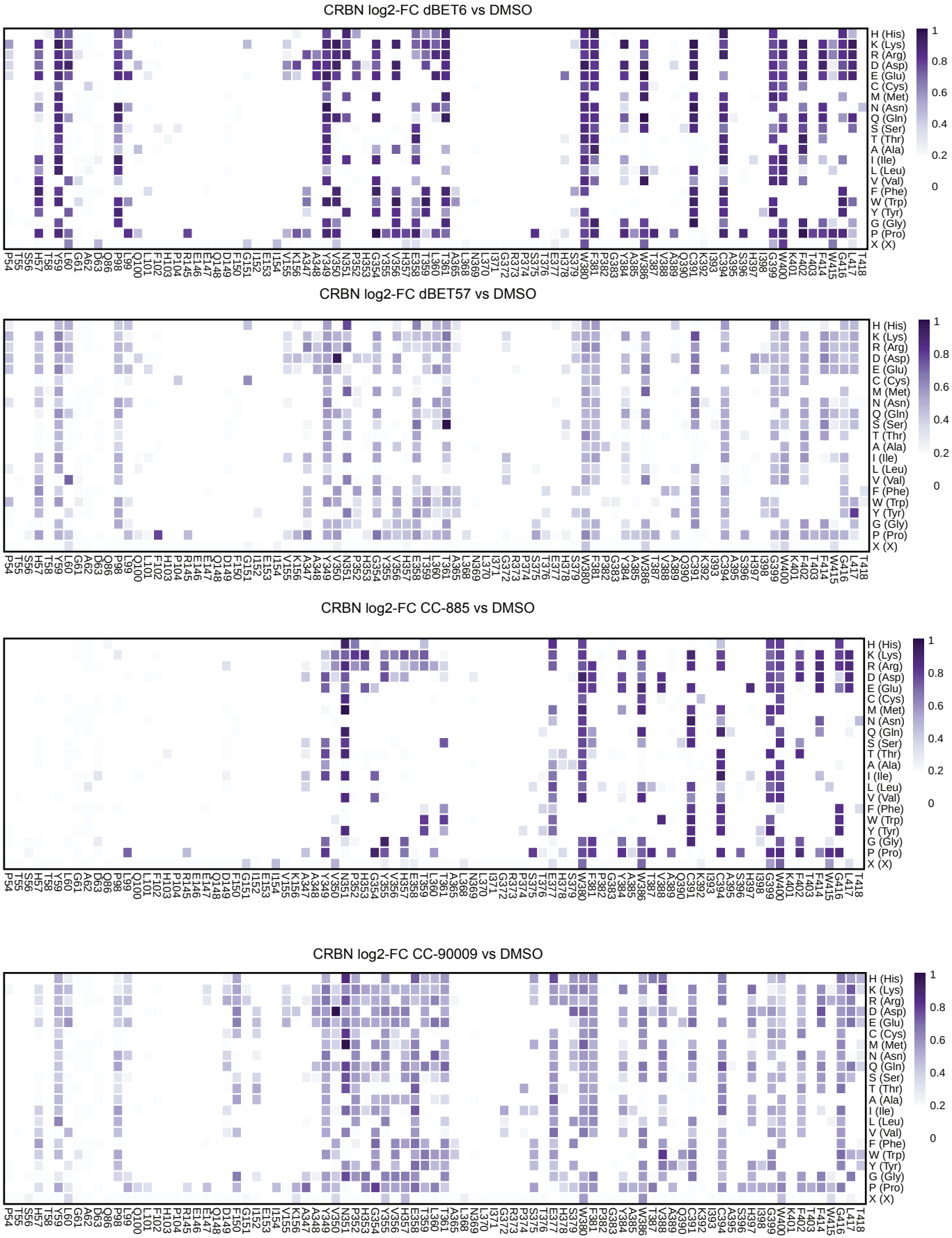

Supplementary Figure 3

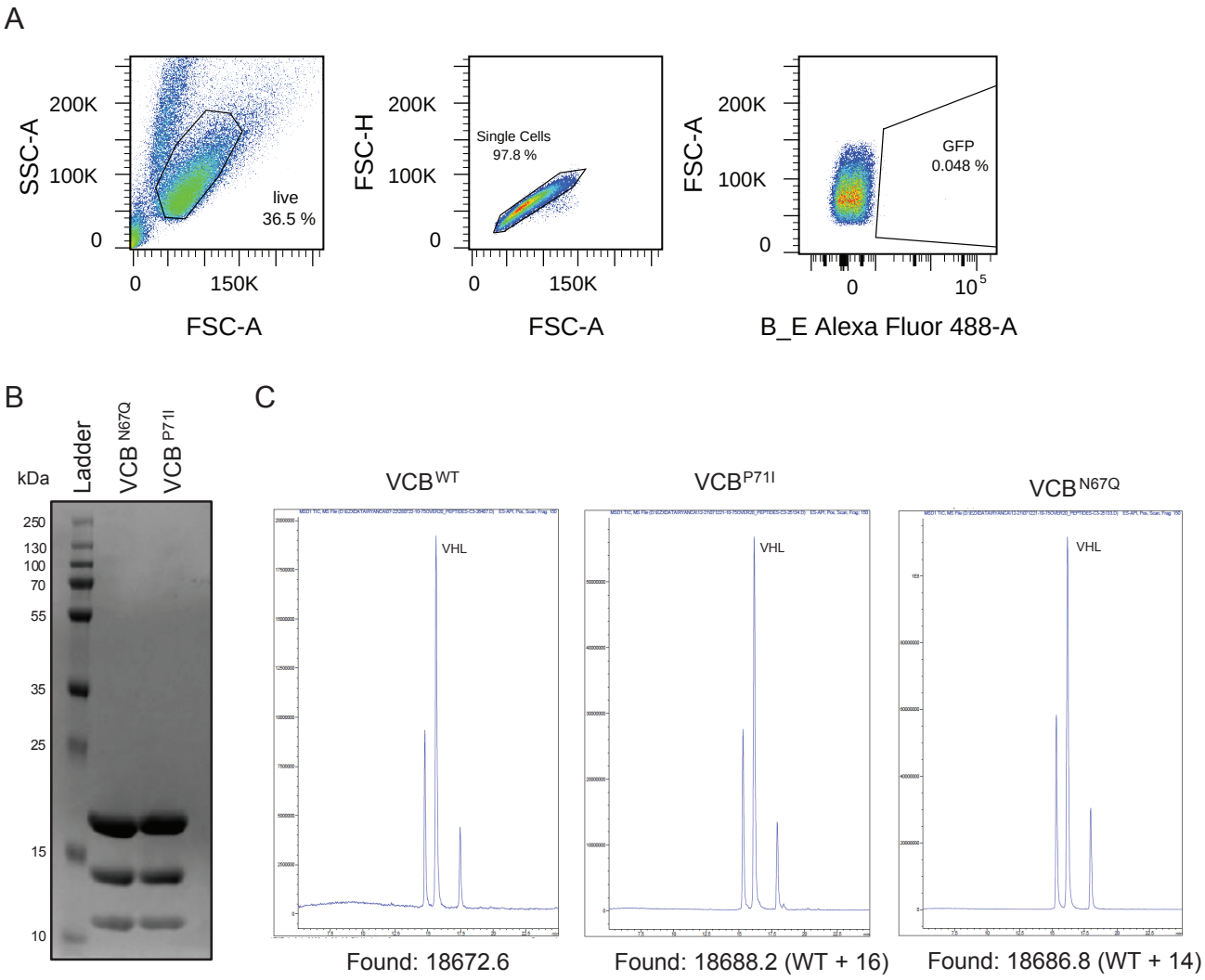

Supplementary Figure 3: Gating Strategy and Characterization of Recombinant Protein
(A) Gating strategy for evaluating the percentage of GFP positive cells related to Extended Data Fig 1B. Shown are untransduced control cells for setting the GFP gate.
(B) Analysis of mutant protein purity and identity following recombinant expression and purification. NuPAGE gel (12% Bis-Tris) of final purified protein sample following staining with InstantBlue with V*BC components running at the expected molecular weights at high purity.
(C) Mass spectrometry chromatogram of final protein samples following separation by HPLC on a C3 column using a gradient of 10 to 75 % acetonitrile over 20 minutes. Data was analysed using an Agilent 6130 quadrupole MS and deconvoluted using Agilent LC/MSD ChemStation and the correct mass shift was identified for each smutant protein when compared to wild-type.

Chemical synthesis of AT7

(2S,4R)-1-((R)-2-(1-fluorocyclopropane-1-carboxamido)-3-methyl-3-(tritylthio)butanoyl)-4-hydroxy-N-(4-(4-methylthiazol-5-yl)benzyl)pyrrolidine-2-carboxamide (3)

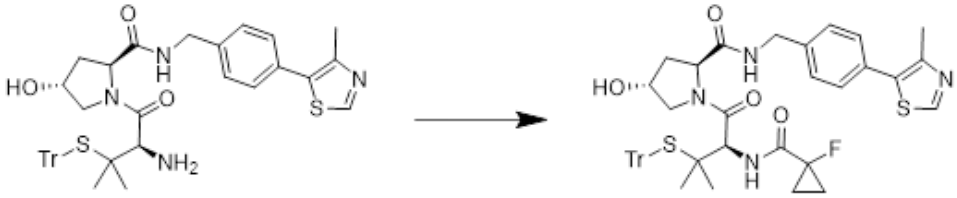

2 **3**

To a solution of **2** (ref. 10) (48 mg, 0.068 mmol) in DMF (0.5 mL) at room temperature, DIPEA (30 µL, 0.172 mmol), HOAT (9mg, 0.068), HATU (26mg, 0.068) and 1-fluorocyclopropanecarboxylic acid (7mg, 0.068 mmol) were added. The mixture was let to react at room temperature for 2 hours. The reaction mixture was cooled to room temperature, filtered and purified by preparative HPLC to give the product (40 mg, 83% yield). MS analysis: $C_{44}H_{45}FN_4O_4S_2$ expected 776.3, found 777.5 [M+H$^+$].

^{1}H NMR (400 MHz, CDCl3) d 8.71 (s, 1H), 7.55 - 7.52 (m, 6H), 7.34 - 7.31 (m, 3H), 7.24 - 7.19 (m, 12H), 4.66 (t, J=8.1 Hz, 1H), 4.37 (br s, 1H), 4.32 - 4.19 (m, 2H), 3.65 (d, J=5.2 Hz, 1H), 3.51 (d, J=11.6 Hz, 1H), 3.26 (dd, J=3.8, 11.6 Hz, 1H), 3.09 (d, J=6.0 Hz, 1H), 2.52 (s, 3H), 2.41 - 2.33 (m, 1H), 2.14 - 2.07 (m, 1H), 1.38 - 1.23 (m, 4H), 1.21 (s, 3H), 0.98 (s, 3H).

^{13}C-NMR (101 MHz, CDCl3, 25 °C) δ: 170.6, 170.4 (J_{C-F} = 20 Hz), 170.0, 150.4, 148.6, 144.4, 138.2, 131.8, 130.9, 129.9, 129.6, 128.04, 127.99, 127.0, 77.4 (J_{C-F} = 207 Hz), 70.2, 68.5, 58.5, 57.0, 56.6, 53.7, 43.0, 36.4, 26.1, 25.7, 16.3, 13.9 (J_{C-F} = 10 Hz), 13.7 (J_{C-F} = 10 Hz).

(*2S,4R*)-1-((*R*)-2-acetamido-3-mercapto-3-methylbutanoyl)-4-hydroxy-*N*-(4-(4-methylthiazol-5-yl)benzyl)pyrrolidine-2-carboxamide (4)

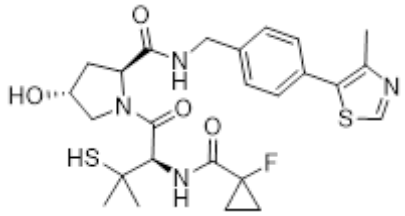

4

Compound **3** (40 mg, 0.057 mmol) was dissolved in 2 mL of DCM. TIPS (0.2 mL) and TFA (0.2 mL) were added, and the yellow mixture was let to react at room temperature for one hour after which LCMS showed complete conversion of the starting material. Volatiles were removed under vacuum and the crude was purified by FCC (from 0 to 15 % of MeOH in DCM) to afford the title compound **4** as a white solid (24 mg, 80% yield). MS analysis: $C_{25}H_{31}FN_4O_4S_2$ expected 534.2, found 535.3 [M+H$^+$].

^{1}H NMR (500 MHz, MeOD) d 8.91 (s, 1H), 8.74 (t, J=5.2 Hz, 1H), 7.72 (d, J=8.3 Hz, 1H), 7.46 (d, J=8.1 Hz, 2H), 7.42 (d, J=7.9 Hz, 2H), 4.93 (d, J=9.0 Hz, 1H), 4.59 (t, J=8.3 Hz, 1H), 4.56 - 4.49 (m, 2H), 4.36 (dd, J=4.8, 15.4 Hz, 1H), 3.96 - 3.85 (m, 2H), 2.47 (s, 3H), 2.25 (dd, J=7.8, 13.1 Hz, 1H), 2.12 - 2.06 (m, 1H), 1.46 (s, 3H), 1.43 - 1.27 (m, 8H).

^{13}C-NMR (101 MHz, CDCl3, 25 °C) δ: 174.2, 171.6 (J_{C-F} = 20 Hz), 170.7, 153.0, 148.7, 140.2, 133.6, 131.4, 130.4, 129.0, 78.2 (J_{C-F} = 230 Hz), 71.0, 61.0, 59.0, 58.1, 47.8, 43.7, 39.0, 30.2, 29.1, 15.7, 14.11 (J_{C-F} = 10 Hz), 14.07 (J_{C-F} = 10 Hz).

(*2S,4R*)-1-((*R*)-2-acetamido-3-((6-aminohexyl)thio)-3-methylbutanoyl)-4-hydroxy-*N*-(4-(4-methylthiazol-5-yl)benzyl)pyrrolidine-2-carboxamide (5)

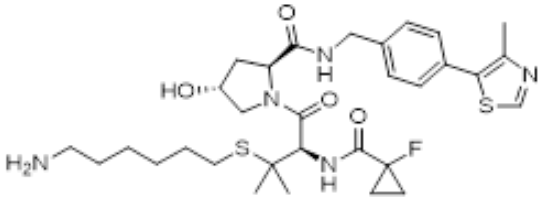

5

Under nitrogen and at 0 °C, a solution of compound **4** (24 mg, 0.045 mmol) in DMF (0.5 mL) was treated with DBU (7.5 µL, 0.049 mmol) followed by *N*-(4-Bromohexyl)phthalimide (15.2 mg, 0.049 mmol). After three hours LCMS indicated the reaction was complete, the reaction mixture was diluted with citric acid solution and extracted with DCM and the volatiles were removed under reduced pressure to afford the crude product. The crude alkylated product was then dissolved in ethanol (2 mL) and treated with hydrazine monohydrate (22 µL, 0.29 mmol) at 70 °C for two hours. The reaction mixture was cooled to room temperature, filtered and purified by preparative HPLC to give the expected amine **5** (17 mg, 60% yield). MS analysis: $C_{31}H_{44}FN_5O_4S_2$ expected 633.3, found 634.5 [M+H$^+$].

^{1}H NMR (500 MHz, MeOD) d 8.88 (s, 1H), 8.55 (s, 1H), 7.47 (d, J=8.5 Hz, 2H), 7.43 (d, J=8.5 Hz, 2H), 4.92 (s, 1H), 4.61 (t, J=8.2 Hz, 1H), 4.56 (d, J=15.4 Hz, 1H), 4.51 (s, 1H), 4.36 (d, J=15.7 Hz, 1H), 3.91 - 3.85 (m, 2H), 2.86 (t, J=7.7 Hz, 2H), 2.59 (t, J=7.2 Hz, 2H), 2.48 (s, 3H), 2.26 (dd, J=8.5, 12.6 Hz, 1H), 2.14 - 2.06 (m, 1H), 1.62 - 1.54 (m, 2H), 1.53 - 1.46 (m, 2H), 1.42 (s, 6H), 1.40 - 1.27 (m, 8H).

^{13}C-NMR (101 MHz, CDCl3, 25 °C) δ: 174.1, 171.4 (J_{C-F} = 20 Hz), 170.7, 152.9, 149.1, 140.2, 133.4, 131.6, 130.4, 128.9, 78.2 (J_{C-F} = 230 Hz), 71.0, 61.1, 58.1, 57.2, 49.9, 43.6, 40.7, 39.1, 30.4, 29.5, 29.2, 28.7, 27.2, 27.1, 25.4, 15.8, 14.0 (J_{C-F} = 10 Hz).

(2S,4R)-1-((R)-3-((6-(2-((S)-4-(4-chlorophenyl)-2,3,9-trimethyl-6H-thieno[3,2-f][1,2,4]triazolo[4,3-a][1,4]diazepin-6-yl)acetamido)hexyl)thio)-2-(1-fluorocyclopropane-1-carboxamido)-3-methylbutanoyl)-4-hydroxy-N-(4-(4-methylthiazol-5-yl)benzyl)pyrrolidine-2-carboxamide (1, AT7)

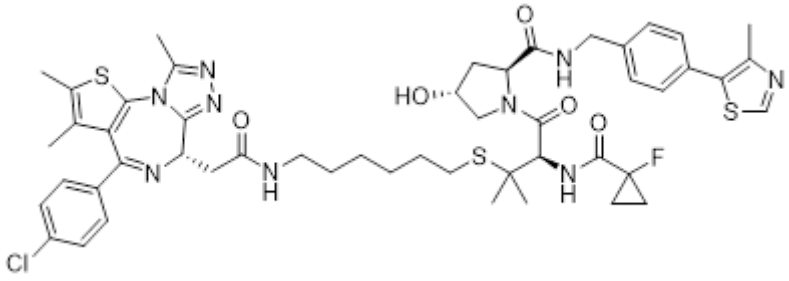

1, AT7

Compound **5** (17 mg, 0.0269 mmol) was dissolved in DMF (0.25 mL) and added to a solution of(*S*)-2-(4-(4-chlorophenyl)-2,3,9-trimethyl-6H-thieno[3,2-f][1,2,4]triazolo[4,3-a][1,4]diazepin-6-yl)acetic acid (+)-JQ1-COOH (11 mg, 0.0269 mmol), COMU (12 mg, 0.0269 mmol), and DIPEA (10 µl, 0.0537 mmol) in DMF (0.25 mL). After stirring at room temperature for 1 h. The crude mixture was dissolved in MeOH, filtered and purified by preparative HPLC to afford the title compound. Obtained 14.6 mg, 53% yield. MS analysis: $C_{50}H_{59}ClFN_9O_5S_3$ expected 1015.35, found 1016.36 [M+H$^+$].

^{1}H NMR (500 MHz, MeOD) d 8.94 (s, 1H), 8.62 (t, J=5.7 Hz, 1H), 7.74 (d, J=9.1 Hz, 1H), 7.49 - 7.42 (m, 9H), 4.94 (d, J=8.5 Hz, 1H), 4.68 - 4.62 (m, 2H), 4.58 (dd, J=10.5, 10.5 Hz, 1H), 4.52 (s, 1H), 4.39

(dd, J=4.9, 15.6 Hz, 1H), 3.94 - 3.87 (m, 2H), 3.44 (dd, J=9.2, 14.8 Hz, 1H), 3.31 - 3.25 (m, 2H), 3.25 - 3.16 (m, 1H), 2.73 (s, 3H), 2.64 - 2.56 (m, 2H), 2.50 (s, 3H), 2.47 (s, 3H), 2.29 (dd, J=7.7, 13.3 Hz, 1H), 2.17 - 2.09 (m, 1H), 1.72 (s, 3H), 1.57 - 1.47 (m, 4H), 1.44 (s, 6H), 1.41 - 1.32 (m, 8H).

^{13}C-NMR (101 MHz, CDCl3, 25 °C) δ: 174.1, 172.6, 171.5 (J_{C-F} = 20 Hz), 170.9, 166.3, 157.0, 153.0, 152.2, 148.8, 140.3, 138.1, 138.0, 133.6, 133.5, 133.4, 132.1, 132.0, 131.4, 131.3, 130.4, 129.8, 128.9, 78.2 (J_{C-F} = 230 Hz), 71.0, 61.1, 58.1, 57.3, 55.2, 49.9, 43.6, 40.4, 39.0, 38.7, 30.6, 30.3, 29.8, 29.3, 27.6, 27.1, 25.6, 15.8, 14.4, 14.1 (J_{C-F} = 10 Hz), 14.0 (J_{C-F} = 10 Hz), 12.9, 11.6.

2.2 Tracing E3 Ligase Abundance Empowers Degrader Discovery at Scale

2.2.1 Interlude

The previous results in section 2.1.2 have demonstrated several key points leading to the conclusion, that additional E3 ligases amendable to small-molecule mediated TPD are desperately needed to improve the prospects of this novel therapeutic paradigm. Firstly, resistance mutations seem to primarily arise at the SR of an E3 ligase, placing this at the center of attention for preventing resistances. Secondly, the frequency and type of mutations is correlated with intrinsic properties of said E3 ligase, where targeting an essential SR seems to lower emergence of resistance. Furthermore, there are even more arguments to expand the targetable E3 ligase space. For PROTACs, ternary complex formation is heavily influenced by the E3 ligase engaged and hence cooperativity measures and resulting degradation efficiencies can vary dramatically between degraders of the same POI. Finally, to date only molecular glue degraders have proven successful in clinical settings, while PROTACs remain under clinical investigation. Together this highlights the need for methods to identify novel small-molecule binders and modulators of E3 ligases.

In the following results part, we report a scalable approach that allows discovery of E3 ligase binders modulating the ligase substrate space. This method is based on initiating a state of auto-degradation where the E3 ligase is ubiquitinating itself, which can be rescued via degrader treatment. We outline a proof-of-concept with the two most commonly adopted E3 ligases in TPD (CRBN and VHL) and show that this approach is potentially viable for hundreds of SRs. Finally, we set out to discover novel molecular glue degraders for the CRL4 SR DCAF15 and in a chemical screen identify dRRM-1. In follow-up experiments we show that dRRM-1 facilitates degradation of RBM39 and RBM23 in a DCAF15 dependent manner validating the use of our presented method for degrader discovery.

The author of this thesis conceptualized this work together with his supervisor Georg Winter and performed all E3 ligase luciferase assays as well as proteomics studies. Cell line generation and validation experiments were performed by the author together with members of the Winter Lab and biochemical characterization of dRRM-1 was contributed by collaborators. The specific author contributions can further be taken from the respective section in the publication.

2.2.2 Results

Results section 2.2.2 contains a full PDF reprint of the manuscript ‘Tracing E3 Ligase Abundance Empowers Degrader Discovery at Scale’ by Alexander Hanzl et al. currently submitted to Cell Chemical Biology. The author of this thesis is an author of the article and thus retains the right to include a reprint in full in this thesis. Other rights remain with the publisher Elsevier Inc. and the journal Cell Chemical Biology.

Tracing E3 Ligase Abundance Empowers Degrader Discovery at Scale

Alexander Hanzl[1], Eleonora Barone[1], Sophie Bauer[1,5], Hong Yue[2,3], Radosław P. Nowak[3,4], Elisa Hahn[1], Eugenia V. Pankevich[1], Christoph Bock[1], Eric S. Fischer[2,3,4], Georg E. Winter[1]

Affiliations

[1] CeMM Research Center for Molecular Medicine of the Austrian Academy of Sciences, 1090 Vienna, Austria

[2] Department of Cancer Biology, Dana-Farber Cancer Institute, Boston, MA, USA

[3] Department of Biological Chemistry and Molecular Pharmacology, Harvard Medical School, Boston, MA, USA

[4] Center for Protein Degradation, Dana-Farber Cancer Institute, Boston, MA, USA

[5] present address: Proxygen GmbH, 1030 Vienna, Austria

[#]correspondence to gwinter@cemm.oeaw.ac.at

Abstract

Chemically inducing proximity between two proteins of interest has bootstrapped many advances in chemical biology including the therapeutic modality called targeted protein degradation. The identification that thalidomide analogues recruit zinc finger proteins to the E3 ligase CRBN marking them for degradation has coined the term molecular glue degraders. While since then development of chemically modular PROtein Targeting Chimeras (PROTACs) has thrived, methods for identification of the small monovalent molecular glue degraders have remained elusive. Here we make use of the NEDD8 - cullin RING ligase regulatory circuity to develop a scalable assay reporting on drug induced changes to the interactome of an E3 ligase of interest. By tracing the abundance of E3 ligase substrate receptors we show that degrader mediated neo-substrate recruitment to CRL^{CRBN} and CRL^{VHL} rescues the ligase from self-inflicted degradation. We next benchmark this method in a proof-of-concept screen using sulfonamides on CRL^{DCAF15} and identify a chemically distinct molecular glue degrader of RBM39 and RBM23. Finally, via global proteomics we chart the space of E3 ligases amendable to this approach in our chosen cellular model and validate in select cases this viability. Together, this method empowers the scalable identification of molecular glue degraders specific to a ligase of interest targeting suitably expressed proteins.

Introduction

Proximity between molecules is a central regulating factor in a wide variety of cellular processes. In the past 30 years, drug discovery efforts have been channeled to chemically induce proximity between two target proteins to elicit a therapeutic response[1]. Next to inhibition of one or both binding partners, the desired effect can also be achieved via gaining neo-morphic functions. The novel pharmacology of targeted protein degradation (TPD) presents such a case, where molecules commonly called degraders recruit proteins of interest (POIs) to E3 ligases ensuing neo-substrate ubiquitination and subsequent proteasomal degradation[2]. Most E3 ligases that have so far been employed for this therapeutic paradigm are of the cullin RING ligase (CRL) family. This family entails approximately 250 distinct ligase complexes centered around one of seven cullin scaffolding proteins[3]. Next to this structural similarity CRLs also share a common layer of activity regulation centered around the deposition and removal of the small ubiquitin like modifier NEDD8. “De-neddylation” from the cullin backbone by the COP9 signalosome (CSN) allows reshaping the CRL ubiquitinated proteome in a cell by exchanging the substrate recruiting factors of CRLs[4]. Conversely, attachment of NEDD8 on the cullin backbone stabilizes an active CRL complex primed for ubiquitination of a substrate, enhancing its enzymatic ability up to 2000 fold[5]. In absence of continuous supply of substrate, this activity can be targeted towards the CRL’s own substrate receptor (SR) in a process termed “auto-degradation”.

Of the large variety of CRLs only few select cases have so far been harnessed for TPD, primarily via so-called hetero-bifunctional proteolysis targeting chimeras (PROTACs)[6]. These degraders bind the E3 ligase and the POI with distinct chemical moieties connected by a linker. While this modular design allows facile chemical and thereby neo-substrate alteration, the degradable proteomic space is limited to ligandable targets. The promise of significantly expanding the druggable proteome via targeted degradation however has so far almost exclusively been fulfilled by a second more elusive class called molecular glue (MG) degraders. These monovalent small molecules stabilize a recognition surface between the ligase and the POI via degrader-protein and protein-protein interactions (PPIs). Mechanistic dissection of the clinically approved immunomodulatory drugs (IMiDs) has unveiled such a mechanism for the $CRL4^{CRBN}$ dependent degradation of zinc finger transcription factors. This notion has further been expanded to the targeted degradation of splicing and translation factors via a select set of E3 ligases including CRL^{DCAF15}.

Recent advances in chemoproteomics workflows have augmented the identification of E3 ligase binders conducive to PROTAC development, yet not necessarily to MG degraders. To empower the latter, a scalable technology measuring the drug induced changes in the E3 ligase interactome would be required. Methods yielding such proteome wide interaction data lack however the throughput to investigate thousands of small molecules. At the same time high throughput screening has traditionally been confined to readouts of pre-defined small molecule mediated PPIs, also in the context of TPD. Here, we leverage the unique regulatory dynamics of CRLs to design a scalable assay informing on drug induced changes to an E3 ligase interactome. We find that degrader mediated neo-substrate recruitment to CRL^{CRBN} rescues the ligase from self-inflicted degradation. By utilizing luciferase tagging and pharmacologic inhibition of the CSN to increase the E3 ligase auto-degratory potential this assay

allows degrader screening in a target agnostic way. We first benchmark this assay with several PORTACs targeting CRL^{VHL} followed by a proof-of-concept screen using sulfonamides on CRL^{DCAF15}. Validation of the hit compound dRRM-1 revealed a chemically distinct molecular glue degrader of RBM39 and RBM23. We furthermore show that a large number of E3 ligases are potentially amendable to this approach in a cell line specific manner by using substrate receptor abundance as a proxy for ligase activity. Taken together, this technology can empower the scalable identification of molecular glue degraders specific to a ligase of interest targeting any expressed protein.

Results

E3 ligase abundance serves as a proxy for neo-substrate recruitment to E3 ligases

CRL activity has been implicated in degrader potency and used for their identification[7,8]. These methods however are limited to targets essential for cellular viability. Active CRLs, in absence of their substrate can ubiquitinate their own substrate receptor in a process termed auto-degradation[3]. This basic mechanism has been implicated in CRL adaptation to substrate availability and cellular stimuli[9]. We envisioned that chemically induced augmentation of CRL substrate availability will affect the E3 ligase auto-degradatory state and hence increase SR abundance (**Figure 1A**). In the near haploid chronic myeloid leukemia cell line HAP1, treatment with the molecular glue degrader CC-885 indeed led to an increase in CRBN levels (**Figure 1B**). Based on the minor increase observed, we surmised that auto-degradation has only a marginal contribution to the proteostasis of CRBN. Given that steady-state Cullin scaffold engagement of each of the ~250 SRs varies greatly[9], also their auto-degradation behavior will depend on factors such as cell type and state. We reasoned that enrichment of active CRLs allows the augmentation of auto-degradation potential in a given cell (**Figure 1A**). NEDD8 is the central post-translational modification governing CRL activity[5] and treatment with the de-neddylation inhibitor CSN5i-3 was previously shown to induce CRL hyper-activity[10]. In HAP1, treatment with 500 nM CSN5i-3 yielded a significant destabilization of the CRBN substrate receptor, which upon engagement via CC-885 was rescued nearly to DMSO treated levels (**Figure 1B**). Such a SR response upon molecular glue treatment could potentially allow identification of degraders at scale. To develop this notion of “ligase tracing” further, we proceeded to validate it with the CRL E3 ligase $CUL2^{VHL}$ which has often been employed for targeted protein degradation via PROTACs[11,12]. Generating Nanoluciferase knock-in HAP1 cells, allowed us to measure VHL abundance in lytic measurements in 384-well plate format. Upon induction of auto-degradation via CSN5i-3 treatment, VHL destabilization was observed in a time-resolved and dose dependent manner also in live-cell measurements (**Figure 1C** and **Figure S1A**). Co-treatment with the BET bromodomain targeting PROTAC ARV-771 showed a sustained rescue of VHL auto-degradation, in line with previous results for $CUL4^{CRBN}$ (**Figure 1C** and **Figure S1A**). Overexpression of luciferase tagged VHL further allowed live-cell tracing of its protein levels under treatment with PROTACs and their inactive counterparts. Both BET PROTACs ARV-771 and MZ1 showed dramatic VHL increases when normalized to CSN5i-3 treatment, but an inactive enantiomer (cis-MZ1) did not elicit a response (**Figure 1D**). This was also validated in assays performed with NLuc-VHL endogenous knock-in cells (**Figure S1A**). Similarly, the SMARCA2/4 degrading PROTAC ACBI1 showed a pattern where only the active compound provoked changes in the auto-

degradation behavior of VHL (**Figure 1D**). As both these negative controls abort VHL recruitment, we next excluded a ligase stabilization via VHL binding alone by treatment with the VHL targeting compound VH-032 (**Figure 1D** and **Figure S1A**). Together these results suggest that CRL substrate receptor abundance can be used as a proxy for substrate engagement via inhibiting auto-degradation. In a state of CRL activity augmentation, this system allows validation of known CRBN and VHL molecular glue and PROTAC degraders.

As the active CRL pool is shaped to the particular cellular needs at any given time, we next explored to which CRL substrate receptors a ligase tracing assay could be expanded in HAP1 cells. To this end we performed global proteomics after 250 nM and 1 uM CSN5i-3 treatment for 8 hours (**Figure 1E** and **Figure S1B**). Most of the destabilized proteins were cullin associated substrate receptors. Among these destabilized CRLs we selected three SRs for a Nanoluciferase knock-in strategy in HAP1 cells and a set of nine different SRs for validation of these results via overexpression. Measuring the SR abundance upon CSN5i-3 induced auto-degradation resulted in dose- and time dependent destabilization, mimicking our previous results (**Figure 1F** and **Figure S1C**). Furthermore, for the overexpressed NLuc-SRs we reasoned that blocking of *de novo* cullin neddylation would reverse this state of hyperactivity. The NAE1 inhibitor MLN4924 abrogates the NEDD8 deposition cascade and leaves CRLs in an inactive conformation reversing the effects of SR auto-degradation across all our tested CRLs (**Figure S1C**). Taken together, these insights provide a proof-of-concept for ligase tracing, using the two best studied E3 ligases in the field of TPD. Furthermore, we show that this approach is amendable to several other CRLs in a cell type specific manner.

Figure 1.

(A) Schematic depiction of the ligase tracing approach. Cullin RING ligase activity is mediated through deposition of NEDD8 (N8) on the Cullin backbone via the COPP9 Signalosome (CSN). Inhibition of the CSN locks Cullin ligases in an active conformation leading to auto-ubiquitination and -degradation of the substrate receptor. Addition of a degrader compound can shield the substrate receptor and rescue its auto-degradation.

(B) Protein levels in KBM7 WT cells pre-treated for 10 min with DMSO or CC-885 (100 nM) followed by treatment with DMSO or CSN5i-3 (500 nM) for 4 h as indicated. Representative images of n = 2 independent measurements.

(C) Lytic luciferase measurement of HAP1 VHL-NanoLuc knock-in cells at the indicated timepoints after treatment with DMSO, CSN5i-3 (100 nM) or CSN5i-3/ARV771 co-treatment (100 nM & 500 nM respectively). Luciferase signal is normalized to DMSO treatment at each timepoint. Mean of n = 2 independent measurements.

(D) Live-cell luciferase measurement of HAP1 VHL-NanoLuc knock-in cells treated with CSN5i-3 (100 nM) or CSN5i-3 and ARV771 (100 nM & 500 nM respectively). Mean of n = 2 independent measurements. Luciferase signal is normalized to DMSO treatment at each timepoint. Representative data of n = 2 experiments.

(E) Volcano plot depicting global $\log_2$-fold changes of protein abundance in HAP1 cells treated with CSN5i-3 (250 nM) for 8 h. CRL substrate receptors are labeled in the indicated colors. SRs selected for validation via luciferase tagging are highlighted. Data of n = 3 replicates.

(F) DMSO normalized live-cell luciferase signal of HAP1 cells harboring endogenous NanoLuc knock-ins for the indicated SRs. Cells were treated with DMSO or CSN5i-3 at indicated concentrations and measured over time. Mean of n = 2 independent measurements.

Figure 1

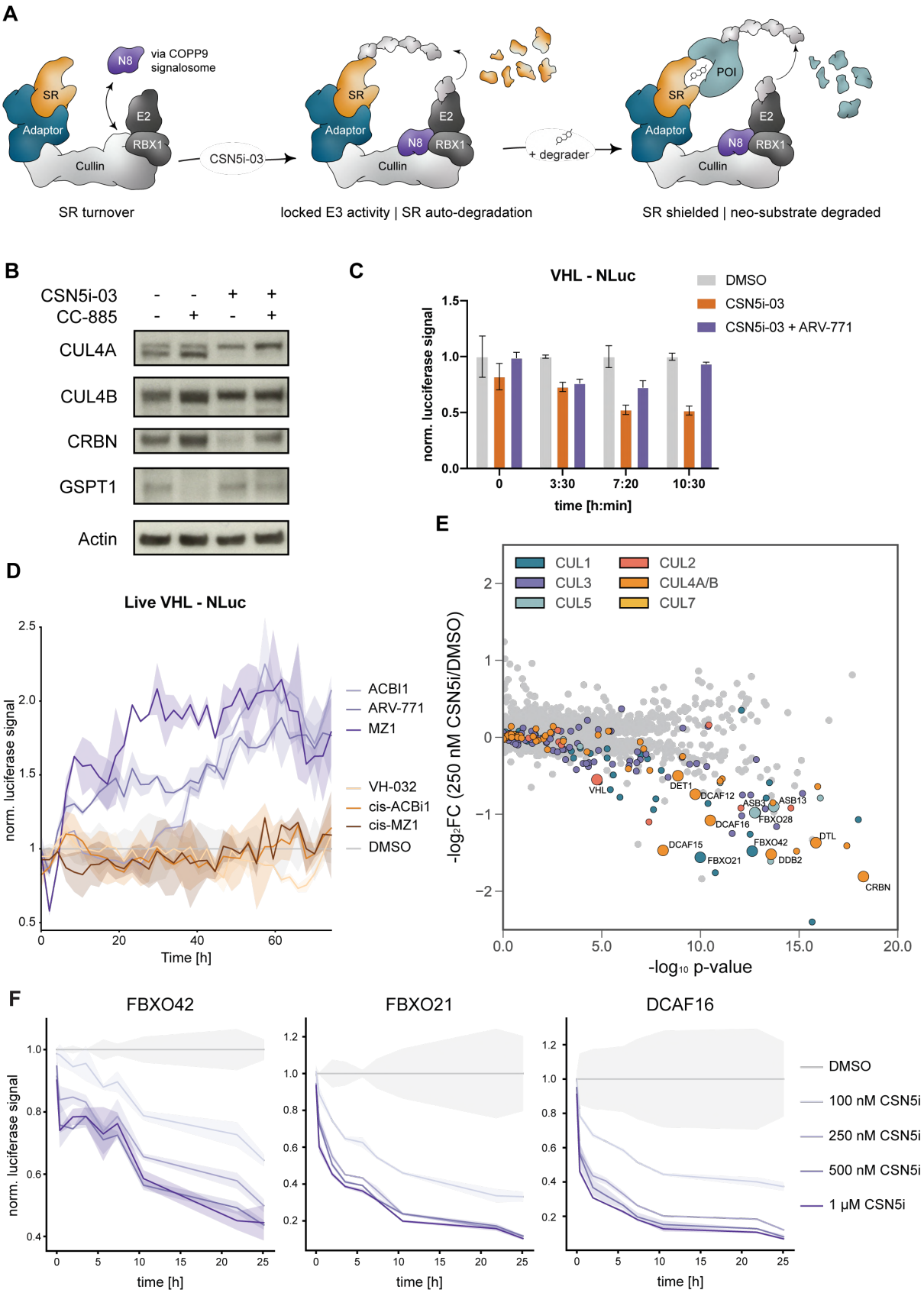
A
N8
via COPP9
signalosome
SR
Adaptor
E2
RBX1
Cullin
CSN5i-03
+ degrader
POI
SR turnover
locked E3 activity | SR auto-degradation
SR shielded | neo-substrate degraded
B
CSN5i-03
CC-885
CUL4A
CUL4B
CRBN
GSPT1
Actin
C
VHL - NLuc
DMSO
CSN5i-03
CSN5i-03 + ARV-771
norm. lucciferase signal
time [h:min]
D
Live VHL - NLuc
norm. luciferase signal
Time [h]
ACBI1
ARV-771
MZ1
VH-032
cis-ACBi1
cis-MZ1
DMSO
E
CUL1
CUL2
CUL3
CUL4A/B
CUL5
CUL7
-log2FC (250 nM CSN5i/DMSO)
-log10 p-value
VHL
DET1
DCAF12
ASB1
ASB13
DCAF16
FBXO28
DTL
DCAF15
FBXO42
FBXO21
DDB2
CRBN
F
FBXO42
FBXO21
DCAF16
norm. luciferase signal
time [h]
DMSO
100 nM CSN5i
250 nM CSN5i
500 nM CSN5i
1 µM CSN5i

Ligase tracing screen identifies a novel RBM39/23 degrader

Discovery of novel molecular glue degraders has historically been driven by chance. After establishing ligase tracing as a viable assay for degrader identification, we next set out to validate it in a chemical screening approach. To leverage already known molecular glue degraders as positive controls, we chose to adopt the ligase tracing approach for $CUL4^{DCAF15}$. DCAF15 can be targeted by aryl sulfonamides such as indisulam to recruit and ubiquitinate the splicing factor RBM39[13,14]. To measure its abundance we chose to overexpress DCAF15 tagged with the split luciferase eleven amino acid peptide HiBit in HEK293t cells[15]. Upon neo-substrate recruitment with indisulam, we observed profound stabilization of HiBit-DCAF15, presumably due to a strong cellular auto-degradation response to the SR overexpression (**Figure 2A**). Similarly, augmenting auto-degradation via CSN inhibition and co-treatment with the molecular glue degrader also led to DCAF15 destabilization and its rescue. Next, we proceeded to determine DCAF15 abundance via lytic split luciferase measurements by adding the complement LgBit luciferase part. Validating our western blot results, we observed destabilization upon CSN5i-3 treatment and profound stabilization of HiBit-DCAF15 by indisulam treatment (**Figure 2B**). Furthermore, we could reproduce this stabilization also in live-cell measurements with a second previously identified RBM39 molecular glue degrader called (dCeMM1) (**Figure 2C**). We also tested this ligase tracing assay in endogenously tagged HiBit-DCAF15 HEK293T cells under CSN5i treatment and could observe an indisulam induced rescue of auto-degradation, even though luciferase signal presented very low (**Figure S2A**). Next, we set out to test whether indisulam mediated stabilization was specific to DCAF15 by performing ligase tracing in overexpression and endogenously tagged NLuc-SR cells. Only in the HiBit-DCAF15 cells we could measure rescue of ligase degradation while DCAF16, FBXO21 and FBXO42 Nanoluciferase knock-ins remained unchanged (**Figure S2B**). Importantly, the increase in DCAF15 abundance was not driven through changes in RNA expression as exemplified by *DCAF15* qPCR (**Figure S2C**). In its initial identification indisulam was shown to be highly dependent on the glycine residue 268 of RBM39[14]. Modification of this amino acid to a valine abrogated the neo-substrate recruitment and induced degradation[16–18]. We therefore used the haploid genetics of HAP1 cells to engineer a $RBM39^{G268V}$ cell line in which we overexpressed NLuc-DCAF15 for ligase tracing (**Figure 2D**). Indisulam only induced a stabilization effect in the $RBM39^{WT}$ cells while no change could be detected in a $RBM39^{G268V}$ background. Of note, the $CUL4^{CRBN}$ molecular glue degrader lenalidomide did not show any stabilization effect (**Figure 2D**). In summary, this highlights how $CUL4^{DCAF15}$ presents a viable system for molecular glue degrader identification via our ligase tracing approach. Stabilization of DCAF15 is observed with different RBM39 degraders and dependent on neo-substrate recruitment.

Having established live-cell ligase tracing for $CUL4^{DCAF15}$ we set out to screen a library of 10,000 sulfonamides for molecular glue degraders in a neo-substrate agnostic fashion. After normalization to DMSO, positive controls (indisulam, dCeMM1) showed a profound stabilization of DCAF15 levels in concordance with previous results (**Figure 2E**). Analysis of other sulfonamides revealed similar stabilization effects via the aryl sulfonamide dRRM-1 which shared some structural similarity to indisulam and dCeMM1 (**Figure 2E and S2D**). Given this similarity, we performed docking of dRRM-1 to a published crystal structure of DCAF15-E7820-RBM39 and identified a shared binding mode to previous sulfonamides, suggesting its mode-of-action via RBM39 degradation (**Figure 2F**). Indeed,

cellular treatment with dRRM-1 showed a similar DCAF15 dependent RBM39 degradation to indisulam and dCeMM1 (**Figure 2G**). We could further validate RBM39 degradation via C-terminal knock-in of HiBit to *RBM39* and measuring its abundance via live-cell luciferase detection (**Figure 2H**). Additionally, via TR-FRET based measurement of E7820 displacement from DCAF15 we detected a similar binding affinity of dRRM-1 as the previously known sulfonamide tasisulam (**Figure S2E**). Global proteomics experiments revealed that not only RBM39 is degraded via dRRM-1 treatment but also the closely related splicing factor RBM23 (**Figure 2I**). RBM23 shares a high sequence similarity to RBM39 and has previously been shown to be targeted by other sulfonamides[18,19]. Intrigued by the preferential degradation of RBM23 over RBM39 by dRRM-1, we generated a C-terminal RBM23-NLuc knock-in HAP1 cell line and measured its abundance upon sulfonamide treatment. Indisulam and dRRM-1 led to similar time dependent RBM23 degradation, which could be rescued by co-treatment with the proteasome inhibitor carfilzomib (**Figure 2J**). Together with the results from the RBM39 knock-in cells and the global proteomics, this suggests that dRRM-1 is preferentially degrading RBM23 over RBM39. In summary, we outline and validate a cullin ligase centric phenotypic screening approach, that allowed us to identify a chemically novel DCAF15 molecular glue degrader. The characterized hit dRRM-1 showed differential target selectivity from previously described sulfonamides while retaining a similar binding mode.

Figure 2.

(A) Protein levels in HEK293t DCAF15$^{-/-}$ cells with reconstitution of HiBit-DCAF15 treated with indisulam (10 uM) or CSN5i-3 (250 nM) for 24 hrs. Representative images of n = 2 independent measurements.

(B) Bar graph depicting DMSO normalized lytic luciferase signal of HEK293t DCAF15$^{-/-}$ cells with reconstitution of HiBit-DCAF15 + LgBit measured at the indicated timepoints after treatment with DMSO, indisulam (10 uM), CSN5i-3 (250 nM) or CSN5i-3/indisulam co-treatment (250 nM & 10 uM respectively). Mean of n = 2 independent measurements. Representative data of n = 2 experiments.

(C) DMSO normalized live-cell luciferase signal of HEK293t DCAF15$^{-/-}$ cells with reconstitution of HiBit-DCAF15 + LgBit treated with indisulam, dCeMM1 or DMSO(10 uM each). Representative data of n = 3 experiments.

(D) Bar graph depicting DMSO normalized live cell luciferase signal of HAP1 WT and RBM39^{G268V} cells with ectopic expression of HiBit-DCAF15 + LgBit measured at the indicated timepoints after treatment with DMSO, indisulam (10 uM) or lenalidomide (10 uM). Mean of n = 3 independent measurements. Representative data of n = 2 experiments.

(E) DMSO normalized live-cell luciferase signal of HEK293t DCAF15$^{-/-}$ cells with reconstitution of HiBit-DCAF15 + LgBit treated with 10 uM control compounds (indisulam, dRRM-1 or DMSO) or screening compounds (10 uM each, 200 compounds shown).

(F) Molecular docking of dRRM-1 in the crystal structure of DCAF15:E7820:RBM39 (PDB: 6Q0R).

(G) Protein levels in HEK293t DCAF15$^{-/-}$ cells with reconstitution of HiBit-DCAF15 treated with indisulam, dCeMM1 or dRRM-1 for 10 hrs. Representative images of n = 2 independent measurements.

(H) DMSO normalized live-cell luciferase signal of HCT116 RBM39-HiBit knock in cells with ectopic expression of LgBit treated with indisulam, dCeMM1, dRRM-1 or neg. control compounds (10 uM each).

(I) Volcano plot depicting global log_2-fold changes of protein abundance in HEK293t DCAF15$^{-/-}$ cells with ectopic expression of HiBit-DCAF15 and LgBit treated with dRRM-1 (10 uM) for 10 hrs. Data of n = 2 replicates.

(J) Bar graph depicting DMSO normalized live cell luciferase signal of HAP1 RBM23-NanoLuc knock in cells measured at the indicated timepoints after treatment with DMSO, indisulam (10 uM) or dRRM-1 (10 uM). Mean of n = 3 independent measurements.

Figure 2

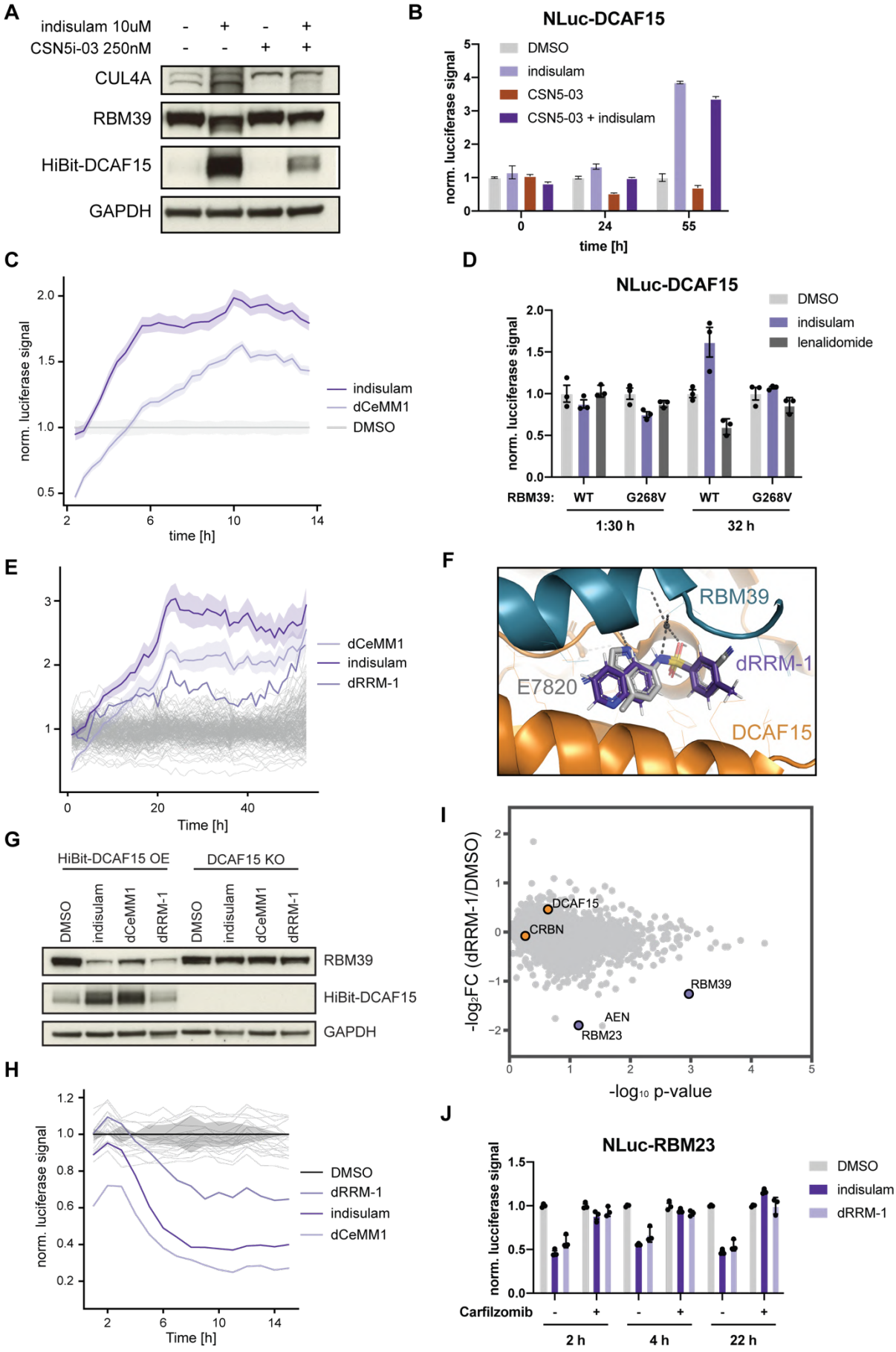
A
indisulam 10uM - + - +
CSN5i-03 250nM - - + +
CUL4A
RBM39
HiBit-DCAF15
GAPDH
B
NLuc-DCAF15
DMSO
indisulam
CSN5-03
CSN5-03 + indisulam
norm. lucciferase signal
time [h]
C
norm. luciferase signal
indisulam
dCeMM1
DMSO
time [h]
D
NLuc-DCAF15
DMSO
indisulam
lenalidomide
norm. lucciferase signal
RBM39: WT G268V WT G268V
1:30 h
32 h
E
dCeMM1
indisulam
dRRM-1
Time [h]
F
RBM39
dRRM-1
E7820
DCAF15
G
HiBit-DCAF15 OE
DCAF15 KO
DMSO
indisulam
dCeMM1
dRRM-1
RBM39
HiBit-DCAF15
GAPDH
H
norm. luciferase signal
DMSO
dRRM-1
indisulam
dCeMM1
Time [h]
I
-log2FC (dRRM-1/DMSO)
DCAF15
CRBN
RBM39
AEN
RBM23
-log10 p-value
J
NLuc-RBM23
norm. lucciferase signal
DMSO
indisulam
dRRM-1
Carfilzomib
2 h
4 h
22 h

Discussion

The rise in popularity of TPD following several seminal discoveries has led to a marked increase in novel chemical matter in this field. Methods based on chemoproteomics have augmented the discovery of covalent E3 ligase binders which in turn have spurred PROTAC development[20,21]. With thousands of functional PROTACs described[22], molecular glue type degraders have remained comparatively elusive. Their inherent dependency on protein-protein interactions via surface complementation in part explains why to date most molecular glue degraders have been identified by chance. Here we outlined a strategy of measuring drug induced changes to the interactome of an E3 ligase of choice by leveraging the regulatory circuits of cullin RING ligases. We benchmark this scalable assay with the two best studied E3 ligases in TPD $CRL4^{CRBN}$ and $CRL2^{VHL}$. By use of the $CRL2^{VHL}$ binding ligand VH-032 we find that the ligase tracing assay specifically reports on neo-substrate recruitment. We further profile all E3 ligases amendable to this approach in our given cell line model and choose to perform a proof-of-concept chemical screen against $CRL4^{DCAF15}$. A single point mutation abrogating MG dependent recruitment of RBM39 to CRL^{DCAF15} was sufficient to disrupt ligase tracing signal highlighting the assay specificity. Among 10,000 sulfonamides tested, we identified dRRM-1 a molecular glue degrader of RBM39 and RBM23 and validate its effects via TR-FRET and global proteomics. We conclude that our ligase tracing assay empowers identification of functional degrader molecules in an E3 ligase driven but target agnostic way.

This allows selection of therapeutically enticing CRL E3 ligases taking into account their characteristics such as disease relevance and expression pattern. In fact, recently we have shown that essentiality of an E3 ligase can have profound impact on emergence of resistance to degrader modalities further highlighting the need to expand the targetable E3 ligase space. In principle, ligase tracing assays target recruitment in a proteome wide fashion. Specific effects of neo-substrate abundance and localization in the cell remain to be understood however. It is imaginable that a target substrate needs to pass a threshold in intracellular abundance based on the mechanism of action employed in this assay, which likely precludes degraders of secreted proteins from discovery. An advantage of ligase tracing over other previously reported methods for molecular glue discovery lies in its independence from the neo-substrate's essentiality status. While discovery of cyclin K molecular glue degraders hinged on their cytotoxicity, the here presented method directly reports on changes to E3 ligase target spectrum.

Nonetheless, ligase tracing comes with some limitations. Firstly, live cell luminescence measurements in multi-well format come with limitations of the amount of conditions that can be measured in a single plate reader. Upscaling of the assay to 1536 well-plates however would be possible. Additionally, one can envision measuring abundance of several E3 ligases in the same cell via fluorescent protein tagging coupled to a microscopy readout. Secondly, ligase tracing is susceptible to inhibitors of autodegradation such as E1- and E2-ubiquitin cascade inhibitors, as outlined in **Figure 1C**. Such small-molecules will however lead to positive signal across most E3 ligases and therefore can be identified and excluded in counter-screening hit validations. Furthermore, this can even be seen as an advantage as similar inhibitors have proven invaluable to deciphering biological systems and effects of drugs. Overall, we believe that the outlined method can be easily adopted to other E3 ligases

of interest and facilitate the *de novo* identification of E3 ligase binders and molecular glue degraders in a target agnostic fashion.

References

1. Stanton, B. Z., Chory, E. J. & Crabtree, G. R. Chemically induced proximity in biology and medicine. *Science* **359**, eaao5902 (2018).
2. Schapira, M., Calabrese, M. F., Bullock, A. N. & Crews, C. M. Targeted protein degradation: expanding the toolbox. *Nat Rev Drug Discov* **18**, 949-963 (2019).
3. Petroski, M. D. & Deshaies, R. J. Function and regulation of cullin-RING ubiquitin ligases. *Nat Rev Mol Cell Biol* **6**, 9-20 (2005).
4. Cavadini, S. et al. Cullin-RING ubiquitin E3 ligase regulation by the COP9 signalosome. *Nature* **531**, 598-603 (2016).
5. Baek, K. et al. NEDD8 nucleates a multivalent cullin-RING-UBE2D ubiquitin ligation assembly. *Nature* **578**, 461-466 (2020).
6. Békés, M., Langley, D. R. & Crews, C. M. PROTAC targeted protein degraders: the past is prologue. *Nat Rev Drug Discov* **21**, 181-200 (2022).
7. Słabicki, M. et al. The CDK inhibitor CR8 acts as a molecular glue degrader that depletes cyclin K. *Nature* **585**, 293-297 (2020).
8. Mayor-Ruiz, C. et al. Rational discovery of molecular glue degraders via scalable chemical profiling. *Nat Chem Biol* **16**, 1199-1207 (2020).
9. Reichermeier, K. M. et al. PIKES Analysis Reveals Response to Degraders and Key Regulatory Mechanisms of the CRL4 Network. *Mol Cell* **77**, 1092-1106.e9 (2020).
10. Mayor-Ruiz, C. et al. Plasticity of the Cullin-RING Ligase Repertoire Shapes Sensitivity to Ligand-Induced Protein Degradation. *Molecular Cell* **75**, 849-858.e8 (2019).
11. Zengerle, M., Chan, K. H. & Ciulli, A. Selective Small Molecule Induced Degradation of the BET Bromodomain Protein BRD4. *ACS Chem Biol* **10**, 1770-1777 (2015).
12. Bondeson, D. P. et al. Catalytic in vivo protein knockdown by small-molecule PROTACs. *Nat Chem Biol* **11**, 611-617 (2015).
13. Uehara, T. et al. Selective degradation of splicing factor CAPERα by anticancer sulfonamides. *Nat Chem Biol* **13**, 675-680 (2017).
14. Han, T. et al. Anticancer sulfonamides target splicing by inducing RBM39 degradation via recruitment to DCAF15. *Science* **356**, eaal3755 (2017).
15. Riching, K. M. et al. Quantitative Live-Cell Kinetic Degradation and Mechanistic Profiling of PROTAC Mode of Action. *ACS Chem Biol* **13**, 2758-2770 (2018).
16. Bussiere, D. E. et al. Structural basis of indisulam-mediated RBM39 recruitment to DCAF15 E3 ligase complex. *Nat Chem Biol* **16**, 15-23 (2020).
17. Du, X. et al. Structural Basis and Kinetic Pathway of RBM39 Recruitment to DCAF15 by a Sulfonamide Molecular Glue E7820. *Structure* **27**, 1625-1633.e3 (2019).
18. Faust, T. B. et al. Structural complementarity facilitates E7820-mediated degradation of RBM39 by DCAF15. *Nature Chemical Biology* **16**, 7-14 (2020).
19. Ting, T. C. et al. Aryl Sulfonamides Degrade RBM39 and RBM23 by Recruitment to CRL4-DCAF15. *Cell Rep* **29**, 1499-1510.e6 (2019).
20. Zhang, X., Crowley, V. M., Wucherpfennig, T. G., Dix, M. M. & Cravatt, B. F. Electrophilic PROTACs that degrade nuclear proteins by engaging DCAF16. *Nat Chem Biol* **15**, 737-746 (2019).
21. Spradlin, J. N. et al. Harnessing the anti-cancer natural product nimbolide for targeted protein degradation. *Nat Chem Biol* **15**, 747-755 (2019).
22. Weng, G. et al. PROTAC-DB: an online database of PROTACs. *Nucleic Acids Res* **49**, D1381-D1387 (2021).
23. Yang, X. et al. A public genome-scale lentiviral expression library of human ORFs. *Nat Methods* **8**, 659-661 (2011).
24. Jaeger, M. G. et al. Selective Mediator dependence of cell-type-specifying transcription. *Nat Genet* **52**, 719-727 (2020).
25. Brand, M. & Winter, G. E. Locus-Specific Knock-In of a Degradable Tag for Target Validation Studies. *Methods Mol Biol* **1953**, 105-119 (2019).

Author contribution:

A.H. and G.E.W. conceptualized this study. A.H. designed and performed E3 ligase luciferase measurements (ligase tracing). A.H., S.B., E.B., E.H. and E.V.P. generated over-expression and knock-in cell lines and conducted immunoblotting and cellular drug sensitivity assays. A.H. generated samples for proteomics experiments and analyzed and visualized resulting data. H.Y. performed TR-FRET assays. R.P.N. performed molecular docking studies. E.S.F. and G.E.W. supervised the work. A.H. generated figures with input from all authors. A.H. and G.E.W. wrote the manuscript with input from all authors.

Acknowledgements:

We thank the Molecular Discovery Platform at CeMM (in particular Anna Koren and Stefan Kubicek) for assistance with luciferase measurements and proteomics experiments. CeMM and the Winter laboratory are supported by the Austrian Academy of Sciences. The Winter lab is further supported by funding from the European Research Council (ERC) under the European Union's Horizon 2020 research and innovation program (grant agreement 851478), as well as by funding from the Austrian Science Fund (FWF, projects P32125, P31690 and P7909).

Financial interest statement

S.B. is an employee at Proxygen, a company that is developing molecular glue degraders. G.E.W. is scientific founder and shareholder at Proxygen and Solgate and coordinates a Research Collaboration between CeMM and Pfizer. This work was supported by a philanthropic gift from Giving | Grousbeck Fazzalari (to E.S.F.), by NCI R01CA2144608 (to E.S.F). E.S.F. is a Damon-Runyon Rachleff Investigator (DRR-50-18). The other authors are not aware of any affiliations, memberships, funding, or financial holdings that might be perceived as affecting the objectivity of this work.

Materials and Methods

Cell lines, tissue culture and lentivirus production

KBM7 cells (a gift from T. Brummelkamp) were grown in IMDM supplemented with 10% Fetal Bovine Serum and 1% penicillin/streptomycin (100 units/ml Penicillin, 100 µg/ml Streptomycin; pen/strep). HAP1 cells were cultured in IMDM supplemented with 10% Fetal Bovine Serum and 1% pen/strep. HEK293t cells (a gift by the Bradner Lab) were grown in in DMEM supplemented with 10% Fetal Bovine Serum and 1% pen/strep. HCT116 cells (a gift by the Superti-Furga Lab) were cultured in DMEM supplemented with 10% Fetal Bovine Serum and 1% pen/strep. pSpCas9(BB)-2A-GFP (PX458) or pSpCas9(BB)-2A-Puro (PX459) was obtained through Addgene (48138 and 62988) and used to transiently express sgRNA against CRBN, VHL, DCAF15 and other genes for knock-out generation. Clones were single cell seeded and checked for gene deletion via PCR on gDNA or Western blotting. For lentiviral production, 293T cells were seeded in 10 cm dishes and transfected at approx. 80 % confluency with 4 µg target vector, 2 µg pMD2.G (Addgene 12259) and 1 µg psPAX2 (Addgene 12260) using PEI and following standard protocol. The viral supernatant was harvested 72 h after transfection

and filtered with a 0.45-µm syringe filter to remove cell debris. Lentivirus was then aliquoted and stored at – 80 °C until transduction of 1 x 10^6 cells in 1 ml of media plus virus in 24 well plates with the addition of 8 µg per ml polybrene (Sigma) and spin inoculation for 1 h at 2,000 r.p.m. Antibiotic selection was performed 24 to 48 h after transduction with 10 µg ml^{-1} blasticidin.

Plasmids and cloning

All plasmids used in this study are summarized in Supplementary Table 1. For ectopic expression of E3 ligases tagged with full length nanoLuciferase, cDNA of the specific genes was ordered in pENTR223 vectors from the BCCM/Belspo consortium as part of the human ORFome library[23]. E3 ligase cDNAs were then cloned into pLenti6.2-ccdB-Nanoluc (Addgene 87075) via gateway LR-recombination cloning (Invitrogen) following manufacturers recommendations.

For cloning of sgRNA cutting plasmids to generate endogenous nanoLuciferase and HiBit knock-ins, we utilized a universal pX330A_sgX_sgPITCh cutting plasmid via adaptation of a published protocol[24]. sgRNAs targeting the endogenous locus (Supplementary Table 1) were selected to lie as close as possible to the start- or stop codon with the minimal predicted off-target activity. They were introduced to the vector via oligonucleotide annealing and subsequent BbsI-mediated restriction cloning. The second part of this micro-homology mediated knock-in strategy was introduced by adapting the pCRIS-PITChv2 repair template plasmid to contain a N-terminal blasticidin-P2A-2xHA-NLuc cassette which was generated via a geneblock and PCR of the flanking PITCh sgRNA target sites. This PCR product was then introduced in MluI linearized pCRIS-PITChv2 vector via NEBuilder 2× HiFi assembly (New England Biolabs). Primers containing 20 to 22 bp homology regions corresponding to the genomic locus 5' and 3' of the sgRNA cleavage were used to PCR this cassette. The resulting repair template introducing a blasticidin marker, and a double HA tagged nanoLuciferase to the genomic locus was reintroduced into MluI linearized pCRIS-PITChv2 vectro backbone with NEBuilder 2× HiFi assembly (New England Biolabs) [25].

Endogenous genome editing for knock-in and mutant generation

To generate cell lines expressing HiBit or NanoLuciferase tagged POIs, HAP1 WT or HCT116 WT cells were seeded into 6-well plates to obtain approximately 70 % confluency the next day. For microhomology mediated knock-in, in each well, PITCh sgRNA/Cas9 and repair template plasmids were transfected at 1.5 µg each via PEI following standard protocol (see Supplementary Table 1 for sgRNA and microhomology sequences). The next day, each condition was split to a 10 cm dish and antibiotic selection for successful editing was started 48 hours after transfection. Single cell selection was ensured by limited dilution into 384 well-plates (seeding at 0.2–1 cells per well in 50 µl) or by picking single colonies directly of the plate. Successful knock-in was characterized via immunoblotting for the introduced HA-tag and/or via genotyping by PCR of the targeted genomic region.

For knock-in of the shorter HiBit-tag in the C-terminus of RBM39 in HCT116, a similar approach was used only that the repair cassette could be introduced via annealed oligos instead of an entire plasmid. For this oligos harboring the 33 bp HiBit-tag flanked by 20 bp homologies from the genomic sgRNA cut site were ordered and co-transfected as described above. Cells were pulse-selected from 24 h post transfection to 72 hrs post transfection for Cas9 expression and subsequently single cell seeded at 0.2–

1 cells per well in a 384 well plate. Single clones were pre-selected by lytic Nanoluc reconstitution under treatment with indisulam or DMSO. Clones that showed loss of luciferase signal under indisulam were subsequently characterized via immunoblotting for the introduced HiBit-tag and via genotyping by PCR of the targeted genomic region.

For generation of the RBM39 G268V mutant HCT116 cells, again annealed oligos were utilized in a similar fashion. After CRISPR/Cas9 mediated cutting at the specific genomic locus a repair template harboring a 40 bp homology and the desired point mutation in its center was used to introduce the mutation. Cells were seeded and transfected with the sgRNA/Cas9 plasmid and the repair oligos as mentioned above followed by pulse-selection for Cas9 expression from 24 h post transfection to 72 hrs post transfection and subsequently single cell seeding. Next, clones were mirror-plated in 96 well plates after initial expansion and pre-selected by treatment with indisulam in one of the mirror plates. Single clones that showed resistance to indisulam were subsequently characterized via genotyping by PCR of the targeted genomic region to identify the specific introduced point mutation.

Transcript quantification via qPCR

1 M HEK293T cells with ectopic expression of HiBit-DCAF15 and LgBit were treated with DMSO or 10 µM indisulam for 12 h, detached and RNA was isolated using the RNeasy Kit and QIAshredder (Qiagen) following standard protocol with DNA digestion. Reverse transcription PCR was performed with the RevertAID First Strand cDNA synthesis kit and Oligo-dT primers (Thermo Scientific). DCAF15 RNA was quantified in a PCR reaction using SYBR select master mix (Fisher Scientific) in the following reaction: 3.75 µl of 1:10 diluted cDNA, 0.75 µl of DCAF15_exon9-11 primer mix (10 µM each), 3 µl H_2O and 7.5 µl SYBR master mix. The reaction mixture was denatured for 3' at 95 °C followed by 45 cycles of 15" at 95 °C, 45" at 60 °C and 15" at 95 °C with a final extension of 1' at 60 °C and 15" at 95 °C in a StepOne Plus real-time PCR cycler (Applied Biosystems). The cycle number for exponential amplification was determined and normalized to DMSO treated samples and visualized with Prism (GraphPad).

Western blot analysis

PBS-washed cell pellets were lysed in RIPA Buffer (50 mM Tris-HCl pH 8.0, 150 mM NaCl, 1% Triton X-100, 0.5% sodium deoxycholate, 0.1% SDS, 1× Halt protease inhibitor cocktail, 25 U ml^{-1} Benzonase). Lysates were cleared by centrifugation for 15 min at 4 °C and 20,000*g*. Protein concentration was measured by BCA according to the manufacturer's protocol (Thermo Scientific™ Pierce™ BCA Protein Assay Kit) and 4X LDS sample buffer was added. Proteins (20 µg) were separated on 4-12% SDS-PAGE gels and transferred to nitrocellulose membranes. Membranes were blocked with 5% milk in TBST for 30 min at RT. Primary antibodies were incubated in milk or TBST alone for 1 h at RT or 4 °C overnight. Secondary antibodies were incubated for 1 h at RT. Blots were developed with chemiluminescence films. Primary antibodies used: BRD4 (1:1000, Abcam, ab128874), BRD3 (1:1000, Bethyl Laboratories, A302-368A), BRD2 (1:1000, Bethyl Laboratories, A302-582A), SMARCA4 (1:1000, Bethyl Laboratories, A300-813A), SMARCA2 (1:1000, Cell Signaling Technology, #6889), cMYC (1:1000, Santa Cruz Biotechnology, sc-764), GSPT1 (1:1000, Abcam, ab49878), CDK9

(1:1000, Cell Signaling Technology, 2316S), CRBN (1:2000, kind gift of R. Eichner and F. Bassermann), VHL (1:1000, Cell Signaling Technology, 2738), ACTIN (1:5000, Sigma-Aldrich, A5441-.2ML), GAPDH (1:1000, Santa Cruz Biotechnology, sc-365062). Secondary antibodies used: Peroxidase-conjugated AffiniPure Goat Anti-Rabbit IgG (1:10000, Jackson ImmunoResearch, 111-035-003) and Peroxidase-conjugated AffiniPure Goat Anti-Mouse IgG (1:10000, Jackson ImmunoResearch, 115-035-003).

E3 ligase luciferase measurements

Live cell measurements

For nanoLuciferase measurements, cells were diluted to 1 M cells ml^{-1} in media and 10 µl of this suspension seeded in a 384-well plate. For large scale chemical screens, compounds were dispensed with an Echo 550 system and resuspended in 10 µl of media prior to cell seeding to obtain a final assay volume of 40 µl and compound concentrations of 10 µM. For small scale luciferase measurements, 10 µl of compound solution was added to each well with cell suspension. Positive (MLN4924) and negative (DMSO) control compounds were scattered over each plate to judge and eliminate plate positional effects. Finally, 20 µl of media supplemented with 50 mM HEPES (Sigma), 1:100 Endurazine Luciferase live cell substrate (Promega) and depending on condition, CSN5i-3 (MedChemExpress) were added to each well. Luciferase measurements were performed every 1 to 2 hours on an EnVision plate reader (PerkinElmer). Results were analysed by employing python (3.8.5), pandas (1.1.3) and numpy (1.19.2) to normalize each timepoint per plate to its relative negative control measurement and depicted using matplotlib (3.3.2) and seaborn (0.11.0).

Lytic measurements

For Lytic endpoint measurements cells were seeded as mentioned above and nanoLuciferase abundance was determined via the Nano-Glo HiBit lytic detection kit (Promega) following manufacturers recommendations. Depending on the cell line used (HiBit- or NLuc tagged protein), LgBit was added to the final measurement mix or not. Results were analysed as described above and visualized with Prism (GraphPad).

Time-resolved Förster resonance energy transfer

Protein constructs, expression and purification were performed as previously described[18]. Titrations of compounds in BodipyFL-E7820 displacement assay were carried out by mixing 200 nM biotinylated Strep-II-Avi-tagged DCAF15 variants, 2 nM terbium-coupled streptavidin in assay buffer containing 50 mM Tris, pH 7.5, 200 mM NaCl, 0.1% Pluronic F-68 solution (Sigma) and 5 µM of BodipyFL-E7820. After dispensing the assay mixture, an increasing concentration of small molecules was dispensed in the 384-well plate (Corning, 4514) using a D300e Digital Dispenser (HP) normalized to 2% DMSO and then incubated for 60 min at room temperature. After excitation of terbium fluorescence at 337 nm, emission at 490 nm (terbium) and 520 nm (BodipyFL) were recorded with a 70-µs delay over 600 µs to reduce background fluorescence, and the reaction was followed over 10 cycles of each data point using a PHERAstar FSX microplate reader (BMG Labtech). The TR-FRET signal of each data point was extracted by calculating the 520/490 nm ratio. The IC_{50} values were estimated using the variable slope

equation in Prism (GraphPad). All TR-FRET results are plotted as mean ± s.d. from three independent replicates ($n = 3$).

Molecular Docking Analysis

The crystal structures of DCAF15-DDB1ΔB-DDA1 complex (PDB: 6Q0R) were prepared using the Protein Preparation Wizard in Maestro (Maestro release 2022-1, Epik version 5.9137). Default settings were used, except that all crystallographic water molecules > 5 Å from heteroatom groups were removed. The docking receptor grid was created using the Receptor Grid Generation module in Glide (Glide version 94137). The grid box and center were set to default by using the active site ligand (E7820), with the active site ligand excluded from the grid. The ligands were prepared using the LigPrep module with OPLS3 force field and default settings (LigPrep version 61137). The docking poses were generated using the LigandDocking protocol as implemented in Schrödinger Suite 2022-1. Default settings were used with the Standard Precision (SP) score function with flexible ligand sampling. Briefly, the grid box and center were set at default using the active site ligand, and no constraints were defined. The top pose with the lowest Glide SP score is shown for dCeMM5. Figures were generated in PyMOL (2.5.1, Schrödinger, LLC).

Expression proteomics

First, we compared overall proteome-wide changes in HAP1 WT cells treated with DMSO or CSN5i-3 (1mM and 250 nM, 8h). Second, we profiled dRRM-1 treatment (10 uM for 10 hrs) in HAP1 DCAF15$^{-/-}$ cells overexpressing HiBit-DCAF15 and LgBit.

Sample preparation

30x10^6 HAP1 cells per condition were collected, washed four times with ice-cold DPBS, the supernatant aspirated and pellets snapfrozen in liquid N2. Each washed cell pellet was lysed separately in 40 mL of freshly prepared lysis buffer containing 50 mM HEPES (pH 8.0), 2% SDS, 0.1 M DTT, 1 mM PMSF, and protease inhibitor cocktail (Sigma-Aldrich). Samples rested at RT for 20 minutes before heating to 99 °C for 5 min. After cooling down to RT, DNA was sheared by sonication using a Covaris S2 high performance ultrasonicator. Cell debris was removed by centrifugation at 20.000 g for 15 min at 20 °C. Supernatent was transferred to fresh eppendorf tubes and protein concentration determined using the BCA protein assay kit (Pierce Biotechnology, Rockford, IL). FASP was performed using a 30 kDa molecular weight cutoff filter (VIVACON 500; Sartorius Stedim Biotech GmbH, 37070 Goettingen, Germany) essentially according to published procedures. In brief, 100 mg total protein per sample were reduced by adding DTT at a final concentration of 83.3 mM followed by incubation at 99 °C for 5 min. After cooling to room temperature, samples were mixed with 200 mL of freshly prepared 8 M urea in 100 mM Tris-HCl (pH 8.5) (UA-solution) in the filter unit and centrifuged at 14.000 3 g for 15 min at 20 °C to remove SDS. Any residual SDS was washed out by a second washing step with 200 mL of UA. The proteins were alkylated with 100 mL of 50 mM iodoacetamide in the dark for 30 min at RT. Afterward, three washing steps with 100 mL of UA solution were performed, followed by three washing steps with 100mL of 50 mM TEAB buffer (Sigma-Aldrich). Proteins were digested with trypsin at a ratio of 1:50 overnight at 37 °C. Peptides were recovered using 40 mL of 50 mM TEAB buffer followed by 50

mL of 0.5 M NaCl (Sigma-Aldrich). Peptides were desalted using C18 solid phase extraction spin columns (The Nest Group, Southborough, MA). After desalting, peptides were labeled with TMT 10plex reagents according to the manufacturer (Pierce, Rockford, IL). After quenching of the labeling reaction, labeled peptides were pooled, organic solvent removed in vacuum concentrator and labeled peptides cleaned via C18 solid phase extraction (SPE).

Offline Fractionation via RP-HPLC at high pH

Tryptic peptides were re-buffered in 20 mM ammonium formiate buffer pH 10, shortly before separation by reversed phase liquid chromatography at pH 10 as described. Peptides were separated into 96 time-based fractions on a Phenomenex C18 RP column (150 3 2.0 mm Gemini-NX 3 mm C18 110A°, Phenomenex, Torrance, CA, USA) using an Agilent 1200 series HPLC system fitted with a binary pump delivering solvent at 100 mL/min. Acidified fractions were consolidated into 36 fractions via a concat-enated strategy described. After solvent removal in a vacuum concentrator, samples were reconstituted in 5% formic acid for LC-MS/MS analysis and kept at 80C until analysis. Mass spectrometry was performed on an Orbitrap Fusion Lumos mass spectrometer (ThermoFisher Scientific, San Jose, CA) coupled to a Dionex Ultimate 3000RSLC nano system (ThermoFisher Scientific, San Jose, CA) via nanoflex source interface. Tryptic peptides were loaded onto a trap column (Pepmap 100 5 mm, 5 3 0.3 mm, ThermoFisher Scientific, San Jose, CA) at a flow rate of 10 mL/min using 2% ACN and 0.05% TFA as loading buffer. After loading, the trap column was switched in-line with a 40 cm, 75 mm inner diameter analytical column (packed in-house with ReproSil-Pur 120 C18-AQ, 3 mm, Dr. Maisch, Ammerbuch-Entringen, Ger- many). Mobile-phase A consisted of 0.4% formic acid in water and mobile-phase B of 0.4% formic acid in a mix of 90% acetonitrile and 9.6% water. The flow rate was set to 230 nL/min and a three-step 90 min gradient applied (6 to 30% solvent B within 81 min, 30 to 65% solvent B within 8 min and, 65 to 100% solvent B within 1 min, 100% solvent B for 6 min before equilibrating at 6% solvent B for 18 min prior to next injection). Analysis on the MS was performed in a data-dependent acquisition (DDA) mode using a max 3 s cycle time. Full MS^1 scans were acquired in the Orbitrap with a scan range of 375 - 1650 m/z and a resolution of 120,000 (at 200 m/z). Auto- matic gain control (AGC) was set to a target of 2 3 10^5 and a maximum injection time of 50 ms. MS^2 -spectra were acquired in the Orbitrap at a resolution of 50,000 (at 200 m/z) with a fixed first mass of 100 m/z. In order to achieve maximum proteome coverage, a classical tandem MS approach was chosen (TMT reporter ion intensities extracted from MS^2-scans) instead of the available synchro- neous precursor selection (SPS)-MS3 approach. The latter provides on average better TMT ratio accuracies but suffers from prolonged duty cycles and reduced identification rates. To minimize TMT ratio compression effects by interence of contaminating coeluting isobaric peptide ion species, precursor isolation width in the quadrupole was set to 0.4 Da and an extended fractionation scheme applied (36 fractions, see above). Monoisotopic peak determination was set to peptides with inclusion of charge states be- tween 2 and 7. Intensity threshold for MS^2 selection was set to 5 3 10^4. Higher energy collision induced dissociation (HCD) was applied with a normalized collision energy (NCE) of 38%. AGC was set to 1 3 10^5 with a maximum injection time of 105 ms. Dynamic exclusion for selected ions was 60 s. A single lock mass

at m/z 445.120024 was employed. Xcalibur version 4.2.28.14 and Tune 3.1 2412.17 were used to operate the instrument.

Data Analysis

Acquired raw data files were processed using the Proteome Discoverer 2.2.0 platform, utilizing the Sequest HT database search en- gine and Percolator validation software node (V3.04) to remove false positives with a false discovery rate (FDR) of 1% on peptide and protein level under strict conditions. Searches were performed with full tryptic digestion against the human SwissProt database v2017.06 with up to two allowed miscleavage sites. Oxidation (+15.9949Da) of methionine was set as variable modification, while carbamidomethylation (+57.0214Da) of cysteine residues and TMT labeling of peptide N-termini and lysine residues were set as fixed modifications. Data was searched with mass tolerances of ± 10 ppm and ± 0.02Da on the precursor and fragment ions, respectively. Results were filtered to include peptide spectrum matches (PSMs) with Sequest HT cross-correlation factor (Xcorr) scores of R 1 and high peptide confidence assigned by Percolator. MS^2 signal-to-noise values (S/N) values of TMT reporter ions were used to estimate peptide/protein abundance changes. PSMs with precursor isolation interference values of R 50% and average TMT-reporter ion S/N % 10 were excluded from quantitation. Only unique peptides were used for TMT quantitation as well as for TOP3 label-free quanti- tation. Isotopic impurity correction and TMT channel-normalization based on total peptide amount were applied. For statistical anal- ysis and p value calculation, the integrated ANOVA hypothesis test was used. TMT ratios with p values below 0.01 were considered as significant. Only proteins with > 1 peptide detected and > 1 unique peptide detected were considered for further analysis. For the calling of destabilized substrate receptors, a log2 fold change threshold (CSN5i/DMSO) of 0.3 was applied. The compar- ison of destabilized substrate receptors in KBM7, AsPC1 and MV4;11 cells was performed on proteins detected across all cell lines. Absolute protein abundance estimates were derived from protein specific TOP3 scores calculated for the sum of all TMT channels. Each protein specific TOP3 score was subsequently multiplied with each sample specific TMT ratio to obtain estimates of protein abundance for each sample.

Supplementary Figures

Supplementary Figure 1.

(A) DMSO normalized live-cell luciferase signal of HAP1 VHL-Nanoluciferase knock-in cells treated with different doses of CSN5i-3 or DMSO (left). On the right, same cells co-treated with CSN5i-3 (250 nM) and ARV-771, MZ-1, VH-032, cis-MZ1 or DMSO (1 µM each). Representative data of n = 3 experiments.

(B) Volcano plot depicting global log_2-fold changes of protein abundance in HAP1 cells treated with CSN5i-3 (1 µM) for 8 h. CRL substrate receptors are labeled in the indicated colors. SRs selected for validation via luciferase tagging are highlighted. Data of *n* = 3 replicates.

(C) DMSO normalized live-cell luciferase signal of HAP1 cells overexpressing the indicated protein in C-terminal fusion with nano-luciferase. Cells were treated with DMSO, CSN5i-03 (500 nM) or CSN5i-03/MLN4924 (500 nM each) and measured at the indicated timepoint after treatment. Mean of n = 2 independent measurements. Representative data of n = 2 experiments.

Supplementary Figure 2.

(A) DMSO normalized live-cell luciferase signal of HEK293t HiBit-DCAF15 endogenous knock-in cells with ectopic expression of LgBit treated with indisulam or DMSO (10 uM). Representative data of n = 3 experiments.

(B) DMSO normalized live-cell luciferase signal of HAP1 cells with endogenous knock-in of Nanoluciferase for the indicated proteins. Cells were treated with DMSO, CSN5i-3 (250 nM, top) or CSN5i-3/indisulam (250 nM and 1 µM, bottom) and measured at the indicated timepoint after treatment. Mean of n = 2 independent measurements. Representative data of n = 2 experiments.

(C) Bar graph depicting fold-change in qPCR cycles of exponential amplification in HEK293t DCAF15$^{-/-}$ cells with reconstitution of HiBit-DCAF15 + LgBit after treatment with indisulam or DMSO for 10 h.

(D) Chemical structure of dRRM-1.

(E) TR-FRET ratio of BodipyFL-E7820 displacement from biotinylated, terbium labeled, Strep-II-Avi-tagged DCAF15 with increasing amounts of tasisulam, dRRM-1, indisulam or positive control E7820. The emission ratio of 520 nm (BodipyFL) over 490 nm (terbium) is calculated and depicted as mean ± s.d. from n = 3 independent replicates.

Supplementary Figure 1

A

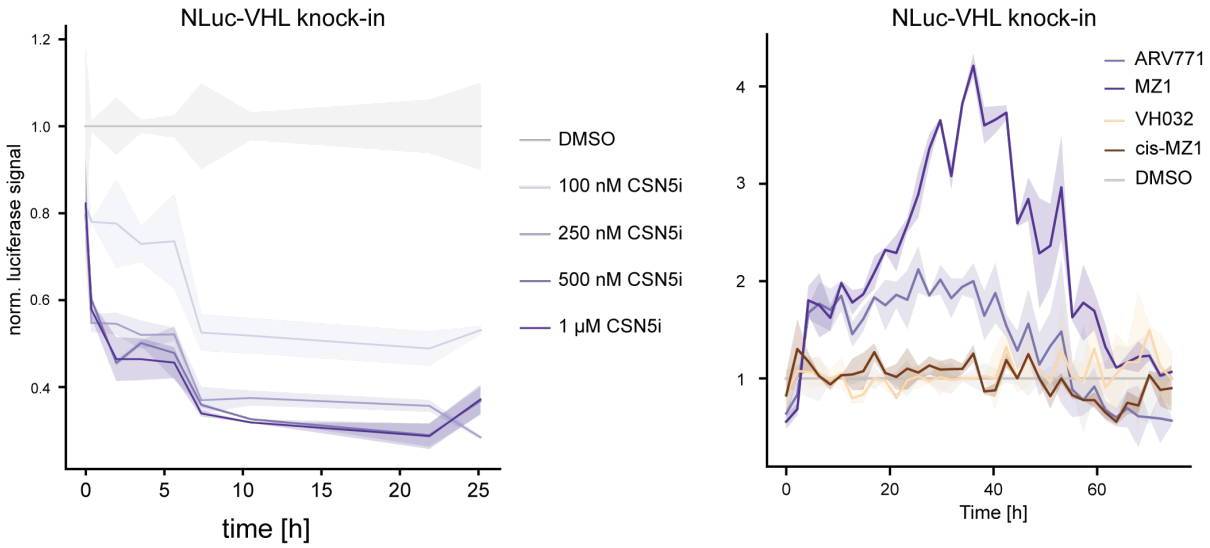

B

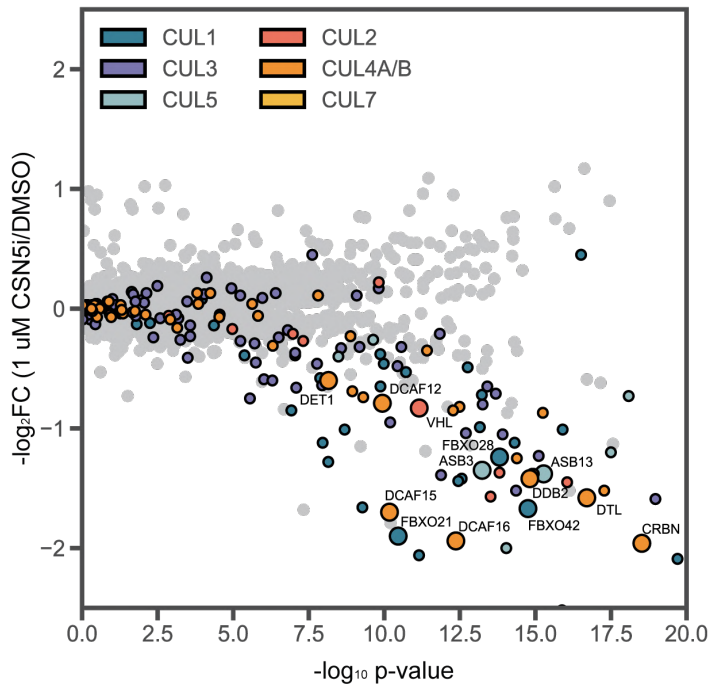

C

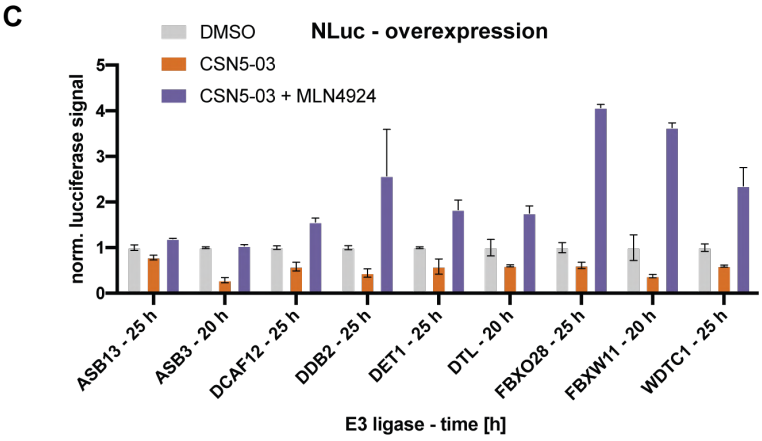

Supplementary Figure 2

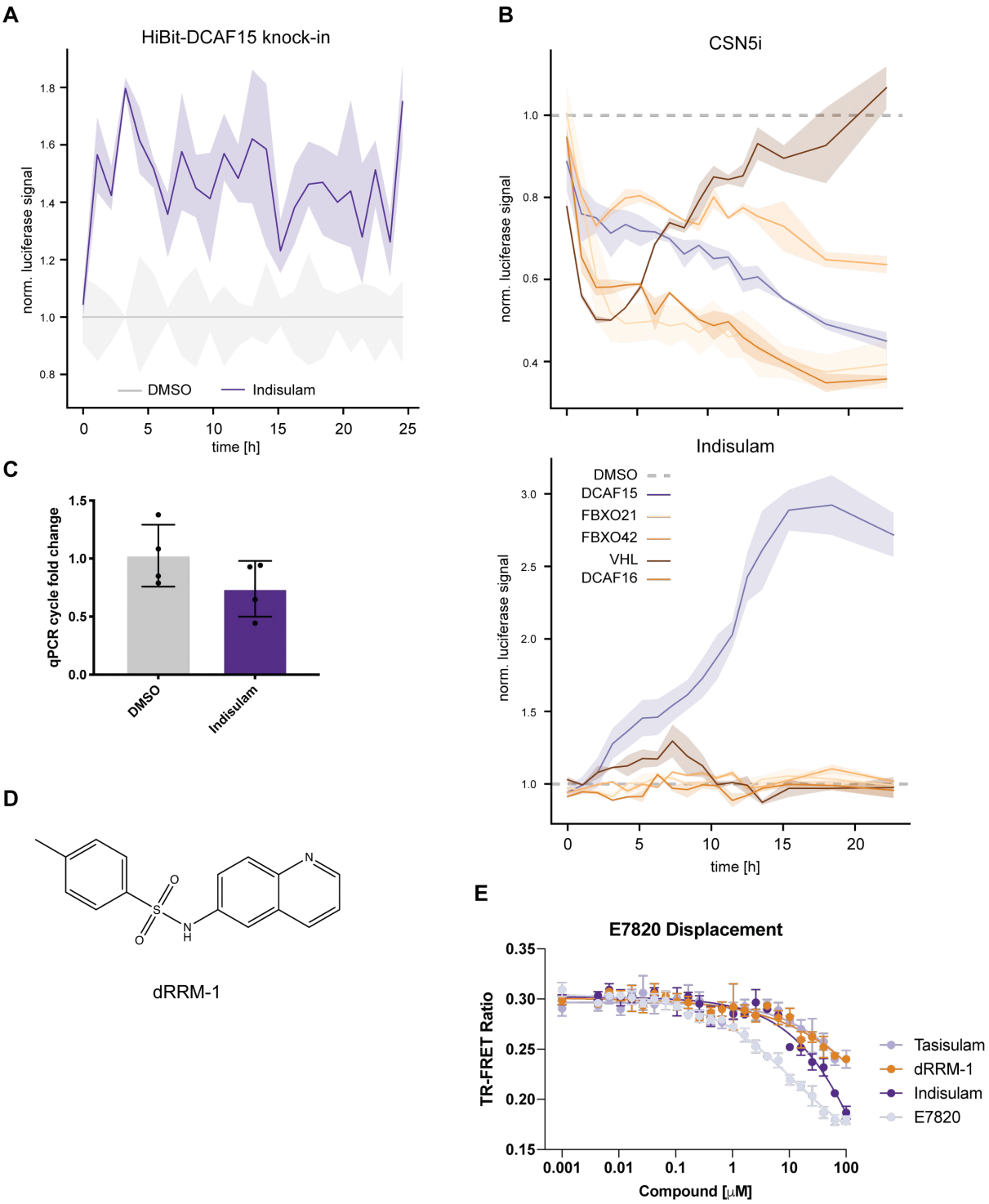

3. Discussion

Targeted protein degradation has seen a lot of excitement in the field of chemical biology due to its several advantages over small-molecule inhibitors. Conceptually, degrader molecules can be roughly characterized in two distinct bins: (i) molecular glue degraders, that facilitate the surface complementation between an E3 and a neo-substrate and (ii) PROTACs, that have two linked chemical warheads engaging the E3 and the neo-substrate respectively (Békés et al., 2022). TPD has fulfilled many of its promises such as increasing drug efficacy (Winter et al., 2015), engineering target selectivity (Brand et al., 2019), and potentially most important, targeting previously 'undruggable' proteins (Matyskiela et al., 2016). However, increasing reports have also highlighted several limitations that will need to be addressed in future studies. In the context of this thesis, we aimed to chart several of these limitations and further provide potential directions how to overcome them in the future.

3.1 Creating Functional Maps of E3 Ligase Surface Topology

At the center of small-molecule driven TPD lies the successful formation of a ternary complex between an E3 ligase, a degrader and a target protein of interest. This complex needs to attain a conformation conducive to target ubiquitination, including not only presentation of accessible lysines but also ensuring adequate PPIs to stabilize the complex (Hughes and Ciulli, 2017) Together these factors contribute to a phenomenon termed cooperativity, which is measured as the increase in binding energy of all three partners over that of only two of the parts (Gadd et al., 2017). The importance of the E3 ligase neo-substrate surface interface is further emphasized in a historic view of targeted protein degradation. Previous to being prescribed to pregnant women in the 1950s, the IMiD molecular glue degrader thalidomide was tested in animal models for safety. Unfortunately, mouse *CRBN* compared to human has several variants within the thalidomide binding pocket. Later studies showed that a single point mutation carried from mouse $CRBN^{I391}$ to human $CRBN^{V388I}$ was sufficient to abrogate degradation of ZF proteins in human models (Fink et al., 2018). Historically, this small difference masked the teratogenic effects during development of thalidomide. Hence, careful consideration and study should be put into understanding ternary complex interfaces and influences of their mutation for TPD.

Currently analysis of trimeric complexes induced by small molecule degraders is mostly performed through structural biology employing x-ray crystallography. This has yielded several advances such as optimizing E3 ligase ligands and PROTACs(Galdeano et al., 2014; Farnaby et al., 2019). Furthermore, it has helped understanding some of the spectacular effects of TPD such as target selectivity(Nowak et al., 2018). Nonetheless, crystallography comes with several drawbacks that limit its extent to unravel functionally relevant information in the field

of TPD. First, assays are typically performed on recombinant proteins, often truncated, which could mask or introduce effects of missing parts and non-physiological protein folding. Second, as these characterizations are performed ex vivo in crystals, they are neglecting the stoichiometry of binding partners in cells and introducing crystallization forces that might affect complex topology. Third, x-ray crystallography always provides a single snapshot of a specific structural conformation. It is known, that degraders can induce different structural alignments and still yield productive degradation of the same target.(Nowak et al., 2018) Therefore, it is safe to assume that these different conformations are found in equilibrium in a cellular state and crystallization pushes this balance into the single complex being measured. Subsequently, different conformations could also be affected distinctly by mutation or changes in degrader markup.

Several of the limitations could be addressed by in solution structural methods such as cryogenic electron microscopy (cryo-EM) or hydrogen exchange mass spectrometry (HDX-MS). In fact, both these methods have recently been employed to understand the allostery of CRBN molecular glue degraders (Watson et al., 2022). In these models degrader binding rearranges CRBN from an ‘open’ to a ‘closed’ conformation, which subsequently allows recognition and binding of the neo-substrate IKZF1. Similarly, investigating BET PROTAC degraders via HDX-MS has suggested considerable differences to structures originating from crystallography (Eron et al., 2021). Taken together, these factors indicate that methods for *in cellulo* functional assessment of ternary complexes may prove vital to deepen our understanding and provide physiologically relevant information for the field of TPD.

In the presented work we devised an approach that would allow us to sample the effect of all possible mutations within a 10 Å window of the degrader binding site of VHL and CRBN. Such a deep mutational scanning methods provide a resolution typically outside the reach of structural characterization of recombinant proteins. This is highlighted by some of the functional consequences we identified in our mutational resistance screens for VHL. The variants VHL^{H110L} and VHL^{P71I} for example lead to a gain in efficacy and resistance to select degraders while having no effect on others. Previously published co-crystal structures failed to rationalize these influences or have proved unobtainable to date (for ARV-771). Our results add an additional layer of functional information upon the surface topology of E3 ligases and together with structural elucidations can provide ample opportunities to optimize degrader molecules.

Several recent accounts have demonstrated that linker design can have large implications for PROTACs affecting their target engagement and off-target degradation. The variety of linker conformations is vastly increasing and several of the degraders selected for clinical trials have made surprising contributions to this variety (Nguyen et al., 2021; Békés et al., 2022).

Interestingly, our results we have indicated functional CRBN hotspots that seem to be selective for degraders with short linker conformations (dBET57) (Nowak et al., 2018). It is plausible that testing different linker and exit vector positions in our assays could yield combinations of PROTACs less prone to resistance.

Finally however, DMS also comes with several drawbacks that should be mentioned and can be managed with the addition of orthogonal assays to complement the data. Generation of mutational libraries is a costly endeavor and thereby only economical for ligases with ample opportunities for degrader testing. Furthermore, the costs involved typically mean that mutation of the full protein is not feasible. This necessitates that information of the degrader binding site and its structural surroundings is available. This structural characterization could potentially also originate from modelling approaches, although the complementation with classical experimental structural data provides many advantages showcased in this thesis' results section (Tunyasuvunakool et al., 2021).

The economical limitation to certain residues also entails that potential distal interactions were not captured in this iteration of mutational scanning. These potential contacts also lie outside the reach of crystallography approaches that don't employ full length proteins. An interesting method to investigate the full scope of factors was recently developed based on CRISPR suppressor scanning (Gosavi et al., 2022). The close overlapping use of a large amount of sgRNAs for genetic deletion of a single gene allows charting functionally important protein sites (Shi et al., 2015). With this, several distal sites on TPD neo-substrates could be identified, which presumably mediate E3 ligase interactions (Gosavi et al., 2022). However, with the tested degraders, these sites only contributed minor effects to the overall degradation efficacy.

Lastly, generation of large mutant libraries are typically performed by *de novo* synthesis, which can be an error prone process. In one of the here tested libraries such a defect lead to drastic overrepresentation of a single point mutant. As this mutant had no functional consequence to degrader treatments and our assays were based on positive selection of resistant mutants, this did lead to relevant biases in our assays. However, given our choice of short read sequencing, capturing relevant synthesis errors such as two mutations in the same construct was less likely. Strategies with longer read sequences or potentially even nanopore long-read sequencing could alleviate such library related problems. Also, since the presented libraries were generated, advances have made it possible to attach barcodes to each variant, thereby greatly reducing sequencing costs and facilitating assay simplicity.

3.2 Resistance to TPD and Strategies to Overcome it

Targeted small-molecule inhibitors against specific proteins have been applied in patient therapy for about 25 years. In clinics, these have greatly improved patient care by increasing survival and decreasing side-effects. Initial approvals of SMIs were obtained by trials in patients with advanced cancers refractory to conventional cytotoxic chemotherapy. Since then, targeted therapies have proven their value also as first-line therapy and in general occupy a large portion of the everyday clinical practice.(Bedard et al., 2020) As such, therapy resistance has rapidly emerged and been described subsequently. Most SMIs are targeted at kinases and resistances revolve around several conceptual mechanisms which are by now relatively well understood (see Chapter 1.3). These include upregulation of genes in the same cellular pathways but also the well described 'gatekeeper' mutations in the active site of the targeted kinase disrupting drug binding.

TPD as a therapeutic modality is however dependent on complex cellular cascades and therefore potentially also subject to different resistance mechanisms than SMIs. This was already acknowledged early in the development of degrader molecules with many insights into the genetic determinants of TPD. Genome wide genetic suppression screens have determined several expected factors important for TPD (Sievers et al., 2018a; Shirasaki et al., 2021; Mayor-Ruiz et al., 2019). These include the specific E3 ligases, but also their regulatory factors such as the COPP9 signalosome or even components of the 26S proteasome. Together these genetic screens however fail to recapitulate naturally occurring resistance mechanisms.

The here presented results aimed to close this gap via approaches to understand spontaneous resistance. Our analysis of genetic defects upon TPD resistance emergence has put spotlight on the substrate receptor of an E3 ligase. While we have identified mutations throughout the E3 ligase complex, most were localized in the degrader binding interface at the SR. Furthermore, by comparing the two E3 ligases most commonly employed for TPD ($CRL4^{CRBN}$ and $CRL2^{VHL}$), we were able to correlate key characteristics such as essentiality of the SR to the frequency and type of genetic alterations. As a comparison of only two E3 ligases for this purpose does not allow statistical certainty, future studies will however still have to consolidate these results. Unfortunately, the low number of E3 ligases amendable for TPD could mean that an indisputable answer to this question might still be years away.

Next to our study, also other approaches have investigated acquired targeted protein degrader resistance mechanisms, focusing also on transcriptional alterations. These have highlighted evasion via exon skipping and transcript downregulation. For instance, in lenalidomide or pomalidomide treated MM patients, frequencies of point mutations in *CRBN* but also copy losses and splicing variants losing exon 10 are increased with progressive IMiD

exposure (Kortüm et al., 2016; Gooding et al., 2021; Barrio et al., 2020). The clear link to the mechanism-of-action of these drugs becomes apparent with almost one-third of pomalidomide refractory patients bearing alterations in *CRBN* (Gooding et al., 2021). Similarly, clonal cell populations outgrowing $CRL2^{VHL}$ based PROTAC treatments have also exhibited exon skipping as a potential resistance mechanism (Zhang et al., 2019). Finally, a recent report has correlated hypermethylation in an active intronic *CRBN* enhancer with decreased *CRBN* expression and IMiD resistance (Haertle et al., 2021). Interestingly, DNA methyltransferase inhibitor treatment induced demethylation and sensitization to IMiD treatments in cell lines, potentially outlining one of many ways to overcome TPD resistance. Together these studies highlight, that resistance mechanisms in TPD are inherently heterogenic, even within a single patient and tumor. Genetic mutations in select genes are likely only contributing a fraction to therapy resistance and transcript variations are at least similarly important. Therefore, a single approach to overcoming resistance is unlikely to resolve every possible evasion mechanism of cancer cells to TPD.

In the presented results we were able to link mutations identified in MM patients to functional E3 ligase hotspots captured in our deep mutational scanning approaches. In our assays these prompted resistance to BET PROTACs and/or to GSPT1 degrading molecular glues. However, not all patient derived point mutations in CRBN elicited a response in the mutational screens. While it is clear, that IMiD activity in MM is linked to ZF degradation via CRBN, the full extent of other contributions is not clear yet (Jan et al., 2021). Hence, resistances following IMiD treatment could potentially be linked to any other drug action or the specific ZF target (most prominently IKZF1 and IKZF3) important for disease progression. As MM models can be troublesome to genetically engineer, we opted to design our screening assays around RKO cells. This prohibited us from directly assaying IMiDs because they show only minor efficacies in this cellular model. Therefore, any resistance mutation identified in patients but also in our mutational scanning approach is likely to be of general relevance to TPD modalities via the targeted ligase. Similarly, patient resistance mutations could be specific to the ZF target degradation they are blocking or even by-stander mutations originating from tumor heterogeneity.

Degrader molecules induce proximity between an E3 and a target protein, therefore resistance mechanisms could conceptually not only be mediated by the E3 ligase and degradation machinery but also to the target binding site. Recently, mutations in CDK12 have been described in cells resistant to a CDK12 degrading PROTAC (Jiang et al., 2021). This was also the first account of target based resistance in TPD. While we included the target genes BRD2/3 and 4 in our sequencing panel, we did not identify any spontaneous genetic alterations in BET PROTAC treated cells. This discrepancy could be explained by several

differences between the CDK12 and BET PRTOACs. Firstly, the assayed BET degraders are based on the inhibitor JQ1, which binds both N-terminal bromodomains on BRD4 with similar affinity and therefore has an intrinsic target redundancy as opposed to the CDK12 degrader (Winter et al., 2017; Raina et al., 2016; Jiang et al., 2021). Hence, escape mutations would necessarily be present in both bromodomains to elicit significant resistance effects. Secondly, the here assayed BET degraders dBET6 and ARV-771 lead to strong catalytic target degradation and therefore a marked increase in cellular efficacy over their parental inhibitor JQ1. At the assayed concentration of 500 nM, the inhibitory effect of these PROTACs on cells is therefore negligible. On the contrary, the discussed CDK12 degrader shows little increase in cellular cytotoxicity over its parental inhibitory component (Jiang et al., 2021). Hence, selection pressure upon treatment is elicited via degradation of the target and inhibition of the target, which overall might favor mutation of the target as opposed to the E3 ligase.

Together all of the above culminates in the question of how to overcome potential resistances to TPD. While our study does not answer this directly, it gives several insights that might steer future advances in the field. First, we identified several resistance mutations which were specific to the recruited substrate or even the specific degrader used. It is thus imaginable, that certain mutations which might become especially prevalent after specific degrader treatment, could be overcome by adapting the ligase interacting moiety. Similarly with PROTACs, we have detected functional E3 ligase hotspots which show selective resistance to degraders based on linker design (see also chapter 3.1). The history of kinase inhibitors might serve as a case example of such emerging resistance mutations followed by chemical adaptation cascades. Ideally, our presented results and future adaptations of the deep mutational scanning approach could allow preemptively responding to similarly emerging resistances in TPD.

Next to degrader and neo-substrate specific resistance mutations, our results highlight also E3 ligase hotspots of general relevance. Mutations in these residues would likely prohibit any chance of chemically adopting the degrader to overcome the resistance. In these cases, degrading the same disease-causing protein via a different E3 ligases could present a possible solution. This is further supported by our analysis of spontaneous resistance mutations which show no overlap between the $CRL4^{CRBN}$ based and the $CRL2^{VHL}$ based PROTAC. Hence, mutations that were acquired, likely don't lead to cross resistance in these cases. Furthermore, our results indicated that essential E3 ligases could present especially interesting for TPD, as they likely lead to lower rates of resistance upon degrader treatment. However, unfortunately the number of E3 ligases amendable to small-molecule mediated TPD is still very limited.

3.3 Unlocking Additional E3 Ligases for TPD

The previous chapter outlines numerous reasons for expanding the pool of E3 ligases which can be bound by small molecules to drive targeted degradation of a POI. Outside of emerging resistances, several advantages of TPD could further prompt the development of novel degrader compounds. The intricate dependencies of ternary complexes in TPD, can serve as an explanation how the same inhibitor warhead can yield functional PROTACs when linked to one E3 ligase binder while not degrading when targeted to a different E3 (Békés et al., 2022). This could also serve as an explanation for the remarkable selectivity of PROTACs over their parental inhibitors (Zengerle et al., 2015). Thus, to expand the degradable protein space but also to fight potential future resistances, targeting a larger fraction of the more than 600 E3 ligases will be a necessity for the future of the TPD field.

Several approaches have aimed to allow screening for novel degrader compounds. A special focus has also been put on identification of molecular glue degraders whose rational design has so far eluded chemical biologists (Słabicki et al., 2020; Mayor-Ruiz et al., 2020). Many of these approaches have been outlined and explained in more detail in chapter 1.8 of this thesis. What to date all E3 ligase and target independent degrader discovery methods share is by design a dependency on cytotoxic effects of the screened compounds. This conversely means that only proteins that are essential in the given cellular model will be targetable with such an approach. Given that such phenotypic screens are often performed in model systems for ease of handling and availability, this can cause severe limitations to drug discovery campaigns (Morgens et al., 2016).

In the presented results we have outlined a strategy to phenotypically screen for small-molecule modulators of Cullin RING E3 ligases. This method is based on intricacies of the regulation of CRLs, which are highly compartmentalized and constantly dynamically adjust their complex compositions in cells (Reitsma et al., 2017). We could show that degrader treatment affects a part of this CRL shuffling termed ‘auto-degradation’ ultimately leading to higher levels of the targeted E3 substrate receptor. Since our ligase tracing assay is dependent on functional modulation of the bespoke ligase, it will identify any compounds that sufficiently change the E3 substrate target spectrum. This conceptually includes degraders of non-essential neo-substrates and presents a main advantage over previously described methods (Słabicki et al., 2020; Mayor-Ruiz et al., 2020). Furthermore, this also includes small molecules that disrupt CRL assembly and regulation as well as downstream factors in ubiquitin dependent protein degradation. Examples of such inhibitors have proven hugely successful in cancer therapy (Richardson et al., 2003; Kuhn et al., 2007) highlighting an additional benefit of the presented method.

Dissecting true from false hits in any small-molecule screening assay presents a bottleneck to a successful drug discovery effort (Feng et al., 2019). Hence, assay design has always been geared towards lowering false hit ratios while ensuring true hit discovery and thereby reducing the signal-to-noise ratio. To that end, screening approaches that report based on gain of signal present conceptually advantageous over assays detecting signal loss (Kaelin, 2017). Thus, considerable effort has been put into designing ‘up’ assays to circumvent these disadvantages. An interesting example of this notion was recently reported where researchers turned the degradation of a POI (loss-of-signal) into a positive selection assay through generation of fusion protein constructs (Koduri et al., 2021) (see also chapter 1.8). The here precented ligase tracing assay was inherently designed to report on E3 ligase stabilization and hence a gain-of-signal assay. Through the induction and enhancement of auto-degradation, the cellular pool of the substrate receptor of interest is depleted. Degrader treatment however recruits a neo-substrate and blocks this self-ubiquitination. Conceptually, this gain in SR abundance poses a significant advantage and could serve as an explanation for the low hit ratio identified in our compound screens.

Since drug discovery efforts ultimately aim to generate benefit for patients, there are two conceptual approaches to identify new potential therapies. On the one hand, empirical approaches tend to measure phenotypic indicators of response in a disease model to discover new small-molecule drugs. Conversely, target-based approaches rationally select a POI to be drugged by an inhibitor or degrader (Swinney, 2013). In the field of TPD, the later approach has several facets to it that can be further investigated. Firstly, degraders function via two typically functionally independent proteins that are brought into proximity. To allow selective targeting of malignant tissue, one can select disease specific E3 ligases or POIs. Hence, chemical screening for binders of a selected E3 ligase can present especially advantageous in the field of TPD. This could allow for preselection not only based on tissue and disease specificity of the E3 but also based on intrinsic characteristics such as essentiality or even predictions of ligandability and probability of PPI induction. So far our presented ligase tracing approach is the only method to allow small-molecule E3 modulator screening in an E3 ligase driven but target agnostic fashion. Recent advances in chemical proteomics to identify covalent and non-covalent binders of proteins (Wang et al., 2019; Kuljanin et al., 2021) could further catalyze PROTAC development in conjunction with ligase tracing. This ‘binders-first’ approach to drug discovery opens several avenues once the molecular underpinnings of a disease state have been sufficiently understood to select POIs to target. However, for identifying novel functional E3 ligase modulators, binding of a small molecule does not guarantee successful degradation, neither on the E3 ligase side nor on the target side

(Donovan et al., 2020). Therefore, caution should be employed in each specific case of degrader development.

3.4 Conclusion and Future Prospects

To date advancements on many technological fronts such as CRISPR-Cas9, mass spectrometry and single-cell omics quantifications made it ever easier to gain insights into disease drivers and thereby increased the list of therapeutically actionable target proteins. Pharmacologic tractability of these targets is however lacking behind this development with only 5 percent of the human proteome successfully targeted by drug discovery (Müller et al., 2022).

TPD presents a revolution in pharmacology and could potentially present a solution to the limited chemical protein tractability. The clinical validation of molecular glue degraders in the form of IMiDs coupled with the rational design principles of PROTACs foretell a bright future and warrant the many degrader programs currently pushing into clinical trials. Factors such as resistances to degraders and expansion towards other E3 ligases have been investigated in the course of this work but will no less need to be further examined in future accounts. Increasing reports of molecular glue degraders are arising. With many of them identified in plants, such as auxin and jasmonic acid (Gray et al., 2001; Chini et al., 2007), their prevalence might be much higher than previously anticipated. Compound classes such as metabolites could serve as especially interesting cases to systematically investigate such molecular mechanisms.

Especially with molecular glues it becomes apparent that the field of TPD is only part of a larger movement in chemical biology termed proximity inducing pharmacology. Direct small molecule mediated target ubiquitination is only one iteration of TPD, with lysosomal and autophagy mediated target depletion mechanisms also described recently (Banik et al., 2020; Takahashi et al., 2019; Li et al., 2020). Similarly, antibodies have been employed to recruit membrane proteins to E3 ligases for subsequent lysosomal degradation (Cotton et al., 2021). However, target degradation presents only one result of forced protein proximity. Examples of dephosphorylating (Yamazoe et al., 2020; Chen et al., 2021), phosphorylating (Siriwardena et al., 2020), acetylating (Wang et al., 2021) and deubiquitinating (Henning et al., 2022) hetero-bifunctional molecules have been described. It remains to be seen how these modalities will translate to clinical success but overall, the potential for neo-morphic functional adaptation of proteins seem to be near limitless.

With the identification of molecular glue compounds in the early 1990s proximity inducing modalities in pharmacology were introduced (Brown et al., 1994; Sabatini et al., 1994). Given

the recent rise of TPD this field has gotten more and more attention and protein-protein interaction inducing agents are coming into the focus of drug hunters (Schreiber, 2021). While there are many established methods to characterize such protein-drug-protein interactions (mass spectrometry, biochemistry, etc.), there identification is still mostly based on chance. Future drug discovery efforts might aim to design saleable assays for rational molecular glue identification. This in turn could catalyze the discovery of neo-morphic glue mediated functions far beyond simple degradation, ultimately allowing drug discovery to catch up in the race of tractability for therapeutically intriguing target proteins.

4. Materials and Methods

All experimental and computational methods performed to obtain the results presented in this thesis are extensively covered in the PDF reprints of the respective manuscripts.

References

Adams, J. (2004). The proteasome: a suitable antineoplastic target. Nat Rev Cancer *4*, 349-360.

Allegra, C. J., Hoang, K., Yeh, G. C., Drake, J. C., and Baram, J. (1987). Evidence for direct inhibition of de novo purine synthesis in human MCF-7 breast cells as a principal mode of metabolic inhibition by methotrexate. J Biol Chem *262*, 13520-13526.

Amable, L., Reed, E., and Chabner, B. A. (2019). Platinum analogues. Cancer Chemotherapy, Immunotherapy and Biotherapy 234-248.

Ashkenazi, A., Fairbrother, W. J., Leverson, J. D., and Souers, A. J. (2017). From basic apoptosis discoveries to advanced selective BCL-2 family inhibitors. Nat Rev Drug Discov *16*, 273-284.

Baek, K., Krist, D. T., Prabu, J. R., Hill, S., Klügel, M., Neumaier, L. M., von Gronau, S., Kleiger, G., and Schulman, B. A. (2020). NEDD8 nucleates a multivalent cullin-RING-UBE2D ubiquitin ligation assembly. Nature *578*, 461-466.

Banik, S. M., Pedram, K., Wisnovsky, S., Ahn, G., Riley, N. M., and Bertozzi, C. R. (2020). Lysosome-targeting chimaeras for degradation of extracellular proteins. Nature *584*, 291-297.

Barrio, S., Munawar, U., Zhu, Y. X., Giesen, N., Shi, C. X., Viá, M. D., Sanchez, R., Bruins, L., Demler, T., Müller, N., Haertle, L., Garitano, A., Steinbrunn, T., Danhof, S., Cuenca, I., Barrio-Garcia, C., Braggio, E., Rosenwald, A., Martinez-Lopez, J., Rasche, L., Raab, M. S., Stewart, A. K., Einsele, H., Stühmer, T., and Kortüm, K. M. (2020). IKZF1/3 and $CRL4^{CRBN}$ E3 ubiquitin ligase mutations and resistance to immunomodulatory drugs in multiple myeloma. Haematologica *105*, e237-e241.

Basset-Séguin, N., Hauschild, A., Kunstfeld, R., Grob, J., Dréno, B., Mortier, L., Ascierto, P. A., Licitra, L., Dutriaux, C., Thomas, L., Meyer, N., Guillot, B., Dummer, R., Arenberger, P., Fife, K., Raimundo, A., Dika, E., Dimier, N., Fittipaldo, A., Xynos, I., and Hansson, J. (2017). Vismodegib in patients with advanced basal cell carcinoma: Primary analysis of STEVIE, an international, open-label trial. Eur J Cancer *86*, 334-348.

Baumeister, W., Walz, J., Zühl, F., and Seemüller, E. (1998). The proteasome: paradigm of a self-compartmentalizing protease. Cell *92*, 367-380.

Bedard, P. L., Hyman, D. M., Davids, M. S., and Siu, L. L. (2020). Small molecules, big impact: 20 years of targeted therapy in oncology. Lancet *395*, 1078-1088.

Bedford, L., Paine, S., Sheppard, P. W., Mayer, R. J., and Roelofs, J. (2010). Assembly, structure, and function of the 26S proteasome. Trends Cell Biol *20*, 391-401.

Behan, F. M., Iorio, F., Picco, G., Gonçalves, E., Beaver, C. M., Migliardi, G., Santos, R., Rao, Y., Sassi, F., Pinnelli, M., Ansari, R., Harper, S., Jackson, D. A., McRae, R., Pooley, R., Wilkinson, P., van der Meer, D., Dow, D., Buser-Doepner, C., Bertotti, A., Trusolino, L., Stronach, E. A., Saez-Rodriguez, J., Yusa, K., and Garnett, M. J. (2019). Prioritization of cancer therapeutic targets using CRISPR-Cas9 screens. Nature *568*, 511-516.

Békés, M., Langley, D. R., and Crews, C. M. (2022). PROTAC targeted protein degraders: the past is prologue. Nat Rev Drug Discov *21*, 181-200.

Bhat, K. P., Ümit Kaniskan, H., Jin, J., and Gozani, O. (2021). Epigenetics and beyond: targeting writers of protein lysine methylation to treat disease. Nat Rev Drug Discov *20*, 265-286.

Bighin, C., Pronzato, P., and Del Mastro, L. (2013). Trastuzumab emtansine in the treatment of HER-2-positive metastatic breast cancer patients. Future Oncol *9*, 955-957.

Boeckman, H. J., Trego, K. S., and Turchi, J. J. (2005). Cisplatin sensitizes cancer cells to ionizing radiation via inhibition of nonhomologous end joining. Mol Cancer Res *3*, 277-285.

Bolli, N., Avet-Loiseau, H., Wedge, D. C., Van Loo, P., Alexandrov, L. B., Martincorena, I., Dawson, K. J., Iorio, F., Nik-Zainal, S., Bignell, G. R., Hinton, J. W., Li, Y., Tubio, J. M., McLaren, S., O' Meara, S., Butler, A. P., Teague, J. W., Mudie, L., Anderson, E., Rashid, N., Tai, Y. T., Shammas, M. A., Sperling, A. S., Fulciniti, M., Richardson, P. G., Parmigiani, G., Magrangeas, F., Minvielle, S., Moreau, P., Attal, M., Facon, T., Futreal, P. A., Anderson, K. C., Campbell, P. J., and Munshi, N. C. (2014). Heterogeneity of genomic evolution and mutational profiles in multiple myeloma. Nat Commun *5*, 2997.

Brand, M., Jiang, B., Bauer, S., Donovan, K. A., Liang, Y., Wang, E. S., Nowak, R. P., Yuan, J. C., Zhang, T., Kwiatkowski, N., Müller, A. C., Fischer, E. S., Gray, N. S., and Winter, G. E. (2019). Homolog-Selective Degradation as a Strategy to Probe the Function of CDK6 in AML. Cell Chem Biol *26*, 300-306.e9.

Brown, E. J., Albers, M. W., Shin, T. B., Ichikawa, K., Keith, C. T., Lane, W. S., and Schreiber, S. L. (1994). A mammalian protein targeted by G1-arresting rapamycin-receptor complex. Nature *369*, 756-758.

Cavadini, S., Fischer, E. S., Bunker, R. D., Potenza, A., Lingaraju, G. M., Goldie, K. N., Mohamed, W. I., Faty, M., Petzold, G., Beckwith, R. E., Tichkule, R. B., Hassiepen, U., Abdulrahman, W., Pantelic, R. S., Matsumoto, S., Sugasawa, K., Stahlberg, H., and Thomä,

N. H. (2016). Cullin-RING ubiquitin E3 ligase regulation by the COP9 signalosome. Nature *531*, 598-603.

Ceppi, P., Volante, M., Novello, S., Rapa, I., Danenberg, K. D., Danenberg, P. V., Cambieri, A., Selvaggi, G., Saviozzi, S., Calogero, R., Papotti, M., and Scagliotti, G. V. (2006). ERCC1 and RRM1 gene expressions but not EGFR are predictive of shorter survival in advanced non-small-cell lung cancer treated with cisplatin and gemcitabine. Ann Oncol *17*, 1818-1825.

Chabner, B. A. Structure and Mechanism of Action. Cancer Chemotherapy, Immunotherapy and Biotherapy

Chapman, M. A., Lawrence, M. S., Keats, J. J., Cibulskis, K., Sougnez, C., Schinzel, A. C., Harview, C. L., Brunet, J. P., Ahmann, G. J., Adli, M., Anderson, K. C., Ardlie, K. G., Auclair, D., Baker, A., Bergsagel, P. L., Bernstein, B. E., Drier, Y., Fonseca, R., Gabriel, S. B., Hofmeister, C. C., Jagannath, S., Jakubowiak, A. J., Krishnan, A., Levy, J., Liefeld, T., Lonial, S., Mahan, S., Mfuko, B., Monti, S., Perkins, L. M., Onofrio, R., Pugh, T. J., Rajkumar, S. V., Ramos, A. H., Siegel, D. S., Sivachenko, A., Stewart, A. K., Trudel, S., Vij, R., Voet, D., Winckler, W., Zimmerman, T., Carpten, J., Trent, J., Hahn, W. C., Garraway, L. A., Meyerson, M., Lander, E. S., Getz, G., and Golub, T. R. (2011a). Initial genome sequencing and analysis of multiple myeloma. Nature *471*, 467-472.

Chapman, P. B., Hauschild, A., Robert, C., Haanen, J. B., Ascierto, P., Larkin, J., Dummer, R., Garbe, C., Testori, A., Maio, M., Hogg, D., Lorigan, P., Lebbe, C., Jouary, T., Schadendorf, D., Ribas, A., O'Day, S. J., Sosman, J. A., Kirkwood, J. M., Eggermont, A. M., Dreno, B., Nolop, K., Li, J., Nelson, B., Hou, J., Lee, R. J., Flaherty, K. T., McArthur, G. A., and BRIM-3, S. G. (2011b). Improved survival with vemurafenib in melanoma with BRAF V600E mutation. N Engl J Med *364*, 2507-2516.

Chauhan, D., Uchiyama, H., Akbarali, Y., Urashima, M., Yamamoto, K., Libermann, T. A., and Anderson, K. C. (1996). Multiple myeloma cell adhesion-induced interleukin-6 expression in bone marrow stromal cells involves activation of NF-kappa B. Blood *87*, 1104-1112.

Chen, P. H., Hu, Z., An, E., Okeke, I., Zheng, S., Luo, X., Gong, A., Jaime-Figueroa, S., and Crews, C. M. (2021). Modulation of Phosphoprotein Activity by Phosphorylation Targeting Chimeras (PhosTACs). ACS Chem Biol *16*, 2808-2815.

Chini, A., Fonseca, S., Fernández, G., Adie, B., Chico, J. M., Lorenzo, O., García-Casado, G., López-Vidriero, I., Lozano, F. M., Ponce, M. R., Micol, J. L., and Solano, R. (2007). The JAZ family of repressors is the missing link in jasmonate signalling. Nature *448*, 666-671.

Ciechanover, A. (2005). Proteolysis: from the lysosome to ubiquitin and the proteasome. Nat Rev Mol Cell Biol *6*, 79-87.

Cochran, A. G., Conery, A. R., and Sims, R. J. (2019). Bromodomains: a new target class for drug development. Nat Rev Drug Discov *18*, 609-628.

Coiffier, B., Haioun, C., Ketterer, N., Engert, A., Tilly, H., Ma, D., Johnson, P., Lister, A., Feuring-Buske, M., Radford, J. A., Capdeville, R., Diehl, V., and Reyes, F. (1998). Rituximab (anti-CD20 monoclonal antibody) for the treatment of patients with relapsing or refractory aggressive lymphoma: a multicenter phase II study. Blood *92*, 1927-1932.

Collins, G. A., and Goldberg, A. L. (2017). The Logic of the 26S Proteasome. Cell *169*, 792-806.

Cortes, J. E., Heidel, F. H., Fiedler, W., Smith, B. D., Robak, T., Montesinos, P., Candoni, A., Leber, B., Sekeres, M. A., Pollyea, D. A., Ferdinand, R., Ma, W. W., O'Brien, T., O'Connell, A., Chan, G., and Heuser, M. (2020). Survival outcomes and clinical benefit in patients with acute myeloid leukemia treated with glasdegib and low-dose cytarabine according to response to therapy. J Hematol Oncol *13*, 92.

Cotton, A. D., Nguyen, D. P., Gramespacher, J. A., Seiple, I. B., and Wells, J. A. (2021). Development of Antibody-Based PROTACs for the Degradation of the Cell-Surface Immune Checkpoint Protein PD-L1. J Am Chem Soc *143*, 593-598.

Dale, B., Cheng, M., Park, K. S., Kaniskan, H. Ü., Xiong, Y., and Jin, J. (2021). Advancing targeted protein degradation for cancer therapy. Nat Rev Cancer *21*, 638-654.

Davies, F. E., Raje, N., Hideshima, T., Lentzsch, S., Young, G., Tai, Y. T., Lin, B., Podar, K., Gupta, D., Chauhan, D., Treon, S. P., Richardson, P. G., Schlossman, R. L., Morgan, G. J., Muller, G. W., Stirling, D. I., and Anderson, K. C. (2001). Thalidomide and immunomodulatory derivatives augment natural killer cell cytotoxicity in multiple myeloma. Blood *98*, 210-216.

Deininger, M., Buchdunger, E., and Druker, B. J. (2005). The development of imatinib as a therapeutic agent for chronic myeloid leukemia. Blood *105*, 2640-2653.

Delgado, J. L., Hsieh, C. M., Chan, N. L., and Hiasa, H. (2018). Topoisomerases as anticancer targets. Biochem J *475*, 373-398.

Delmore, J. E., Issa, G. C., Lemieux, M. E., Rahl, P. B., Shi, J., Jacobs, H. M., Kastritis, E., Gilpatrick, T., Paranal, R. M., Qi, J., Chesi, M., Schinzel, A. C., McKeown, M. R., Heffernan, T. P., Vakoc, C. R., Bergsagel, P. L., Ghobrial, I. M., Richardson, P. G., Young, R. A., Hahn,

W. C., Anderson, K. C., Kung, A. L., Bradner, J. E., and Mitsiades, C. S. (2011). BET bromodomain inhibition as a therapeutic strategy to target c-Myc. Cell *146*, 904-917.

Domostegui, A., Nieto-Barrado, L., Perez-Lopez, C., and Mayor-Ruiz, C. (2022). Chasing molecular glue degraders: screening approaches. Chem Soc Rev *51*, 5498-5517.

Donovan, K. A., Ferguson, F. M., Bushman, J. W., Eleuteri, N. A., Bhunia, D., Ryu, S., Tan, L., Shi, K., Yue, H., Liu, X., Dobrovolsky, D., Jiang, B., Wang, J., Hao, M., You, I., Teng, M., Liang, Y., Hatcher, J., Li, Z., Manz, T. D., Groendyke, B., Hu, W., Nam, Y., Sengupta, S., Cho, H., Shin, I., Agius, M. P., Ghobrial, I. M., Ma, M. W., Che, J., Buhrlage, S. J., Sim, T., Gray, N. S., and Fischer, E. S. (2020). Mapping the Degradable Kinome Provides a Resource for Expedited Degrader Development. Cell *183*, 1714-1731.e10.

Douer, D. (2016). Efficacy and Safety of Vincristine Sulfate Liposome Injection in the Treatment of Adult Acute Lymphocytic Leukemia. Oncologist *21*, 840-847.

Druker, B. J., Tamura, S., Buchdunger, E., Ohno, S., Segal, G. M., Fanning, S., Zimmermann, J., and Lydon, N. B. (1996). Effects of a selective inhibitor of the Abl tyrosine kinase on the growth of Bcr-Abl positive cells. Nat Med *2*, 561-566.

Duan, R., Du, W., and Guo, W. (2020). EZH2: a novel target for cancer treatment. J Hematol Oncol *13*, 104.

Emanuele, M. J., Elia, A. E., Xu, Q., Thoma, C. R., Izhar, L., Leng, Y., Guo, A., Chen, Y. N., Rush, J., Hsu, P. W., Yen, H. C., and Elledge, S. J. (2011). Global identification of modular cullin-RING ligase substrates. Cell *147*, 459-474.

Eron, S. J., Huang, H., Agafonov, R. V., Fitzgerald, M. E., Patel, J., Michael, R. E., Lee, T. D., Hart, A. A., Shaulsky, J., Nasveschuk, C. G., Phillips, A. J., Fisher, S. L., and Good, A. (2021). Structural Characterization of Degrader-Induced Ternary Complexes Using Hydrogen-Deuterium Exchange Mass Spectrometry and Computational Modeling: Implications for Structure-Based Design. ACS Chem Biol *16*, 2228-2243.

Falkenberg, K. J., and Johnstone, R. W. (2014). Histone deacetylases and their inhibitors in cancer, neurological diseases and immune disorders. Nat Rev Drug Discov *13*, 673-691.

Farber, S., and Diamond, L. K. (1948). Temporary remissions in acute leukemia in children produced by folic acid antagonist, 4-aminopteroyl-glutamic acid. N Engl J Med *238*, 787-793.

Farnaby, W., Koegl, M., Roy, M. J., Whitworth, C., Diers, E., Trainor, N., Zollman, D., Steurer, S., Karolyi-Oezguer, J., Riedmueller, C., Gmaschitz, T., Wachter, J., Dank, C., Galant, M., Sharps, B., Rumpel, K., Traxler, E., Gerstberger, T., Schnitzer, R., Petermann, O.,

Greb, P., Weinstabl, H., Bader, G., Zoephel, A., Weiss-Puxbaum, A., Ehrenhöfer-Wölfer, K., Wöhrle, S., Boehmelt, G., Rinnenthal, J., Arnhof, H., Wiechens, N., Wu, M. Y., Owen-Hughes, T., Ettmayer, P., Pearson, M., McConnell, D. B., and Ciulli, A. (2019). BAF complex vulnerabilities in cancer demonstrated via structure-based PROTAC design. Nat Chem Biol *15*, 672-680.

Feng, T., Basu, P., Sun, W., Ku, H. T., and Mack, W. J. (2019). Optimal design for high-throughput screening via false discovery rate control. Stat Med *38*, 2816-2827.

Ferguson, F. M., and Gray, N. S. (2018). Kinase inhibitors: the road ahead. Nat Rev Drug Discov *17*, 353-377.

Ferlay, J., Colombet, M., Soerjomataram, I., Parkin, D. M., Piñeros, M., Znaor, A., and Bray, F. (2021). Cancer statistics for the year 2020: An overview. Int J Cancer

Ferrara, N., Hillan, K. J., Gerber, H. P., and Novotny, W. (2004). Discovery and development of bevacizumab, an anti-VEGF antibody for treating cancer. Nat Rev Drug Discov *3*, 391-400.

Fink, E. C., McConkey, M., Adams, D. N., Haldar, S. D., Kennedy, J. A., Guirguis, A. A., Udeshi, N. D., Mani, D. R., Chen, M., Liddicoat, B., Svinkina, T., Nguyen, A. T., Carr, S. A., and Ebert, B. L. (2018). $Crbn^{I391V}$ is sufficient to confer in vivo sensitivity to thalidomide and its derivatives in mice. Blood *132*, 1535-1544.

Fischer, K. R., Durrans, A., Lee, S., Sheng, J., Li, F., Wong, S. T., Choi, H., El Rayes, T., Ryu, S., Troeger, J., Schwabe, R. F., Vahdat, L. T., Altorki, N. K., Mittal, V., and Gao, D. (2015). Epithelial-to-mesenchymal transition is not required for lung metastasis but contributes to chemoresistance. Nature *527*, 472-476.

Flaherty, K. T., Robert, C., Hersey, P., Nathan, P., Garbe, C., Milhem, M., Demidov, L. V., Hassel, J. C., Rutkowski, P., Mohr, P., Dummer, R., Trefzer, U., Larkin, J. M., Utikal, J., Dreno, B., Nyakas, M., Middleton, M. R., Becker, J. C., Casey, M., Sherman, L. J., Wu, F. S., Ouellet, D., Martin, A. M., Patel, K., Schadendorf, D., and METRIC, S. G. (2012). Improved survival with MEK inhibition in BRAF-mutated melanoma. N Engl J Med *367*, 107-114.

Fornasier, G., Francescon, S., and Baldo, P. (2018). An Update of Efficacy and Safety of Cetuximab in Metastatic Colorectal Cancer: A Narrative Review. Adv Ther *35*, 1497-1509.

Fruman, D. A., Chiu, H., Hopkins, B. D., Bagrodia, S., Cantley, L. C., and Abraham, R. T. (2017). The PI3K Pathway in Human Disease. Cell *170*, 605-635.

Futreal, P. A., Coin, L., Marshall, M., Down, T., Hubbard, T., Wooster, R., Rahman, N., and Stratton, M. R. (2004). A census of human cancer genes. Nat Rev Cancer *4*, 177-183.

Gadd, M. S., Testa, A., Lucas, X., Chan, K. H., Chen, W., Lamont, D. J., Zengerle, M., and Ciulli, A. (2017). Structural basis of PROTAC cooperative recognition for selective protein degradation. Nat Chem Biol *13*, 514-521.

Galdeano, C., Gadd, M. S., Soares, P., Scaffidi, S., Van Molle, I., Birced, I., Hewitt, S., Dias, D. M., and Ciulli, A. (2014). Structure-guided design and optimization of small molecules targeting the protein-protein interaction between the von Hippel-Lindau (VHL) E3 ubiquitin ligase and the hypoxia inducible factor (HIF) alpha subunit with in vitro nanomolar affinities. J Med Chem *57*, 8657-8663.

Gandhi, A. K., Kang, J., Havens, C. G., Conklin, T., Ning, Y., Wu, L., Ito, T., Ando, H., Waldman, M. F., Thakurta, A., Klippel, A., Handa, H., Daniel, T. O., Schafer, P. H., and Chopra, R. (2014). Immunomodulatory agents lenalidomide and pomalidomide co-stimulate T cells by inducing degradation of T cell repressors Ikaros and Aiolos via modulation of the E3 ubiquitin ligase complex CRL4(CRBN.). Br J Haematol *164*, 811-821.

Gerson, S. L. (2004). MGMT: its role in cancer aetiology and cancer therapeutics. Nat Rev Cancer *4*, 296-307.

Gooding, S., Ansari-Pour, N., Towfic, F., Ortiz Estévez, M., Chamberlain, P. P., Tsai, K. T., Flynt, E., Hirst, M., Rozelle, D., Dhiman, P., Neri, P., Ramasamy, K., Bahlis, N., Vyas, P., and Thakurta, A. (2021). Multiple cereblon genetic changes are associated with acquired resistance to lenalidomide or pomalidomide in multiple myeloma. Blood *137*, 232-237.

Goodman, L., and Wintrobe, M. (1946). Nitrogen mustard therapy; use of methyl-bis (beta-chloroethyl) amine hydrochloride and tris (beta-chloroethyl) amine hydrochloride for Hodgkin's disease, lymphosarcoma, leukemia and certain allied and miscellaneous disorders. J Am Med Assoc *132*, 126-132.

Gosavi, P. M., Ngan, K. C., Yeo, M. J. R., Su, C., Li, J., Lue, N. Z., Hoenig, S. M., and Liau, B. B. (2022). Profiling the Landscape of Drug Resistance Mutations in Neosubstrates to Molecular Glue Degraders. ACS Cent Sci *8*, 417-429.

Gounder, M., Schöffski, P., Jones, R. L., Agulnik, M., Cote, G. M., Villalobos, V. M., Attia, S., Chugh, R., Chen, T. W., Jahan, T., Loggers, E. T., Gupta, A., Italiano, A., Demetri, G. D., Ratan, R., Davis, L. E., Mir, O., Dileo, P., Van Tine, B. A., Pressey, J. G., Lingaraj, T., Rajarethinam, A., Sierra, L., Agarwal, S., and Stacchiotti, S. (2020). Tazemetostat in advanced

epithelioid sarcoma with loss of INI1/SMARCB1: an international, open-label, phase 2 basket study. Lancet Oncol *21*, 1423-1432.

Gray, W. M., Kepinski, S., Rouse, D., Leyser, O., and Estelle, M. (2001). Auxin regulates SCF(TIR1)-dependent degradation of AUX/IAA proteins. Nature *414*, 271-276.

Haertle, L., Barrio, S., Munawar, U., Han, S., Zhou, X., Vogt, C., Fernández, R. A., Bittrich, M., Ruiz-Heredia, Y., Da Viá, M., Zovko, J., Garitano-Trojaola, A., Bolli, N., Ruckdeschel, A., Stühmer, T., Chatterjee, M., Kull, M., Krönke, J., Agirre, X., Martin-Subero, J. I., Raab, P., Einsele, H., Rasche, L., Martinez-Lopez, J., Haaf, T., and Kortüm, K. M. (2021). Cereblon enhancer methylation and IMiD resistance in multiple myeloma. Blood *138*, 1721-1726.

Hales, B. F. (1999). Thalidomide on the comeback trail. Nat Med *5*, 489-490.

Hanahan, D. (2022). Hallmarks of Cancer: New Dimensions. Cancer Discov *12*, 31-46.

Hanahan, D., and Weinberg, R. A. (2000). The hallmarks of cancer. Cell *100*, 57-70.

Hanahan, D., and Weinberg, R. A. (2011). Hallmarks of cancer: the next generation. Cell *144*, 646-674.

Harbeck, N., Beckmann, M. W., Rody, A., Schneeweiss, A., Müller, V., Fehm, T., Marschner, N., Gluz, O., Schrader, I., Heinrich, G., Untch, M., and Jackisch, C. (2013). HER2 Dimerization Inhibitor Pertuzumab - Mode of Action and Clinical Data in Breast Cancer. Breast Care (Basel) *8*, 49-55.

Heidelberger, C., Caudhuri, N. K., Dannenberg, P., Mooren, D., Griesbach, L., Duschinsky, R., Schnitzer, R. J., Pleven, E., and Scheiner, J. (1957). Fluorinated pyrimidines, a new class of tumour-inhibitory compounds. Nature *179*, 663-666.

Henning, N. J., Boike, L., Spradlin, J. N., Ward, C. C., Liu, G., Zhang, E., Belcher, B. P., Brittain, S. M., Hesse, M. J., Dovala, D., McGregor, L. M., Valdez Misiolek, R., Plasschaert, L. W., Rowlands, D. J., Wang, F., Frank, A. O., Fuller, D., Estes, A. R., Randal, K. L., Panidapu, A., McKenna, J. M., Tallarico, J. A., Schirle, M., and Nomura, D. K. (2022). Deubiquitinase-targeting chimeras for targeted protein stabilization. Nat Chem Biol *18*, 412-421.

Hicke, L. (2001). Protein regulation by monoubiquitin. Nat Rev Mol Cell Biol *2*, 195-201.

Hodi, F. S., O'Day, S. J., McDermott, D. F., Weber, R. W., Sosman, J. A., Haanen, J. B., Gonzalez, R., Robert, C., Schadendorf, D., Hassel, J. C., Akerley, W., van den Eertwegh, A. J., Lutzky, J., Lorigan, P., Vaubel, J. M., Linette, G. P., Hogg, D., Ottensmeier, C. H., Lebbé, C., Peschel, C., Quirt, I., Clark, J. I., Wolchok, J. D., Weber, J. S., Tian, J., Yellin, M. J., Nichol,

G. M., Hoos, A., and Urba, W. J. (2010). Improved survival with ipilimumab in patients with metastatic melanoma. N Engl J Med *363*, 711-723.

Hopkins, A. L., and Groom, C. R. (2002). The druggable genome. Nature Reviews Drug Discovery *1*, 727-730.

Hughes, S. J., and Ciulli, A. (2017). Molecular recognition of ternary complexes: a new dimension in the structure-guided design of chemical degraders. Essays Biochem *61*, 505-516.

Ito, T., Ando, H., Suzuki, T., Ogura, T., Hotta, K., Imamura, Y., Yamaguchi, Y., and Handa, H. (2010). Identification of a primary target of thalidomide teratogenicity. Science *327*, 1345-1350.

Ivan, M., Kondo, K., Yang, H., Kim, W., Valiando, J., Ohh, M., Salic, A., Asara, J. M., Lane, W. S., and Kaelin, W. G. (2001). HIFalpha targeted for VHL-mediated destruction by proline hydroxylation: implications for O2 sensing. Science *292*, 464-468.

Jaakkola, P., Mole, D. R., Tian, Y. M., Wilson, M. I., Gielbert, J., Gaskell, S. J., von Kriegsheim, A., Hebestreit, H. F., Mukherji, M., Schofield, C. J., Maxwell, P. H., Pugh, C. W., and Ratcliffe, P. J. (2001). Targeting of HIF-alpha to the von Hippel-Lindau ubiquitylation complex by O2-regulated prolyl hydroxylation. Science *292*, 468-472.

Jacobson, L. O., Spurr, C. L., Barron, E. S. G., Smith, T., Lushbaugh, C., and Dick, G. F. (1946). Nitrogen mustard therapy: Studies on the effect of methyl-bis (beta-chloroethyl) amine hydrochloride on neoplastic diseases and allied disorders of the hemopoietic system. Journal of the American Medical Association *132*, 263-271.

Jan, M., Sperling, A. S., and Ebert, B. L. (2021). Cancer therapies based on targeted protein degradation - lessons learned with lenalidomide. Nat Rev Clin Oncol *18*, 401-417.

Jiang, B., Gao, Y., Che, J., Lu, W., Kaltheuner, I. H., Dries, R., Kalocsay, M., Berberich, M. J., Jiang, J., You, I., Kwiatkowski, N., Riching, K. M., Daniels, D. L., Sorger, P. K., Geyer, M., Zhang, T., and Gray, N. S. (2021). Discovery and resistance mechanism of a selective CDK12 degrader. Nat Chem Biol *17*, 675-683.

Kaelin, W. G. (2017). Common pitfalls in preclinical cancer target validation. Nat Rev Cancer *17*, 425-440.

Kamura, T., Koepp, D. M., Conrad, M. N., Skowyra, D., Moreland, R. J., Iliopoulos, O., Lane, W. S., Kaelin, W. G., Elledge, S. J., Conaway, R. C., Harper, J. W., and Conaway, J.

W. (1999). Rbx1, a component of the VHL tumor suppressor complex and SCF ubiquitin ligase. Science *284*, 657-661.

Kantarjian, H., Issa, J. P., Rosenfeld, C. S., Bennett, J. M., Albitar, M., DiPersio, J., Klimek, V., Slack, J., de Castro, C., Ravandi, F., Helmer, R., Shen, L., Nimer, S. D., Leavitt, R., Raza, A., and Saba, H. (2006). Decitabine improves patient outcomes in myelodysplastic syndromes: results of a phase III randomized study. Cancer *106*, 1794-1803.

Kawakami, T., Chiba, T., Suzuki, T., Iwai, K., Yamanaka, K., Minato, N., Suzuki, H., Shimbara, N., Hidaka, Y., Osaka, F., Omata, M., and Tanaka, K. (2001). NEDD8 recruits E2-ubiquitin to SCF E3 ligase. EMBO J *20*, 4003-4012.

King, M. C., Marks, J. H., Mandell, J. B., and New, Y. B. C. S. G. (2003). Breast and ovarian cancer risks due to inherited mutations in BRCA1 and BRCA2. Science *302*, 643-646.

Koduri, V., Duplaquet, L., Lampson, B. L., Wang, A. C., Sabet, A. H., Ishoey, M., Paulk, J., Teng, M., Harris, I. S., Endress, J. E., Liu, X., Dasilva, E., Paulo, J. A., Briggs, K. J., Doench, J. G., Ott, C. J., Zhang, T., Donovan, K. A., Fischer, E. S., Gygi, S. P., Gray, N. S., Bradner, J., Medin, J. A., Buhrlage, S. J., Oser, M. G., and Kaelin, W. G. (2021). Targeting oncoproteins with a positive selection assay for protein degraders. Sci Adv *7*, eabd6263.

Komander, D., Clague, M. J., and Urbé, S. (2009). Breaking the chains: structure and function of the deubiquitinases. Nat Rev Mol Cell Biol *10*, 550-563.

Komander, D., and Rape, M. (2012). The ubiquitin code. Annu Rev Biochem *81*, 203-229.

Kortüm, K. M., Mai, E. K., Hanafiah, N. H., Shi, C. X., Zhu, Y. X., Bruins, L., Barrio, S., Jedlowski, P., Merz, M., Xu, J., Stewart, R. A., Andrulis, M., Jauch, A., Hillengass, J., Goldschmidt, H., Bergsagel, P. L., Braggio, E., Stewart, A. K., and Raab, M. S. (2016). Targeted sequencing of refractory myeloma reveals a high incidence of mutations in CRBN and Ras pathway genes. Blood *128*, 1226-1233.

Krönke, J., Udeshi, N. D., Narla, A., Grauman, P., Hurst, S. N., McConkey, M., Svinkina, T., Heckl, D., Comer, E., Li, X., Ciarlo, C., Hartman, E., Munshi, N., Schenone, M., Schreiber, S. L., Carr, S. A., and Ebert, B. L. (2014). Lenalidomide causes selective degradation of IKZF1 and IKZF3 in multiple myeloma cells. Science *343*, 301-305.

Kufe, D. W., Munroe, D., Herrick, D., Egan, E., and Spriggs, D. (1984). Effects of 1-beta-D-arabinofuranosylcytosine incorporation on eukaryotic DNA template function. Mol Pharmacol *26*, 128-134.

Kuhn, D. J., Chen, Q., Voorhees, P. M., Strader, J. S., Shenk, K. D., Sun, C. M., Demo, S. D., Bennett, M. K., van Leeuwen, F. W., Chanan-Khan, A. A., and Orlowski, R. Z. (2007). Potent activity of carfilzomib, a novel, irreversible inhibitor of the ubiquitin-proteasome pathway, against preclinical models of multiple myeloma. Blood *110*, 3281-3290.

Kuljanin, M., Mitchell, D. C., Schweppe, D. K., Gikandi, A. S., Nusinow, D. P., Bulloch, N. J., Vinogradova, E. V., Wilson, D. L., Kool, E. T., Mancias, J. D., Cravatt, B. F., and Gygi, S. P. (2021). Reimagining high-throughput profiling of reactive cysteines for cell-based screening of large electrophile libraries. Nat Biotechnol *39*, 630-641.

Ledford, H. (2016). Cocktails for cancer with a measure of immunotherapy. Nature *532*, 162-164.

Li, J., Cai, Z., Vaites, L. P., Shen, N., Mitchell, D. C., Huttlin, E. L., Paulo, J. A., Harry, B. L., and Gygi, S. P. (2021). Proteome-wide mapping of short-lived proteins in human cells. Mol Cell *81*, 4722-4735.e5.

Li, Y., Gazdoiu, S., Pan, Z. Q., and Fuchs, S. Y. (2004). Stability of homologue of Slimb F-box protein is regulated by availability of its substrate. J Biol Chem *279*, 11074-11080.

Li, Z., Zhu, C., Ding, Y., Fei, Y., and Lu, B. (2020). ATTEC: a potential new approach to target proteinopathies. Autophagy *16*, 185-187.

Lingaraju, G. M., Bunker, R. D., Cavadini, S., Hess, D., Hassiepen, U., Renatus, M., Fischer, E. S., and Thomä, N. H. (2014). Crystal structure of the human COP9 signalosome. Nature *512*, 161-165.

Liu, J., Song, T., Zhou, W., Xing, L., Wang, S., Ho, M., Peng, Z., Tai, Y. T., Hideshima, T., Anderson, K. C., and Cang, Y. (2019). A genome-scale CRISPR-Cas9 screening in myeloma cells identifies regulators of immunomodulatory drug sensitivity. Leukemia *33*, 171-180.

Lohr, J. G., Stojanov, P., Carter, S. L., Cruz-Gordillo, P., Lawrence, M. S., Auclair, D., Sougnez, C., Knoechel, B., Gould, J., Saksena, G., Cibulskis, K., McKenna, A., Chapman, M. A., Straussman, R., Levy, J., Perkins, L. M., Keats, J. J., Schumacher, S. E., Rosenberg, M., Multiple, M. R. C., Getz, G., and Golub, T. R. (2014). Widespread genetic heterogeneity in multiple myeloma: implications for targeted therapy. Cancer Cell *25*, 91-101.

Lord, C. J., and Ashworth, A. (2017). PARP inhibitors: Synthetic lethality in the clinic. Science *355*, 1152-1158.

Lu, G., Middleton, R. E., Sun, H., Naniong, M., Ott, C. J., Mitsiades, C. S., Wong, K. K., Bradner, J. E., and Kaelin, W. G. (2014). The myeloma drug lenalidomide promotes the cereblon-dependent destruction of Ikaros proteins. Science *343*, 305-309.

Lu, Y., Lee, B. H., King, R. W., Finley, D., and Kirschner, M. W. (2015). Substrate degradation by the proteasome: a single-molecule kinetic analysis. Science *348*, 1250834.

Lulla, P. D., Hill, L. C., Ramos, C. A., and Heslop, H. E. (2018). The use of chimeric antigen receptor T cells in patients with non-Hodgkin lymphoma. Clin Adv Hematol Oncol *16*, 375-386.

Lynch, T. J., Bell, D. W., Sordella, R., Gurubhagavatula, S., Okimoto, R. A., Brannigan, B. W., Harris, P. L., Haserlat, S. M., Supko, J. G., Haluska, F. G., Louis, D. N., Christiani, D. C., Settleman, J., and Haber, D. A. (2004). Activating mutations in the epidermal growth factor receptor underlying responsiveness of non-small-cell lung cancer to gefitinib. N Engl J Med *350*, 2129-2139.

Martincorena, I., Raine, K. M., Gerstung, M., Dawson, K. J., Haase, K., Van Loo, P., Davies, H., Stratton, M. R., and Campbell, P. J. (2017). Universal Patterns of Selection in Cancer and Somatic Tissues. Cell *171*, 1029-1041.e21.

Matyskiela, M. E., Lu, G., Ito, T., Pagarigan, B., Lu, C. C., Miller, K., Fang, W., Wang, N. Y., Nguyen, D., Houston, J., Carmel, G., Tran, T., Riley, M., Nosaka, L., Lander, G. C., Gaidarova, S., Xu, S., Ruchelman, A. L., Handa, H., Carmichael, J., Daniel, T. O., Cathers, B. E., Lopez-Girona, A., and Chamberlain, P. P. (2016). A novel cereblon modulator recruits GSPT1 to the CRL4(CRBN) ubiquitin ligase. Nature *535*, 252-257.

Mayor-Ruiz, C., Bauer, S., Brand, M., Kozicka, Z., Siklos, M., Imrichova, H., Kaltheuner, I. H., Hahn, E., Seiler, K., Koren, A., Petzold, G., Fellner, M., Bock, C., Müller, A. C., Zuber, J., Geyer, M., Thomä, N. H., Kubicek, S., and Winter, G. E. (2020). Rational discovery of molecular glue degraders via scalable chemical profiling. Nat Chem Biol *16*, 1199-1207.

Mayor-Ruiz, C., Jaeger, M. G., Bauer, S., Brand, M., Sin, C., Hanzl, A., Mueller, A. C., Menche, J., and Winter, G. E. (2019). Plasticity of the Cullin-RING Ligase Repertoire Shapes Sensitivity to Ligand-Induced Protein Degradation. Molecular Cell *75*, 849-858.e8.

Migden, M. R., Guminski, A., Gutzmer, R., Dirix, L., Lewis, K. D., Combemale, P., Herd, R. M., Kudchadkar, R., Trefzer, U., Gogov, S., Pallaud, C., Yi, T., Mone, M., Kaatz, M., Loquai, C., Stratigos, A. J., Schulze, H. J., Plummer, R., Chang, A. L., Cornélis, F., Lear, J. T., Sellami, D., and Dummer, R. (2015). Treatment with two different doses of sonidegib in patients with locally advanced or metastatic basal cell carcinoma (BOLT): a multicentre, randomised, double-blind phase 2 trial. Lancet Oncol *16*, 716-728.

Milanovic, M., Fan, D. N. Y., Belenki, D., Däbritz, J. H. M., Zhao, Z., Yu, Y., Dörr, J. R., Dimitrova, L., Lenze, D., Monteiro Barbosa, I. A., Mendoza-Parra, M. A., Kanashova, T., Metzner, M., Pardon, K., Reimann, M., Trumpp, A., Dörken, B., Zuber, J., Gronemeyer, H., Hummel, M., Dittmar, G., Lee, S., and Schmitt, C. A. (2018). Senescence-associated reprogramming promotes cancer stemness. Nature *553*, 96-100.

Moreira, A. L., Sampaio, E. P., Zmuidzinas, A., Frindt, P., Smith, K. A., and Kaplan, G. (1993). Thalidomide exerts its inhibitory action on tumor necrosis factor alpha by enhancing mRNA degradation. J Exp Med *177*, 1675-1680.

Morgens, D. W., Deans, R. M., Li, A., and Bassik, M. C. (2016). Systematic comparison of CRISPR/Cas9 and RNAi screens for essential genes. Nat Biotechnol *34*, 634-636.

Müller, S., Ackloo, S., Al Chawaf, A., Al-Lazikani, B., Antolin, A., Baell, J. B., Beck, H., Beedie, S., Betz, U. A. K., Bezerra, G. A., Brennan, P. E., Brown, D., Brown, P. J., Bullock, A. N., Carter, A. J., Chaikuad, A., Chaineau, M., Ciulli, A., Collins, I., Dreher, J., Drewry, D., Edfeldt, K., Edwards, A. M., Egner, U., Frye, S. V., Fuchs, S. M., Hall, M. D., Hartung, I. V., Hillisch, A., Hitchcock, S. H., Homan, E., Kannan, N., Kiefer, J. R., Knapp, S., Kostic, M., Kubicek, S., Leach, A. R., Lindemann, S., Marsden, B. D., Matsui, H., Meier, J. L., Merk, D., Michel, M., Morgan, M. R., Mueller-Fahrnow, A., Owen, D. R., Perry, B. G., Rosenberg, S. H., Saikatendu, K. S., Schapira, M., Scholten, C., Sharma, S., Simeonov, A., Sundström, M., Superti-Furga, G., Todd, M. H., Tredup, C., Vedadi, M., von Delft, F., Willson, T. M., Winter, G. E., Workman, P., and Arrowsmith, C. H. (2022). Target 2035 - update on the quest for a probe for every protein. RSC Med Chem *13*, 13-21.

Nguyen, T. M., Deb, A., Kokkonda, P., Sreekanth, V., Tiwari, P. K., Shoba, V., Lai, S., Chaudhary, S. K., Mercer, J. A. M., and Jan, M. (2021). Proteolysis Targeting Chimeras With Reduced Off-targets. bioRxiv

Nowak, R. P., DeAngelo, S. L., Buckley, D., He, Z., Donovan, K. A., An, J., Safaee, N., Jedrychowski, M. P., Ponthier, C. M., Ishoey, M., Zhang, T., Mancias, J. D., Gray, N. S., Bradner, J. E., and Fischer, E. S. (2018). Plasticity in binding confers selectivity in ligand-induced protein degradation. Nat Chem Biol *14*, 706-714.

O'Neil, N. J., Bailey, M. L., and Hieter, P. (2017). Synthetic lethality and cancer. Nat Rev Genet *18*, 613-623.

Ogitani, Y., Aida, T., Hagihara, K., Yamaguchi, J., Ishii, C., Harada, N., Soma, M., Okamoto, H., Oitate, M., Arakawa, S., Hirai, T., Atsumi, R., Nakada, T., Hayakawa, I., Abe, Y., and Agatsuma, T. (2016). DS-8201a, A Novel HER2-Targeting ADC with a Novel DNA

Topoisomerase I Inhibitor, Demonstrates a Promising Antitumor Efficacy with Differentiation from T-DM1. Clin Cancer Res *22*, 5097-5108.

Ohata, Y., Shimada, S., Akiyama, Y., Mogushi, K., Nakao, K., Matsumura, S., Aihara, A., Mitsunori, Y., Ban, D., Ochiai, T., Kudo, A., Arii, S., Tanabe, M., and Tanaka, S. (2017). Acquired Resistance with Epigenetic Alterations Under Long-Term Antiangiogenic Therapy for Hepatocellular Carcinoma. Mol Cancer Ther *16*, 1155-1165.

Oshimori, N., Oristian, D., and Fuchs, E. (2015). TGF-β promotes heterogeneity and drug resistance in squamous cell carcinoma. Cell *160*, 963-976.

Ostrem, J. M., Peters, U., Sos, M. L., Wells, J. A., and Shokat, K. M. (2013). K-Ras(G12C) inhibitors allosterically control GTP affinity and effector interactions. Nature *503*, 548-551.

Pak, E., and Segal, R. A. (2016). Hedgehog Signal Transduction: Key Players, Oncogenic Drivers, and Cancer Therapy. Dev Cell *38*, 333-344.

Pierce, N. W., Lee, J. E., Liu, X., Sweredoski, M. J., Graham, R. L., Larimore, E. A., Rome, M., Zheng, N., Clurman, B. E., Hess, S., Shan, S. O., and Deshaies, R. J. (2013). Cand1 promotes assembly of new SCF complexes through dynamic exchange of F box proteins. Cell *153*, 206-215.

Pon, J. R., and Marra, M. A. (2015). Driver and passenger mutations in cancer. Annu Rev Pathol *10*, 25-50.

Pui, C. H., Campana, D., Pei, D., Bowman, W. P., Sandlund, J. T., Kaste, S. C., Ribeiro, R. C., Rubnitz, J. E., Raimondi, S. C., Onciu, M., Coustan-Smith, E., Kun, L. E., Jeha, S., Cheng, C., Howard, S. C., Simmons, V., Bayles, A., Metzger, M. L., Boyett, J. M., Leung, W., Handgretinger, R., Downing, J. R., Evans, W. E., and Relling, M. V. (2009). Treating childhood acute lymphoblastic leukemia without cranial irradiation. N Engl J Med *360*, 2730-2741.

Quaresma, M., Coleman, M. P., and Rachet, B. (2015). 40-year trends in an index of survival for all cancers combined and survival adjusted for age and sex for each cancer in England and Wales, 1971-2011: a population-based study. Lancet *385*, 1206-1218.

Rahbari, N. N., Kedrin, D., Incio, J., Liu, H., Ho, W. W., Nia, H. T., Edrich, C. M., Jung, K., Daubriac, J., Chen, I., Heishi, T., Martin, J. D., Huang, Y., Maimon, N., Reissfelder, C., Weitz, J., Boucher, Y., Clark, J. W., Grodzinsky, A. J., Duda, D. G., Jain, R. K., and Fukumura, D. (2016). Anti-VEGF therapy induces ECM remodeling and mechanical barriers to therapy in colorectal cancer liver metastases. Sci Transl Med *8*, 360ra135.

Raina, K., Lu, J., Qian, Y., Altieri, M., Gordon, D., Rossi, A. M., Wang, J., Chen, X., Dong, H., Siu, K., Winkler, J. D., Crew, A. P., Crews, C. M., and Coleman, K. G. (2016). PROTAC-induced BET protein degradation as a therapy for castration-resistant prostate cancer. Proc Natl Acad Sci U S A *113*, 7124-7129.

Raza, S., Safyan, R. A., and Lentzsch, S. (2017). Immunomodulatory Drugs (IMiDs) in Multiple Myeloma. Curr Cancer Drug Targets *17*, 846-857.

Reed, S. I. (2006). The ubiquitin-proteasome pathway in cell cycle control. Results Probl Cell Differ *42*, 147-181.

Reichermeier, K. M., Straube, R., Reitsma, J. M., Sweredoski, M. J., Rose, C. M., Moradian, A., den Besten, W., Hinkle, T., Verschueren, E., Petzold, G., Thomä, N. H., Wertz, I. E., Deshaies, R. J., and Kirkpatrick, D. S. (2020). PIKES Analysis Reveals Response to Degraders and Key Regulatory Mechanisms of the CRL4 Network. Mol Cell *77*, 1092-1106.e9.

Reitsma, J. M., Liu, X., Reichermeier, K. M., Moradian, A., Sweredoski, M. J., Hess, S., and Deshaies, R. J. (2017). Composition and Regulation of the Cellular Repertoire of SCF Ubiquitin Ligases. Cell *171*, 1326-1339.e14.

Richardson, P. G., Barlogie, B., Berenson, J., Singhal, S., Jagannath, S., Irwin, D., Rajkumar, S. V., Srkalovic, G., Alsina, M., Alexanian, R., Siegel, D., Orlowski, R. Z., Kuter, D., Limentani, S. A., Lee, S., Hideshima, T., Esseltine, D. L., Kauffman, M., Adams, J., Schenkein, D. P., and Anderson, K. C. (2003). A phase 2 study of bortezomib in relapsed, refractory myeloma. N Engl J Med *348*, 2609-2617.

Richardson, P. G., Oriol, A., Beksac, M., Liberati, A. M., Galli, M., Schjesvold, F., Lindsay, J., Weisel, K., White, D., Facon, T., San Miguel, J., Sunami, K., O'Gorman, P., Sonneveld, P., Robak, P., Semochkin, S., Schey, S., Yu, X., Doerr, T., Bensmaine, A., Biyukov, T., Peluso, T., Zaki, M., Anderson, K., Dimopoulos, M., and OPTIMISMM, T. I. (2019). Pomalidomide, bortezomib, and dexamethasone for patients with relapsed or refractory multiple myeloma previously treated with lenalidomide (OPTIMISMM): a randomised, open-label, phase 3 trial. Lancet Oncol *20*, 781-794.

Roche-Lestienne, C., Soenen-Cornu, V., Grardel-Duflos, N., Laï, J. L., Philippe, N., Facon, T., Fenaux, P., and Preudhomme, C. (2002). Several types of mutations of the Abl gene can be found in chronic myeloid leukemia patients resistant to STI571, and they can pre-exist to the onset of treatment. Blood *100*, 1014-1018.

Rosenberg, S. A., and Restifo, N. P. (2015). Adoptive cell transfer as personalized immunotherapy for human cancer. Science *348*, 62-68.

Roskoski, R. (2016). Classification of small molecule protein kinase inhibitors based upon the structures of their drug-enzyme complexes. Pharmacol Res *103*, 26-48.

Rossari, F., Minutolo, F., and Orciuolo, E. (2018). Past, present, and future of Bcr-Abl inhibitors: from chemical development to clinical efficacy. J Hematol Oncol *11*, 84.

Russo, M., Siravegna, G., Blaszkowsky, L. S., Corti, G., Crisafulli, G., Ahronian, L. G., Mussolin, B., Kwak, E. L., Buscarino, M., Lazzari, L., Valtorta, E., Truini, M., Jessop, N. A., Robinson, H. E., Hong, T. S., Mino-Kenudson, M., Di Nicolantonio, F., Thabet, A., Sartore-Bianchi, A., Siena, S., Iafrate, A. J., Bardelli, A., and Corcoran, R. B. (2016). Tumor Heterogeneity and Lesion-Specific Response to Targeted Therapy in Colorectal Cancer. Cancer Discov *6*, 147-153.

Sabatini, D. M., Erdjument-Bromage, H., Lui, M., Tempst, P., and Snyder, S. H. (1994). RAFT1: a mammalian protein that binds to FKBP12 in a rapamycin-dependent fashion and is homologous to yeast TORs. Cell *78*, 35-43.

Sahasranaman, S., Howard, D., and Roy, S. (2008). Clinical pharmacology and pharmacogenetics of thiopurines. Eur J Clin Pharmacol *64*, 753-767.

Santi, D. V., McHenry, C. S., and Sommer, H. (1974). Mechanism of interaction of thymidylate synthetase with 5-fluorodeoxyuridylate. Biochemistry *13*, 471-481.

Savitski, M. M., Zinn, N., Faelth-Savitski, M., Poeckel, D., Gade, S., Becher, I., Muelbaier, M., Wagner, A. J., Strohmer, K., Werner, T., Melchert, S., Petretich, M., Rutkowska, A., Vappiani, J., Franken, H., Steidel, M., Sweetman, G. M., Gilan, O., Lam, E. Y. N., Dawson, M. A., Prinjha, R. K., Grandi, P., Bergamini, G., and Bantscheff, M. (2018). Multiplexed Proteome Dynamics Profiling Reveals Mechanisms Controlling Protein Homeostasis. Cell *173*, 260-274.e25.

Schirrmacher, V. (2019). From chemotherapy to biological therapy: A review of novel concepts to reduce the side effects of systemic cancer treatment (Review). Int J Oncol *54*, 407-419.

Schlierf, A., Altmann, E., Quancard, J., Jefferson, A. B., Assenberg, R., Renatus, M., Jones, M., Hassiepen, U., Schaefer, M., Kiffe, M., Weiss, A., Wiesmann, C., Sedrani, R., Eder, J., and Martoglio, B. (2016). Targeted inhibition of the COP9 signalosome for treatment of cancer. Nat Commun *7*, 13166.

Schreiber, S. L. (2021). The Rise of Molecular Glues. Cell *184*, 3-9.

Shi, J., Wang, E., Milazzo, J. P., Wang, Z., Kinney, J. B., and Vakoc, C. R. (2015). Discovery of cancer drug targets by CRISPR-Cas9 screening of protein domains. Nat Biotechnol *33*, 661-667.

Shibue, T., and Weinberg, R. A. (2017). EMT, CSCs, and drug resistance: the mechanistic link and clinical implications. Nat Rev Clin Oncol *14*, 611-629.

Shirasaki, R., Matthews, G. M., Gandolfi, S., de Matos Simoes, R., Buckley, D. L., Raja Vora, J., Sievers, Q. L., Brüggenthies, J. B., Dashevsky, O., Poarch, H., Tang, H., Bariteau, M. A., Sheffer, M., Hu, Y., Downey-Kopyscinski, S. L., Hengeveld, P. J., Glassner, B. J., Dhimolea, E., Ott, C. J., Zhang, T., Kwiatkowski, N. P., Laubach, J. P., Schlossman, R. L., Richardson, P. G., Culhane, A. C., Groen, R. W. J., Fischer, E. S., Vazquez, F., Tsherniak, A., Hahn, W. C., Levy, J., Auclair, D., Licht, J. D., Keats, J. J., Boise, L. H., Ebert, B. L., Bradner, J. E., Gray, N. S., and Mitsiades, C. S. (2021). Functional Genomics Identify Distinct and Overlapping Genes Mediating Resistance to Different Classes of Heterobifunctional Degraders of Oncoproteins. Cell Rep *34*, 108532.

Sievers, Q. L., Gasser, J. A., Cowley, G. S., Fischer, E. S., and Ebert, B. L. (2018a). Genome-wide screen identifies cullin-RING ligase machinery required for lenalidomide-dependent CRL4^{CRBN} activity. Blood *132*, 1293-1303.

Sievers, Q. L., Petzold, G., Bunker, R. D., Renneville, A., Słabicki, M., Liddicoat, B. J., Abdulrahman, W., Mikkelsen, T., Ebert, B. L., and Thomä, N. H. (2018b). Defining the human C2H2 zinc finger degrome targeted by thalidomide analogs through CRBN. Science *362*, eaat0572-11.

Simonetta, K. R., Taygerly, J., Boyle, K., Basham, S. E., Padovani, C., Lou, Y., Cummins, T. J., Yung, S. L., von Soly, S. K., Kayser, F., Kuriyan, J., Rape, M., Cardozo, M., Gallop, M. A., Bence, N. F., Barsanti, P. A., and Saha, A. (2019). Prospective discovery of small molecule enhancers of an E3 ligase-substrate interaction. Nat Commun *10*, 1402.

Singh, S., Kumar, N. K., Dwiwedi, P., Charan, J., Kaur, R., Sidhu, P., and Chugh, V. K. (2018). Monoclonal Antibodies: A Review. Curr Clin Pharmacol *13*, 85-99.

Singhal, S., Mehta, J., Desikan, R., Ayers, D., Roberson, P., Eddlemon, P., Munshi, N., Anaissie, E., Wilson, C., Dhodapkar, M., Zeddis, J., and Barlogie, B. (1999). Antitumor activity of thalidomide in refractory multiple myeloma. N Engl J Med *341*, 1565-1571.

Siriwardena, S. U., Munkanatta Godage, D. N. P., Shoba, V. M., Lai, S., Shi, M., Wu, P., Chaudhary, S. K., Schreiber, S. L., and Choudhary, A. (2020). Phosphorylation-Inducing Chimeric Small Molecules. J Am Chem Soc *142*, 14052-14057.

Słabicki, M., Kozicka, Z., Petzold, G., Li, Y. D., Manojkumar, M., Bunker, R. D., Donovan, K. A., Sievers, Q. L., Koeppel, J., Suchyta, D., Sperling, A. S., Fink, E. C., Gasser, J. A., Wang, L. R., Corsello, S. M., Sellar, R. S., Jan, M., Gillingham, D., Scholl, C., Fröhling, S., Golub, T. R., Fischer, E. S., Thomä, N. H., and Ebert, B. L. (2020). The CDK inhibitor CR8 acts as a molecular glue degrader that depletes cyclin K. Nature *585*, 293-297.

Soucy, T. A., Smith, P. G., Milhollen, M. A., Berger, A. J., Gavin, J. M., Adhikari, S., Brownell, J. E., Burke, K. E., Cardin, D. P., Critchley, S., Cullis, C. A., Doucette, A., Garnsey, J. J., Gaulin, J. L., Gershman, R. E., Lublinsky, A. R., McDonald, A., Mizutani, H., Narayanan, U., Olhava, E. J., Peluso, S., Rezaei, M., Sintchak, M. D., Talreja, T., Thomas, M. P., Traore, T., Vyskocil, S., Weatherhead, G. S., Yu, J., Zhang, J., Dick, L. R., Claiborne, C. F., Rolfe, M., Bolen, J. B., and Langston, S. P. (2009). An inhibitor of NEDD8-activating enzyme as a new approach to treat cancer. Nature *458*, 732-736.

Speirs, A. (1962). Thalidomide and congenital abnormalities. Lancet *1*, 303-305.

Spring, L. M., Wander, S. A., Andre, F., Moy, B., Turner, N. C., and Bardia, A. (2020). Cyclin-dependent kinase 4 and 6 inhibitors for hormone receptor-positive breast cancer: past, present, and future. Lancet *395*, 817-827.

Stratton, M. R., Campbell, P. J., and Futreal, P. A. (2009). The cancer genome. Nature *458*, 719-724.

Swinney, D. C. (2013). Phenotypic vs. target-based drug discovery for first-in-class medicines. Clin Pharmacol Ther *93*, 299-301.

Takahashi, D., Moriyama, J., Nakamura, T., Miki, E., Takahashi, E., Sato, A., Akaike, T., Itto-Nakama, K., and Arimoto, H. (2019). AUTACs: Cargo-Specific Degraders Using Selective Autophagy. Mol Cell *76*, 797-810.e10.

Tarakhovsky, A. (2010). Tools and landscapes of epigenetics. Nat Immunol *11*, 565-568.

Thrower, J. S., Hoffman, L., Rechsteiner, M., and Pickart, C. M. (2000). Recognition of the polyubiquitin proteolytic signal. EMBO J *19*, 94-102.

Townsend, A. J., and Cheng, Y. C. (1987). Sequence-specific effects of ara-5-aza-CTP and ara-CTP on DNA synthesis by purified human DNA polymerases in vitro: visualization of chain elongation on a defined template. Mol Pharmacol *32*, 330-339.

Tunyasuvunakool, K., Adler, J., Wu, Z., Green, T., Zielinski, M., Žídek, A., Bridgland, A., Cowie, A., Meyer, C., Laydon, A., Velankar, S., Kleywegt, G. J., Bateman, A., Evans, R., Pritzel, A., Figurnov, M., Ronneberger, O., Bates, R., Kohl, S. A. A., Potapenko, A., Ballard,

A. J., Romera-Paredes, B., Nikolov, S., Jain, R., Clancy, E., Reiman, D., Petersen, S., Senior, A. W., Kavukcuoglu, K., Birney, E., Kohli, P., Jumper, J., and Hassabis, D. (2021). Highly accurate protein structure prediction for the human proteome. Nature *596*, 590-596.

Vasan, N., Baselga, J., and Hyman, D. M. (2019). A view on drug resistance in cancer. Nature *575*, 299-309.

Vyas, S., and Chang, P. (2014). New PARP targets for cancer therapy. Nat Rev Cancer *14*, 502-509.

Walker, B. A., Mavrommatis, K., Wardell, C. P., Ashby, T. C., Bauer, M., Davies, F. E., Rosenthal, A., Wang, H., Qu, P., Hoering, A., Samur, M., Towfic, F., Ortiz, M., Flynt, E., Yu, Z., Yang, Z., Rozelle, D., Obenauer, J., Trotter, M., Auclair, D., Keats, J., Bolli, N., Fulciniti, M., Szalat, R., Moreau, P., Durie, B., Stewart, A. K., Goldschmidt, H., Raab, M. S., Einsele, H., Sonneveld, P., San Miguel, J., Lonial, S., Jackson, G. H., Anderson, K. C., Avet-Loiseau, H., Munshi, N., Thakurta, A., and Morgan, G. J. (2018). Identification of novel mutational drivers reveals oncogene dependencies in multiple myeloma. Blood *132*, 587-597.

Wang, W. W., Chen, L. Y., Wozniak, J. M., Jadhav, A. M., Anderson, H., Malone, T. E., and Parker, C. G. (2021). Targeted Protein Acetylation in Cells Using Heterobifunctional Molecules. J Am Chem Soc *143*, 16700-16708.

Wang, Y., Dix, M. M., Bianco, G., Remsberg, J. R., Lee, H. Y., Kalocsay, M., Gygi, S. P., Forli, S., Vite, G., Lawrence, R. M., Parker, C. G., and Cravatt, B. F. (2019). Expedited mapping of the ligandable proteome using fully functionalized enantiomeric probe pairs. Nat Chem *11*, 1113-1123.

Wani, M. C., and Horwitz, S. B. (2014). Nature as a remarkable chemist: a personal story of the discovery and development of Taxol. Anticancer Drugs *25*, 482-487.

Watson, E. R., Novick, S. J., and Matyskiela…, M. E. (2022). Molecular glue CELMoD compounds are allosteric regulators of cereblon conformation. bioRxiv

Weinstein, I. B. (2002). Addiction to oncogenes-the Achilles heal of cancer. Science *297*, 63-64.

Weng, G., Li, D., Kang, Y., and Hou, T. (2021). Integrative Modeling of PROTAC-Mediated Ternary Complexes. J Med Chem *64*, 16271-16281.

Wilson, L. J., Linley, A., Hammond, D. E., Hood, F. E., Coulson, J. M., MacEwan, D. J., Ross, S. J., Slupsky, J. R., Smith, P. D., Eyers, P. A., and Prior, I. A. (2018). New Perspectives,

Opportunities, and Challenges in Exploring the Human Protein Kinome. Cancer Res *78*, 15-29.

Winter, G. E., Buckley, D. L., Paulk, J., Roberts, J. M., Souza, A., Dhe-Paganon, S., and Bradner, J. E. (2015). DRUG DEVELOPMENT. Phthalimide conjugation as a strategy for in vivo target protein degradation. Science *348*, 1376-1381.

Winter, G. E., Mayer, A., Buckley, D. L., Erb, M. A., Roderick, J. E., Vittori, S., Reyes, J. M., di Iulio, J., Souza, A., Ott, C. J., Roberts, J. M., Zeid, R., Scott, T. G., Paulk, J., Lachance, K., Olson, C. M., Dastjerdi, S., Bauer, S., Lin, C. Y., Gray, N. S., Kelliher, M. A., Churchman, L. S., and Bradner, J. E. (2017). BET Bromodomain Proteins Function as Master Transcription Elongation Factors Independent of CDK9 Recruitment. Mol Cell *67*, 5-18.e19.

Wolf, D. A., Zhou, C., and Wee, S. (2003). The COP9 signalosome: an assembly and maintenance platform for cullin ubiquitin ligases. Nat Cell Biol *5*, 1029-1033.

Wu, Q., Yang, Z., Nie, Y., Shi, Y., and Fan, D. (2014). Multi-drug resistance in cancer chemotherapeutics: mechanisms and lab approaches. Cancer Lett *347*, 159-166.

Yamazoe, S., Tom, J., Fu, Y., Wu, W., Zeng, L., Sun, C., Liu, Q., Lin, J., Lin, K., Fairbrother, W. J., and Staben, S. T. (2020). Heterobifunctional Molecules Induce Dephosphorylation of Kinases-A Proof of Concept Study. J Med Chem *63*, 2807-2813.

Yau, R. G., Doerner, K., Castellanos, E. R., Haakonsen, D. L., Werner, A., Wang, N., Yang, X. W., Martinez-Martin, N., Matsumoto, M. L., Dixit, V. M., and Rape, M. (2017). Assembly and Function of Heterotypic Ubiquitin Chains in Cell-Cycle and Protein Quality Control. Cell *171*, 918-933.e20.

Yu, H. A., Arcila, M. E., Hellmann, M. D., Kris, M. G., Ladanyi, M., and Riely, G. J. (2014). Poor response to erlotinib in patients with tumors containing baseline EGFR T790M mutations found by routine clinical molecular testing. Ann Oncol *25*, 423-428.

Zaidman, D., Prilusky, J., and London, N. (2020). PRosettaC: Rosetta Based Modeling of PROTAC Mediated Ternary Complexes. J Chem Inf Model *60*, 4894-4903.

Zecha, J., Meng, C., Zolg, D. P., Samaras, P., Wilhelm, M., and Kuster, B. (2018). Peptide Level Turnover Measurements Enable the Study of Proteoform Dynamics. Mol Cell Proteomics *17*, 974-992.

Zengerle, M., Chan, K. H., and Ciulli, A. (2015). Selective Small Molecule Induced Degradation of the BET Bromodomain Protein BRD4. ACS Chem Biol *10*, 1770-1777.

Zhang, L., Riley-Gillis, B., Vijay, P., and Shen, Y. (2019). Acquired Resistance to BET-PROTACs (Proteolysis-Targeting Chimeras) Caused by Genomic Alterations in Core Components of E3 Ligase Complexes. Mol Cancer Ther *18*, 1302-1311.

Zhao, L., Zhao, J., Zhong, K., Tong, A., and Jia, D. (2022). Targeted protein degradation: mechanisms, strategies and application. Signal Transduct Target Ther *7*, 113.

Zhong, L., Li, Y., Xiong, L., Wang, W., Wu, M., Yuan, T., Yang, W., Tian, C., Miao, Z., Wang, T., and Yang, S. (2021). Small molecules in targeted cancer therapy: advances, challenges, and future perspectives. Signal Transduct Target Ther *6*, 201.

Curriculum Vitae

Personal Information

Name:	Alexander Hanzl
Date of birth:	May 28th, 1991
Nationality:	Austrian
Email:	alexander.hanzl@gmail.com

Education

2017 - **PhD in Molecular Medicine**
CeMM Research Center for Molecular Medicine, Vienna (AT)
Supervisor: Georg E. Winter
Title: “Identifying Novel Degraders and Resistance Mechanisms in Targeted Protein Degradation”

2015 - 2016 **Master thesis, Vienna University of Technology**
Friedrich Miescher Institute for Biomedical Research, Basel (CH)
Supervisor: Antoine H.F.M. Peters
Title: “The Role of Histone Chaperone DAXX during Meiotic Sex Chromosome Inactivation and its Interaction with Polycomb Repressive Complex“

2014 - 2016 **Master of science in Technical Chemistry**
Vienna University of Technology, Vienna (AT)
Specialization: Biotechnology and Bioanalytics
GPA: 1.5 (best 1, worst 5)

2010 - 2014 **Bachelor of science in Technical Chemistry**
Vienna University of Technology, Vienna (AT)
Supervisor: Marko D.Mihovilovic
Title: “Sythesis of Magnolol-Derivatives as PPARg and GABAA agonists”
GPA: 1.9 (best 1, worst 5)

2007 - 2008 **South High School**
Minneapolis, Minnesota (USA)

2001 - 2009 **Gymnasium BGXIII**
Fichtnergasse, Vienna (AT)
Matura (General Qualification for University Entrance)
GPA: 1,8 (best 1, worst 5)

Professional Experience

2017 -	**Predoctoral Fellow, Georg Winter Lab** *CeMM Research Center for Molecular Medicine, Vienna (AT)*
2019 - 2021	**Consultant** *ICONS consulting by students, Vienna (AT)*
2015 - 2016	**Undergraduate Scientist, Antoine Peters Lab** *Friedrich Miescher Institute for Biomedical Research, Basel (CH)*
2014	**Guest Scientist, Stefan Kubicek Lab** *CeMM Research Center for Molecular Medicine, Vienna (AT)*
2009 - 2010	**Officer Candidate, Austrian Army** *Freistadt, Amstetten, Baden (AT)*

Conferences and Meetings

2022 Degraders Down Under, WEHI, Melbourne (AUS)
Invited oral presentation

2022 Ubiquitin and Friends Symposium, Vienna (AT)
Poster presentation

2020 European Targeted Protein Degradation Congress, Basel (CH)

2020 CeMM Scientific Advisory Board Meeting
Oral presentation

2020 CeMM Scientific Recess
Oral presentation

2019 Ubiquitin and Friends Symposium, Vienna (AT)

2019 CeMM Scientific Recess
Oral presentation

2018 CeMM Scientific Recess
Poster presentation

List of publications

1. **Functional E3 ligase hotspots and resistance mechanisms to small-molecule degraders.**

   Alexander Hanzl, Ryan Casement*, Hana Imrichova*, Scott J. Hughes, Eleonora Barone, Andrea Testa, Sophie Bauer, Jane Wright, Matthias Brand, Alessio Ciulli and Georg E. Winter (2020); *these authors contributed equally
   Nature Chemical Biology, *accepted manuscript*

2. **Tracing E3 Ligase Abundance Empowers Degrader Discovery at Scale**

   Alexander Hanzl, Eleonora Barone, Sophie Bauer, Hong Yue, Radosław P. Nowak, Elisa Hahn, Eugenia V. Pankevich, Christoph Bock, Eric S. Fischer, Georg E. Winter
   Cell Chemical Biology, *submitted manuscript*

3. **Targeted protein degradation: current and future challenges.**

   Alexander Hanzl, and Georg E. Winter (2020)
   Current Opinions in Chemical Biology *56*, 35-41.

4. **Selective Mediator dependence of cell-type-specifying transcription.**

   Martin G. Jaeger, Björn Schwalb, Sebastian D. Mackowiak, Taras Velychko , Alexander Hanzl, Hana Imrichova, Matthias Brand, Benedikt Agerer, Someth Chorn, Behnam Nabet, Fleur M. Ferguson, André C. Müller, Andreas Bergthaler, Nathanael S. Gray, James E. Bradner, Christoph Bock, Denes Hnisz, Patrick Cramer and Georg E. Winter (2020)
   Nature Genetics *52*, 719-727

5. **Plasticity of the Cullin-RING Ligase Repertoire Shapes Sensitivity to Ligand-Induced Protein Degradation.**

   Cristina Mayor-Ruiz*, Martin G. Jaeger*, Sophie Bauer, Matthias Brand, Celine Sin, Alexander Hanzl, Andre C. Mueller, Jörg Menche, and Georg E. Winter (2019) *these authors contributed equally
   Molecular Cell *75*, 849-858.e8

6. **Genome-scale CRISPR screens are efficient in non-homologous end-joining deficient cells.**

   Joana Ferreira da Silva, Sejla Salic, Marc Wiedner, Paul Datlinger, Patrick Essletzbichler, Alexander Hanzl, Giulio Superti-Furga, Christoph Bock, Georg E. Winter & Joanna I. Loizou (2019)
   Scientific Reports *9*, 15751